NASA CR-120869
TRW 14549-6001-RO-00

FINAL REPORT

HYDROGEN-OXYGEN CATALYTIC IGNITION AND THRUSTER INVESTIGATION

VOLUME I

CATALYTIC IGNITION AND LOW PRESSURE THRUSTER EVALUATIONS

By
R. J. JOHNSON

PREPARED FOR
NATIONAL AERONAUTICS AND SPACE ADMINISTRATION
NASA Lewis Research Center
Contract 3-14347

P. N. HERR,
Project Manager

NOTICE

This report was prepared as an account of Government-sponsored work. Neither the United States, nor the National Aeronautics and Space Administration (NASA), nor any person acting on behalf of NASA;

A. Makes any warranty or representation, expressed or implied, with respect to the accuracy, completeness, or usefulness of the information contained in this report, or that the use of any information, apparatus, method, or process disclosed in this report may not infringe privately-owned rights; or

B. Assumes any liabilities with respect to the use of, or for damages resulting from the use of, any information, apparatus, method or process disclosed in this report.

As used above, "person acting on behalf of NASA" includes any employee or contractor of NASA, or employee of such contractor, to the extent that such employee or contractor of NASA or employee of such contractor prepares, disseminates, or provides access to any information pursuant to this employment or contract with NASA, or his employment with such contractor.

Requests for copies of this report should be referred to

National Aeronautics and Space Administration
Scientific and Technical Information Facility
P. O. Box 33
College Park, Maryland 20740

1. Report No.	2. Government Accession No.	3. Recipient's Catalog No.
NASA CR-120869		

4. Title and Subtitle	5. Report Date
HYDROGEN-OXYGEN CATALYTIC IGNITION AND THRUSTER INVESTIGATION Vol. I — Catalytic Ignition and Low Pressure Thruster Evaluations	November 1972 6. Performing Organization Code

7. Author(s)	8. Performing Organization Report No.
R. J. Johnson	10. Work Unit No.

9. Performing Organization Name and Address	11. Contract or Grant No.
TRW SystemsGroup One Space Park, Redondo Beach, California 90278	NAS 3-14347

12. Sponsoring Agency Name and Address	13. Type of Report and Period Covered
National Aeronautics and Space Administration Washington, D.C. 20546	Final 14. Sponsoring Agency Code

15. Supplementary Notes

Project Manager, P. N. Herr, NASA Lewis Research Center, Cleveland, Ohio

16. Abstract

An experimental and analytical program was conducted to evaluate catalytic igniter operational limits, igniter scaling criteria, and delivered performance of cooled, flightweight gaseous hydrogen-oxygen reaction control thrusters. Specific goals were to establish operating life and environmental effects for both Shell 405-ABSG and Engelhard MFSA catalysts, provide generalized igniter design guidelines for high response without flashback, and to determine overall performance of thrusters at chamber pressures of 15 and 300 psia (103 and 2068 kN/m^2) and thrust levels of 30 and 1500 lbf (133 and 6672 N), respectively. The experimental results have demonstrated the feasibility of reliable, high response (less than 25 msec) catalytic ignition and the effectiveness of ducted chamber cooling (1800 second single firing) for a high performance flightweight thruster. This volume presents the results of the catalytic igniter and low pressure thruster evaluations. Analytical and experimental evaluations of the high pressure thruster are reported in Volume II, NASA CR-120870.

17. Key Words (Suggested by Author(s))	18. Distribution Statement
Catalytic Ignition Hydrogen-Oxygen Low Pressure Thruster Duct Cooling	

19. Security Classif. (of this report)	20. Security Classif. (of this page)	21. No. of Pages	22. Price*
Unclassified	Unclassified	213	

* For sale by the National Technical Information Service, Springfield, Virginia 22151

NASA CR-120869
TRW 14549-6001-R0-00

FINAL REPORT

HYDROGEN-OXYGEN CATALYTIC IGNITION AND THRUSTER INVESTIGATION

Volume I

Catalytic Ignition and Low Pressure Thruster Evaluations

by

R. J. Johnson

TRW SYSTEMS GROUP
One Space Park
Redondo Beach, California 90278

prepared for

NATIONAL AERONAUTICS AND SPACE ADMINISTRATION

November 14, 1972

CONTRACT NAS 3-14347

NASA Lewis Research Center
Cleveland, Ohio

P. N. Herr, Project Manager
Liquid Rocket Technology Branch

ONE SPACE PARK • REDONDO BEACH • CALIFORNIA

FOREWORD

This report was prepared by the Applied Technology Division of the TRW Systems Group, One Space Park, Redondo Beach, California, under Contract NAS 3-14347. The contract was administered by the Lewis Research Center of the National Aeronautics and Space Administration, Cleveland, Ohio. The NASA Project Manager for the contract was Mr. P. N. Herr of the Liquid Rocket Technology Branch. This is the final report on the subject contract and summarizes the technical effort conducted during the period from June 1970 to December 1971. Volume I describes the catalytic ignition and low chamber pressure thruster evaluations, and Volume II presents the results of the high pressure thruster evaluations begun during March 1971.

ACKNOWLEDGEMENTS

The following personnel at TRW contributed to the technical accomplishments of this program: R. J. Johnson, Program Manager; B. J. Heckert, High Pressure Thruster Development and Evaluation; B. G. Morton, Igniter Evaluations; H. L. Burge and S. J. VanGrouw, Technical Advisors; E. P. Koutsoukos, M. J. Santy, and T. B. Hurst, Laboratory Investigations; H. W. Beck, K. J. Mock, and E. W. Woodell, Design; P. Y. Hsieh, Stress Analysis; F. B. Muenzer, Dynamic Analysis; F. Scott, Heat Transfer Analysis; J. T. Gardner and J. T. Fitzgerald, Engineering Liaison; J. R. Augustson, L. L. Gassert, F. E. Robinett, and R. C. Sorensen, Test Operations; D. S. Landgreen and G. P. Starr, Data Acquisition.

CONTENTS

CONTENTS

ILLUSTRATIONS

ILLUSTRATIONS (Continued)

ILLUSTRATIONS (Continued)

ILLUSTRATIONS (Continued)

ILLUSTRATIONS (Continued)

ILLUSTRATIONS (Continued)

ILLUSTRATIONS (Continued)

ILLUSTRATIONS (Continued)

TABLES

TABLES

ABSTRACT

An experimental and analytical program was conducted to evaluate catalytic igniter operational limits, igniter scaling criteria, and delivered performance of cooled, flightweight gaseous hydrogen-oxygen reaction control thrusters. Specific goals were to establish operating life and environmental effects for both Shell 405-ABSG and Engelhard MFSA catalysts, provide generalized igniter design guidelines for high response without flashback, and to determine overall performance of thrusters at chamber pressures of 15 and 300 psia (103 and 2068 kN/m^2) and thrust levels of 30 and 1500 lbf (133 and 6672 N), respectively. The experimental results have demonstrated the feasibility of reliable, high response (less than 25 msec) catalytic ignition and the effectiveness of ducted chamber cooling (1800 second single firing) for a high performance flightweight thruster. This volume presents the results of the catalytic igniter and low pressure thruster evaluations. Analytical and experimental evaluations of the high pressure thruster are reported in Volume II, NASA CR-120870.

1. SUMMARY

1. SUMMARY

The experimental results of Contract NAS 3-14347 have demonstrated the feasibility of reliable, high response catalytic ignition of gaseous hydrogen-oxygen thrusters and have proven the effectiveness of ducted chamber cooling for a high perforamnce, flightweight reaction control thruster. Catalytic igniter operational limits, igniter scaling criteria, and delivered performance of cooled, flightweight thrusters were evaluated over a wide range of environmental and propellant inlet conditions.

Laboratory experiments and igniter test firings performed with Shell 405-ABSG and Engelhard MFSA catalysts led to the following conclusions:

- Either catalyst will effectively promote the reaction of GH_2/GO_2 for steady-state durations of at least 4,000 seconds without degrading thermal response or physical characteristics of the catalyst. Test results indicate that single firings of even longer durations are attainable without loss of reactor performance at ambient bed and propellant temperatures.

- At least 5,000 pulses can be performed with both the Shell and Engelhard catalyst with ambient temperature propellants. High response reaction can be achieved with the Shell 405-ABSG catalyst at propellant and initial bed temperatures of -250°F (117°K) after the completion of at least 1000 pulse cycles.

- Igniter flashback can be prevented by maintaining minimum mixing section velocities of 50 ft/sec (15 m/sec) and avoiding mixture ratios above 1.5 O/F upstream of the catalyst bed during transients. Flashback could not be completely arrested by diffusion ball beds. The type of catalyst, Shell or Engelhard, did not affect flashback limits.

- Overall igniter response times of less than 25 msec (to effluent temperature sufficient for thruster ignition) can be attained by injection of oxygen downstream of the catalyst bed. This represents a 100:1 reduction in the catalytic igniter response as previously demonstrated in NAS 3-11227. Preheating and insulating the catalyst bed resulted in minor reduction in overall response, compared to downstream injection.

- Both Shell 405-ABSG and Engelhard MFSA catalysts exposed to simulated shuttle vehicle environmental exposures of earth stay (30 days polluted, humid air) and reentry (1 hour at 1500°F [1089°K], 3.5 psia [24 kN/m^2] air) were reduced in low temperature activity for the initial firing; however, original response was achieved after a single ambient bed firing. Hydrogen purging and/or heating of the catalyst bed was recommended to reverse environmental effects of strongly adsorbed oxygen.

Analysis and correlation of the igniter test data from this program and NAS 3-11227 provided generalized design guidelines for catalytic igniters, which were incorporated into specific igniter designs for 1500 lbf (6672 N) thrusters operating at chamber pressures of 15 psia (103 kN/m^2) and 300 psia (2068 kN/m^2).

Design and cooling analyses were performed for a 30 lbf (133 N) thrust, 15 psia (103 kN/m^2) chamber pressure flightweight thruster. Test firings were conducted to determine delivered altitude performance and durability. The low pressure thruster investigations are summarized as follows:

- The triplet injector designed during this program was found to be superior to the impinging sheet injector (NAS 3-11227) in both cold flow mixing results and test firing performance, and was selected by the NASA/LeRC Project Manager for cooled thruster evaluations.

- Measured altitude performance of 375 lbf-sec/lbm (3677 Nsec/kg) I_{sp} at e = 5 was achieved with a flightweight duct cooled thrust chamber.

- Steady-state and pulse-mode cooled thruster firings were performed with propellant temperatures from ambient to -250°F (117°K). Repeatable pulses were attained for thruster on times from 500 to 80 msec.

- An 1800-second duration steady-state firing was successfully completed with injector and thrust chamber hardware in excellent condition except for surface pits and hairline fatigue cracks in the OFHC copper duct exit. Berylco BE-10 copper alloy was recommended as a superior duct material. Maximum chamber temperature measured during the durability test was 1258°F (953°K) at e = 3.5.

Generalized design guidelines and scaling criteria for catalytic igniters were developed through analysis of the experimental results of this program. Basic thermal and performance data were also acquired for duct cooled hydrogen-oxygen thrusters.

2. INTRODUCTION

2. INTRODUCTION

The "Hydrogen-Oxygen Catalytic Ignition and Thruster Investigation" program, NASA/LeRC Contract NAS 3-14347, was comprised of an experimental and supporting analytical evaluation of catalyst bed operational limitations, igniter scaling criteria, and delivered performance for gaseous hydrogen-oxygen reaction control thrusters. The basic igniter and thruster design criteria previously developed during the performance of NAS 3-11227 were extended to flightweight cooled thrusters, and catalytic igniter operating characteristics were further defined. The specific objectives of this program were:

- Establish catalyst operational life, flashback criteria, and methods of enhancing response time for catalytic pilot bed igniters
- Provide a set of generalized design guidelines for hydrogen-oxygen thruster igniters, based upon a scaling analysis of catalytic igniter designs and experimental results (including NAS 3-11227 data)
- Investigate the effects of environmental conditions on performance of catalytic igniters
- Evaluate the overall performance, operating characteristics, and durability of cooled, flightweight gaseous hydrogen-oxygen thrusters

To accomplish these goals, the following experimental and analytical tasks were conducted:

- Steady-state and pulse mode igniter tests with both Shell 405-ABSG and Engelhard MFSA catalysts
- Analysis of the scaling of catalytic igniter designs for wide ranges of operating conditions
- Laboratory and igniter test firing evaluations of environmental effects on catalyst activity
- Thruster/system interaction analyses
- Cooling analysis, design, and fabrication of flightweight reaction control-type thrusters
- Altitude test firings of flightweight thruster assemblies for both pulse-mode and extended duration (up to 1800 seconds) steady state operation

Flightweight cooled thrusters were developed for both high and low chamber pressure levels. A 15 psia (103 kN/m^2) chamber pressure triplet injector, designed for a vacuum thrust of 30 lbf (133 N) at $\epsilon = 5$, was test evaluated along with the residual low Pc impinging sheet injector from NAS 3-11227. The high Pc thruster, 300 psia (2068 kN/m^2) chamber pressure, was designed for 1500 lbf (6672 N) altitude thrust at $\epsilon = 40$.

Numerous igniter configurations and operational techniques were evaluated to enhance the overall response and reliability of the catalytic igniter. These igniter evaluations and the low pressure thruster investigations are described in the subsequent report sections. The high pressure thruster evaluation results are presented in Volume II of this contract report.

3. CATALYTIC IGNITER INVESTIGATIONS

3. CATALYTIC IGNITER INVESTIGATIONS

A series of experimental tests and supporting analyses were performed to determine the operational limitations and design criteria for catalytic igniters. These investigations were conducted for catalytic reactors capable of igniting gaseous hydrogen-oxygen thrusters over a wide range of thrust and chamber pressure levels. The objectives of this task effort were:

- Establish catalyst operational life, flashback criteria, and methods of enhancing response time for a catalytic pilot bed igniter
- Provide a set of generalized design guidelines for hydrogen-oxygen thruster igniters, based upon a scaling analysis of catalytic igniter designs and experimental results
- Investigate the effects of environmental conditions on performance of a catalytic igniter.

Both steady-state and pulse-mode igniter firings were performed to determine catalyst life, flashback limits, and response characteristics. An igniter scaling analysis was next conducted, based upon results of these tests and NAS 3-11227 (Reference 1). Finally, as a supplementary task, the effects of typical shuttle vehicle operational environments on catalyst activity were also investigated.

3.1 CATALYST LIFE EVALUATION

The purpose of this task was to determine the operational life of the Shell 405-ABSG and Engelhard MFSA catalysts for both steady-state and cyclic (pulse-mode) firing conditions with gaseous hydrogen-oxygen propellants. The specific objectives of the test series were:

- Conduct long-duration continuous igniter firings to establish the steady-state life of each catalyst type with ambient temperature propellants
- Determine the cyclic operational life of each catalyst by performing a series of pulse-mode test firings
- Perform visual and laboratory chemisorption evaluations of each catalyst load from the life tests to determine the extent of physical degradation or loss of activity of the catalyst.

3.1.1 Steady-State Life Tests

Reactor firings of 4000 seconds continuous operation were conducted to determine the steady-state durability of the Shell 405-ABSG and Engelhard MFSA catalysts with gaseous hydrogen-oxygen propellants. The following paragraphs describe the reactor hardware and test stand installation, and discuss the experimental results obtained.

3.1.1.1 Reactor Hardware and Stand Installation

The basic reactor hardware used for the steady-state catalyst life tests is shown in Figures 1 and 2. This reactor assembly (Part No. X-404318) was fabricated and tested during the performance of NASA/LeRC Contract NAS3-11227 (Reference 1). As shown in Figure 1, reactor instrumentation ports were provided to obtain both pressure and temperature measurements at various locations within the mixing zone, catalyst bed, and downstream chamber volume. The disassembled view of the reactor in Figure 2 shows the internal details of the reactor assembly.

The overall test stand installation for the steady-state life tests is shown in Figure 3. Only one of the two reactor mounting positions was utilized for the steady-state tests. Both positions were later used for simultaneous pulse-mode tests with each catalyst type. Figure 4 is a closeup view of the reactor test installation.

Each catalyst bed was carefully loaded in a "clean room" environment and the pre- and post-test catalyst weights measured with a precision electronic scale, as shown in Figure 5. Catalyst load weights were recorded to the nearest one-tenth milligram (0.0001 gram) before and after the long duration firings.

3.1.1.2 Steady-State Firing Test Results

Continuous firings of 4000 seconds duration were successfully completed with each catalyst type. Target test conditions of 100 psia (690 kN/m^2) chamber pressure and reactor effluent temperatures of 1800°F (1256°K) were attained with both the Shell and Engelhard catalysts. Tables 1 and 2 present data obtained during the 4000 second test firings. Measured C* performance of nearly 97% of theoretical equilibrium C* for these propellants and mixture ratios was attained for both long duration tests, after equilibrium operating temperature of the reactor hardware was reached. Chamber pressures, mixture ratios, and reactor effluent and catalyst bed temperatures remained essentially constant during the 4000 second firings, as shown in Tables 1 and 2.

Immediately following each long-duration firing (after cooldown of the catalyst bed to ambient temperature) a 20-second firing was conducted to determine if the thermal response of the catalyst bed had been affected by the extended duration operation. Figures 6 through 9 compare the catalyst bed and reactor effluent thermal response before and after 4000 seconds of operation with each catalyst type. It should be noted that the life test reactor hardware and catalyst bed configurations were not designed for

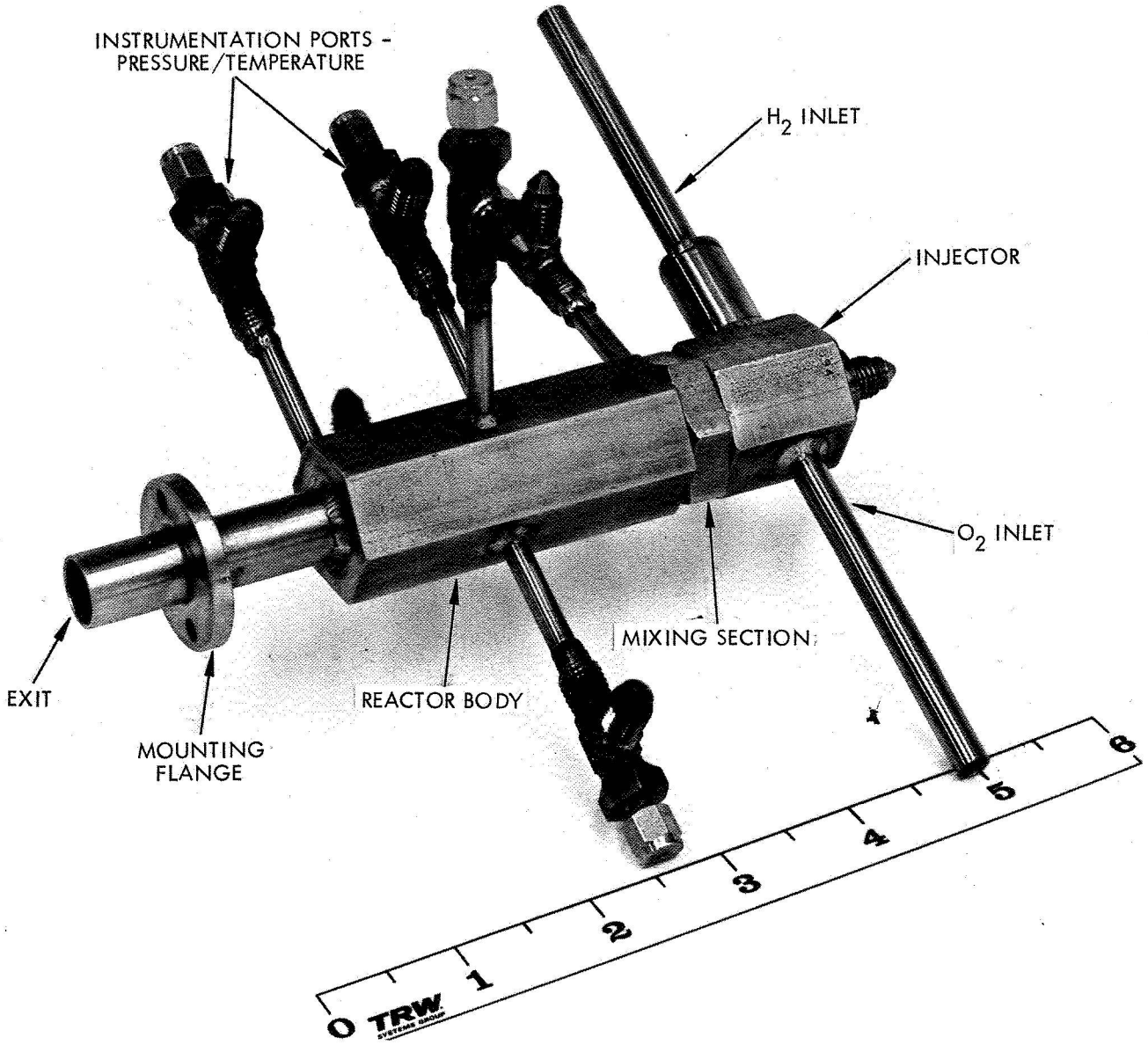

Figure 1. Experimental Catalytic Reactor Igniter Assembly - High Chamber Pressure (Residual from NAS-11227)

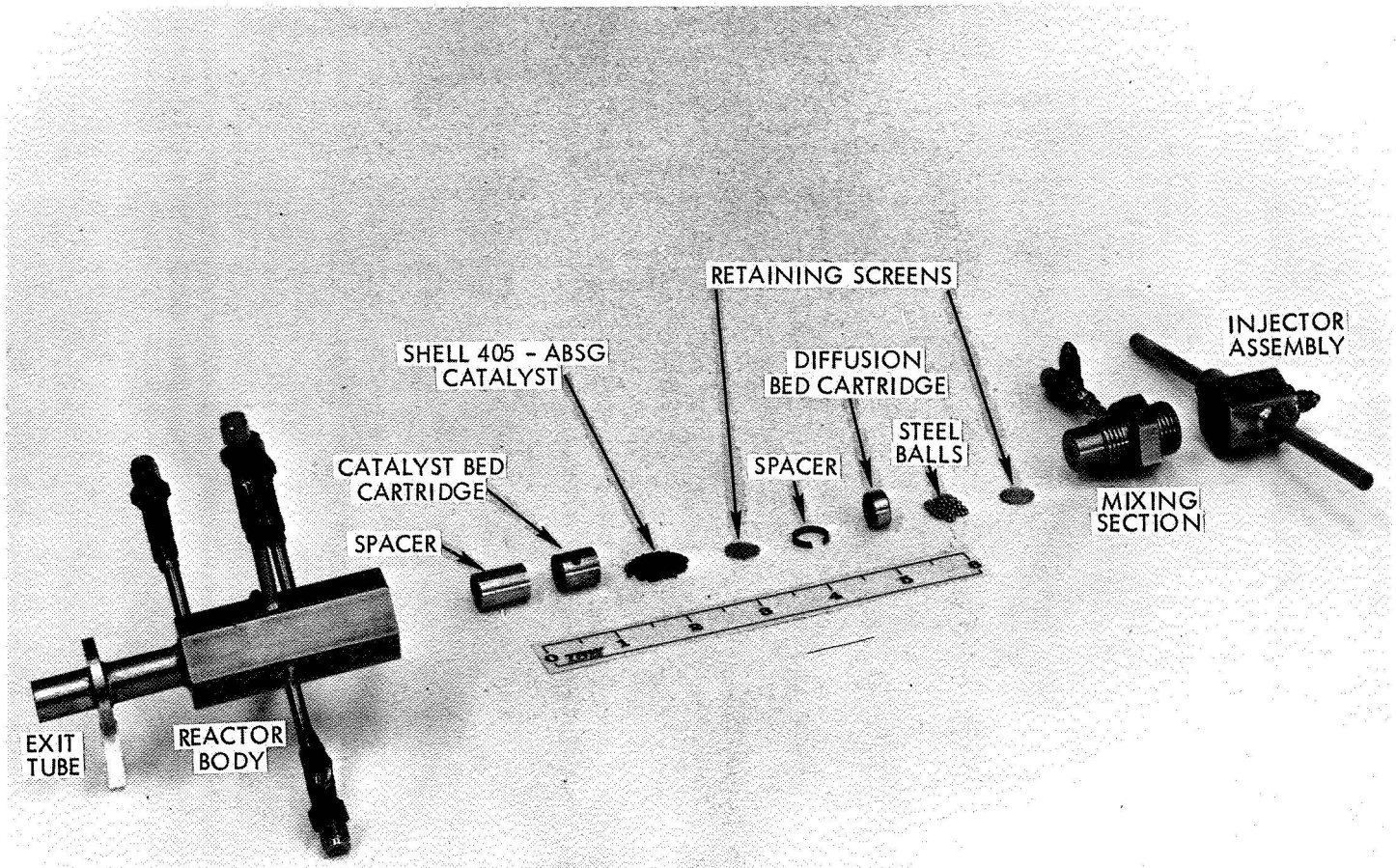

Figure 2. Disassembled Catalytic Reactor Igniter - High Chamber Pressure

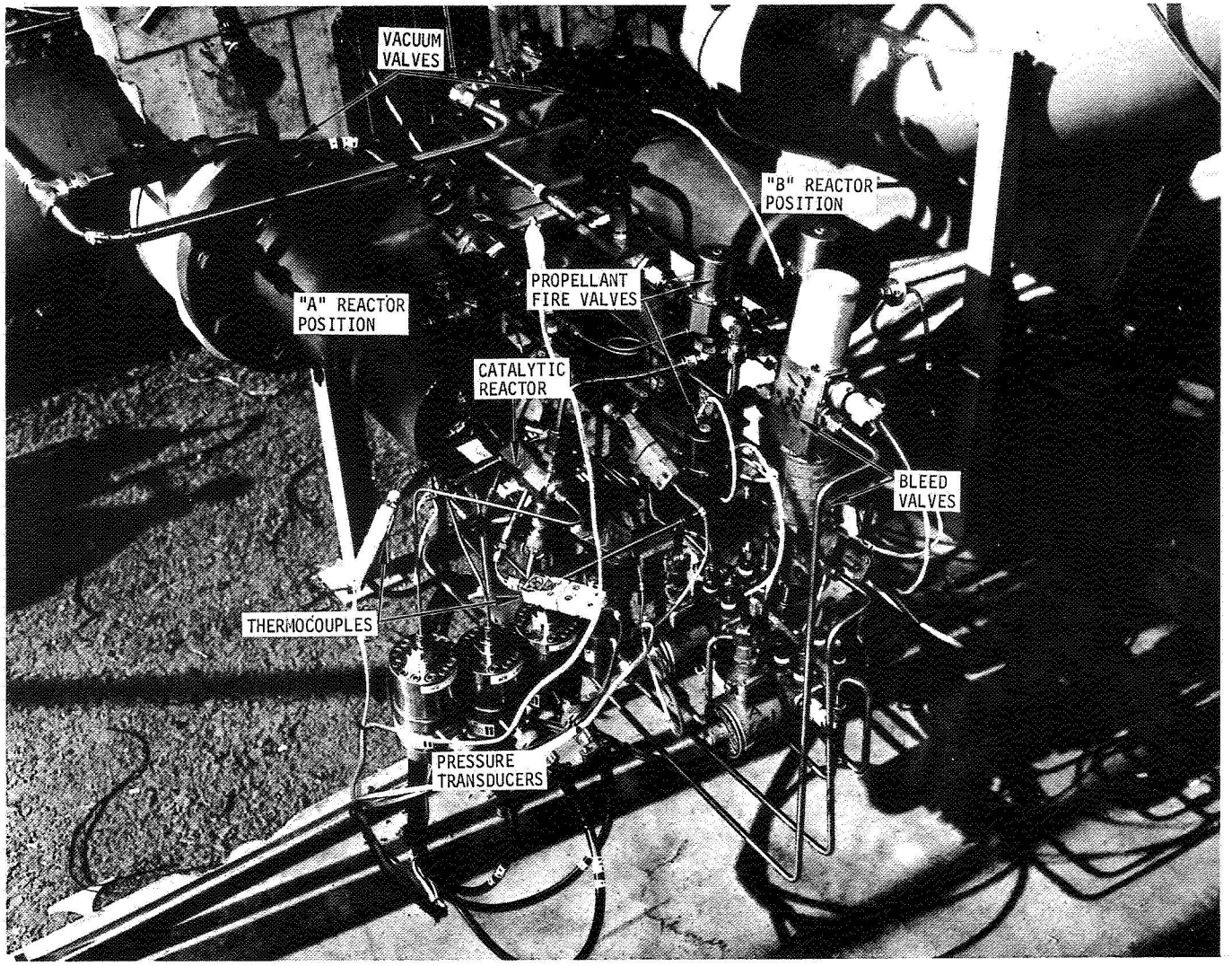

Figure 3. Catalyst Steady-State Reactor Test Installation

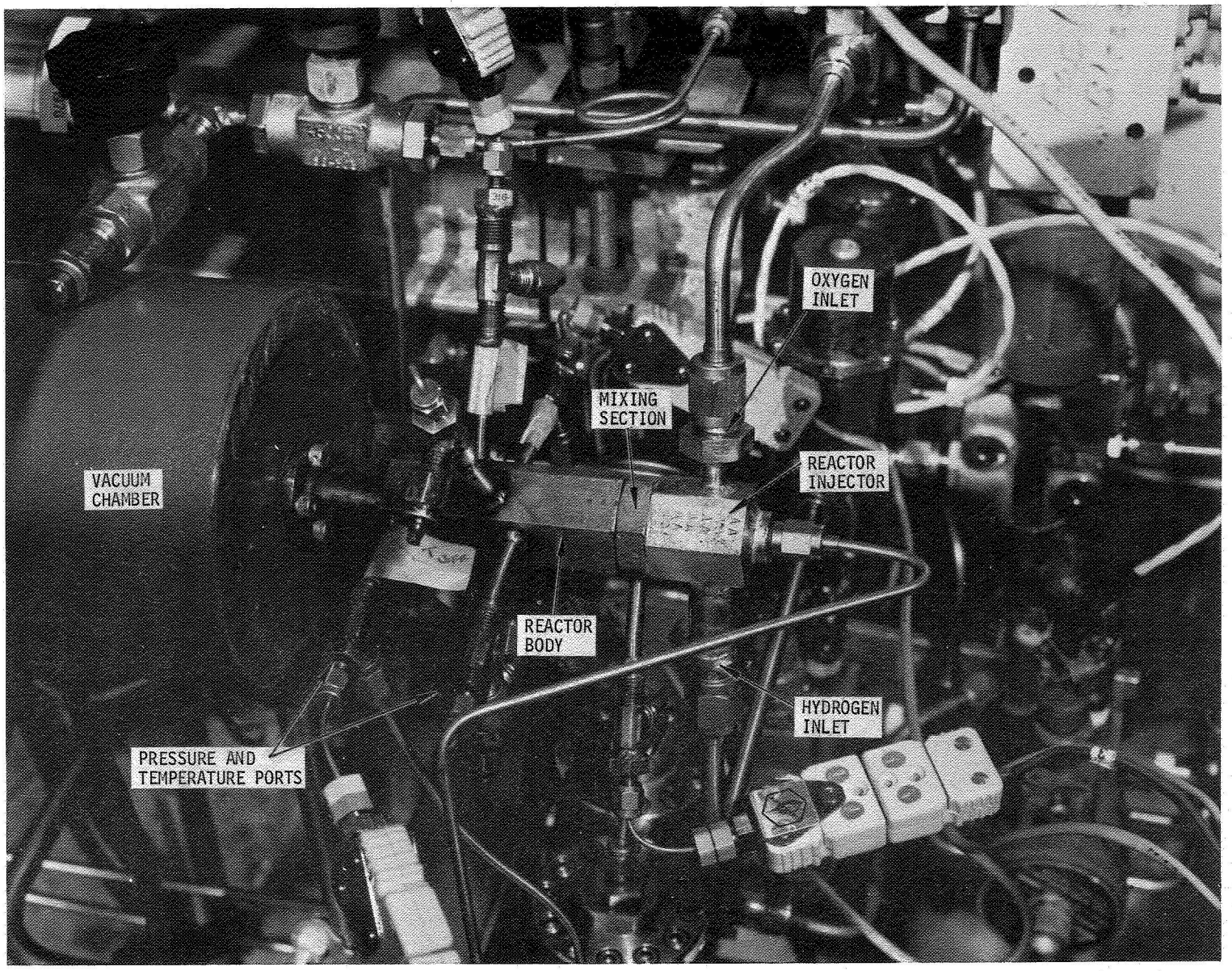

Figure 4. Closeup View of Steady-State Reactor Installation

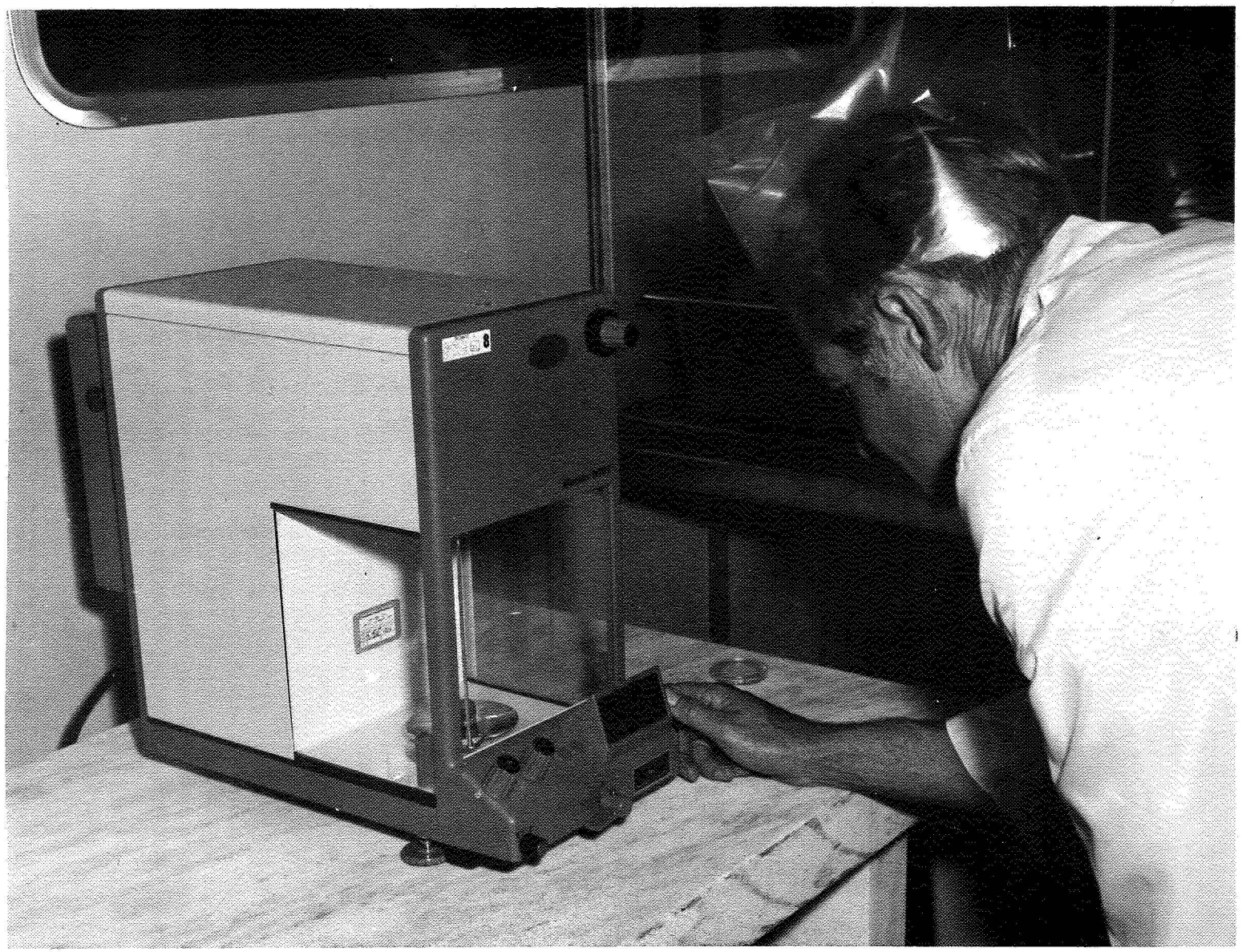

Figure 5. Weighing of Catalyst Bed Load for Life Tests

Table 1. Catalyst Steady-State Life Test Data
Shell 405-ABSG Catalyst - Run 014

Time	P_{CD}		$\dot{W}_T$		MR	T_{Bed-2}(1)		$T_{Effluent}$		η_C*(2)
sec	psia	kN/m^2	lb/sec	kg/sec	O/F	°F	°K	°F	°K	%
5	90.36	623.0	0.00393	0.00171	1.017	1,807	748.5	1,594	630.2	88.0
10	93.17	642.4	0.00393	0.00171	1.017	1,808	749.1	1,648	660.2	90.7
50	97.95	675.3	0.00393	0.00171	1.021	1,817	754.1	1,799	744.1	95.2
100	98.27	677.5	0.00393	0.00171	1.024	1,825	758.5	1,804	746.9	95.5
500	98.75	680.9	0.00394	0.00172	1.028	1,835	764.1	1,801	745.2	95.7
1,000	99.07	683.1	0.00395	0.00172	1.030	1,840	766.9	1,801	753.0	96.3
2,000	99.51	686.1	0.00395	0.00172	1.036	1,854	774.6	1,815	753.0	96.3
3,000	99.53	686.2	0.00394	0.00172	1.041	1,862	779.1	1,821	756.3	96.4
4,000	99.75	687.8	0.00394	0.00172	1.046	1,873	785.2	1,855	755.2	96.7

(1) Thermocouple located at center of catalyst bed

(2) Uncorrected combustion efficiency

Table 2. Catalyst Steady-State Life Test Data
Engelhard MSFA Catalyst - Run 018

Time	P_{CD}		$\dot{W}_T$		MR	T_{Bed-2}(1)		$T_{Effluent}$		η_C*(2)
sec	psia	kN/m^2	lb/sec	kg/sec	O/F	°F	°K	°F	°K	%
5	91.83	633.1	0.00395	0.00172	1.041	1,692	684.6	1,614	641.3	88.8
10	94.29	650.1	0.00396	0.00173	1.040	1,688	682.4	1,657	665.2	91.0
50	98.16	676.8	0.00396	0.00173	1.042	1,693	685.2	1,807	748.5	94.7
100	98.59	679.8	0.00396	0.00173	1.042	1,696	686.9	1,842	768.0	95.1
500	98.72	680.7	0.00395	0.00172	1.042	1,692	684.6	1,845	769.6	95.4
1,000	98.15	676.7	0.00394	0.00172	1.046	1,699	688.5	1,849	771.9	95.1
2,000	99.20	684.0	0.00394	0.00172	1.045	1,703	690.7	1,851	773.0	96.0
3,000	98.41	678.5	0.00394	0.00172	1.045	1,700	689.1	1,842	768.0	95.3
4,000	99.53	686.2	0.00393	0.00171	1.045	1,698	688.0	1,838	765.7	96.7

(1) Thermocouple located at center of catalyst bed

(2) Uncorrected combustion efficiency

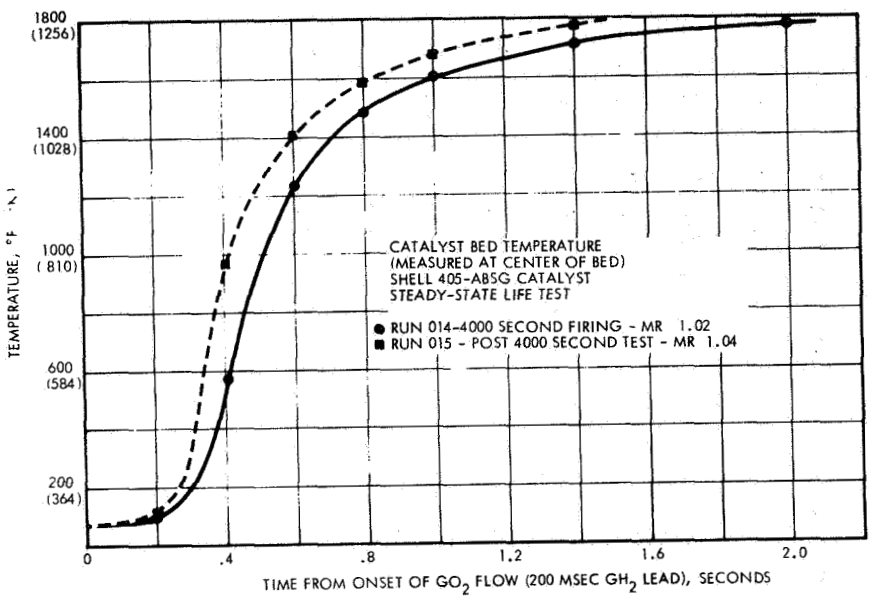

Figure 6. Catalyst Bed Response Data - Shell Catalyst Steady-State Life Tests

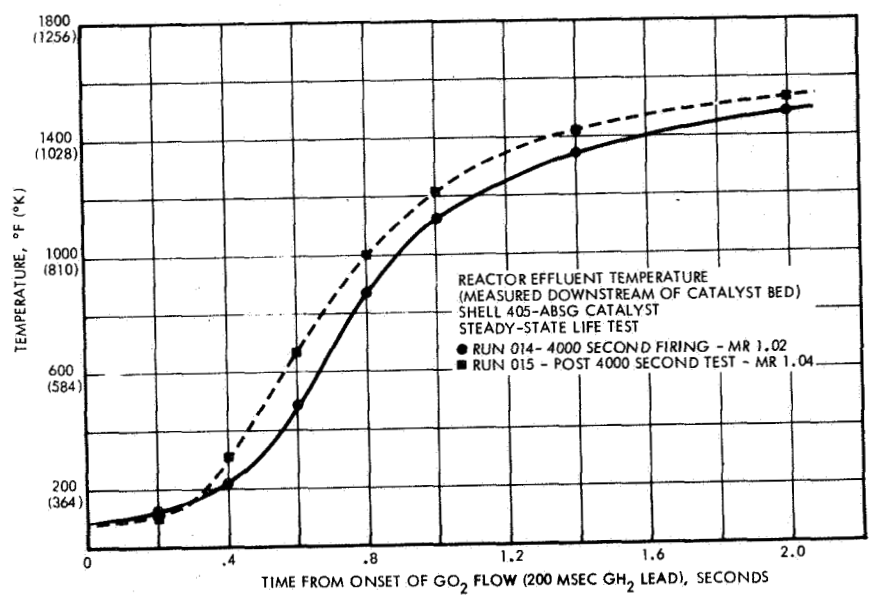

Figure 7. Reactor Effluent Response Data - Shell Catalyst Steady-State Life Tests

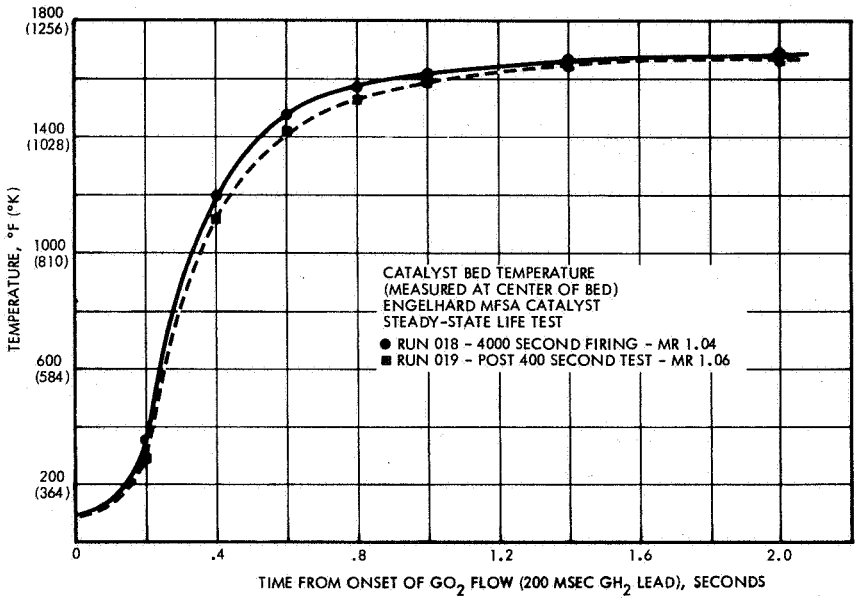

Figure 8. Catalyst Bed Response Data - Engelhard Catalyst Steady-State Life Tests

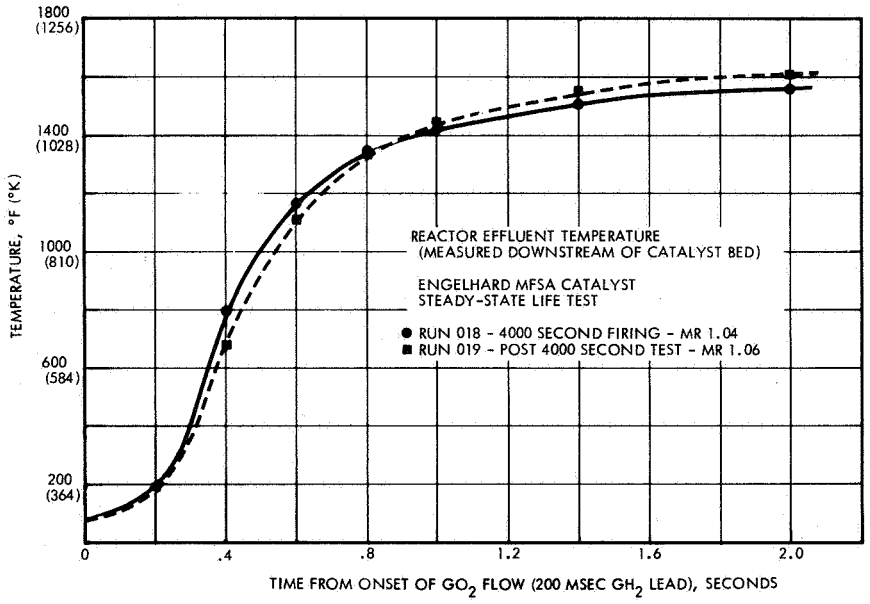

Figure 9. Reactor Effluent Response Data - Engelhard Catalyst Steady-State Life Tests

optimum bed response, and that these test results are not indicative of the minimum attainable catalyst bed thermal response times. Data from the Shell catalyst steady-state life tests in Figures 6 and 7 indicate that the long duration firing had no detrimental effect on the reactor thermal response with ambient temperature propellants. Temperatures and response rates were even slightly higher for the post-firing test 019, which was approximately 2% higher in mixture ratio than test 018.

The data plotted in Figures 8 and 9 for the Engelhard catalyst life tests also indicate that 4000 seconds of steady-state operation had no effect on the capability of the catalyst to initiate reaction with gaseous hydrogen-oxygen propellants.

Visual examination of each catalyst load after the long duration firing revealed no crumbling or erosion of the catalyst pellets. Figures 10 and 11 compare the appearance of "as received" Shell and Engelhard catalysts with typical catalyst pellets that had been fired in the 4000 second tests. No apparent differences can be seen between the fired and unfired catalyst samples of each type.

The weights of the catalyst beds before and after the 4000 second steady-state tests are listed in Table 3.

Table 3. Catalyst Bed Weights - Steady State Life Tests

	Shell 405-ABSG	Englehard MFSA
Catalyst weight loaded	3.6681 grams	1.7398 grams
Post-firing weight	3.5714 grams	1.6539 grams
Weight loss	0.0967 grams	0.0859 grams

The weight loss of less than 0.1 grams for each catalyst bed can partly be accounted for by loss of particles in loading and unloading the reactor, although care was employed to retain all fines. The catalyst bed dimensions were the same for both steady-state life tests, 0.430 inch (1.09 cm) diameter by 1.0 inch (2.54 cm) long, but the higher metal content and packing density of the Shell catalyst resulted in bed weights of about twice that of the Engelhard catalyst beds.

3.1.1.3 Laboratory Analysis of Fired Catalyst

After completion of the 4000-second steady-state life tests with the Shell 405-ABSG and Engelhard MFSA catalysts, each catalyst bed was subjected to a series of laboratory tests to determine the total and active surface area degradation. The total and active surface areas of both catalysts in their as received conditions were also determined to serve as a baseline to which the fired catalysts could be compared.

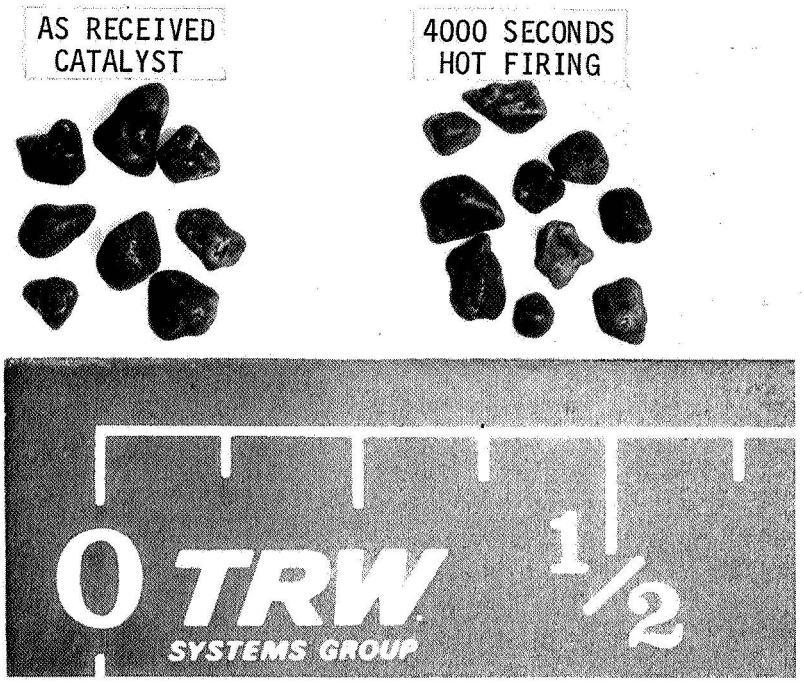

Figure 10. Shell 405-ABSG Catalyst After 4,000 Second Steady-State Life Test

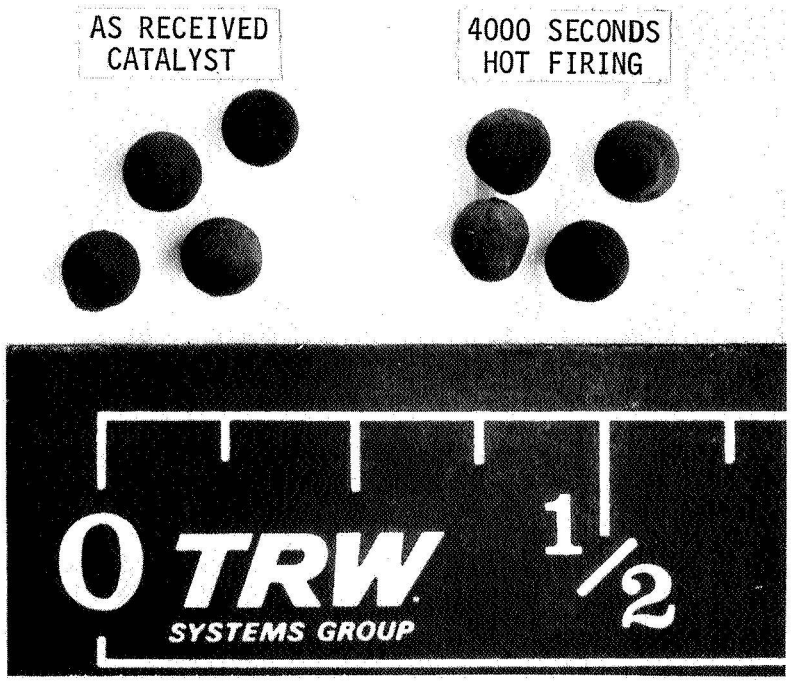

Figure 11. Engelhard MFSA Catalyst After 4,000 Second Steady-State Life Test

A constant volume gas adsorption apparatus was used to measure total surface areas by the physical adsorption technique of Brunauer, Emmett, and Teller (BET theory) (Reference 2). Figure 12 is a schematic diagram of the system. The system was constructed of glass and consisted of a manifold, gas bulbs, sample bulb, pressure measuring devices, and a high vacuum pumping system. A one liter bulb of high purity krypton gas at 1 atmosphere pressure was sealed onto the manifold. This bulb served as the krypton supply for all of the surface area determinations. By opening or closing the stopcocks connecting the gas bulbs to the manifold, the total dead space of the system could be varied by as much as a factor of 5. In this way, the total number of molecules adsorbed on a sample per unit drop in the pressure could be varied by as much as a factor of 5.

A typical surface area measurement on a catalyst sample was conducted in the following fashion: The sample tube containing a catalyst sample which had been pretreated [16 hours at 300°C (575°K) under high vacuum] was immersed in a Dewar flask filled with liquid nitrogen. To insure the achievement of steady-state temperature, about one hour was allowed to elapse before proceeding with the surface area determination. To start the adsorption measurements, the system was isolated from the main vacuum line by closing the stopcock connecting the vacuum line to the manifold and sample bulb. The stopcock connecting the manifold and sample tube was also closed. The amount of dead space of the system was adjusted by opening or closing the stopcocks connecting the gas bulbs to the manifold. Krypton gas was then bled into the manifold and connected gas bulbs from the krypton storage bulb. The pressure for the first adsorption point was allowed to build up to about 0.1 mm and then the krypton storage bulb was sealed from the system by closing the connecting stopcock. From the known volume of the manifold and connecting gas bulbs and the pressure indicated on the Pirani gauge, the number of moles of krypton initially in the gas phase could be calculated. The stopcock connecting the sample tube and the manifold was then opened and the krypton gas introduced into the sample tube. As the krypton adsorbed on the sample, the pressure decreased. The initial rate of adsorption is usually very fast, but the last 5% of the gas adsorption requires between 15 and 30 minutes. When there was no further change in pressure, the system was at equilibrium and the final pressure was recorded. From the known dead space of the manifold, sample tube,and gas bulbs, the number of moles of krypton remaining in the gas phase could be calculated. The difference between the original and final number of moles of krypton in the gas phase was the number of moles of krypton adsorbed on the sample at liquid nitrogen temperature (-195°C or 78°K) and the final equilibrium pressure. The amount of gas adsorbed at the final equilibrium pressure, thus, represented one point on the adsorption isotherm. The stopcock connecting the sample tube to the manifold was then closed, fresh krypton was admitted to the manifold and the process repeated. A new, higher, equilibrium pressure was then obtained with a corresponding larger quantity of gas adsorbed. This process was repeated up to an equilibrium pressure of about 0.3 torr (mm Hg). With the experimental determination of the krypton adsorption isotherm, it was then possible to calculate the surface area of the catalyst sample utilizing the BET method.

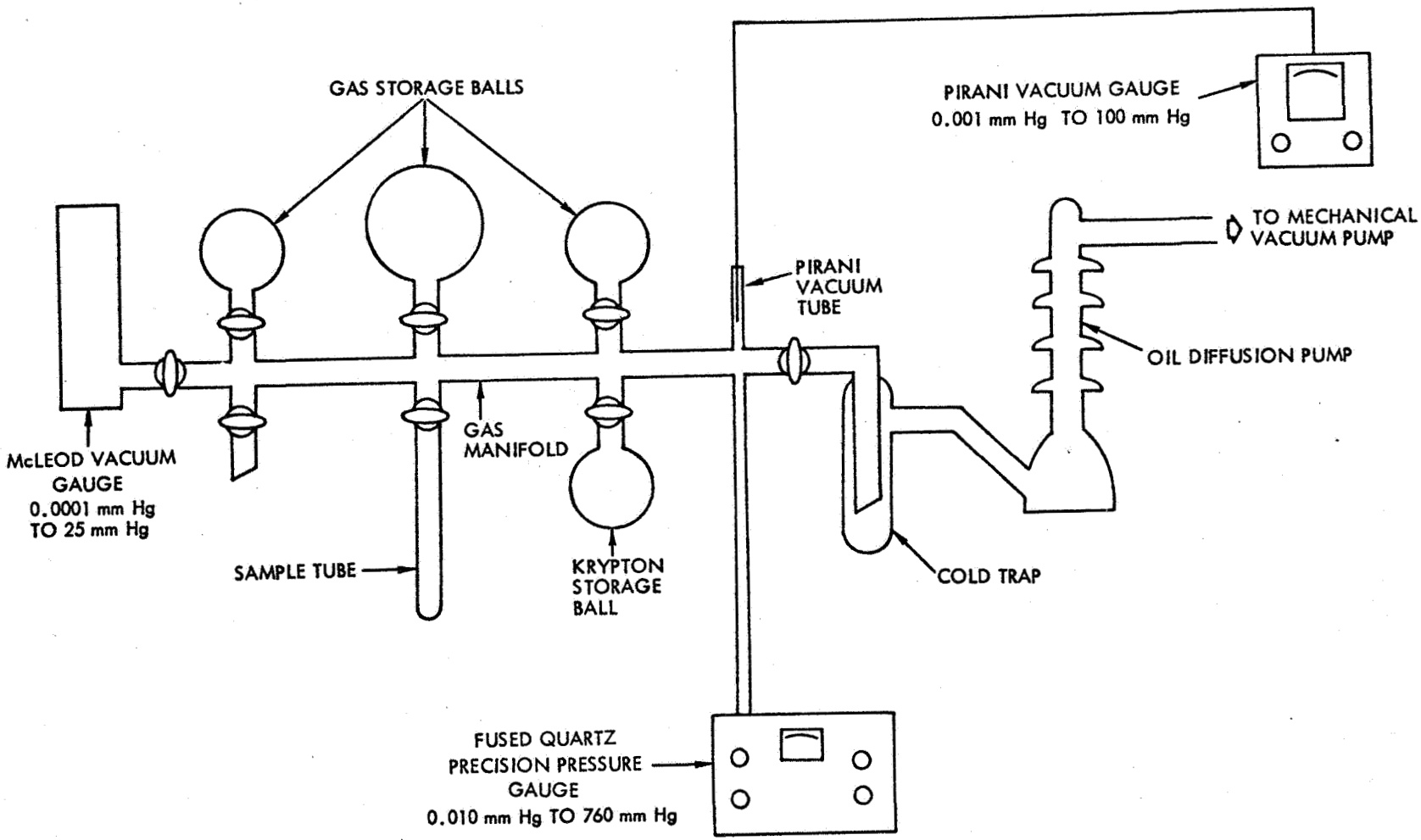

Figure 12. Schematic Diagram of the Surface Area Determination Apparatus

Table 4 shows the results of the total surface area measurements on both the Shell 405 and Engelhard MFSA catalysts. The results show that the Shell 405 catalyst lost a greater portion of its total surface area (64.4%) than the Engelhard MFSA catalyst (48.5%).

Table 4. Total Surface Areas of Shell 405 and Engelhard MFSA Catalysts

	Total Surface Area (Sq meters/gram)	
Catalyst	As Received	Post 4000 Second Ignition
Shell 405	112 (Run SA-1)	40 (Run SA-2)
Englehard MFSA	180 (Run SA-3)	93 (Run SA-4)

Note: Replicate experiments were run with the as-received Englehard MFSA catalyst and reproducibility was found to be $\pm$ 2 sq. meters/gram.

It has been found (NASA Contract NAS 7-520, Reference 3) that the determination of adsorption isotherms of hydrogen on catalysts provide a very sensitive measure of the amount of active surface metal available to catalyze chemical reactions. Hence, chemisorption measurements provided a simple and rapid method of determining what effect a 4000-second steady-state firing in a hydrogen-oxygen igniter had on the active catalyst surface.

The chemisorption apparatus is an all-glass, constant volume, adsorption system. It consists of a manifold and gas sample bulb, catalyst sample tube thermally isolated from the manifold, gas analysis sampling outlet, high vacuum pumping system, sample furnace, temperature measurement and control systems, and a very precise pressure measuring system. Figure 13 shows a schematic diagram of the apparatus. The amount of gas adsorbed on a sample of catalyst is determined by measuring the pressure drop in the calibrated constant volume system.

To make an equilibrium adsorption isotherm measurement a known weight of catalyst was pretreated and then was allowed to thermally equilibrate at the predetermined isotherm temperature of 200°C (473°K). A quantity of gas was initially bled into the evacuated manifold from the gas storage bulb. The number of molecules initially in the gas phase was calculated from the known volume of the manifold and the measured manifold pressure. A stopcock connecting the evactuated sample tube to the gas manifold was then opened and the gas introduced into the sample tube. As the gas species (e.g., hydrogen) adsorbed on the catalyst sample, the pressure decreased. When there was no appreciable further change in pressure, the system was assumed to be at equilibrium and the final gas phase pressure was recorded. The number of molecules of gas remaining in the gas phase was calculated from the known dead space of the manifold and sample tube. The difference

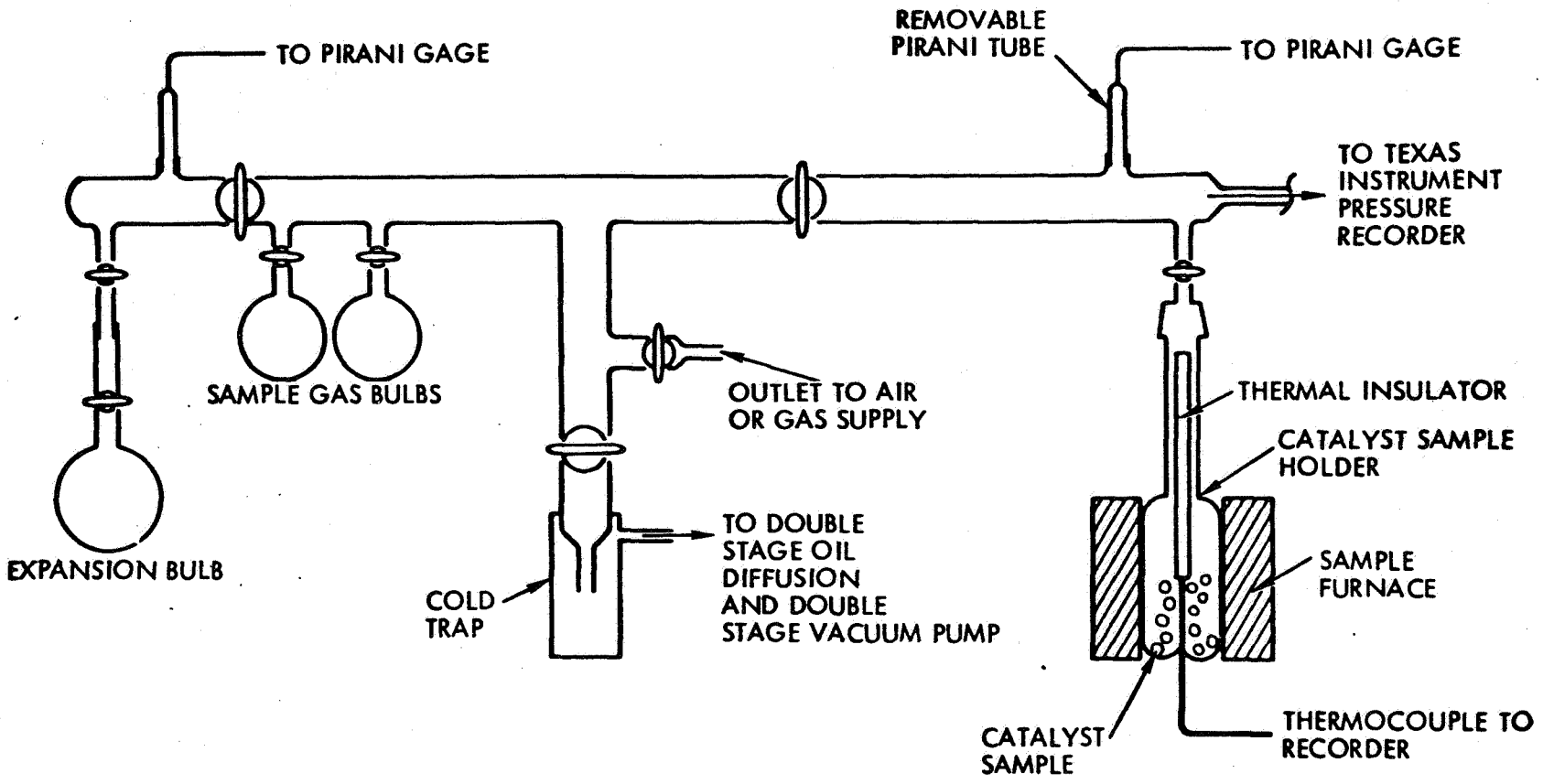

Figure 13. Schematic Diagram of the All Glass Constant Volume Adsorption System

between the original and the final number of molecules in the gas phase was the number of molecules adsorbed on the sample at the isotherm temperature and the final equilibrium pressure. The amount of gas adsorbed at the final equilibrium pressure thus represents one point on the adsorption isotherm. The stopcock connecting the sample tube to the gas manifold was then closed, fresh gas admitted to the manifold, and the process repeated. A new higher equilibrium pressure was obtained with a corresponding larger quantity of gas adsorbed. This process was repeated up to an equilibrium pressure of 220 torr (mm Hg).

Table 5 is a summary of the hydrogen chemisorption data for both the Shell 405 and Engelhard MFSA catalysts. The data indicated a reduction in hydrogen adsorption at an equilibrium pressure of 200 torr (mm Hg) and a temperature of 200°C (473°K) of 69.1% for the Shell 405 and 34.5% for the Engelhard MFSA catalysts. Since the amount of hydrogen chemisorption was proportional to the amount of active surface area (active surface metal) available to promote the reaction, a like amount of reduction in active surface metal occurred. The results are plotted in Figures 14 and 15.

Table 5. Summary of Hydrogen Chemisorption Isotherm Experiments

Catalyst	Sample History (All samples were pretreated)*	Equilibrium Hydrogen Adsorption at 473°K and 200 Torr (mm Hg) Hydrogen Atoms x 10^{-18}
Shell 405	As received	415 ± 5** (Runs HA-1, HA-2)
Shell 405	Post 4000 sec run	128 ± 8 (Runs HA-5, HA-6)
Englehard MFSA	As received	22.3 ± 3.0 (Runs HA-3, HA-4)
Englehard MFSA	Post 4000 sec run	14.6 ± 1.5 (Runs HA-7, HA-8)

*The standard pretreatment to remove very strongly adsorbed oxygen (from air exposure of the catalyst) consists of 16 hours evacuation at 473°K followed by exposure to 200 torr hydrogen at 773°K for 7 hours followed by 16 hours evacuation at 873°K in 10^{-6} torr vacuum.

**Duplicate experiments were run for each of these cases and the listed uncertainty represents the span between the experiments.

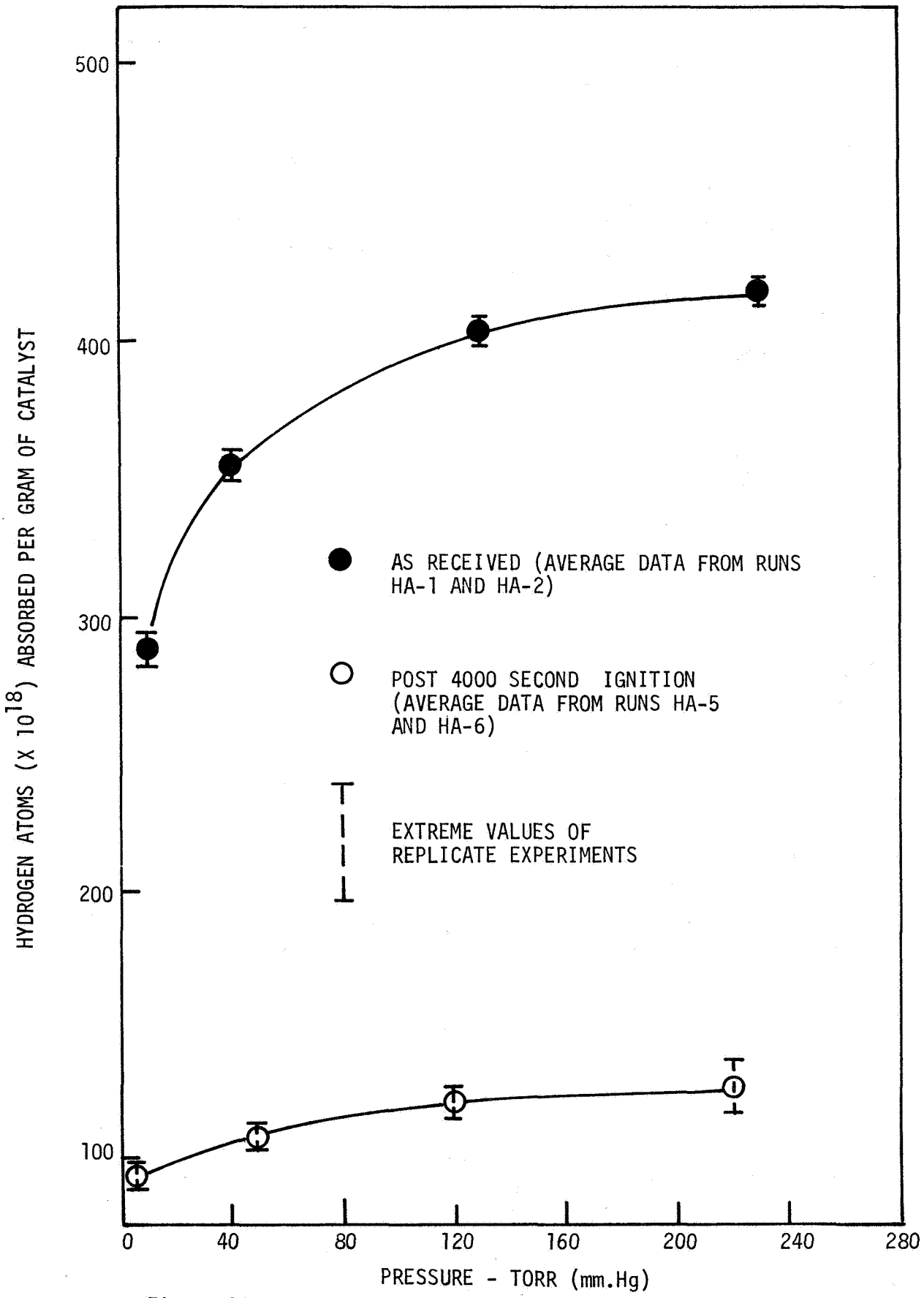

Figure 14. Hydrogen Adsorption Isotherms on Shell 405 Catalyst at 200°C (473°K)

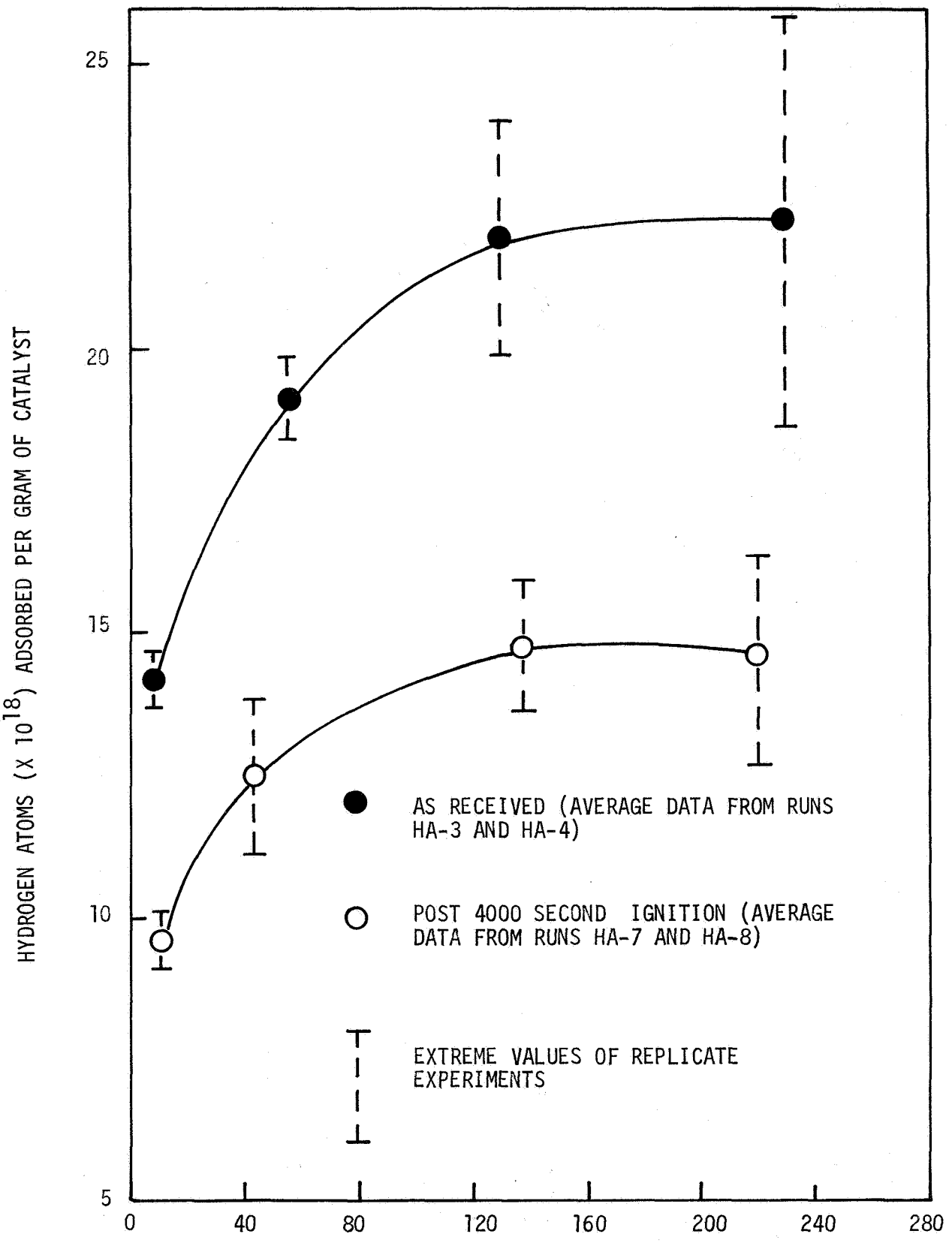

Figure 15. Hydrogen Adsorption Isotherms on Engelhard MFSA Catalyst at 200°C (473°K)

3.1.1.4 Conclusions From Experimental Results

Based on the test firing performance of the catalyst beds and the post-firing laboratory analysis of the catalysts, the conclusions resulting from the steady-state life tests were:

- Both the Shell 405-ABSG and the Engelhard MFSA catalysts effectively promote the reaction of gaseous hydrogen and oxygen for steady-state run durations of at least 4000 seconds. Test results indicate that single test firings of even longer durations are attainable without loss of reactor performance at ambient bed and propellant temperatures, even though laboratory tests indicated some loss of catalyst activity occurred.

- Thermal response of the Shell and Engelhard catalyst beds with ambient temperature propellants was not affected by the 4000-second duration firings.

- Physical appearance of either catalyst was not notably affected by the 4000-second firing. No shattering or erosion of the catalyst pellets were observed, and measured weight loss of each catalyst bed was less than five percent.

3.1.2 Cyclic Life Tests

A series of igniter pulse mode tests was performed to determine the cyclic operational life of the Shell 405-ABSG and Engelhard MFSA catalysts. Cyclic life tests of 5000 pulses were completed with each catalyst at ambient temperature propellant conditions. Low temperature cyclic tests of 150, 700, and 1000 pulses each were conducted with the Shell 405-ABSG catalyst at propellant temperatures of -250°F (117°K). The following paragraphs describe the cyclic reactor hardware and test conditions, and discuss the experimental results.

3.1.2.1 Ambient Temperature Propellant Cyclic Tests

Modifications to the basic reactor hardware were performed to incorporate a cooling manifold around the catalyst bed for the pulse-mode tests. The reactor assembly is shown in Figure 16. Details of the modified reactor are presented in Figure 17. This hardware differs from the reactor used for the steady-state life tests only in the added cooling jacket and the method of retaining the catalyst. For the cyclic tests, the catalyst bed cartridge was eliminated and a spring added to maintain an axial compressive load on the catalyst bed to preclude channeling in the bed due to possible migration of pellets during pulse operation. A second, identical reactor assembly was also fabricated to allow simultaneous cyclic testing of the Shell and Englehard catalysts. A schematic of the igniter stand installation for the catalyst life tests is presented in Figure 18. Dual igniter mounting ports were provided to enable pulse-mode tests to be conducted simultaneously with two different catalyst formulations. Stand installation of the cooled reactor for pulse-mode catalyst life tests is shown in Figure 19.

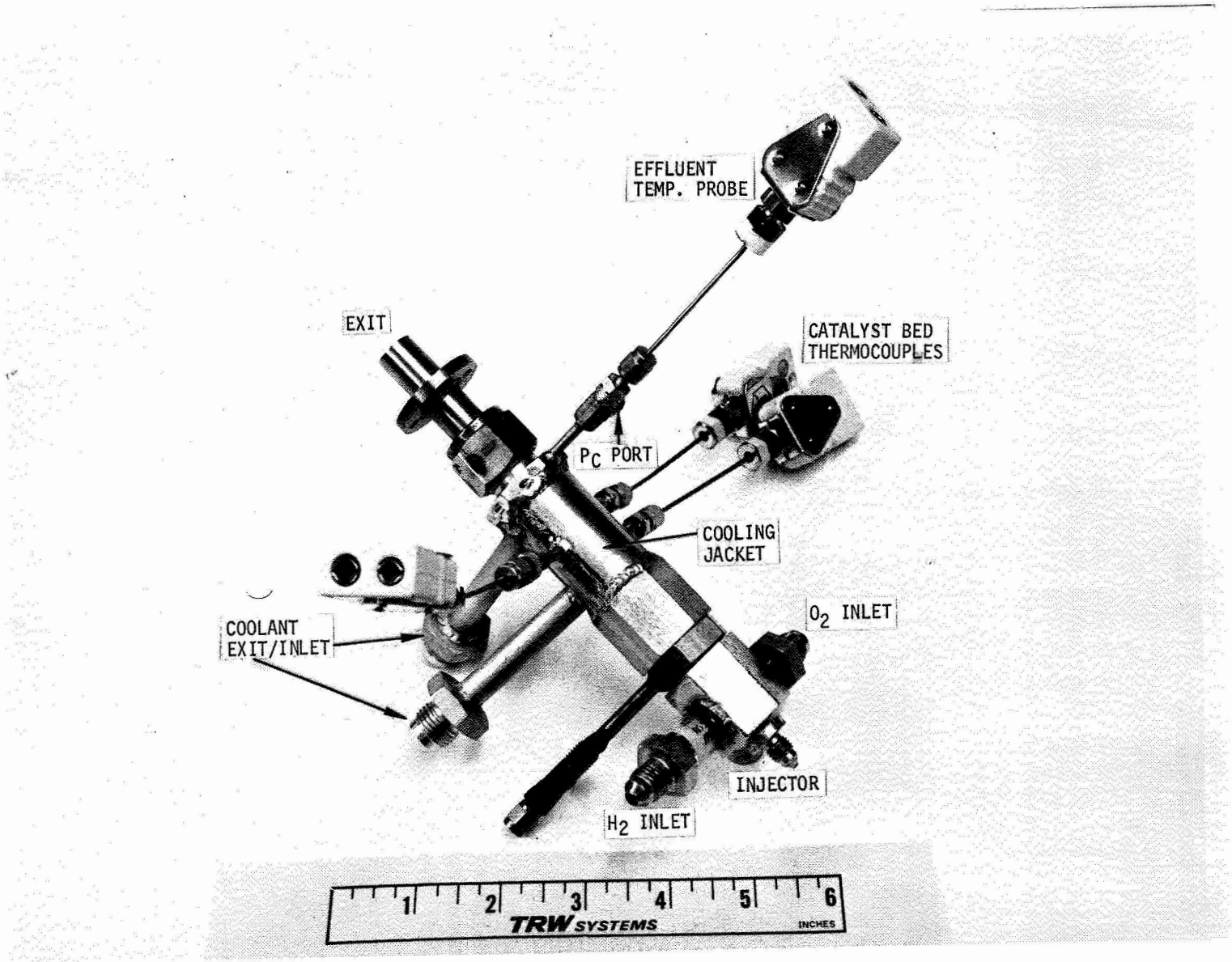

Figure 16. Catalytic Reactor Assembly with Cooling Jacket Modification

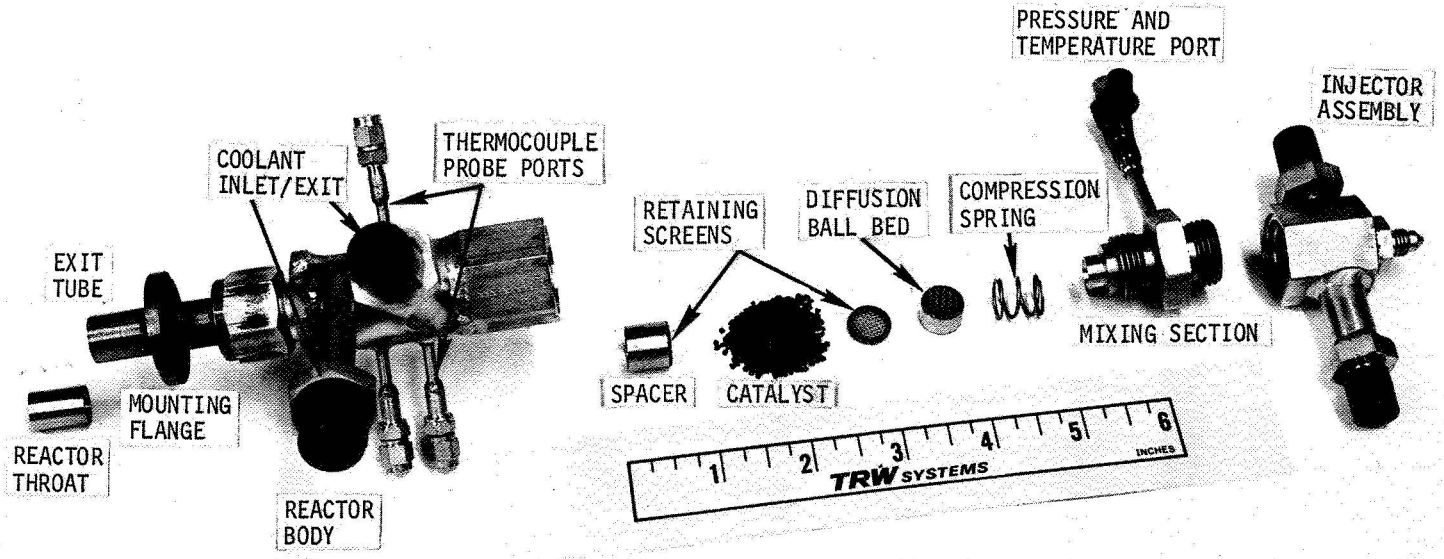

Figure 17. Disassembled Cooled Reactor Assembly

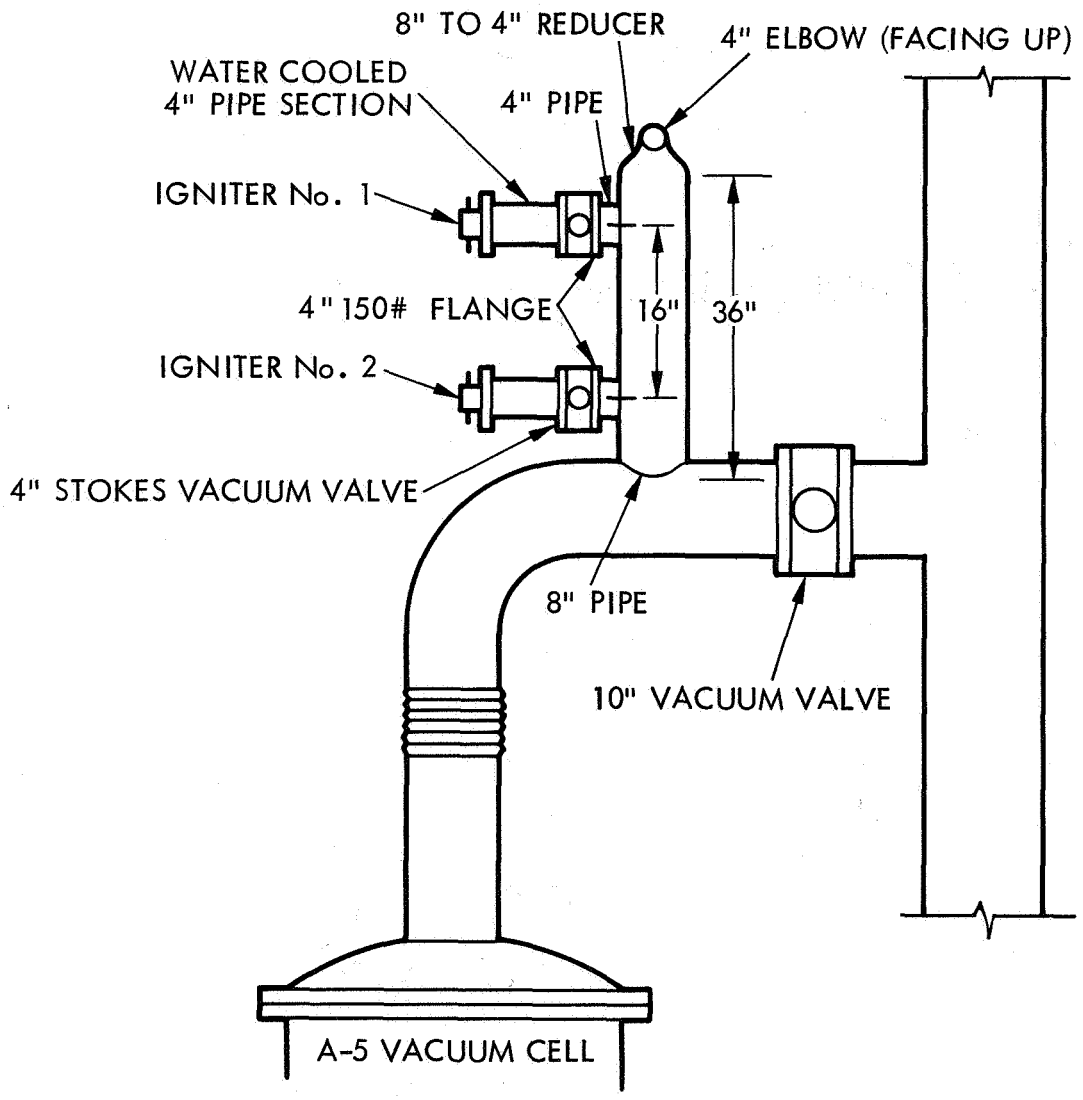

Figure 18. HEPTS Position A-5 Installation for H_2-O_2 Igniter Life Tests

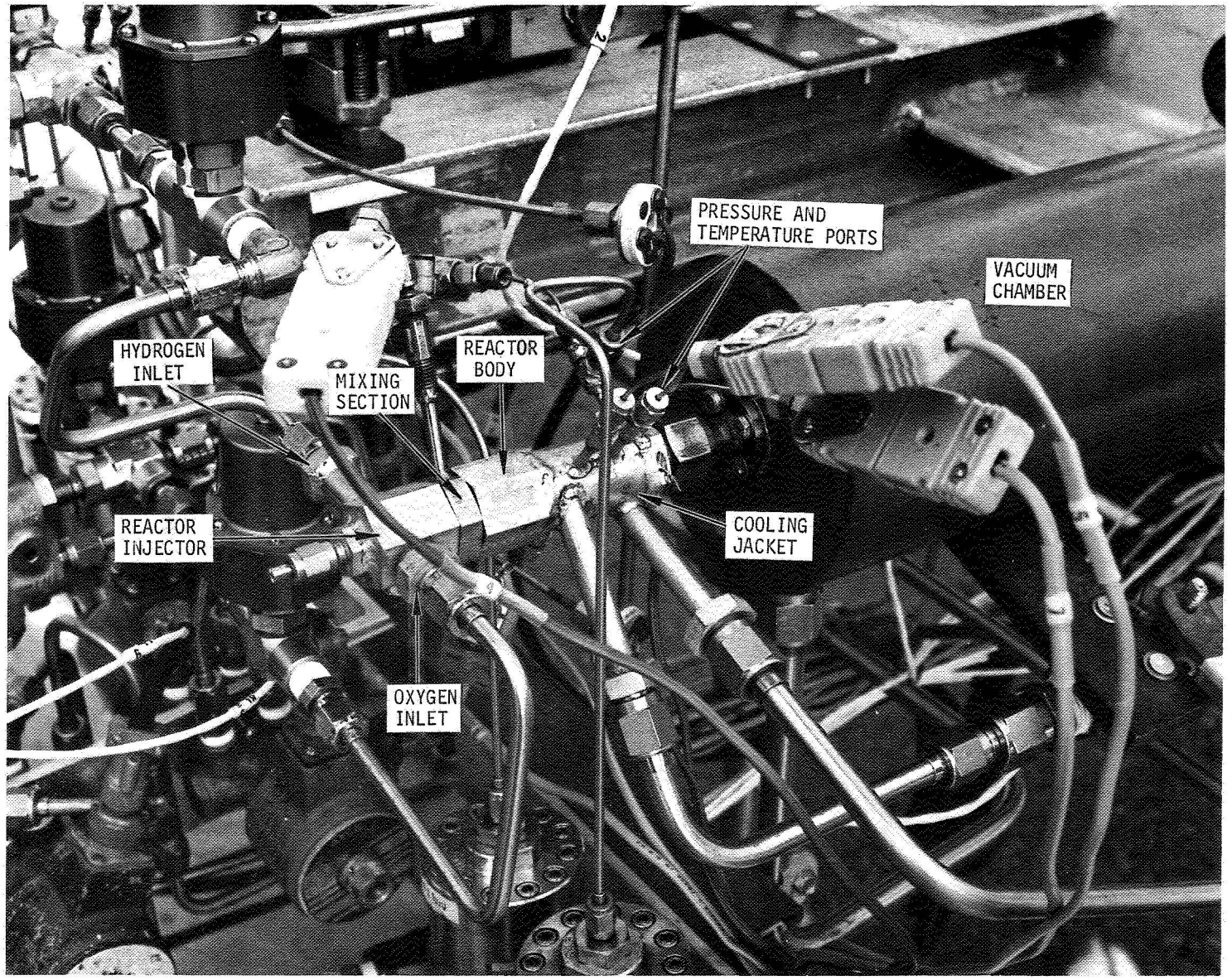

Figure 19. Closeup View of Pulse-Mode Reactor Installation

Electronic control equipment for conducting the cyclic tests was designed and fabricated. The reactor firing test console and pulse sequence timer are shown in Figure 20. The digital dials on the timer could be set to vary any valve start or shutdown by 1 millisecond increments. The timer started each pulse when the catalyst bed had cooled to the preselected temperature, fired the reactors for the required duration, and also controlled startup and shutdown of the oscillograph and tape data acquisition systems.

The ambient temperature propellant cyclic life evaluations were performed at nominal test conditions of 100 psia (690 kN/m^2) chamber pressure and 1800°F (1256°K) catalyst bed temperatures, with cooldown of the catalyst bed to 1000°F (810°K) or below between pulses. Data from these tests are listed in Tables 6 and 7 for the Shell and Engelhard catalysts, respectively.

Results of the cyclic life tests are presented in Figures 21 through 24, which compare the catalyst bed and reactor effluent temperature response before and after 5000 pulses (15,000 seconds total firing time) with each catalyst type. It should again be noted that the life test reactor hardware and catalyst bed configurations were not designed for optimum bed response, and that these test results are not indicative of the minimum attainable catalyst bed thermal response times.

Data from the Shell catalyst cyclic life tests in Figures 21 and 22 and from the Engelhard catalyst tests in Figures 23 and 24 indicate that some degradation of catalyst bed response and reduction in reactor effluent temperatures occurred after 5000 cycles of operation. However, in each case, the catalysts were still able to support the reaction of ambient temperature hydrogen-oxygen.

Visual examination of each catalyst load after the cyclic life tests revealed some erosion of the catalyst pellets. Figures 25 and 26 compare "as received" Shell and Engelhard catalysts with typical pellets from the 5000 pulse cycle tests. Some sintering together of the Shell catalyst is indicated in Figure 25, although most of the catalyst bed remained as individual pellets. Figure 26 reveals that slight erosion and cracking of the Engelhard catalyst pellets occurred during the 5000 pulse firings. Weight loss of each catalyst bed was about seven percent, as indicated in Table 8.

After completion of the cyclic life tests, each catalyst bed was subjected to a series of laboratory tests to determine both the total and active surface area degradation. The laboratory apparatus and experimental procedures employed in the surface area measurements were previously described in detail in Section 3.1.1.3 of this report. The results of the total surface area measurements utilizing the BET method (Reference 2) are listed in Table 9. A loss of nearly 90% of the surface area of the Shell catalyst occurred, while the Engelhard catalyst retained about 50% of its original surface areas, as shown in Table 9.

Figure 20. Reactor Firing Test Console and Pulse Sequence Timer

Table 6. Catalyst Cyclic Life Test Data - 5000 Pulses
Shell 405-ABSG Catalyst - Ambient Propellants

Pulse[1] No.	P_{CD} psia	P_{CD} kN/m^2	$\dot{W}_T$ lb/sec	$\dot{W}_T$ kg/sec	MR O/F	T_{Bed-2}[2] °F	T_{Bed-2} °K	$T_{Effluent}$ °F	$T_{Effluent}$ °K	η_{C^*}[3] %
1	98.22	677.2	0.00427	0.00194	0.979	1867	1293	1568	1126	88.3
5	99.05	682.9	0.00427	0.00194	0.979	1870	1294	1593	1140	89.1
400	98.43	678.7	0.00423	0.00192	0.951	1738	1221	1498	1088	89.6
800	95.87	661.0	0.00413	0.00188	1.000	1820	1266	1514	1096	88.9
1200	98.15	676.7	0.00422	0.00191	0.990	1847	1281	1497	1087	89.3
1600	98.74	680.8	0.00426	0.00193	0.965	1798	1254	1476	1075	89.1
2000	95.61	659.2	0.00412	0.00187	1.010	1876	1297	1511	1095	88.8
2400	95.12	655.8	0.00412	0.00187	0.985	1800	1255	1526	1103	88.5
2600	98.10	676.4	0.00421	0.00191	0.983	1852	1284	1455	1064	89.4
3200	95.51	658.5	0.00413	0.00188	0.982	1841	1278	1504	1091	88.7
3600	98.61	679.9	0.00414	0.00190	0.973	1749	1227	1601	1145	90.5
4000	96.73	666.9	0.00422	0.00191	0.968	1886	1303	1573	1129	88.1
4400	93.84	647.0	0.00411	0.00187	0.967	1880	1300	1454	1063	87.8
4800	91.76	632.7	0.00406	0.00184	1.000	1904	1313	1365	1014	86.7
5000	95.84	660.8	0.00426	0.00193	0.972	1864	1291	1383	1024	86.4

(1) Data taken at end of 3-second duration pulse

(2) Thermocouple located at center of catalyst bed

(3) Uncorrected combustion efficiency

Table 7. Catalyst Cyclic Life Test Data - 5000 Pulses
Engelhard MFSA Catalyst - Ambient Propellants

Pulse[1] No.	P_{CD} psia	P_{CD} kN/m^2	$\dot{W}_T$ lb/sec	$\dot{W}_T$ kg/sec	MR O/F	T_{Bed-2}[2] °F	T_{Bed-2} °K	$T_{Effluent}$ °F	$T_{Effluent}$ °K	η_{C^*}[3] %
1	92.14	635.3	0.00427	0.00194	0.977	1707	1204	1758	1232	87.5
5	93.98	648.0	0.00427	0.00194	0.978	1727	1215	1795	1253	89.2
400	92.20	635.7	0.00423	0.00192	0.950	1174	1785	1247	1247	88.7
800	92.87	640.3	0.00413	0.00188	1.000	1665	1180	1821	1267	90.8
1200	94.50	651.6	0.00422	0.00191	0.990	1676	1186	1892	1306	90.7
1600	93.80	646.7	0.00426	0.00193	0.965	1645	1169	1829	1271	89.4
2000	93.21	642.7	0.00412	0.00187	1.010	1749	1227	1881	1300	91.3
2400	91.09	628.0	0.00412	0.00187	0.985	1683	1190	1813	1263	89.4
2600	94.40	650.9	0.00422	0.00191	0.983	1690	1194	1835	1275	90.7
3200	92.62	638.6	0.00413	0.00188	0.982	1684	1191	1879	1299	90.7
3600	92.95	640.9	0.00419	0.00190	0.973	1660	1178	1862	1290	90.5
4000	93.43	644.2	0.00422	0.00191	0.968	1599	1144	1833	1274	89.8
4400	90.98	627.3	0.00411	0.00198	0.967	1628	1160	1833	1274	89.9
4800	91.75	632.6	0.00406	0.00184	1.000	1654	1174	1892	1306	91.5
5000	92.58	638.3	0.00426	0.00193	0.972	1571	1128	1720	1211	88.1

(1) Data taken at end of 3-second duration pulse

(2) Thermocouple located at center of catalyst bed

(3) Uncorrected combustion efficiency

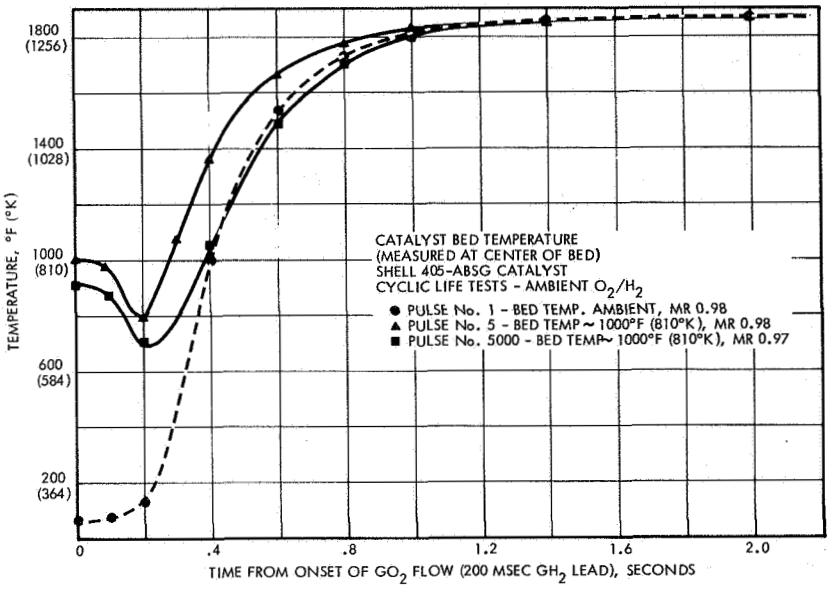

Figure 21. Catalyst Bed Response Data - Shell Catalyst Cyclic Life Tests, Ambient Temperature

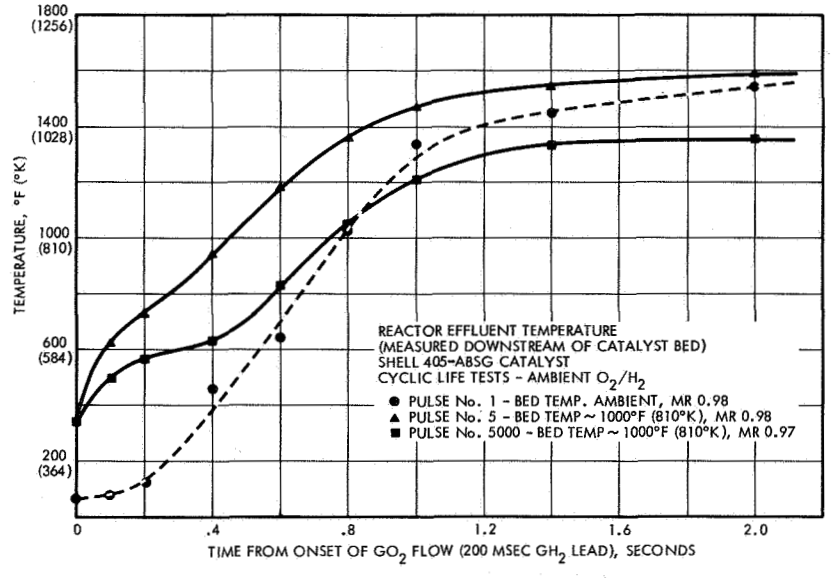

Figure 22. Reactor Effluent Response Data - Shell Catalyst Cyclic Life Tests, Ambient Temperature

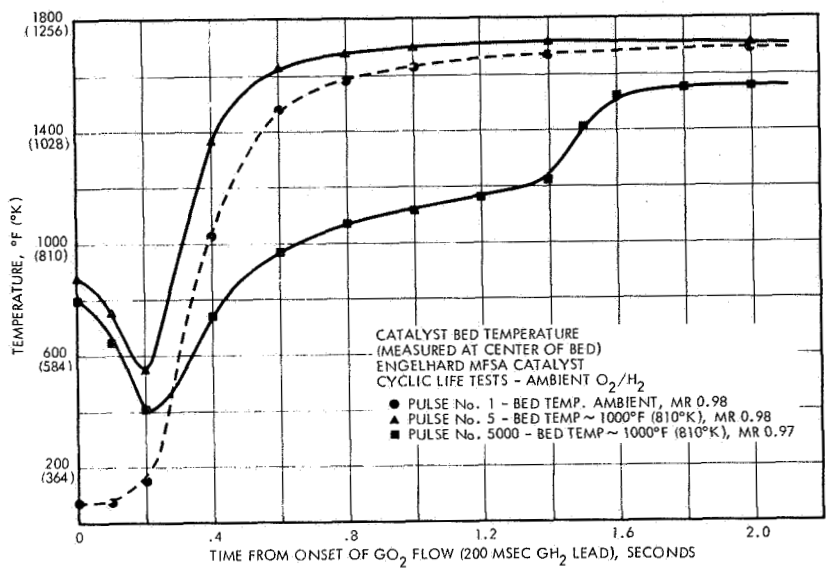

Figure 23. Catalyst Bed Response Data - Engelhard Catalyst Cyclic Life Tests, Ambient Temperature

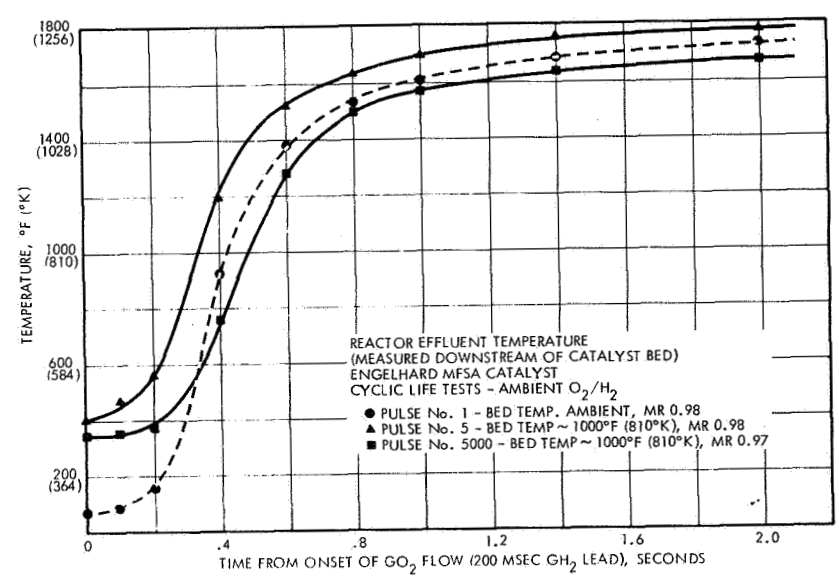

Figure 24. Reactor Effluent Response Data - Engelhard Catalyst Cyclic Life Tests, Ambient Temperature

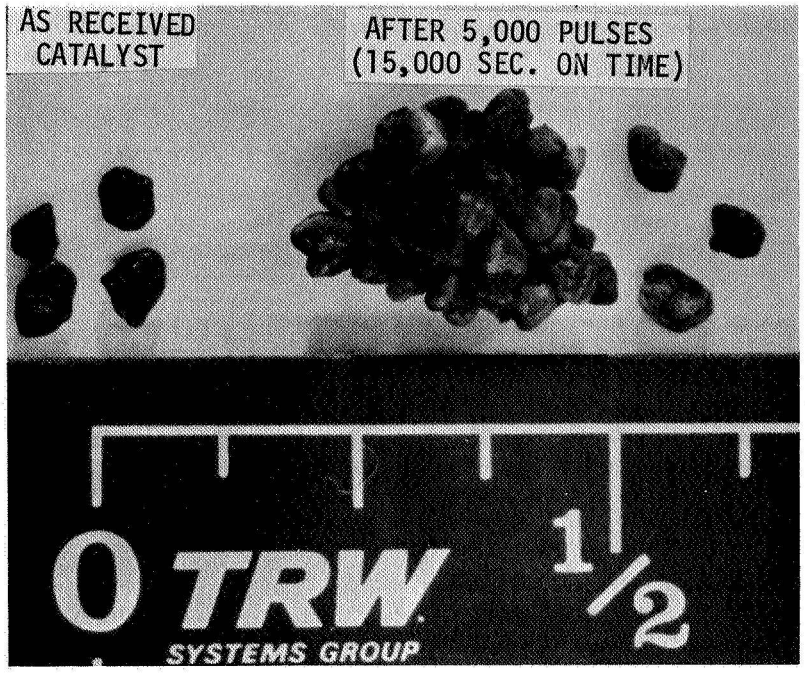

Figure 25. Shell 405-ABSG Catalyst After 5000 Pulse Cyclic Life Test

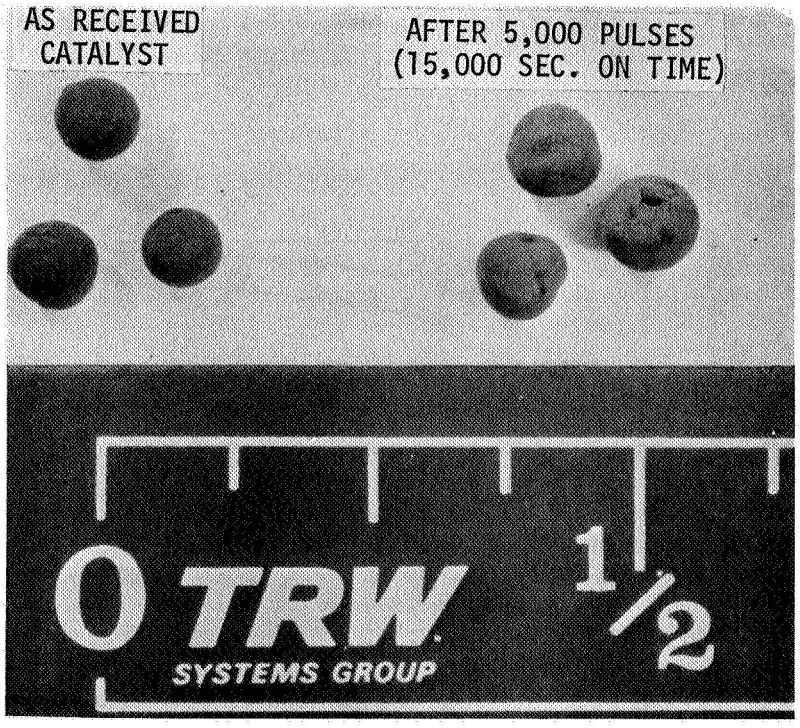

Figure 26. Engelhard MFSA Catalyst After 5000 Pulse Cyclic Life Tests

Table 8. Catalyst Bed Weights-Cyclic Life Tests
(5000 Pulses-15,000 Seconds Total Firing Time)

	Shell 405-ABSG	Engelhard MFSA
Catalyst weight loaded	4.9943 grams	2.3397 grams
Post-firing weight	4.6565 grams	2.1805 grams
Weight loss	0.3478 grams	0.1592 grams

Table 9. Total Surface Areas of Shell 405
and Engelhard MFSA Catalysts

	Total Surface Area - Square Meters/Gram	
Catalyst	As Received	Post 5000 Pulses
Shell 405	112 (Run SA-1)	15 + 1.5 (Runs $\overline{SA}$-5, SA-6)
Engelhard MFSA	180 (Run SA-3)	85 + 7.0 (Runs $\overline{SA}$-7, SA-8)

The loss of active surface area (active surface metal) of each catalyst as determined by hydrogen chemisorption is shown in Table 10. This table also includes the results of the 4000 second steady-state tests for comparison .

The data indicates that severe loss of active surface area of the Shell catalyst occurred during the cyclic life tests. The hydrogen chemisorption data for each catalyst are also shown graphically in Figure 27.

The results of the cyclic life tests with ambient temperature hydrogen-oxygen verified that at least 5000 pulses could be achieved with both the Shell 405-ABSG and Engelhard MFSA catalysts, even though major loss of active surface occurred.

3.1.2.2 Low Temperature Propellant Cyclic Tests

Cyclic tests were conducted with the Shell 405-ABSG catalyst at propellant and initial bed temperatures of -250°F (117°K). The objective of this test series was to complete 5000 pulses of the reactor, during which the catalyst would be heated to 1800°F (1256°K) and then cooled by external means to -250°F (117°K) prior to the next pulse. A liquid nitrogen cooling jacket was utilized to externally cool the catalyst bed between pulses.

The reactor hardware for the low temperature propellant cyclic tests was previously operated for 5000 cycles with ambient temperature propellants and water as a coolant. During performance of the first cyclic test series with -250°F (117°K) propellant and bed temperatures, a crack developed in the reactor wall between the catalyst bed and the liquid nitrogen cooling

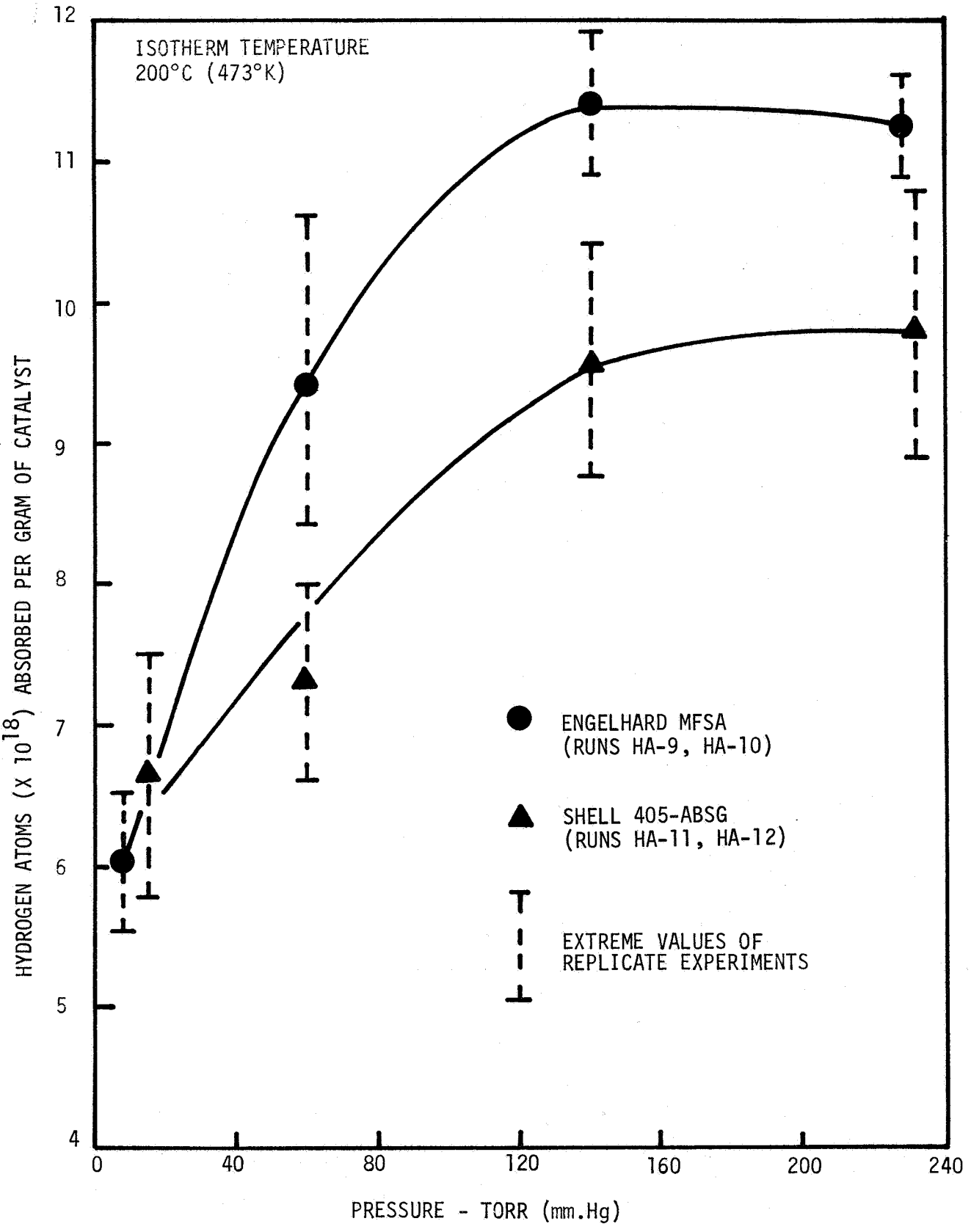

Figure 27. Hydrogen Adsorption Isotherms for Engelhard MFSA and Shell 405 Catalysts after 5000 Pulse Firings

Table 10. Summary of Hydrogen Chemisorption Isotherm Experiments

Catalyst	Sample History (All Samples Were Pretreated)*	Equilibrium Hydrogen Adsorption at 473°K and 200 Torr (mm Hg) Hydrogen Atoms X 10^{-18}
Shell 405-ABSG	As received	415 ± 5** (Runs HA-1, HA-2)
Shell 405-ABSG	After 4000 sec steady-state run	128 ± 8 (Runs HA-5, HA-6)
Shell 405-ABSG	After 5000 pulses (15,000 sec on time)	9.7 ± 1.0 (Runs HA-11, HA-12)
Engelhard MFSA	As received	22.3 ± 3.0 (Runs HA-3, HA-4)
Engelhard MFSA	After 4000 sec run	14.6 ± 1.5 (Runs HA-7, HA-8)
Engelhard MFSA	After 5000 pulses (15,000 sec on time)	11.3 ± .4 (Runs HA-9, HA-10)

*The standard pretreatment to remove very strongly adsorbed oxygen (from air exposure of the catalyst) consists of 16 hours evacuation at 473°K followed by exposure to 200 torr hydrogen at 773°K for 7 hours followed by 16 hours evacuation at 873°K in 10^{-6} torr vacuum.

**Duplicate experiments were run for each of these cases and the listed uncertainty represents the span between the experiments.

manifold. An abnormal increase in the catalyst bed cooldown rate indicated that liquid nitrogen from the cooling manifold was leaking into the catalyst bed between pulses. This leak occurred after approximately 150 pulses had been completed.

After a pressure test had verified that a leak did exist, the reactor was cut open, as shown in Figure 28. Analysis of the failure indicated that thermal expansion and contraction of the reactor wall was sufficient to have caused the fatigue crack, as identified in Figure 28.

Data from the low temperature cyclic tests obtained before the reactor wall leak occurred are presented in Figures 29 and 30. Figure 29 indicates that the catalyst bed temperature was reduced after 150 pulses, but this was a result of a decrease in propellant mixture ratio, as noted in the figure legend.

Reactor effluent temperatures were nearly identical for the 1st and 150th pulses, as shown in Figure 30. The initial delay in the effluent temperature thermocouple response was caused by ice built up on the thermocouple during chilldown between pulses. The point where the temperature

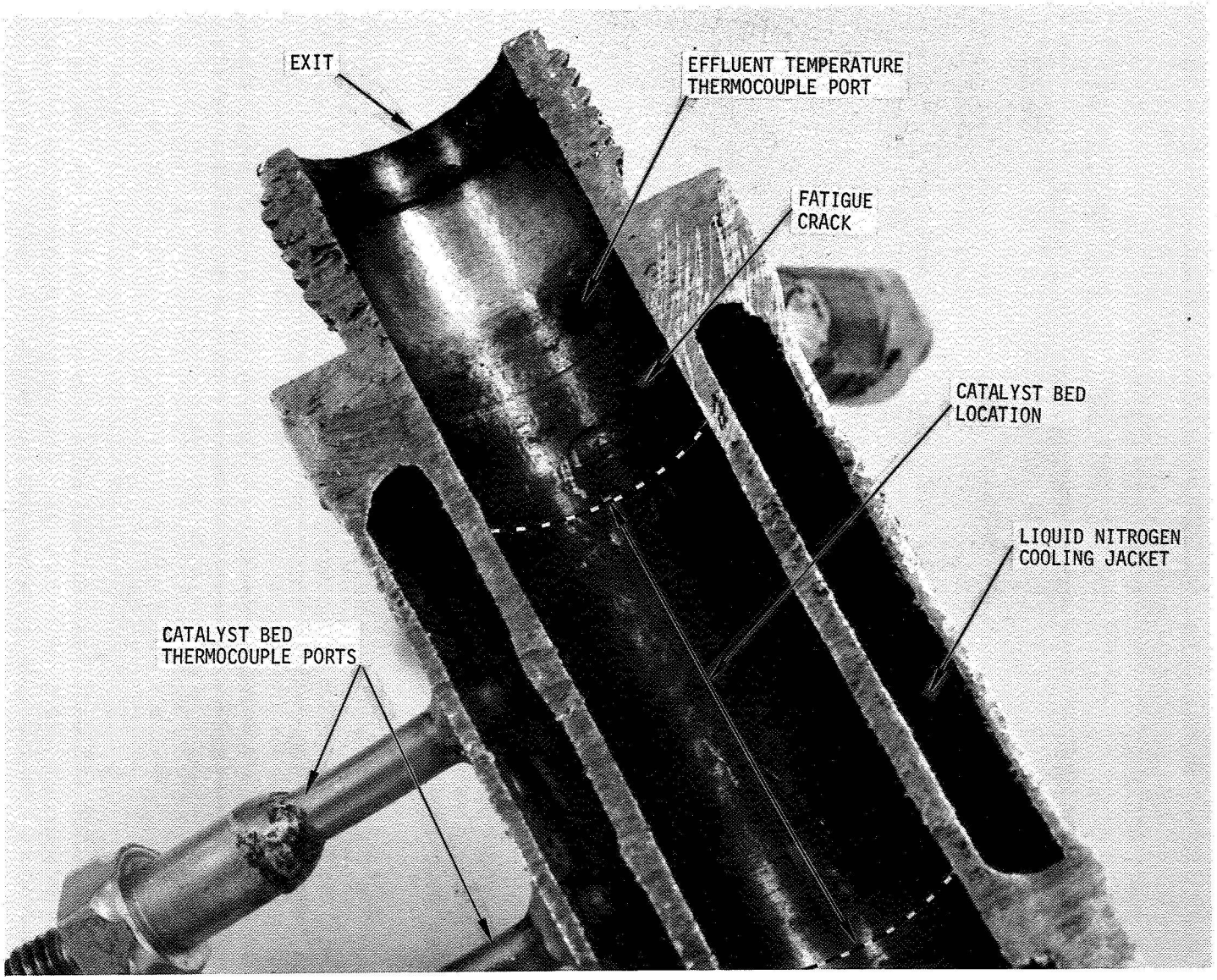

Figure 28. Initial Cooled Reactor Hardware - Sectioned to Show Fatigue Crack

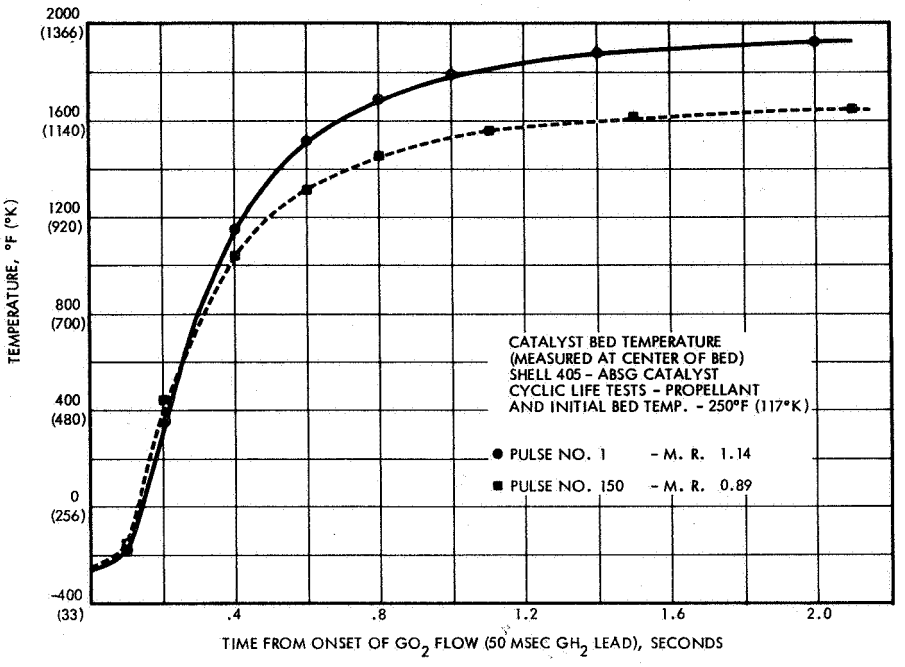

Figure 29. Catalyst Bed Response Data - Shell Catalyst Low Temperature Cyclic Life Tests

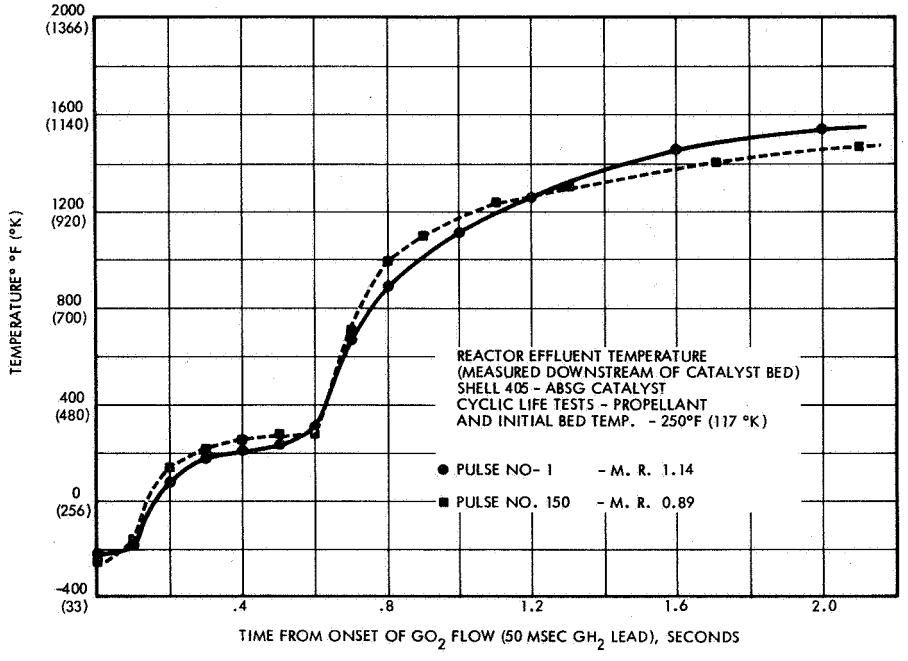

Figure 30. Reactor Effluent Response Data - Shell Catalyst Low Temperature Cyclic Life Tests

rapidly rises corresponds to the liquid saturation temperature for water at the reactor chamber pressure. At mixture ratio 1.0, the O_2/H_2 reaction products are one-half H_2O by weight.

The cooled reactor hardware was then redesigned to incorporate a thermal expansion joint, as shown in Figure 31. Fabrication of this new reactor was completed, and the low temperature cyclic tests were resumed. However, fatigue cracking also occurred in this hardware, as shown in Figure 32. Although the expansion joint allowed for axial extension and retraction of the reactor sleeve during thermal cycling, it was apparent that the joint was too stiff to allow radial expansion, resulting in the fatigue crack due to bending (No. 1, Figure 32). A second crack was observed between the two thermocouple port bosses (No. 2, Figure 32).

A re-evaluation of the cyclic test reactor design was made, and the hardware shown in Figures 33 and 34 was designed and fabricated. A stainless steel bellows was utilized to seal the cooling jacket while allowing unrestrained axial and radial expansion of the reactor sleeve. In addition, the sleeve was fabricated from Invar (36% nickel/iron alloy), which has a coefficient of thermal expansion approximately 70% of the coefficient for the stainless steel previously used, significantly reducing the stress due to thermal cycling.

As shown in Figure 33, the catalyst bed thermocouple was inserted through the downstream bed retaining screen, rather than through the reactor sleeve wall, to avoid any discontinuities in the sleeve which could result in recurrence of cracks. Using the reactor assembly shown in Figure 34, the low temperature cyclic tests were resumed. This design did show a marked improvement over the previous cooled reactors. However, after 700 cycles of operation, a crack also occurred in the reactor wall between the catalyst bed and the liquid nitrogen coolant, as shown in Figure 35.

Completion of 700 successive low-temperature pulses verified that satisfactory reaction of hydrogen-oxygen could be attained with the Shell 405-ABSG catalyst at -250°F (117°K) temperatures when the catalyst surface was pretreated by adsorption of hydrogen, as previously determined during the investigations of NAS 3-11227 (Reference 1). No degradation of the catalyst activity or physical appearance was observed after 700 pulses when the reactor crack occurred.

The rapid cooldown of the reactor wall from 1800°F (1256°K) to liquid nitrogen temperatures during cyclic testing imposed thermal gradients and stresses which would not have been present during reactor pulsing without the external LN_2 cooling jacket. However, no practical method of completing 5000 cycles was evident without some technique of rapid cooldown between pulses being employed. Completion of this task was rescheduled to utilize a new igniter design incorporating downstream injection of oxygen, as described in the following paragraphs.

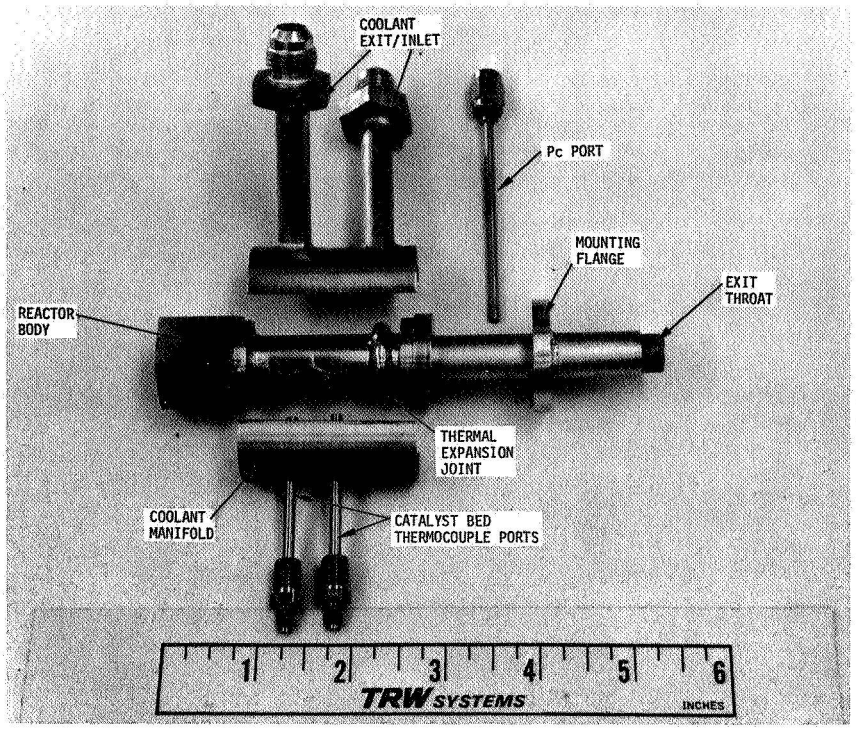

Figure 31. Redesigned Cooled Reactor Hardware - Incorporating Thermal Expansion Joints

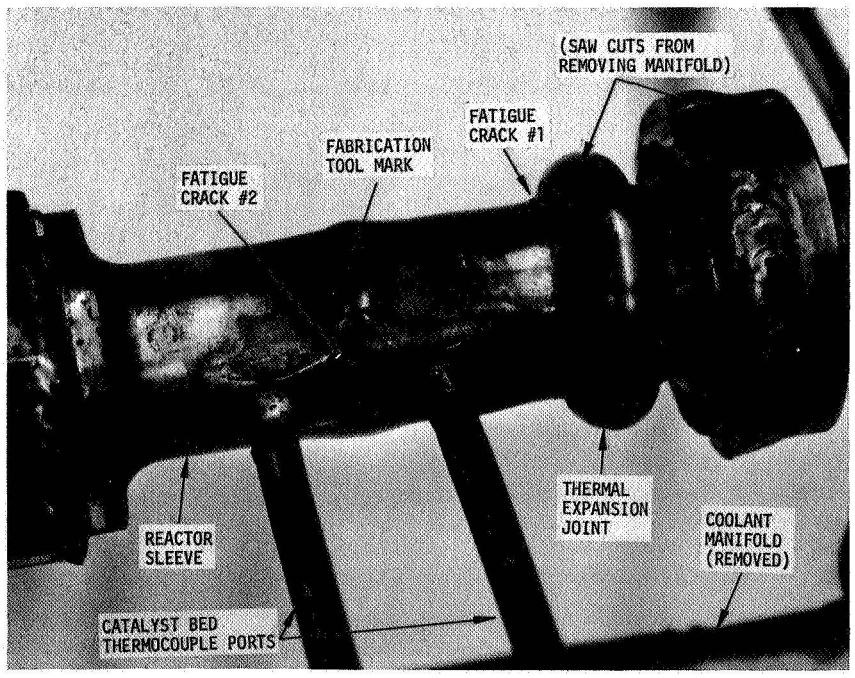

Figure 32. Cooled Reactor Hardware with Expansion Joint - Sectioned to Show Fatigue Cracks

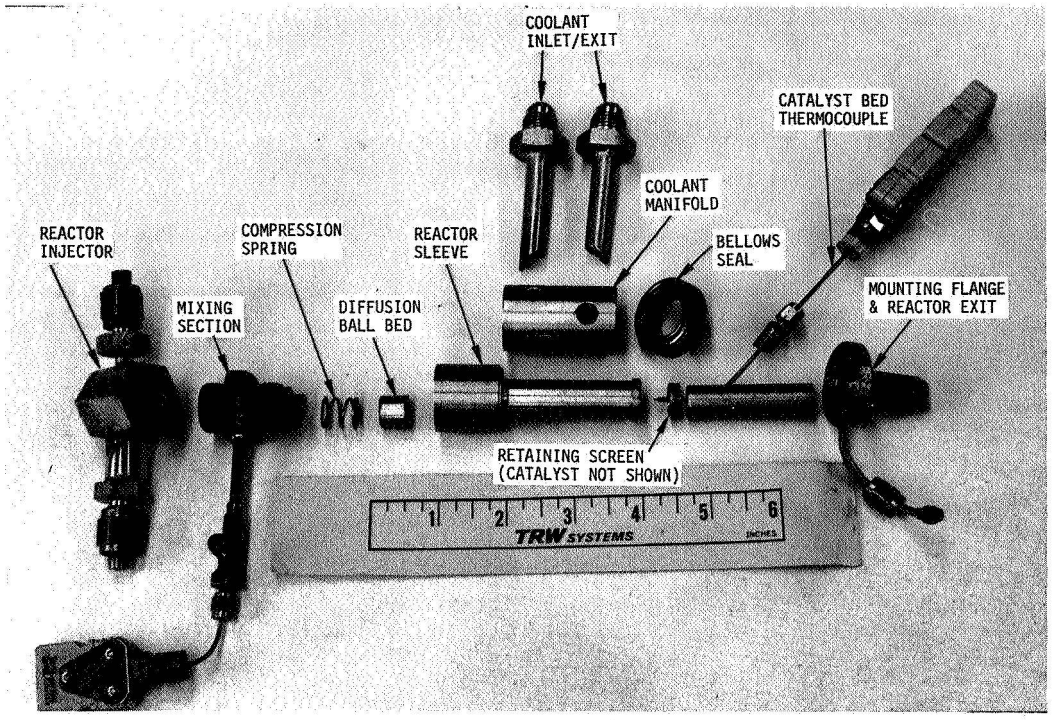

Figure 33. Disassembled Cooled Reactor - Bellows Seal

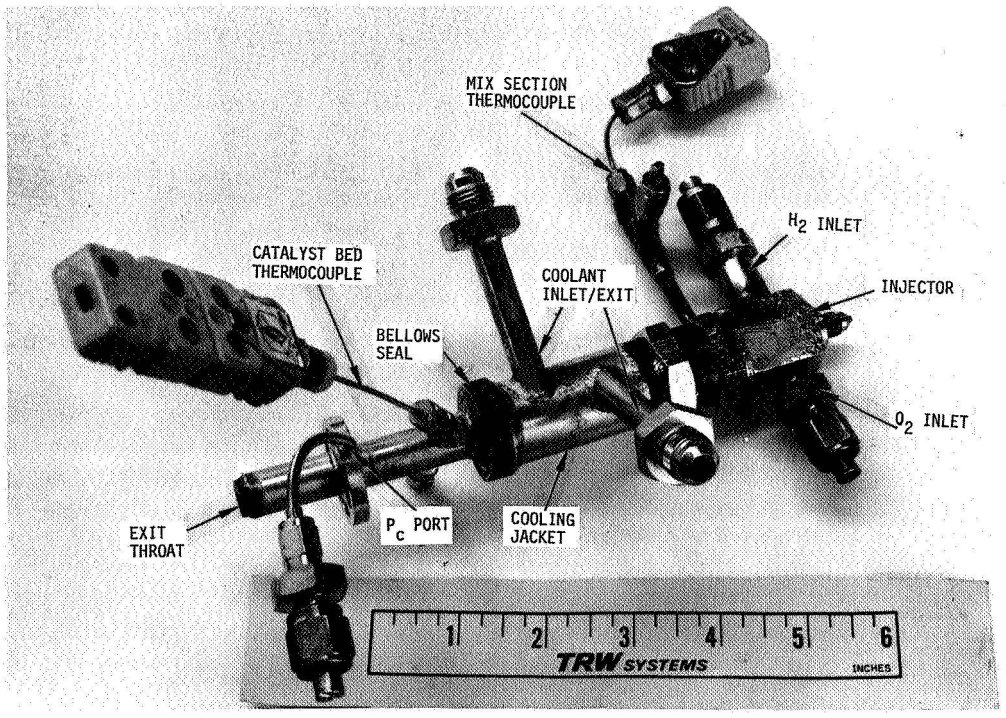

Figure 34. Catalytic Reactor Assembly - Bellows Cooling Jacket Seal

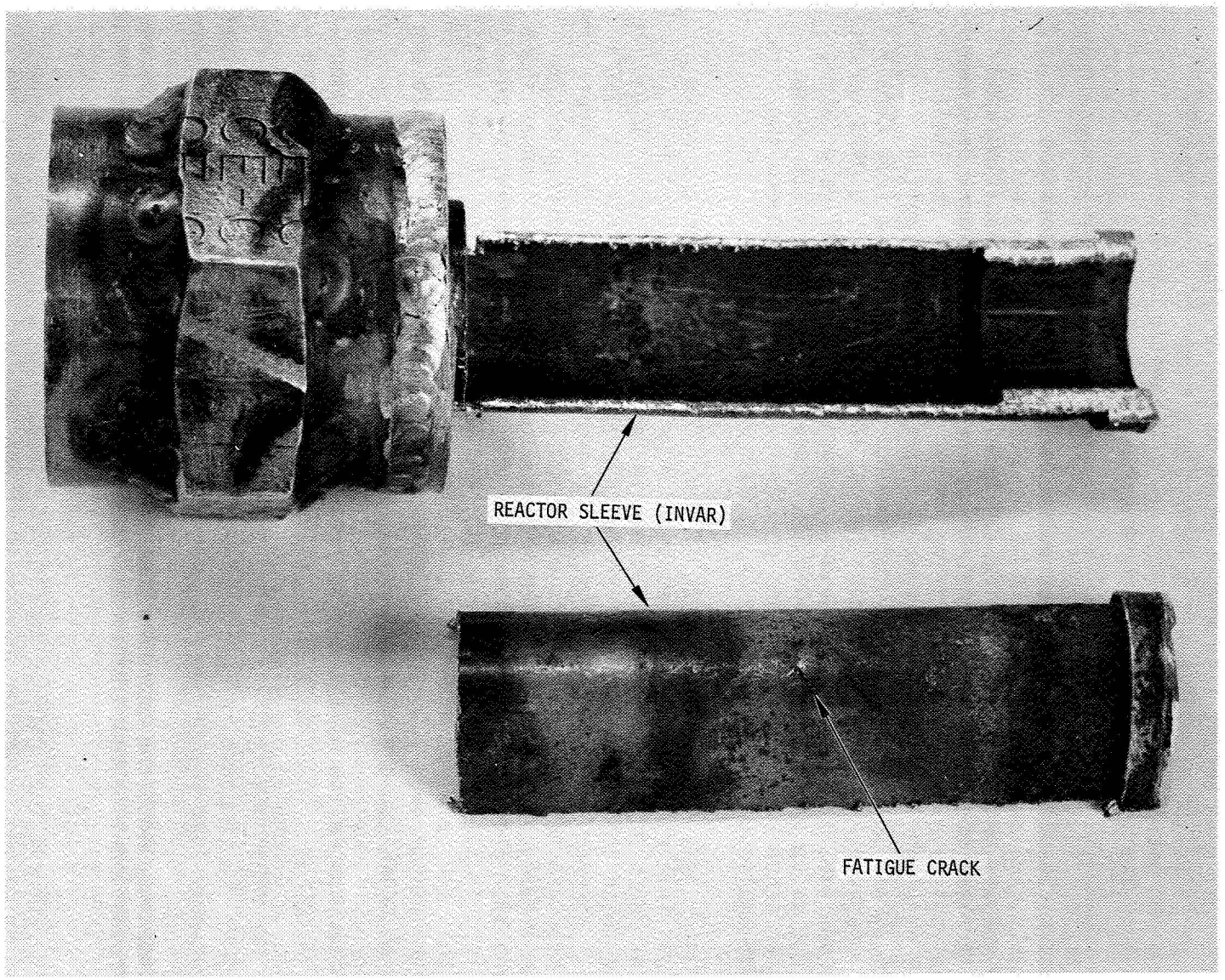

Figure 35. Sectioned Sleeve From Bellows Seal Cooled Reactor Showing Fatigue Crack

3.1.2.3 Downstream Injection Igniter Cyclic Tests

The high pressure, downstream oxygen injection igniter hardware, shown in Figures 36 and 37, was designed and fabricated as part of the high pressure, high thrust task effort added to the original program. Downstream injection of oxygen was selected as a means of significantly enhancing the overall response of the catalytic igniter, as described in detail in Section 3.2.2 of this report.

Cyclic life tests with this igniter were conducted by firing 1000 consecutive 250-millisecond duration pulses with ambient temperature propellants, followed by pulse tests of the same catalyst load with low temperature propellants to verify ignition capability. Oscillograph traces of these tests are presented in Figures 38 and 39. Figure 38 shows the final pulses of a 1000 cycle firing series performed with the Shell 405-ABSG catalyst in the high pressure downstream injection igniter (Figures 36 and 37). Nominal measured results were: 135 psia (931 kN/m^2) chamber pressure, 1.0 overall mixture ratio, and 0.215 lb/sec (0.0975 kg/sec) total propellant flow rate. Although an occasional valve misfire occurred during the pulse series, as indicated in Figure 38, no discernible change in igniter response or pulse chamber pressure was observed between the first and 1000th pulse.

Immediately following the last of the 1000 ambient pulses, a pulse series was initiated with low temperature propellants conditioned in a liquid nitrogen heat exchanger. As shown in Figure 39, repeatable, high response pulse ignitions were attained with propellants initially at -250°F (117°K). However, as pulsing continued and propellant temperatures approached liquid nitrogen temperature of less than -300°F (89°K), the gaseous oxygen began to liquify, progressively quenching the catalyst bed reaction as shown in Figure 39. Eventually the chamber pressure line became frozen, as shown at the left in Figure 39. It is evident from the repeatability of the initial pulses that the catalyst was capable of high response low temperature ignition after performance over 1000 pulse firings. The catalyst did not exhibit any erosion or cracking, and appeared visually in "as received" condition.

After completion of the cyclic life tests with the downstream oxygen injection igniter, laboratory tests (as described in Section 3.1.1.3) were performed to determine any degradation in either total or active surface area of the Shell 405-ABSG catalyst. The catalyst fired for 1000 pulses followed by low temperature ignitions was analyzed and compared with catalyst fired for only five pulses and "as received" catalyst, as shown in Table 11.

Comparing both the total surface area loss and active surface degradation (proportional to equilibrium hydrogen absorption) of Table 11 with the previous life test results in Table 10, it is evident that catalyst degradation is greatly reduced with the downstream injection igniter. With this igniter, effluent temperatures sufficient for main thruster ignition were attained by oxygen injection downstream of the catalyst bed, allowing the catalyst itself to operate at temperatures as low as 400°F (478°K), compared with bed temperatures of 1800°F (1255°K) with the initial igniter design where all of the oxygen was passed through the catalyst bed. Operation at the lower bed temperature reduced catalyst sintering and significantly

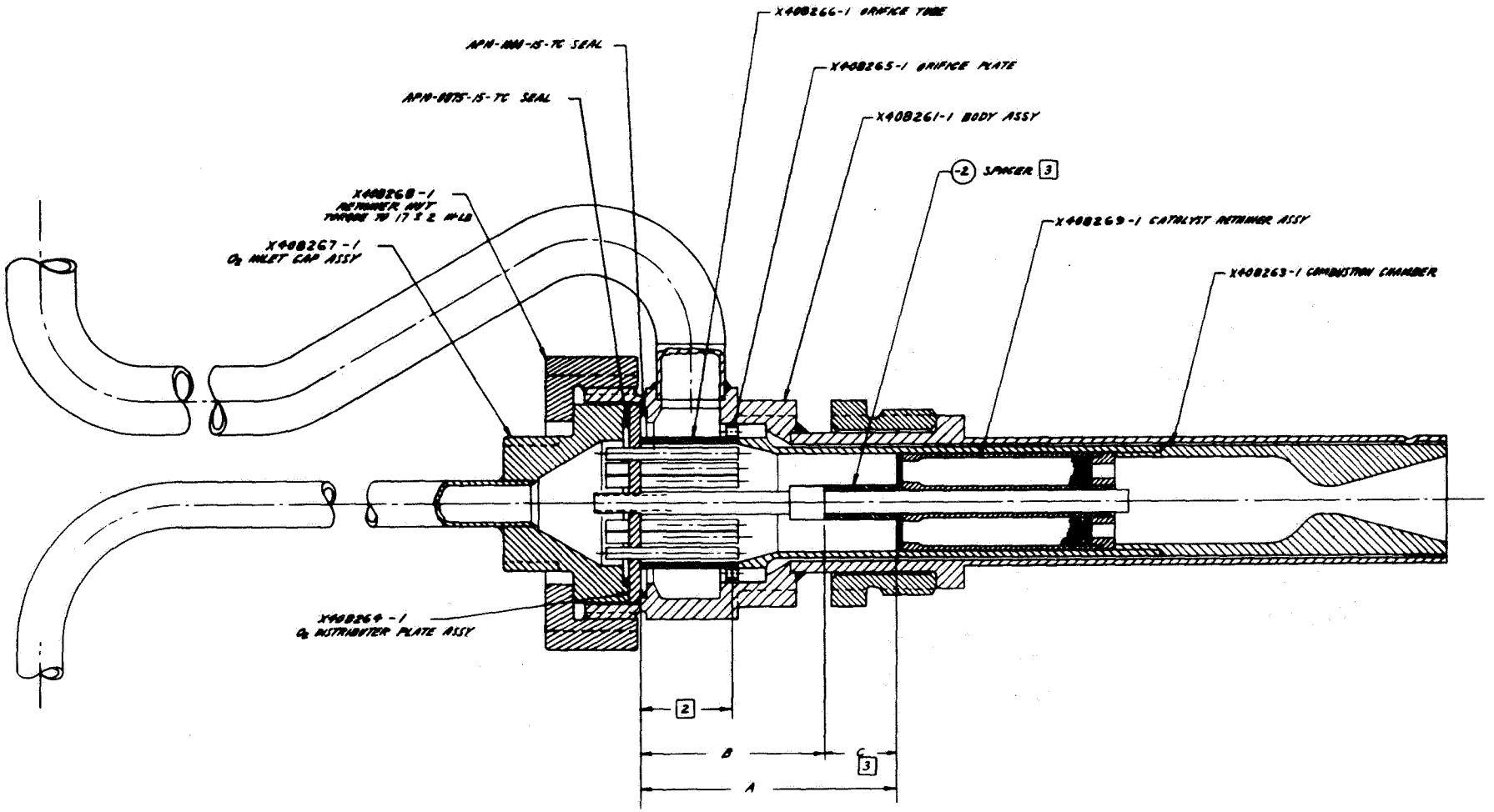

Figure 36. Catalytic Reactor - Downstream O_2 Injection

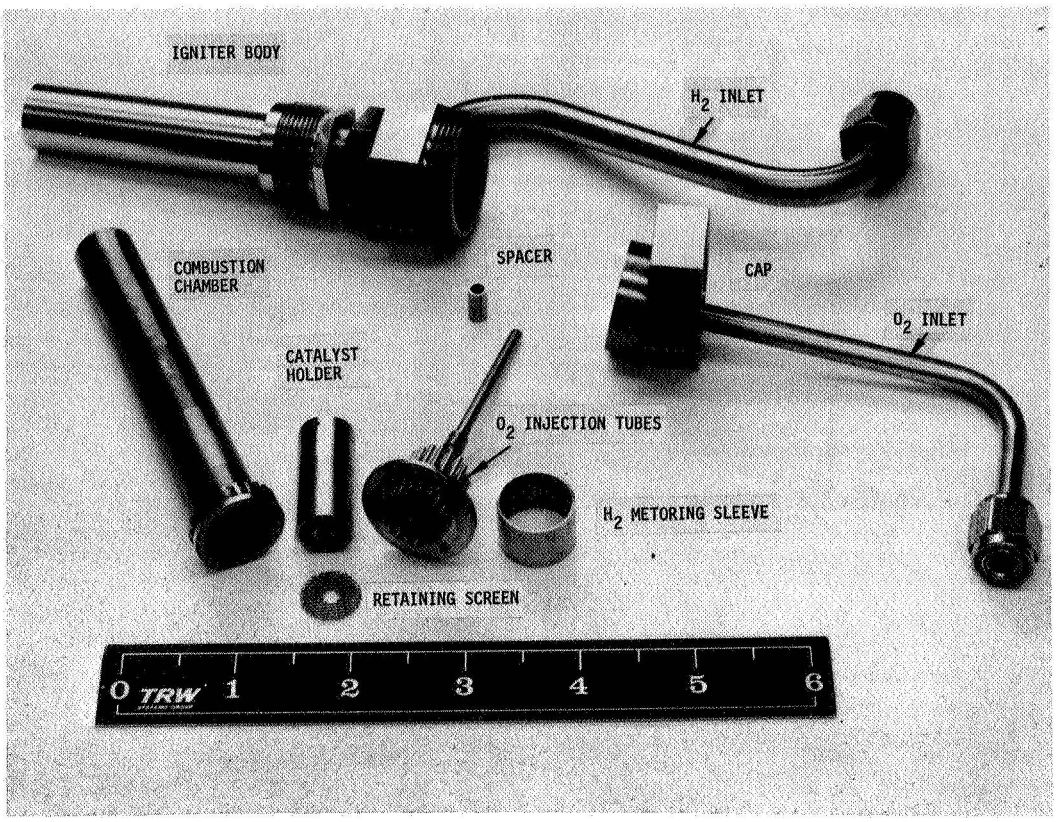

Figure 37. Disassembled Catalytic Igniter - High P_c Thruster

Design Detail Summary -

Mixing Section

1. 36 O_2 tubes, .007" (.018 cm) I.D. by .720" (1.84 cm) length.
2. H_2 radial metering ports, 8 places, .021" (.054) I.D.
3. 90% of H_2 is by passed for c-oling of the CU combustion tube.
4. Overall MR 1:1
5. Mixing length set by axial diffusion for single O_2 jet in a flowing H_2 field.

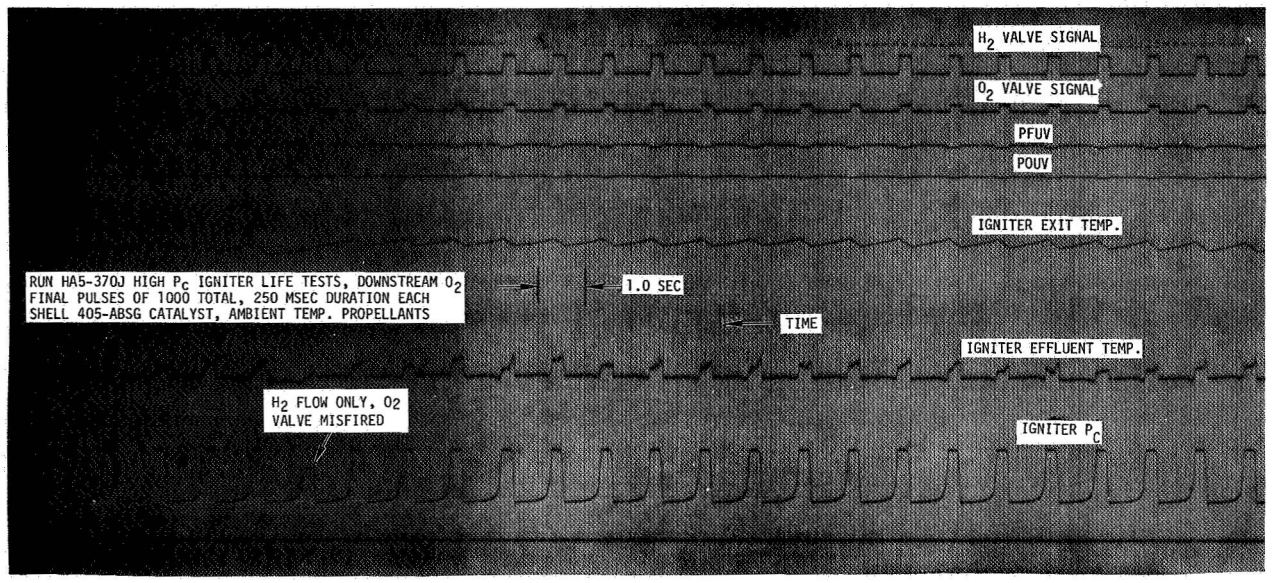

Figure 38. High P_C Igniter Life Tests, Downstream O_2 Injection
Final Pulses of 1000 Total, Shell Catalyst

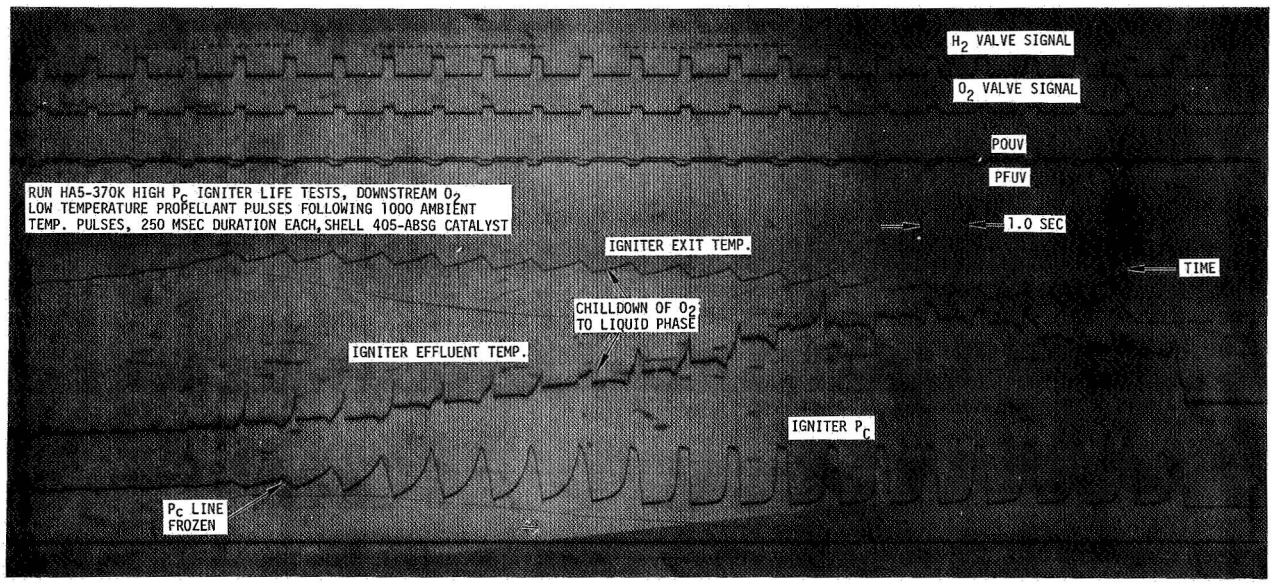

Figure 39. Low Temperature Ignitions Following 1000 Pulses
High P_C Igniter, Downstream Injection

Table 11. Summary of Laboratory Analyses of Shell 405-ABSG Catalyst After Cyclic Life Tests With Downstream Injection Igniter

Sample History (All samples pretreated)*	Total Surface Area (square meters/gram)	Equilibrium Hydrogen Absorption at 473°K and 200 Torr (mm Hg) Hydrogen Atoms X 10^{-18}
As received	112	485
After 5 pulses	111	468
After 1000 pulses	76	430

*Pretreatment consisted of vacuum soak for 16 hours at 473°K, followed by 200 torr hydrogen exposure at 773°K for 7 hours, followed by 16 hours at 873°K and 10^{-6} torr vacuum.

improved durability of the catalyst. The difference in active surface area between catalyst samples subjected to 5 and 1000 pulses (Table 11) was only 7%, which indicates excellent stability in catalyst activity up to at least 1000 pulses.

3.1.2.4 Conclusions from Experimental Results

Based on the pulse firing performance of the catalyst beds and the post-firing laboratory analyses, the conclusions resulting from the cyclic tests were:

- At least 5000 pulses can be performed with both the Shell 405-ABSG and Engelhard MFSA catalysts with ambient temperature propellants even though major reduction in active catalyst surface occurred.
- Satisfactory reaction can be achieved with the Shell 405-ABSG catalyst at propellant and initial bed temperatures of -250°F (117°K).
- The downstream oxygen injection igniter concept not only greatly enhances overall response, but significantly improves catalyst life by allowing lower bed operating temperatures.

3.2 IGNITER DESIGN OPTIMIZATION

An experimental and analytical evaluation of catalytic igniter operational characteristics and limitations was conducted to establish generalized igniter design guidelines. The objectives of this design optimization were:

- Investigate the variables influencing/controlling flashback of flame front from the catalyst bed to the mixing injector.
- Determine baseline catalyst bed response and evaluate methods of improving overall igniter response.
- Develop generalized design guidelines for catalytic igniters, including scaling criteria.

3.2.1 Flashback Limit Determination

A series of test firings was conducted to determine the effects of variations in igniter internal geometry, flow velocity, and mixture ratio on igniter flashback characteristics. The following paragraphs describe the test installation and procedures, and present the experimental results.

3.2.1.1 Test Hardware and Stand Installation

The catalytic reactor hardware utilized for the flashback investigations was previously fabricated during the performance of NASA/LeRC Contract NAS 3-11227. Figure 40 is a section view of the low Pc reactor, and shows the relative locations of the injector, mixing section, diffusion and catalyst beds, and the temperature and pressure instrumentation ports. The high Pc reactor is identical in concept but reduced in size. The mixing section between the injector and catalyst bed contained interchangeable sleeve and orifice plate inserts, which provided the capability of varying the gas velocity through the mix section. Further variation of velocity was accomplished by using a motorized throat plug (Figure 40, 41) to increase pressures, which resulted in decreased flow velocity at constant propellant mass flow rates (controlled by sonic orifices). For each igniter configuration, mixing zone velocity was progressively reduced in attempting to induce flashback. Occurrence of flashback was detected by the mix section thermocouple, as shown in Figure 40, and the test was automatically terminated. The overall test stand installation is presented in Figure 42.

3.2.1.2 Input Flow Velocity Effects

Investigations of the effects of varying the propellant flow rate into the catalyst bed on the initiation of flashback were conducted for each pressure level igniter. Mixing section flow velocities were systematically reduced by changing the mixing diameter and/or increasing igniter pressures using the adjustable throat plug (Figure 41). For these tests, a minimal hydrogen lead on start-up and an overall mixture ratio of 1.0 were maintained. Data from these tests are listed in Table 12 and described as follows.

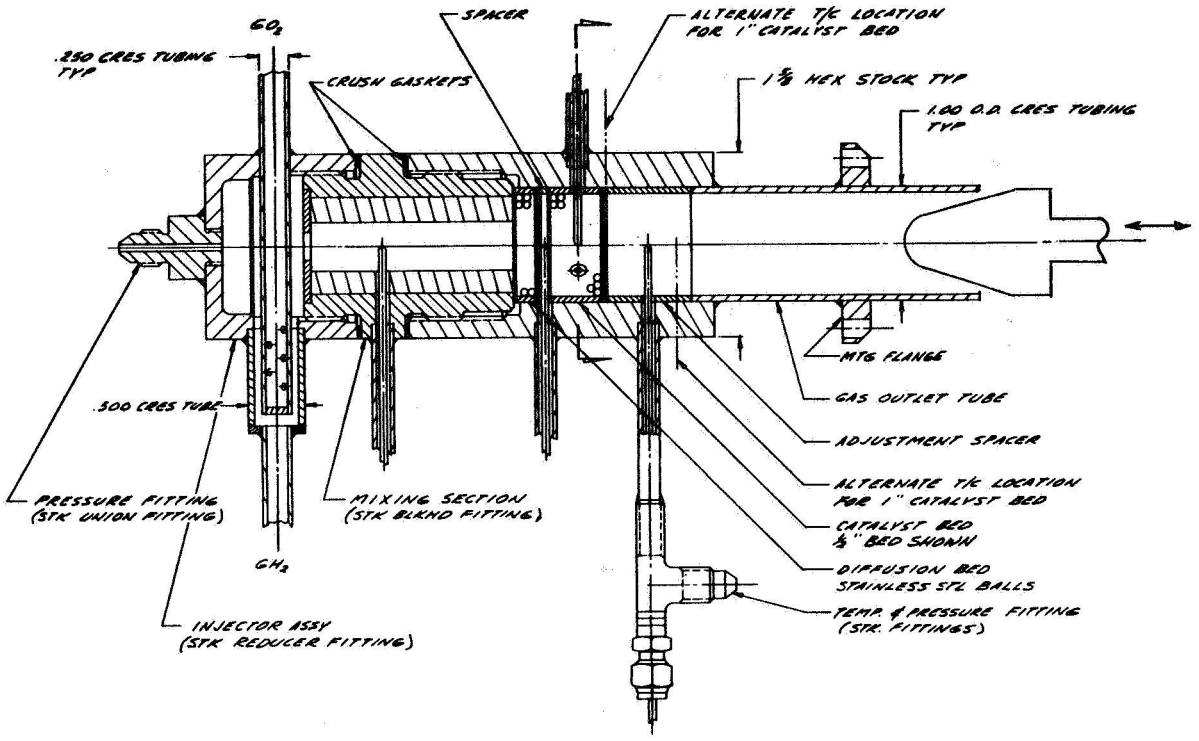

Figure 40. Catalytic Reactor Igniter - Low Chamber Pressure (Motorized Throat Plug Shown) For Flashback Evaluations

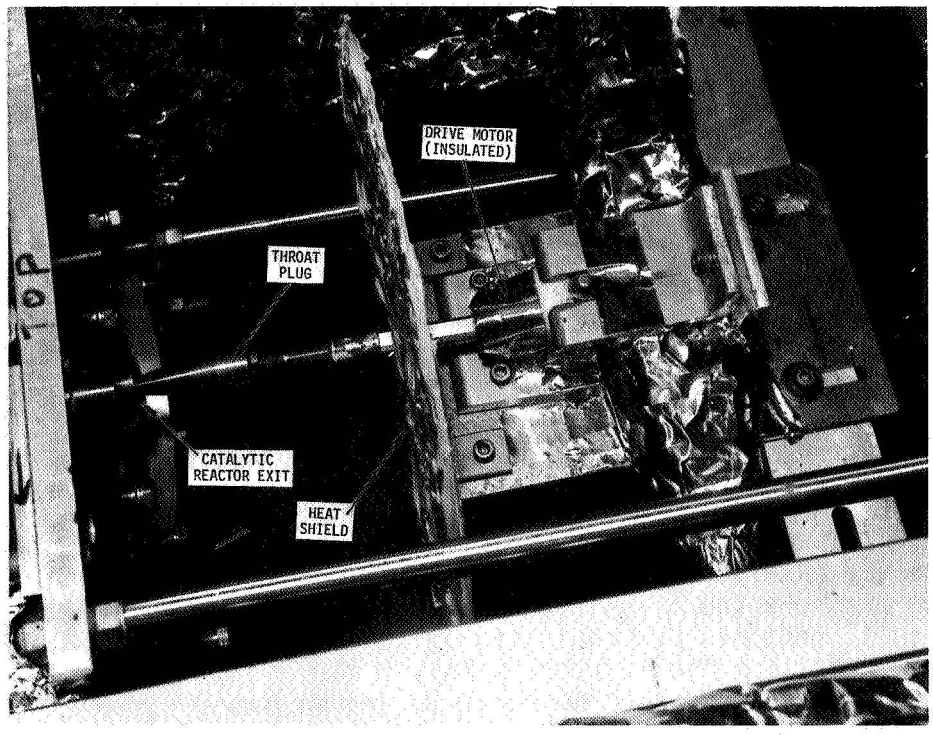

Figure 41. Motorized Throat Plug Installation - Igniter Flashback Investigation Tests

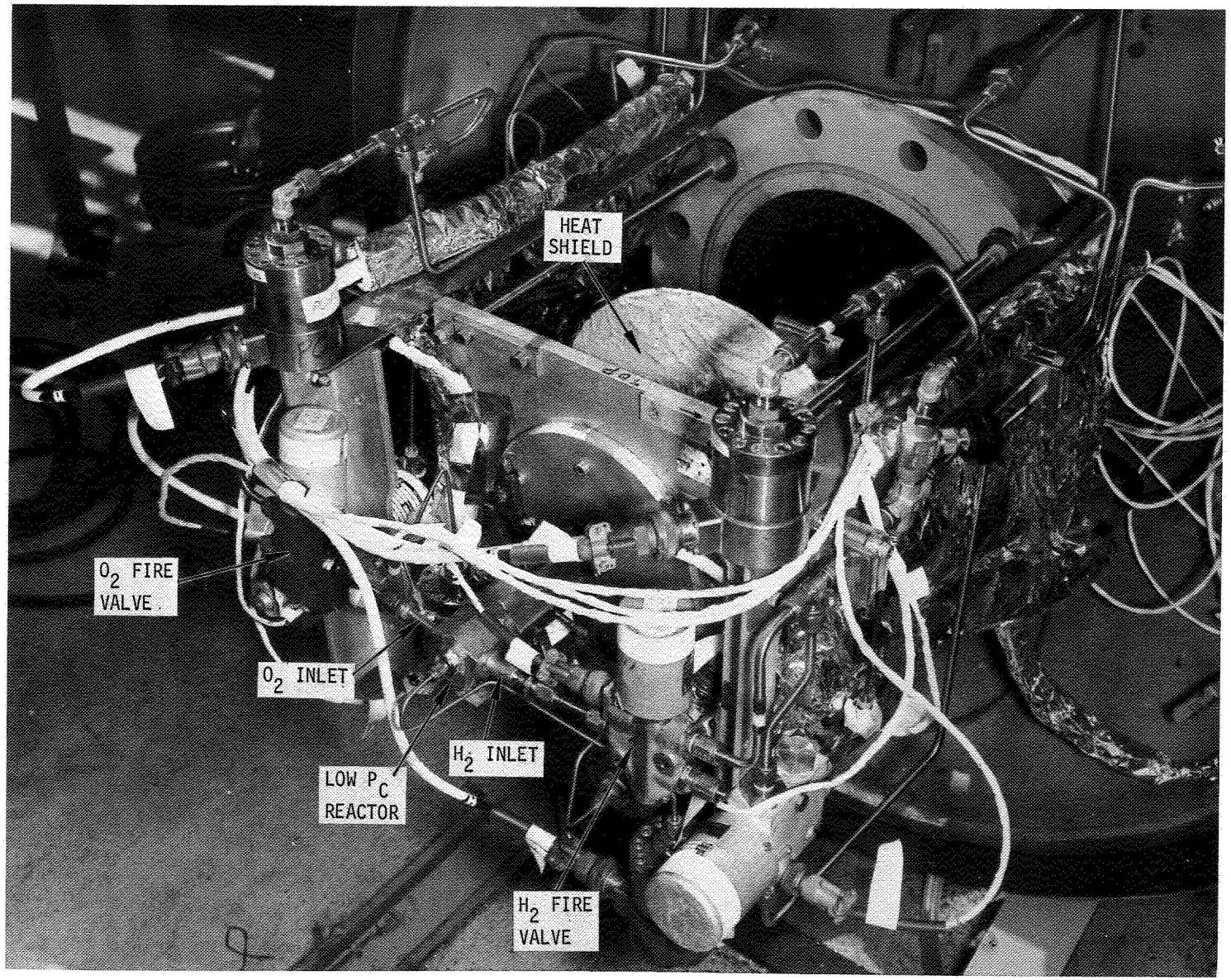

Figure 42. Igniter Flashback Investigation Test Installation

Table 12. Igniter Flashback Investigation Tests - Input Flow Velocity Effects[1]

Test No. (HA5-)	P_{CD} (lbf/in^2)	P_{CD} (kN/m^2)	P_{mix} (lbf/in^2)	P_{mix} (kN/m^2)	V_{mix} (ft/sec)	V_{mix} (m/sec)	$\dot{W}_{total}$ (lbm/sec)	$\dot{W}_{total}$ (g/sec)	Reynolds[2] Number	Flashback	Comments
129-A	41.4	285.4	45.8	315.8	279.8	85.29	.00426	1.94	24,800		Low pressure reactor Engelhard catalyst Mixing section diameter 0.40 inch (1.02 cm)
129-C	68.7	473.7	71.0	489.5	188.2	57.37	.00426	1.94	24,800		
129-B	15.0	103.4	17.6	121.3	274.3	83.61	.00158	0.719	9,220		
129-B	23.2	160.0	25.6	176.5	188.6	57.49	.00158	0.719	9,220		
129-D	15.0	103.4	17.6	121.3	57.5	17.53	.00153	0.696	4,350		Same as above except mixing section diameter 0.875 inch (2.22 cm)
129-E	21.2	146.2	23.8	164.1	42.5	12.95	.00153	0.696	4,350		
129-E	53.3	367.5	58.0	399.9	49.1	14.97	.00430	1.96	11,500		
129-E	67.5	465.4	71.0	489.5	40.0	12.19	.00430	1.96	11,500		
129-F	27.7	191.0	32.0	220.6	55.7	16.98	.00265	1.21	7,150		
129-F	41.0	282.7	43.0	296.5	41.5	12.65	.00265	1.21	7,150		
141-D	16.5	113.8	26.0	179.3	41.7	12.71	.00167	0.760	4,150		Low pressure reactor Shell catalyst Mixing section diameter 0.875 inch (2.22 cm)
141-E	51.7	356.5	67.0	461.9	41.1	12.53	.00425	1.93	11,500		
141-F	55.5	382.7	70.0	482.6	39.4	12.01	.00425	1.93	11,500		
143-A	40.8	281.3	44.0	303.4	23.7	7.22	.00161	0.732	4,350	X	
180-A	14.0	96.5	15.8	108.9	63.1	19.23	.00164	0.732	4,350		Same as above except Engelhard catalyst
180-B	45.1	310.9	45.8	315.8	21.9	6.68	.00160	0.728	4,350	X	
180-D	47.2	325.4	48.0	330.9	20.6	6.28	.00165	0.751	4,350	X	
181-A	86.0	592.9	88.0	606.7	30.7	9.36	.00428	1.95	11,500	X	
181-B	80.4	554.3	82.0	565.4	35.5	10.82	.00430	1.96	11,500	X	
231-B	273.6	1886.0	281.9	1994.0	158.6	48.34	.00370	1.68	42,500		High pressure reactor Engelhard catalyst Mixing section diameter 0.20 inch (0.51 cm)
231-D	214.8	1895.0	284.1	1959.0	157.6	48.04	.00372	1.69	42,500		
232-I	431.3	2974.0	437.4	3016.0	104.5	31.85	.00358	1.63	42,500		
233-A	277.6	1914.0	278.7	1922.0	68.2	20.79	.00148	0.673	17,600		
233-B	151.3	1043.0	153.8	1060.0	124.9	38.07	.00147	0.669	17,600		
233-C	248.1	1711.0	249.6	1721.0	76.1	23.20	.00148	0.673	17,600		
233-E	257.8	1777.0	259.2	1787.0	72.7	22.16	.00145	0.660	17,600		
234-A	92.9	640.5	114.7	790.8	84.3	25.70	.00369	1.68	20,400		Same as above except mixing section diameter 0.43 inch (1.19 cm)
234-G	496.5	3423.0	500.4	3450.0	19.3	5.88	.00370	1.68	20,400		
234-L	466.6	3217.0	487.4	3360.0	20.8	6.34	.00369	1.68	20,400		
235-B	119.0	820.5	136.2	939.0	29.3	8.93	.00151	0.687	8,300		
235-G	259.1	1786.0	265.8	1833.0	14.9	4.54	.00151	0.687	8,300		
246-C	95.4	657.7	150.1	1035.0	39.6	12.07	.00440	2.00	24,400		High pressure reactor Shell catalyst Mixing section diameter 0.43 inch (1.19 cm)
246-D	98.6	679.8	156.4	1078.0	38.1	11.61	.00440	2.00	24,400		
247-A	122.0	841.1	208.0	1434.0	28.7	8.75	.00440	2.00	24.400		
247-F	322.4	2223.0	357.0	2461.0	16.7	5.09	.00440	2.00	24,400		

[1] Ambient temperature H_2/O_2 propellants at a mixture ratio of 1.0 O/F and a 1.0 inch (2.54 cm) long catalyst bed were employed throughout test series.

[2] Reynolds number is based on diameter of mix section and indicates turbulent flow for all tests.

Tests 129A-C: Low pressure reactor tests with the Engelhard catalyst and a mixing section diameter of 0.40 inch (1.02 cm) did not result in flashback at flow rates from 2 to 5% of nominal thruster flows and mix section velocities as low as 188 ft/sec (57.4 m/sec). More than one data point was frequently obtained during a test as the motorized throat plug was moved during the firing. Calculated Reynolds number values indicated turbulent flow for all tests.

Tests 129D-F: Increasing the mixing section diameter equal to the catalyst bed diameter of 0.875 inch (2.22 cm) still did not induce flashback with the low Pc reactor at mix velocities as low as 40 ft/sec (12.2 m/sec).

Tests 141D-F, 143A: These low pressure tests were performed with the Shell catalyst to determine if catalyst type had any influence on flashback velocity limits. Flashback was attained when mix velocity was reduced to 23.7 ft/sec (7.22 m/sec) at an igniter flow rate equal to 2% of nominal thruster flow. Even with the maximum mixing section diameter (equal to catalyst bed diameter), flashback velocities occurred only when chamber pressure was increased from the nominal 15 psia (103.4 kN/m^2) to 40.8 psia (281.3 kN/m^2).

Tests 180A-181B: Verifying the limiting flashback velocity for the low Pc reactor with the Engelhard catalyst resulted in flashback at mix velocities of 21.9 ft/sec (6.68 m/sec) at 2% thruster flows and 35.5 ft/sec (10.82 m/sec) at flow rates equal to 5% of nominal thruster flows. Again, flashback occurred only at chamber pressures approximately three times the nominal 15 psia (103.4 kN/m^2) design operating pressure.

Results of the high pressure reactor flashback tests listed in the lower half of Table 12 were as follows:

Tests 231B-233E: No flashbacks resulted from high Pc reactor tests with Engelhard catalyst at mix velocities as low as 72.7 ft/sec (22.16 m/sec) with a 0.20 inch (0.51 cm) mixing diameter over a flow range from 2 to 5% of thruster flow.

Tests 234A-235G: Increasing mixing diameter equal to catalyst bed diameter of 0.43 inch (1.19 cm) did not induce flashback with Engelhard catalyst at mix velocities as low as 14.9 ft/sec (4.54 m/sec) and chamber pressures up to 496.5 psia (3423 kN/m^2), five times the nominal design operating pressure.

Tests 246C-247F: Repeating the above tests with the Shell catalyst did not induce flashback at mix velocities as low as 16.7 ft/sec (5.09 m/sec).

Although flashback had not been attained with the high pressure reactor, further reduction of mix section velocities would have required increasing mix diameters to impractical limits (greater than catalyst bed diameter) and/or a substantial increase in operating pressures, requiring feed system modification.

Results of the flashback velocity limit tests with both the low and high chamber pressure igniters are summarized in Figure 43. Average flow velocity through the mixing section during each test is plotted versus mix section pressure in atmospheres. Each line decreasing in velocity and increasing in pressure from left to right represents a series of tests from Table 12 in which the igniter throat plug was inserted to increase pressure and thus reduce velocities at a constant flow rate. Each data line is identified to indicate mix section diameter and igniter flow rate as a percentage of nominal thruster flow. Flashback data points are noted for the low chamber pressure igniter, and limiting velocities appear to be the same for either Shell or Engelhard catalysts tested.

With a minimal igniter hydrogen lead on start-up, flashback did not occur with the low Pc igniter at pressures less than three times nominal operating pressure. No flashbacks were experienced with the high Pc igniter even at chamber pressures five times nominal design pressure and catalyst bed input velocities as low as 14.9 ft/sec (4.54 m/sec). Results of this flashback velocity limit investigation were further analyzed and incorporated into generalized design criteria during the igniter scaling analysis effort described later in Section 3.2.3.

3.2.1.3 Increased Initial Mixture Ratio Effects

The second flashback test series was performed to investigate the effects of high initial oxidizer/fuel mixture ratio on flashback initiation. Previous occurrences of flashback had been initiated by O_2 surges during the start-up transient, and these tests were attempted to duplicate these transient conditions.

Figure 44 shows the technique used to attain a high O/F mixture ratio during the start transient. The variable volume plenum between the igniter oxygen fire valve and the oxidizer sonic flow control orifice provided a controlled surge of oxygen during the start transient, while the fuel flow rate remained constant. Valve timing was set to provide a fuel lead on start-up, followed by an oxygen surge of less than 100 milliseconds, and then an overall mixture ratio of 1:1, unless the test was terminated by flashback.

Data from the high initial mixture ratio tests are presented in Table 13 and the results were as follows:

Tests 190J-K: The initial low pressure reactor tests without a diffusion bed upstream of the catalyst resulted in flashback when the igniter flow rate was increased from 2 to 5 percent of nominal thruster flows with the surge volume at 0.1104 in^3 (1.809 cm^3). The ratio of oxidizer supply pressure to fuel supply pressure (proportional to propellant mixture ratio), Pos/Pfs was held constant for these two tests.

Tests 192I-J: Flashback occurred on test 192I with reduced surge volume but increased Pos/Pfs. A very minimal reduction in mixture ratio (note Pos/Pfs) for test 192J resulted in no flashback. Later

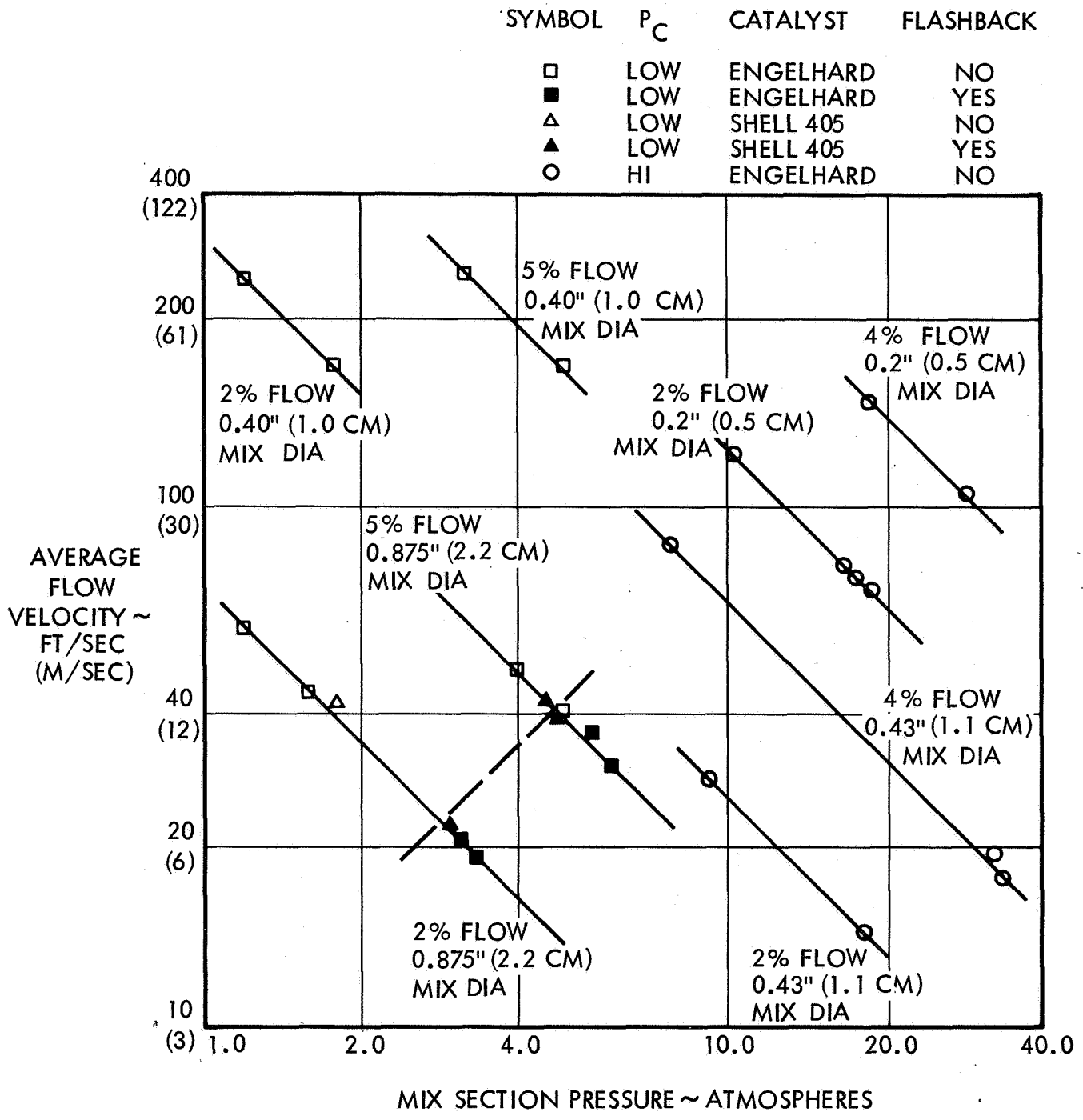

Figure 43. Igniter Flashback Test Data

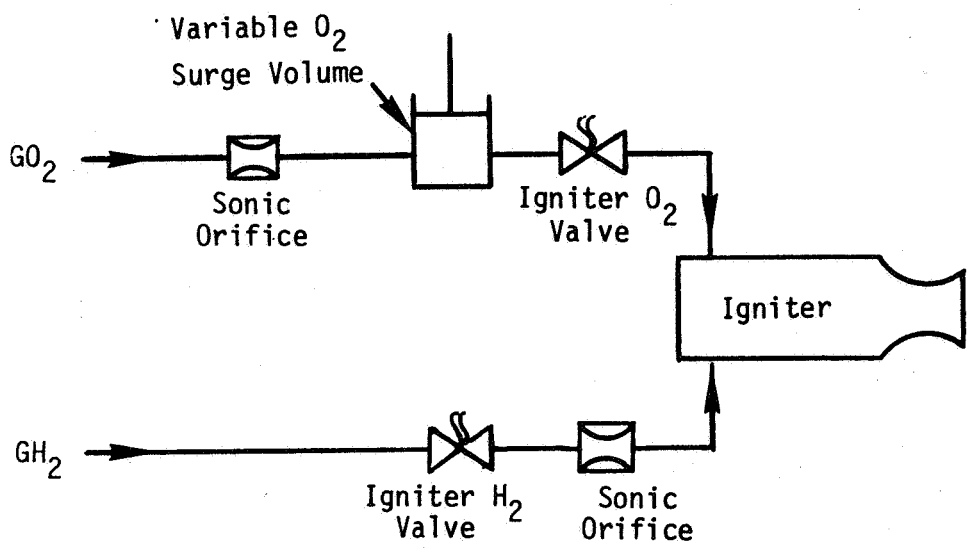

Figure 44. High Initial Mixture Ratio Test Feed System Schematic

tests also verified that a very slight increase in Pos/Pfs resulted in flashback, when the limiting mixture ratio was attained.

Tests 193C-195C: For these tests, diffusion beds of copper or steel shot were installed upstream of the catalyst bed (see Figure 40) to attempt arrest of flashback. The low Pc diffusion bed holders of different lengths are shown at the top of Figure 45. These test results indicate that although flashback limits could be extended somewhat by the use of diffusion beds of steel or copper shot upstream of the catalyst bed, these beds were not capable of completely arresting flashback under all igniter transient flow conditions.

Tests 239F-Q: Initial tests of the high pressure reactor without diffusion beds resulted in flashback at lower mixture ratios (lower Pos/Pfs and lower surge volumes) compared to the low Pc reactor tests. A very slight (4 percent) increase in surge volume between tests 239F and 239Q reduced the Pos/Pfs at which flashback occurred.

Tests 240A-245N: These tests constituted a systematic evaluation of the effects of various diffusion bed configurations and materials on influencing flashback limits. The high Pc diffusion bed holders and the copper and steel shot used are shown in Figure 45. The steel shot at the right was mechanically "roughened" to irregular shapes. The copper shot was no more effective than the steel ball beds in modifying flashback limits, and no significant difference was observed in the effects of the "smooth" and "roughened" steel balls on flashback limits. Increasing the copper diffusion bed length to 1.1 inches (2.79 cm) for tests 245 M, N increased considerably the initial mixture ratio (indicated by increased surge volume and Pos/Pfs) required before flashback occurred; however, even this relatively large mass of copper shot could not completely quench flashback.

Table 13. Igniter Flashback Investigation Tests - Increased Initial Mixture Ratio Effects[1]

Test No. (HA-5-)	P_{CD} lbf/in^2	P_{CD} kN/m^2	$\dot{W}_{Total}$ lbm/sec	$\dot{W}_{Total}$ g/sec	Surge Volume[2] in^3	Surge Volume[2] cm^3	Diffusion Bed Material	Diffusion Bed Length (in/cm)	P_{OS}/P_{FS}[3]	Flashback	Comments
190-J	13.9	95.8	0.00217	0.984	0.1104	1.809	None	-	0.553		
190-K	6.1	42.1	0.00436	1.978	0.1104	1.809	↓	-	0.555	X	Low Pressure Reactor
192-I	7.1	49.0	0.00163	0.739	0.1094	1.793	↓	-	0.573	X	
192-J	16.3	112.4	0.00161	0.730	↓	↓	Copper	-	0.570		Engelhard Catalyst
193-C	14.3	98.6	0.00164	0.744	↓	↓	↓	.25/.64	0.593		
193-D	7.3	50.3	0.00164	0.744	↓	↓	↓	.25/.64	0.603	X	Mixing Section Diameter .875 inch (2.22 cm)
194-G	7.8	53.8	0.00428	1.941	↓	↓	↓	.125/.32	0.552	X	
194-H	15.4	106.2	0.00429	1.946	↓	↓	↓	.125/.32	0.548		
195-B	14.7	101.4	0.00432	1.960	↓	↓	Steel	.25/.64	0.554		
195-C	7.3	50.3	0.00434	1.969	↓	↓	↓	.25/.64	0.565	X	
239-F	50.3	346.8	0.00183	0.830	0.1005	1.647	None	-	0.438		
239-M	60.1	414.4	0.00390	1.769	0.1005	1.647	↓	-	0.472	X	
239-P	81.2	559.9	0.00386	1.751	0.1041	1.706	↓	-	0.359		
239-Q	70.1	483.3	0.00409	1.855	↓	↓	↓	-	0.407	X	
240-A	83.7	577.1	0.00407	1.846	↓	↓	Copper	.25/.64	0.409		
240-B	58.8	405.4	0.00425	1.928	↓	↓	↓	↓	0.448	X	
240-C	84.4	581.9	0.00427	1.937	0.1005	1.647	↓	↓	0.449		High Pressure Reactor
240-D	57.8	398.5	0.00439	1.991	0.1005	1.647	↓	↓	0.470	X	
241-A	84.5	582.6	0.00409	1.855	0.0951	1.558	None	-	0.409		Engelhard Catalyst
241-B	69.8	481.3	0.00428	1.941	↓	↓	None	-	0.449	X	
242-A	75.3	519.2	0.00408	1.851	↓	↓	Steel	.25/.64	0.408		Mixing Section Diameter .43 inch (1.19 cm)
242-B	80.0	551.6	0.00428	1.941	↓	↓	↓	↓	0.449		
242-C	40.9	282.0	0.00437	1.982	↓	↓	↓	↓	0.469	X	
243-A	80.6	555.7	0.00410	1.860	↓	↓	Copper	.125/.32	0.409		
243-B	82.1	566.1	0.00427	1.937	↓	↓	↓	↓	0.448		
243-C	42.0	289.6	0.00441	2.000	↓	↓	↓	↓	0.468	X	
244-A	87.8	605.4	0.00408	1.851	↓	↓	Steel[4]	.25/.64	0.408		
244-B	96.2	663.3	0.00429	1.946	↓	↓	↓	↓	0.429		
244-C	96.8	667.4	0.00432	1.960	↓	↓	↓	↓	0.432		
244-D	56.6	390.2	0.00438	1.987	↓	↓	↓	↓	0.438	X	
245-M	85.0	586.1	0.00469	2.127	0.1562	2.560	Copper	1.1/2.79	0.469		
245-N	45.5	313.7	0.00493	2.236	0.1562	2.560	Copper	1.1/2.79	0.493	X	

[1] Ambient temperature H_2/O_2 propellants and a 1.0 inch (2.54 cm) long catalyst bed were employed throughout this test series.

[2] Variable surge volume between the O_2 fire valve and sonic flow orifice utilized to induce a high mixture ratio start transient.

[3] The ratio of the oxidizer and fuel supply pressures is proportional to propellant mixture ratio.

[4] The diffusion bed steel balls were mechanically "roughened" to irregular shapes for these tests.

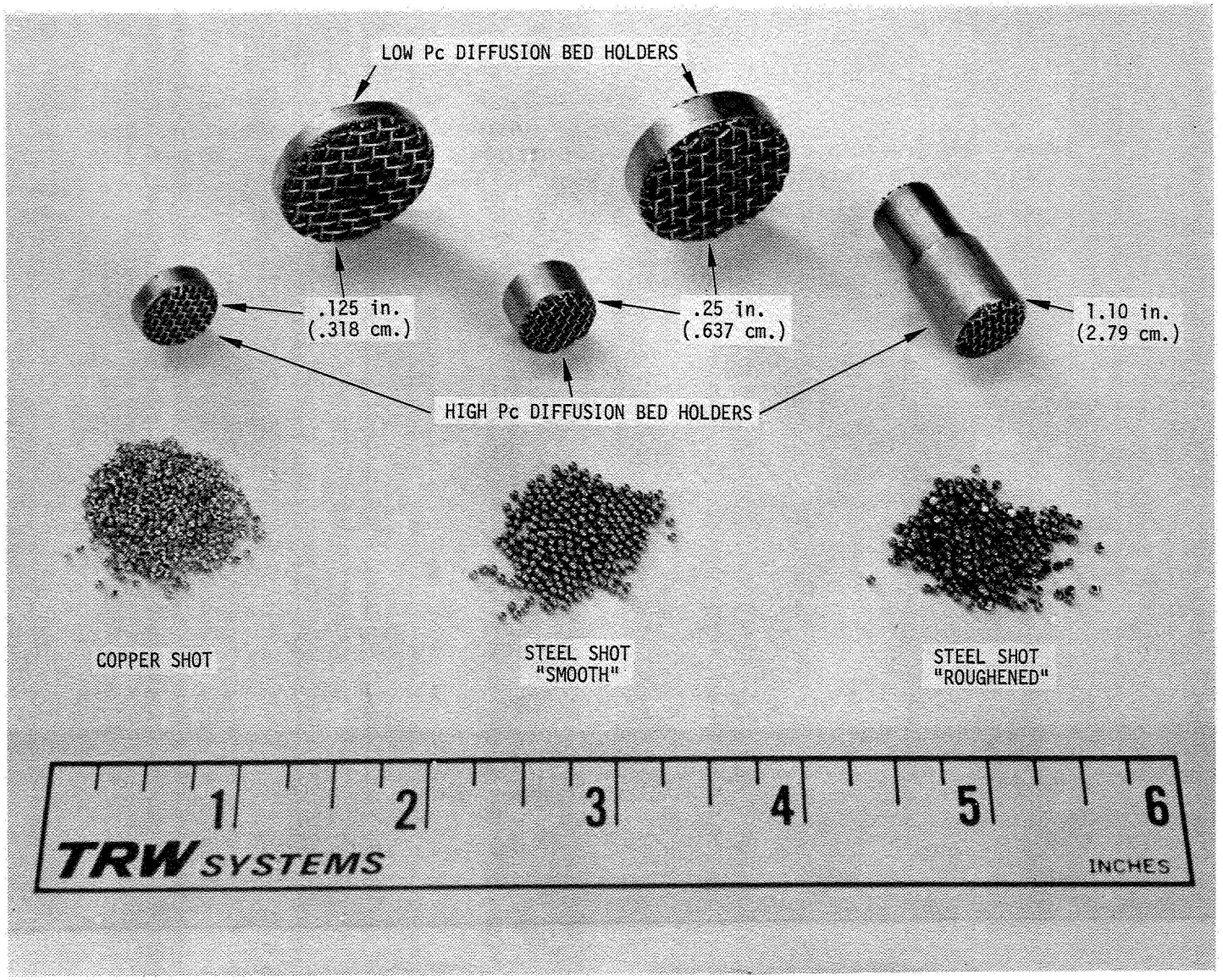

Figure 45. Igniter Diffusion Bed Configurations -
Sizes of Shot were as Follows:
Copper - 20/30 mesh, Steel - .032" (.081 cm)

Results of the high transient mixture ratio tests were later correlated through computer analysis during the igniter design scaling task (section 3.2.3). A high initial mixture ratio was also under evaluation as a means of improving igniter bed response; however, these tests results indicated that flashback could readily occur unless initial mixture ratios were carefully controlled.

3.2.1.4 Induced Injection Streaking Effects

The final flashback tests were conducted to investigate the effects on flashback of variations in mixture ratio distribution through the mixing section and catalyst bed. High mixture ratio "streaks" were induced by injecting pure oxygen through a tube installed in each reactor injector. Figure 46 shows the "streak" tube installation for the high Pc reactor. Up to 20 percent of the total oxygen flow was diverted through the "streak" tube at varied distances from the upstream surface of the catalyst be. Overall propellant mixture ratio was held at 1:1 and a minimal hydrogen lead on start-up was maintained.

Results of the induced streaking effects tests are listed in Table 14 and described as follows.

Tests 197E-I: Low pressure reactor tests with 13.5 percent of the oxygen injected at a point 1.62 inches (4.11 cm) upstream of the catalyst bed were completed with no flashbacks. These tests were performed without a diffusion bed and at igniter flow rates of 2 and 5 percent of nominal thruster flows.

Tests 198A-199B: Moving the oxygen streak injection point to 0.25 inch (0.64 cm) from the catalyst bed resulted in flashback at all flow rates, even after a steel ball diffusion bed (Figure 45) had been installed. Inspection of the hardware after tests 198B and 199B revealed that a hole was burned in the upstream catalyst retaining screen.

Tests 237D-E: High pressure reactor tests performed with 20 percent oxygen injected as a streak 1.0 inch (2.54 cm) from the catalyst bed did not exhibit flashback; however, a hole was found in the upstream catalyst retaining screen after test 237E, as shown at the right in Figure 46, resulting from the high local mixture ratio combustion temperature.

Tests 238A-C: No flashbacks occurred when 237D was repeated with a copper diffusion bed (Figure 45) as expected. No catalyst screen erosion was noted after three firings, indicating that the copper bed did help to further mix the propellants before they entered the catalyst bed.

The results of the induced streaking tests indicate that flashback is not initiated unless a very severe oxidizer streak is injected at a point close enough to the catalyst bed that essentially no mixing can take place. Diffusion ball beds may be of value to insure minimal propellant mixing, although an injector designed for reasonable propellant mixing should preclude this type of flashback initiation.

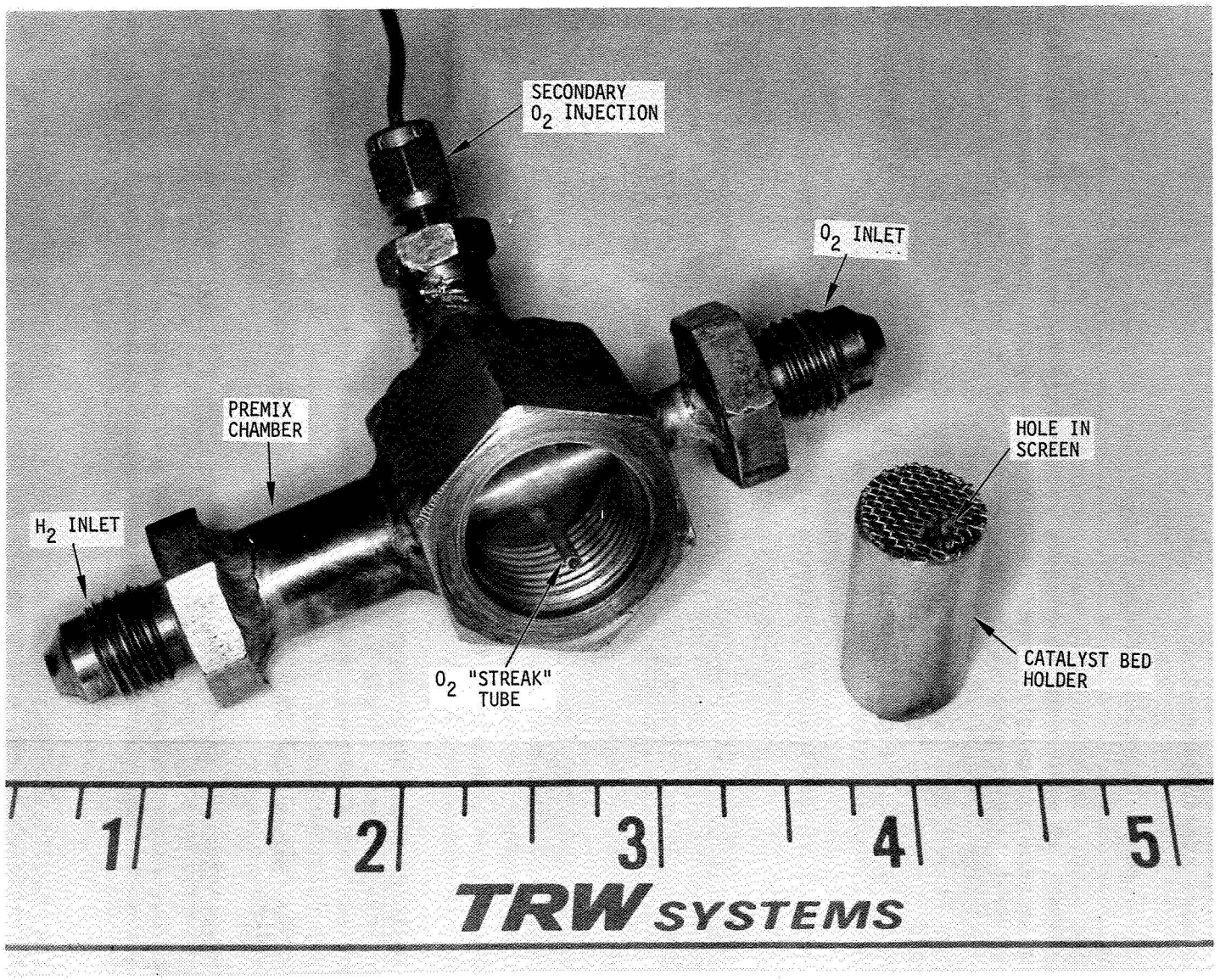

Figure 46. High Pressure Reactor Injector With Oxygen Injection "Streak Tube"

Table 14. Igniter Flashback Investigation Tests - Induced Injector Streaking Effects[1]

Test No. (HA5-)	P_{CD} lbf/in^2	P_{CD} kN/m^2	P_{mix} lbf/in^2	P_{mix} kN/in^2	$\dot{W}_{Total}$ lbm/sec	$\dot{W}_{Total}$ g/sec	% $\dot{W}_{ox}$ in Streak Tube	L[2] (in/cm)	Diffusion Bed Material	Diffusion Bed Length (in/cm)	Flashback	Comments
197-E	13.5	93.0	23.0	158.6	0.00427	1.94	13.5	1.62/4.11	None	-		Low Pressure Reactor
197-F	13.5	93.1	22.8	157.2	0.00425	1.93	13.5	1.62/4.11	None	-		Engelhard Catalyst
197-G	14.3	98.6	17.1	117.9	0.00175	0.796	13.5	1.62/4.11	None	-		Mixing Section Diameter
197-H	13.1	90.3	15.4	106.2	0.00162	0.737	13.5	1.62/4.11	None	-		0.875 inch (2.22 cm)
197-I	14.9	102.7	17.0	117.2	0.00162	0.737	13.5	1.62/4.11	None	-		A hole in upper catalyst
198-A	11.8	81.3	13.1	90.3	0.00166	0.755	13.5	.25/.64	None	-	X	retaining screen was found
198-B	16.6	114.4	23.3	160.6	0.00431	1.96	13.5	.25/.64	None	-	X	after tests 198-B and 199-B.
199-A	11.7	80.7	12.0	82.7	0.00167	0.760	13.5	.25/.64	Steel	.125/.32	X	
199-B	10.9	75.1	12.0	82.7	0.00168	0.764	13.5	.25/.64	Steel	.125/.32	X	
237-D	132.0	910.0	147.0	1013.0	0.00406	1.85	20.0	1.0/2.54	None	-		High Pressure Reactor
237-E	136.0	938.0	146.0	1007.0	0.00407	1.85	20.0	1.0/2.54	None	-		Engelhard Catalyst
238-A	108.0	745.0	136.0	938.0	0.00407	1.85	20.0	1.0/2.54	Copper	.25/.64		Mixing Section Diameter
238-B	132.0	910.0	155.0	1069.0	0.00408	1.86	20.0	1.0/2.54	Copper	.25/.64		0.43 inch (1.19 cm)
238-C	145.0	1000.0	167.0	1151.0	0.00408	1.86	20.0	1.0/2.54	Copper	.25/.64		A hole in upstream catalyst retaining screen was found after test 237-E. No damage observed after test 238-C.

[1] Ambient temperature H_2/O_2 propellants at a mixture ratio of 1.0 O/F and a 1.0 inch (2.54 cm) long catalyst bed were employed throughout the test series.

[2] L is the distance from the exit of the oxidizer streak injection tube to the catalyst bed upstream surface.

3.2.1.5 Conclusions From Experimental Results

The results of the igniter flashback limit determination tests led to the following conclusions:

- Flashback could not be induced with the high Pc igniter at pressures up to five times nominal chamber pressure with a hydrogen lead on start-up.
- Flashback was induced with the low Pc igniter only at pressures approximately three times nominal design pressure and with a mix diameter as large as the catalyst bed diameter.
- The type of catalyst, Shell 405 ABSG or Engelhard MFSA, did not affect the flashback limits.
- Flashback could be induced with either pressure level igniter by high initial mixture ratios resulting from surges in oxygen flow during the start transient.
- Although flashback limits could be modified by the use of diffusion beds of steel or copper shot upstream of the catalyst bed, diffusion beds were not capable of completely arresting flashback under all igniter transient flow conditions.
- Flashback could be induced by severe oxidizer-rich streaks, which could be dissipated by diffusion beds, but should not occur with a reasonable amount of injector propellant mixing.

Detailed analysis and correlation of the flashback test data were performed as part of the igniter scaling analysis, described in Section 3.2.3 of this report.

3.2.2 Response Enhancement Investigation

The objectives of these tests were to determine the baseline thermal response for the catalytic igniter and to evaluate methods of improving this response. Response effects were experimentally evaluated for variables such as catalyst bed configuration, initial bed and propellant temperature, thermal insulation of the catalyst bed, and propellant mixture ratio.

The same catalytic igniter assemblies and test installation used for the flashback tests were employed, with modifications to the catalyst bed configurations and/or operating conditions selected to enhance the response. The following paragraphs describe the performance of the response enhancement tests and present the experimental results and conclusions.

3.2.2.1 Baseline Response Tests

A series of igniter tests was conducted to establish baseline response at each chamber pressure level with both the Shell 405-ABSG and Engelhard MFSA catalysts. Three different catalyst bed configurations were evaluated to determine effects on overall response. The first bed configuration tested was the plain cylindrical bed utilized during the catalyst life tests and flashback limit investigations. The two additional igniter configurations, shown in Figure 47, were the bed injection and downstream oxygen injection designs.

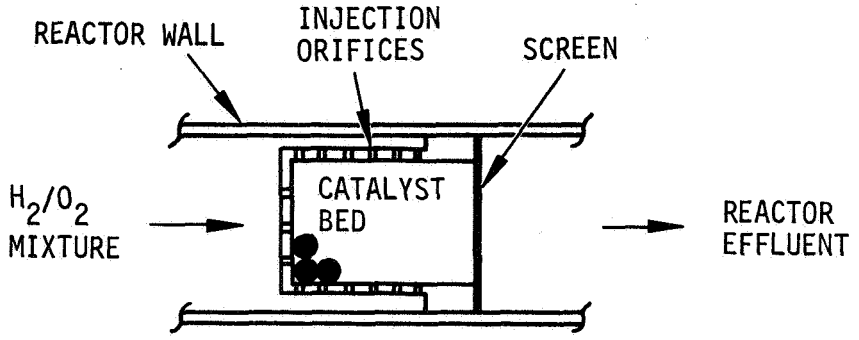

(a) Pre-mixed H_2/O_2 injection into catalyst bed

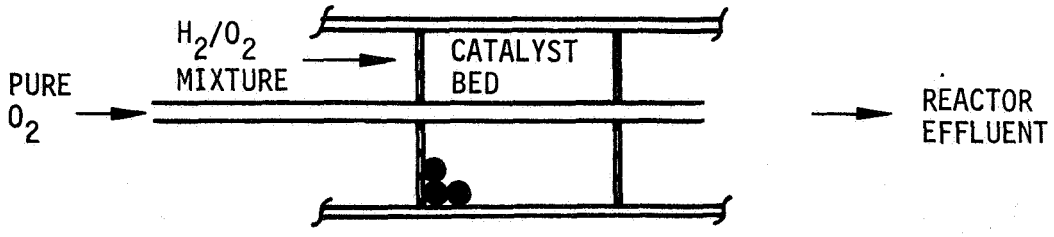

(b) Pure O_2 injection downstream of catalyst bed

Figure 47. Catalyst Bed/Reactor Configurations

The bed injection configuration attempted to enhance response by injecting the hydrogen-oxygen mixture into the bed along the sides as well as from the upstream end, significantly increasing the surface area of the bed initially exposed to incoming propellants, compared to the plain cylindrical bed (Figure 40). Catalyst bed holders were constructed from wire screen material with spacers to center the bed holder in the reactor body. Bed holders of two different lengths for the high pressure igniter are shown in Figure 48.

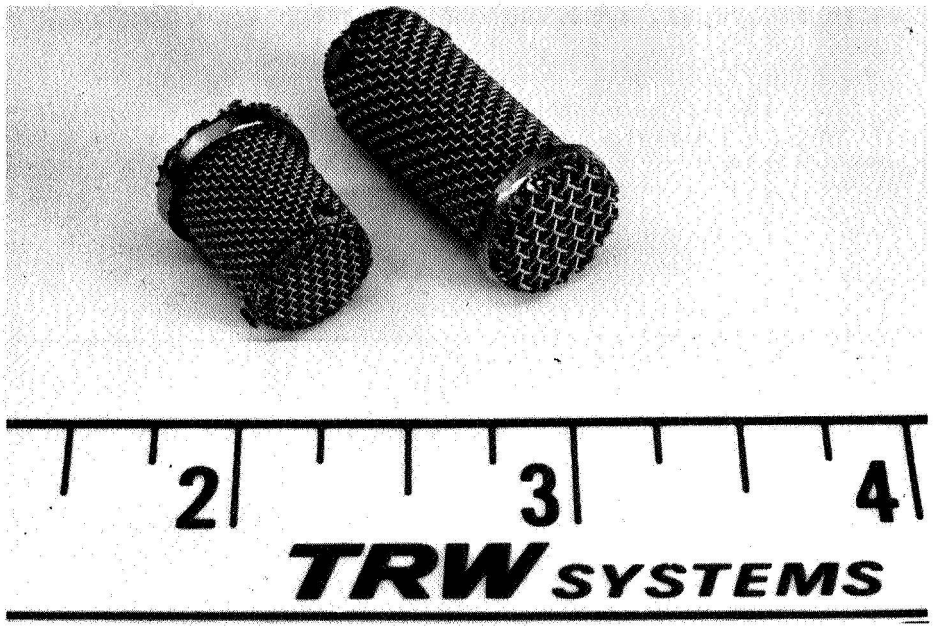

Figure 48. Bed Injection Catalyst Bed Holders

The downstream oxygen injection technique, illustrated schematically in Figure 49, was evaluated as a means of improving response by raising the mixture ratio at the downstream surface of the catalyst bed during the start transient only. Increasing mixture ratio upstream of the bed was previously found to initiate flashback (Section 3.2.1.3). It was also considered that since most of the response time of the igniter consisted of thermal delay of the catalyst bed, overall igniter response would be improved if ignition could be initiated downstream of the catalyst bed. Secondary oxygen flow was injected downstream by inserting a tube through the catalyst bed, as shown in Figure 50.

Data from the baseline response tests are listed in Tables 15 and 16 for the high and low pressure reactors, respectively. The only realistic definition of overall igniter response is the time required for the effluent gases to reach a temperature sufficient for ignition of the main thruster, approximately 1200°F (920°K). The results of these tests are described as follows.

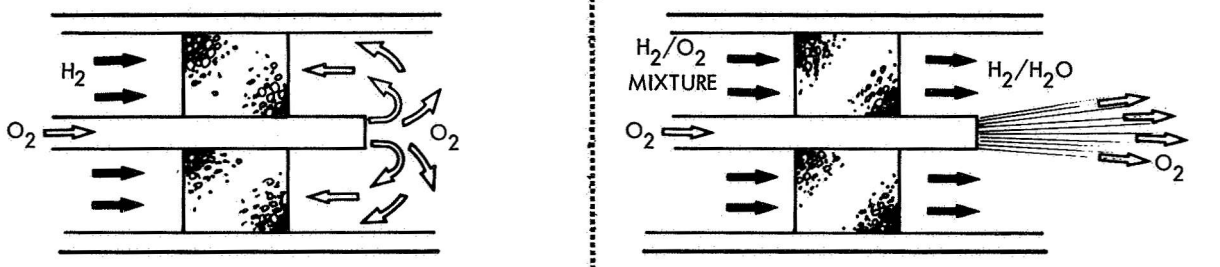

(a) IGNITION AT DOWNSTREAM SURFACE OF CATALYST BED, M.R > 10

(b) STEADY-STATE OPERATION:
H_2/O_2 MIXTURE THROUGH CATALYST BED, M.R. ~ 1.0
PURE O_2 INJECTED DOWNSTREAM

Figure 49. Downstream Oxygen Injection Technique

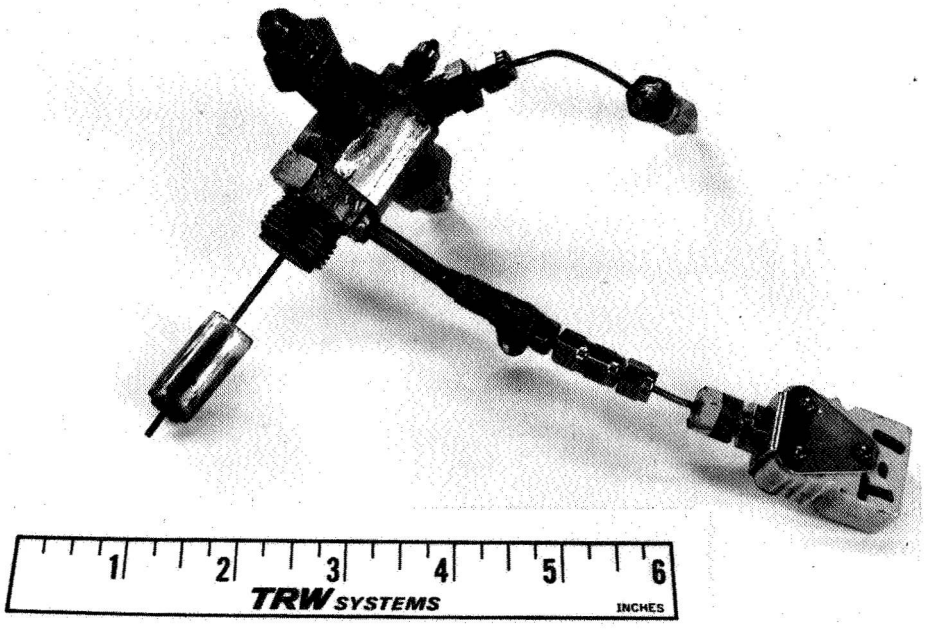

Figure 50. Experimental Downstream Oxygen Injection Test Configuration - High Pressure Igniter

Table 15. Ignitor Response Enhancement - Baseline Tests, High Pressure Reactor

Test No. (HA5-)	P_{CD} (lb_f/in^2)	P_{CD} (kN/m^2)	Prop Temp (°F)	Prop Temp (°K)	Initial Bed Temp (°F)	Initial Bed Temp (°K)	$\dot{W}_{Total}$ (lb_m/sec)	$\dot{W}_{Total}$ (g/sec)	Initial Mixture Ratio (O/F)	Time to 1200°F (920°K) (sec)	Comments
265-A	115	792	Amb	Amb	80	300	.0015	.681	0.88	1.64	
265-B	126	868	↕	↕	100	311	.0016	.726	1.0	1.02	
265-C	127	875	↕	↕	139	333	.0016	.726	1.0	0.93	Cylindrical Bed Configuration Shell Catalyst
265-G	107	738	Amb	Amb	165	347	.0032	1.45	0.88	0.57	
266-B	87.7	604	-156	169	-176	158	.0029	1.32	0.93	0.80	
278-F	127	875	Amb	Amb	143	335	.0018	.818	1.25	0.84	
278-G	145	999	↕	↕	217	376	.0018	.818	1.25	0.86	
278-H	240	1655	↕	↕	143	335	.0018	.818	1.25	0.81	
278-I	307	2115	↕	↕	113	318	.0018	.818	1.25	0.76	
278-J	84	579	↕	↕	99	311	.0037	1.68	1.06	1.55	
278-K	113	779	↕	↕	91	306	.0038	1.73	1.11	0.74	
278-L	127	876	↕	↕	152	329	.0038	1.73	1.11	0.57	
278-M	148	1020	↕	↕	182	357	.0038	1.73	1.11	0.51	
278-N	162	1118	↕	↕	212	373	.0038	1.73	1.11	0.44	Cylindrical Bed Engelhard Catalyst
278-O	388	2670	↕	↕	86	303	.0038	1.73	1.11	0.43	
278-P	585	4035	Amb	Amb	80	300	.0038	1.73	1.11	0.53	
281-H	103.7	714	- 97	202	-81	211	.0039	1.77	0.95	--	
281-I	267.4	1842	- 93	204	-75	214	.0037	1.68	1.05	0.72	
281-J	366.4	2530	-107	196	-92	205	.0037	1.68	1.05	0.93	
281-K	498.1	3430	- 99	201	-85	209	.0037	1.68	1.05	0.73	
281-T	134.9	929	- 98	201	-73	215	.0036	1.64	1.12	1.31	
275-B	144	993	Amb	Amb	135	331	.0016	.726	1.00	2.24	
275-C	127	876	↕	↕	91	307	.0016	.726	1.00	2.58	
275-D	228	1571	↕	↕	100	311	.0016	.726	1.00	2.73	
275-E	212	1462	↕	↕	113	318	.0016	.726	1.00	2.35	
275-G	108	744	↕	↕	135	331	.0034	1.54	0.89	2.56	
275-H	298	2053	↕	↕	121	323	.0034	1.54	0.89	1.43	
275-I	342	2357	↕	↕	86	304	.0034	1.54	0.89	1.25	
275-J	483	3330	Amb	Amb	108	316	.0034	1.54	0.89	1.32	Bed Injection Configuration Shell Catalyst
276-Q	118.0	814	-185	153	-186	154	.0034	1.54	0.89	1.38	
276-R	132.2	912	-182	155	-186	154	.0034	1.54	0.89	1.51	
276-S	444.4	3063	-166	164	-170	161	.0034	1.54	0.89	2.59	
276-T	245.3	1690	-182	155	-186	151	.0034	1.54	0.89	0.98	
276-V	165.9	1144	-210	139	-218	135	.0034	1.54	0.89	2.02	
276-X	264.3	1821	-220	133	-226	130	.0034	1.54	0.89	1.81	
276-Y	330.7	228	-220	133	-225	131	.0034	1.54	0.89	2.14	

Table 15. Ignitor Response Enhancement - Baseline Tests, High Pressure Reactor (Continued)

Test No. (HA5-)	P_{CD} (lb_f/in^2)	P_{CD} (kN/m^2)	Prop Temp (°F)	Prop Temp (°K)	Initial Bed Temp (°F)	Initial Bed Temp (°K)	$\dot{W}_{Total}$ (lb_m/sec)	$\dot{W}_{Total}$ (g/sec)	Initial Mixture Ratio (O/F)	Time to 1200°F (920°K) (sec)	Comments
265-E	125	861	Amb	Amb	182	357	.0042	1.91	4.25	.042	
265-F	108	744			142	335	.0070	3.18	7.75	.051	
265-M	76	523			142	335	.0088	4.00	4.0	.170	
265-N	79	544			121	323	.0097	4.41	4.70	.027	
265-O	50	344			126	326	.0097	4.41	4.70	.025	Downstream O_2 Injection Shell Catalyst
265-U	64	441	Amb	Amb	100	311	.0100	4.54	4.88	.023	
266-D	127.4	878	-156	169	-176	158	.0083	3.77	4.53	.044	
266-E	164.9	1135	-155	168	-170	161	.0082	3.72	4.53	.040	
279-E	123	848	Amb	Amb	126	326	.0046	2.09	4.75	.060	
279-F	135	931			95	309	.0046	2.09	4.75	.070	
279-J	144	992			135	331	.0046	2.09	4.75	.102	
279-K	148	1020			139	333	.0046	2.09	4.75	.120	
279-L	144	992			108	316	.0046	2.09	4.75	.075	
279-O	155	1068			156	343	.0046	2.09	4.75	.108	
279-R	158	1089			187	359	.0046	2.09	4.75	.089	Downstream O_2 Injection Engelhard Catalyst
279-S	148	1020			204	369	.0046	2.09	4.75	.094	
279-T	153	1054			178	355	.0046	2.09	4.75	.081	
279-U	135	931			117	321	.0093	4.22	4.17	.105	
279-X	214	1475			95	309	.0093	4.22	4.17	.021	
279-Z	148	1020			100	311	.0093	4.22	4.17	.023	
279-Z3	189	1303			80	300	.0093	4.22	4.17	.020	
279-Z5	259	1785	Amb	Amb	91	306	.0093	4.22	4.17	.019	

Table 16. Igniter Response Enhancement - Baseline Tests, Low Pressure Reactor

Test No. (HA5-)	P_{CD} (lb_f/in^2)	P_{CD} (kN/m^2)	Prop Temp (°F)	Prop Temp (°K)	Initial Bed Temp (°F)	Initial Bed Temp (°K)	$\dot{W}_{Total}$ (lb_m/sec)	$\dot{W}_{Total}$ (g/sec)	Initial Mixture Ratio (O/F)	Time to 1200°F (920°K) (sec)	Comments
289-K	8.7	59.9	Amb	Amb	230	384	.0019	.863	1.11	5.60	
289-L	17.4	120			221	379	.0019	.863	1.11	5.17	
289-M	22.7	157			247	393	.0019	.863	1.11	5.35	Cylindrical Bed Configuration Shell Catalyst
289-N	9.3	64.1			178	354	.0041	1.86	1.05	2.53	
289-O	21.1	146			173	352	.0041	1.86	1.05	2.65	
289-P	28.6	197			178	354	.0041	1.86	1.05	2.59	
298-D	13.9	95.7			121	323	.0019	.863	1.11	2.98	
298-E	15.8	109			139	333	.0020	.908	1.22	2.88	
298-F	20.2	139			143	335	.0020	.908	1.22	2.78	
298-G	10.5	72.4			143	335	.0041	1.86	1.05	1.51	Cylindrical Bed Configuration Engelhard Catalyst
298-H	17.2	119			165	348	.0041	1.86	1.05	1.51	
298-I	25.8	178			178	354	.0041	1.86	1.05	1.49	
298-J	23.7	163			187	360	.0041	1.86	1.05	1.48	
291-M	17	117			195	364	.0046	2.09	4.11	-	
291-O	28	193			221	379	.0046	2.09	4.11	.098	
291-Z4	28	193			113	318	.0070	3.18	6.78	.039	
291-Z7	63	434			113	318	.0070	3.18	6.78	.027	
291-Z8	75	516			99	311	.0070	3.18	6.78	.030	Downstream O_2 Injection Shell Catalyst
291-Z25	26	179			114	319	.0138	6.27	5.90	.052	
291-Z31	42	289			116	320	.0138	6.27	5.90	.065	
291-Z38	57	392			108	316	.0138	6.27	5.90	.025	
291-Z39	58	399			102	312	.0138	6.27	5.90	.030	
298-M	12.3	84.8			156	343	.0138	6.27	5.90	.092	
298-N	12.2	84.1			130	328	.0159	7.23	6.95	.058	
298-O	12.3	84.8			130	328	.0159	7.23	6.95	.052	
298-U	15.0	104			113	319	.0159	7.23	6.95	.072	Downstream O_2 Injection Engelhard Catalyst
298-V	12.7	87.5			121	323	.0159	7.23	6.95	.067	
298-Y	20.6	142			113	319	.0159	7.23	6.95	.060	
298-Z	15.7	108	Amb	Amb	152	340	.0159	7.23	6.95	.029	

Tests 265A - 266B: High Pc reactor cylindrical bed tests with the Shell catalyst showed some improvement in response as flow rates were increased. Minimum response time with ambient temperature propellants was 0.57 second. Low temperature propellants (test 266B) resulted in increased response time at flow rates comparable to test 265G.

Tests 278F - 281T: Cylindrical bed tests with Engelhard catalyst yielded a minimum response time of 0.43 second with ambient propellants and 0.72 second with reduced temperature propellants. Response was somewhat improved compared to Shell catalyst tests (265-6), which was expected because of the lower mass of the Engelhard catalyst load, thus less energy was required to heat the catalyst bed. Low temperature propellants tests also resulted in increased response times.

Tests 275B - 276Y: Bed injection tests (Figures 47a, 48) with the Shell catalyst indicated an increase in response time compared to the cylindrical bed tests 265-6. Apparently a sufficient amount of hydrogen and/or oxygen entered the sides of the catalyst bed too far downstream for complete reaction, and cooled the effluent gases through dilution of the reacted propellants.

Tests 265E - 266E: Downstream oxygen injection tests (Figures 47b, 49 and 50) yielded a major improvement in igniter overall response time. Response times as low as 23 milliseconds (0.023 second) were attained in test 265-U. Oscillograph traces from tests 265-O and 266-E are reproduced in Figure 51, indicating a response time of 25 msec with ambient propellants and 40 msec with temperatures as low as -200°F (145°K).

Tests 279E - 279Z5: Downstream injection tests with the Engelhard catalyst also resulted in greatly improved response times compared to tests with other igniter configurations. Minimum response time was 19 msec with ambient temperature propellants, slightly less than the response with the Shell catalyst.

Results of the low chamber pressure reactor tests are presented in Table 16 and described as follows:

Tests 289K-P: Low pressure tests with a cylindrical bed of Shell catalyst showed an appreciable increase in response time compared to the high Pc tests, most of this delay due to the increased thermal mass of the larger catalyst bed.

Tests 298D-J: Engelhard catalyst low pressure tests showed a response improvement over the Shell catalyst tests due to the reduced mass of this catalyst in the bed load. Response also improved as flow rates were increased.

Tests 291M - Z39: Downstream oxygen injection tests with the Shell catalyst improved response by nearly two orders of magnitude compared to the cylindircal bed tests - from over two seconds to 25 milliseconds.

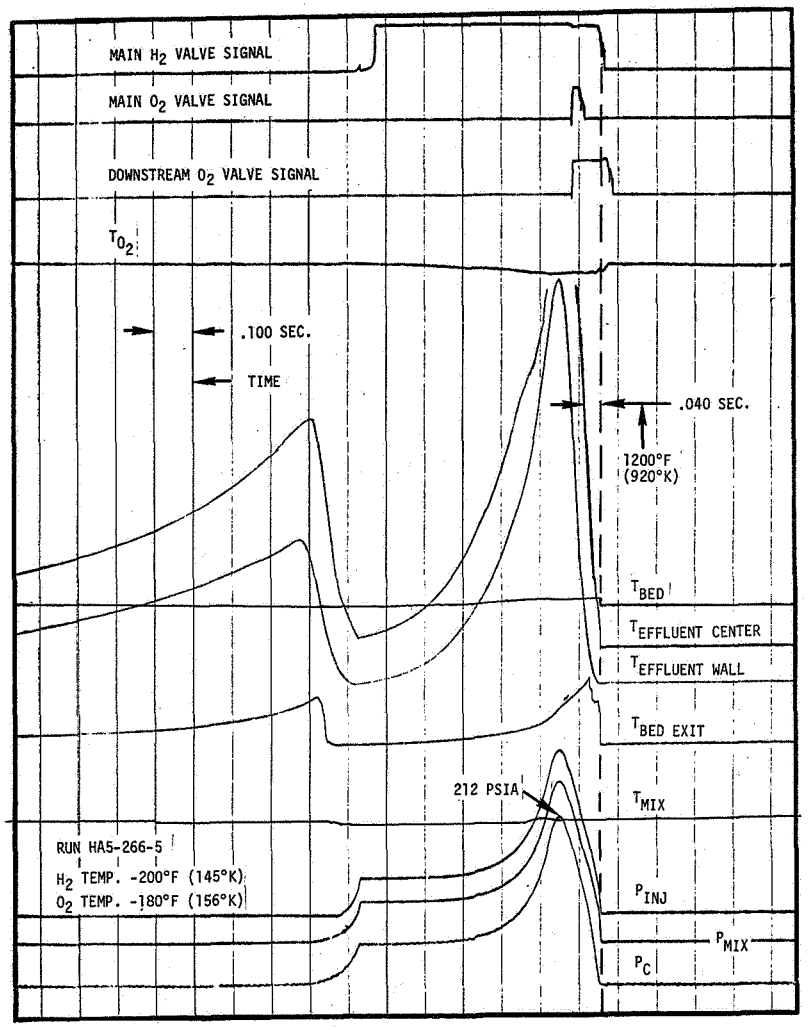

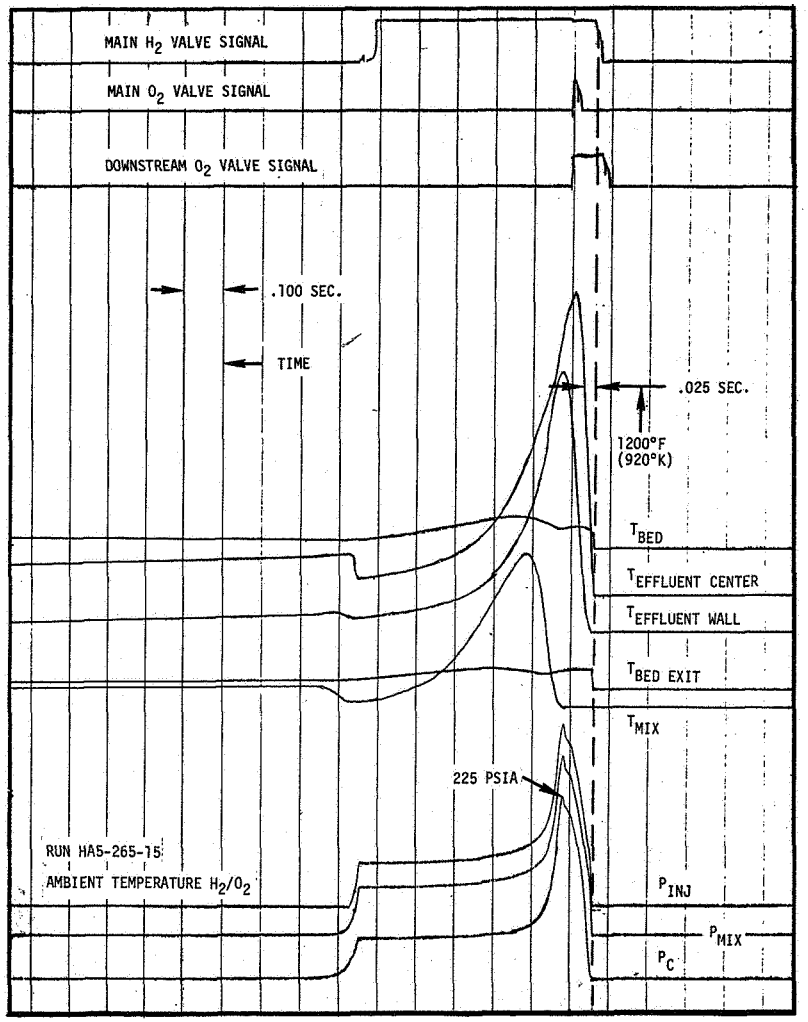

Figure 51. Catalytic Igniter Response - High Chamber Pressure, Downstream Injection, 80% of O_2 Injected Downtream

Tests 298M-Z: Engelhard catalyst tests with downstream injection yielded response times as low as 29 milliseconds with ambient temperature propellants.

Results of the baseline response tests indicated that overall response of the catalytic igniter could be reduced to one-hundredth of previous response times by injection of oxygen downstream of the catalyst bed on ignition. This accomplishment represented a major breakthrough in the development of a practical catalytic igniter for hydrogen-oxygen thrusters.

3.2.2.2 Heat Transfer Effects

The next series of response enhancement tests was performed to determine the effects of both heating and thermally insulating the catalyst bed on overall response. Heat loss from the bed to the reactor walls was minimized by containing the catalyst in dimpled 0.002 inch (0.005 cm) stainless steel holders to reduce thermal contact. The insulating foil catalyst holders for each pressure level igniter are shown in Figure 52.

The low chamber pressure igniter heat transfer tests were performed first and are described as follows. Data from these tests are listed in Table 17.

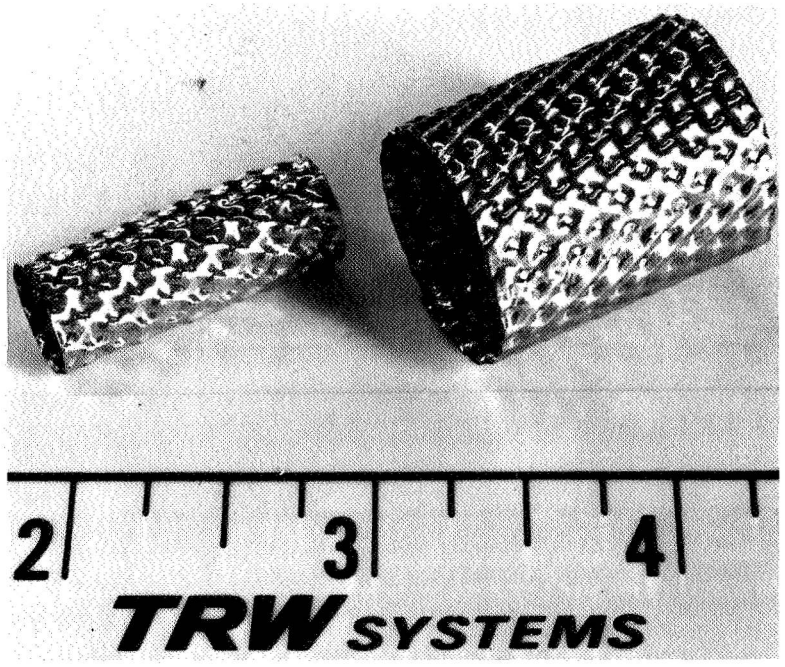

Figure 52. Catalyst Bed Insulators-
Minimum Thermal Contact

Table 17. Igniter Response Enhancement - Heat Transfer/Warm Bed Tests, Low Chamber Pressure

Test No. (HA-5)	P_{CD} (lb_f/in^2)	P_{CD} (kN/m^2)	Prop Temp (°F)	Prop Temp (°K)	Initial Bed Temp (°F)	Initial Bed Temp (°K)	$\dot{W}_{Total}$ (lb_m/sec)	$\dot{W}_{Total}$ (g/sec)	Initial Mixture Ratio (O/F)	Time to 1200°F (920°K) (sec)	Comments
299-J	14.8	102.0	Amb	Amb	110	316	.004	1.82	1.0	1.98	
299-K	15.2	104.8			112	317	.004	1.82	1.0	1.99	
299-L	15.2	104.8			108	315	.004	1.82	1.0	2.10	
299-P	15.7	108.2			493	528	.004	1.82	1.0	1.10	
299-Q	15.8	108.9			490	527	.004	1.82	1.0	1.63	
299-R	15.9	109.6			494	529	.004	1.82	1.0	-	
299-T	16.2	111.7			969	793	.004	1.82	1.0	1.21	
299-U	16.5	113.8			973	795	.004	1.82	1.0	1.17	
299-V	16.8	115.8			973	795	.004	1.82	1.0	1.18	
299-X	16.3	112.4			1179	909	.004	1.82	1.0	0.92	Cylindrical Bed Configuration Shell Catalyst
299-Y	16.6	114.4			1181	910	.004	1.82	1.0	0.96	
299-Z	16.8	115.9	Amb	Amb	1196	918	.004	1.82	1.0	0.98	
301-A	11.7	80.6	-232	127	-217	135	.004	1.82	1.0	>5.2	
301-C	22.9	157.7	-40	234	+91	306	.004	1.82	1.0	3.17	
301-G	16.8	115.9	-97	202	491	951	.004	1.82	1.0	3.18	
301-H	17.4	119.9	-93	204	484	524	.004	1.82	1.0	-	
301-O	16.3	112.3	-43	232	1180	909	.004	1.82	1.0	2.90	
301-P	16.6	114.5	-73	215	1156	897	.004	1.82	1.0	4.58	
301-Q	16.9	116.5	-98	201	1150	894	.004	1.82	1.0	>4.5	
304-B	16.2	111.7	Amb	Amb	95	308	.0033	1.50	1.06	2.07	
304-D	17.5	120.6			493	952	.0033	1.50	1.06	1.10	
304-E	18.3	126.1			493	952	.0033	1.50	1.06	1.02	
304-F	18.8	129.7			497	954	.0033	1.50	1.06	1.18	
304-H	19.4	133.8			947	780	.0033	1.50	1.06	0.41	
304-I	20.0	137.9			960	788	.0033	1.50	1.06	0.55	
304-J	20.4	140.6			960	788	.0033	1.50	1.06	0.50	
304-L	19.0	131.0			1137	886	.0033	1.50	1.06	0.26	
304-M	19.5	134.4			1154	896	.0033	1.50	1.06	0.21	
304-N	20.0	137.8	Amb	Amb	1162	900	.0033	1.50	1.06	0.19	
306-B	16.3	112.4	+18	266	80	300	.0036	1.64	1.25	1.51	Cylindrical Bed Configuration Engelhard Catalyst
306-D	19.5	134.5	+9	261	930	772	.0043	1.95	0.87	.49	
306-E	20.5	141.3	-5	253	939	776	.0043	1.95	0.87	.46	
306-G	22.0	151.7	-25	242	1074	851	.0043	1.95	0.87	.29	
306-H	22.9	157.9	-66	219	1086	857	.0043	1.95	0.87	.17	
306-J	20.9	143.0	-1	255	493	529	.0043	1.95	0.87	1.05	
306-K	20.7	142.8	+4	258	493	529	.0043	1.95	0.87	1.15	
306-L	20.7	142.8	+9	261	493	529	.0043	1.95	0.87	1.16	
306-O	18.8	129.7	+14	263	80	300	.0043	1.95	0.87	1.66	
306-P	18.9	130.3	+18	266	126	325	.0043	1.95	0.87	1.61	
306-R	16.7	115.1	-87	207	80	300	.0043	1.95	0.87	2.64	
306-S	17.0	117.2	-87	207	68	293	.0043	1.95	0.87	2.57	

Figure 17. Igniter Response Enhancement - Heat Transfer/Warm Bed Tests, Low Chamber Pressure (Continued)

Test No. (HA-5)	P_{CD} (lb_f/in^2)	P_{CD} (kN/m^2)	Prop Temp (°F)	Prop Temp (°K)	Initial Bed Temp (°F)	Initial Bed Temp (°K)	$\dot{W}_{Total}$ (lb_m/sec)	$\dot{W}_{Total}$ (g/sec)	Initial Mixture Ratio (O/F)	Time to 1200°F (920°K) (sec)	Comments
300-H	46.1	318	Amb	Amb	118	321	.0160	7.27	7.0	.075	
300-I	46.8	322	↑	↑	111	317	.0160	7.27	7.0	.058	
300-N	36.1	249	↕	↕	488	526	.0160	7.27	7.0	.039	
300-P	37.1	256	↕	↕	976	797	.0160	7.27	7.0	.034	
300-R	45.2	311	Amb	Amb	1177	908	.0160	7.27	7.0	.031	
302-A	36.9	254	+6	259	-4	252	.0160	7.27	7.0	.090	
302-D	38.9	268	-11	249	210	372	.0150	6.82	6.5	.050	Downstream O_2 Injection Shell Catalyst
303-H	40.0	276	-6	252	37	276	.0150	6.82	6.5	.059	
303-M	30.8	212	+40	278	492	528	.0160	7.27	7.0	.069	
303-R	23.5	162	-16	247	54	285	.0160	7.27	7.0	.150	
303-S	39.9	275	+20	267	52	284	.0160	7.27	7.0	.040	
303-V	41.6	287	+7	260	980	800	.0160	7.27	7.0	.085	
303-X	41.8	288	-2	255	973	796	.0150	6.82	6.5	.072	
305-I	15.8	108.8	Amb	Amb	117	320	.0153	6.95	8.56	.054	
305-J	15.6	107.5	↑	↑	161	345	.0153	6.95	8.56	.049	
305-M	14.8	102.0			493	529	.0153	6.95	8.56	.045	
305-O	14.0	96.5			493	529	.0153	6.95	8.56	.040	
305-Q	8.6	59.3			926	768	.0153	6.95	8.56	.030	
305-S	10.0	68.9			943	779	.0153	6.95	8.56	.030	
305-U	11.3	77.9	↓	↓	1099	865	.0153	6.95	8.56	.025	
305-W	9.0	62.1	Amb	Amb	1074	851	.0153	6.95	8.56	.025	Downstream O_2 Injection Engelhard Catalyst
307-E	14.3	98.5	+14	263	744	668	.0143	6.50	5.22	.050	
307-G	11.0	75.8	-5	253	964	790	.0153	6.95	5.65	.031	
307-I	11.3	77.9	41	278	510	538	.0153	6.95	5.65	.055	
307-J	11.5	79.3	37	276	502	534	.0153	6.95	5.65	-	
307-L	15.0	103.4	+4	258	80	300	.0153	6.95	5.65	.040	
307-M	14.3	98.5	-55	225	-40	233	.0153	6.95	5.65	.069	

Tests 299J - 301Q: Insulated bed tests with Shell catalyst resulted in response times approximately 20% less than with uninsulated beds (Table 16, tests 289N-P), at comparable flow rates and initial bed temperatures. Increasing initial catalyst bed temperatures as high as 1196°F (918°K) further reduced response to slightly under one second. Low temperature propellants significantly increased response times, probably due in part to some leakage of cold gases around the catalyst bed between the foil liner and the reactor wall.

Tests 304B - 306S: Engelhard catalyst tests also indicated some improvement in igniter response compared to unheated, uninsulated bed tests, but no response reductions comparable to those achieved with downstream bed injection were achieved.

Tests 300H - 303X: Response tests of combined effects of downstream oxygen injection, bed heating, and bed thermal insulation indicated no significant improvement over downstream injection tests with ambient temperature, uninsulated catalyst beds.

Tests 305I - 307M: Engelhard catalyst tests verified the above Shell catalyst test results - that heated, insulated catalyst beds had no major effect on response when applied to the downstream injection igniter configuration.

Table 18 presents the high chamber pressure heat transfer effects tests. Results of these tests with Shell catalyst were:

Tests 308H - 309Y: Tests of the insulated cylindrical bed configuration (Figure 52) indicated no noticeable response improvement compared to uninsulated bed tests 265G and 266B (Table 15).

Tests 309K - Z3: Downstream oxygen injection tests with heated, insulated catalyst beds did not achieve the response of uninsulated bed tests 265E - 266E (Table 15), the apparent difference being the increased initial mixture ratio of tests 309K - Z3.

The results of the heat transfer effects tests revealed that response time may be reduced to approximately one-half by heating an insulated bed to nearly 1200°F (920°K). This improvement is relatively minor compared to the one-hundredth fold response enhancement of downstream oxygen injection and would require an external energy source to maintain the catalyst bed at an elevated temperature.

3.2.2.3 Mixture Ratio Effects

The effects of a momentary high mixture ratio pulse during the start transient on overall igniter response was next investigated. Oxidizer surges had previously been found to initiate flashback, as described in Section 3.2.1.3. For these tests, high initial mixture ratios were attained by initiating a hydrogen lead at a low flow rate ("trickle" flow) followed by an oxygen flow sufficient to provide an initial mixture ratio from 10 to 50 O/F. After a selected pulse time (up to ten milliseconds) at this mixture ratio, a second fuel valve was opened to decrease the overall propellant

Table 18. Igniter Response Enhancement - Heat Transfer/Warm Bed Tests, High Pressure Reactor

Test No. (HA5-)	P_{CD} (lb_f/in^2)	P_{CD} (kN/m^2)	Prop Temp (°F)	Prop Temp (°K)	Initial Bed Temp (°F)	Initial Bed Temp (°K)	$\dot{W}_{Total}$ (lb_m/sec)	$\dot{W}_{Total}$ (g/sec)	Initial Mixture Ratio (O/F)	Time to 1200°F (920°K) (sec)	Comments
308-H	397	2739	Amb	Amb	251	395	.0041	1.86	1.05	0.80	Cylindrical Bed Configuration Shell Catalyst
308-I	404	2785			152	340	.0041	1.86	1.05	0.89	
308-J	408	2810			169	349	.0041	1.86	1.05	0.85	
308-K	308	2123			217	376	.0041	1.86	1.05	1.00	
308-M	362	2495			502	534	.0041	1.86	1.05	0.54	
308-N	358	2468			511	539	.0041	1.86	1.05	0.93	
309-Y	302	2081			260	399	.0042	1.91	1.33	0.519	
309-K	181	1247			68	293	.0161	7.32	7.05	0.048	Downstream O_2 Injection Shell Catalyst
309-Z	263	1813			493	529	.0162	7.36	8.00	0.085	
309-Z3	206	1420	Amb	Amb	632	617	.0162	7.36	8.00	0.095	

mixture ratio to 1:1. The data from these tests with each pressure level igniter are presented in Table 19 and the results are described as follows.

Tests 292C - 293J: Low pressure reactor tests with Shell catalyst at mixture ratios of 23.4 and below did not cause flashback but showed no response improvement over baseline tests (Table 16).

Tests 294A - 296D: Increasing initial mixture ratio of the low Pc reactor to 30.8 and 44.4 resulted in flashback with ambient temperature propellants. Flashback was initiated with low temperature propellants at initial mixture ratios as low as 11.4 O/F.

Tests 283A-K: High pressure tests with Engelhard catalyst were conducted with flashback at mixture ratio 19.8 but no flashback at 22.9 O/F, indicating some inconsistency in results. Again, no response improvement over baseline tests (Table 15) was observed.

Tests 285Z - 288K: Engelhard catalyst tests of the high Pc reactor did not result in flashback at mixture ratio 29 with low total flowrate, but flashback occurred at mixture ratio 20.6 with increased flows. Initial mixture ratios of 40 and 50 O/F caused flashback even at reduced total flow.

The results of the mixture ratio effects tests indicated that high initial mixture ratios up to 50:1 during the igniter start transient resulted in flashback before any significant improvement in response occurred. Detonations in the oxygen feed systems also occurred on two occasions during these tests, one in the O_2 injection pressure line and another in the tubing of the O_2 propellant thermal conditioning system.

The first detonation resulted in the burn-through of the O_2 injection pressure line, as shown in Figure 53, and the rupture of the O_2 injection pressure transducer, shown in Figure 54. The detonation may have been caused by contamination in the line and/or transducer; however, it occurred after numerous tests had been conducted with the same setup. Since these tests were conducted with an H_2 lead in a vacuum system, it is very likely that H_2 was present within the O_2 injection pressure line and transducer when the O_2 valve was first opened. It is possible that an explosive H_2/O_2 mixture may have been ignited by adiabatic compression when the O_2 valve opened. No damage to the igniter or catalyst bed occurred.

The second detonation occurred within the O_2 thermal conditioning system which consisted of coiled copper tubing within a liquid nitrogen container. Figure 55 shows the rupture in the copper tubing. The test was conducted with ambient propellants; therefore, the hand valve at the inlet to the heat exchanger was closed, no propellants were flowing through the heat exchanger, and the by-pass hand valve was open. Apparently, the detonation in the oxidizer feed system "dead headed" (stagnated) at this location.

Table 19. Igniter Response Enhancement - Mixture Ratio Effects Tests

Test No. (HA5-)	P_{CD} (lb_f/in^2)	P_{CD} (kN/m^2)	Prop[1] Temp (°F)	Prop[1] Temp (°K)	Initial Bed Temp (°F)	Initial Bed Temp (°K)	$\dot{W}_{Total}$ (lb_m/sec)	$\dot{W}_{Total}$ (g/sec)	Initial Mixture Ratio (O/F)	Flash Back	Comments
292-C	7.2	49.6	Amb	Amb	111	318	.00217	.985	11.8	No	Low Pressure Reactor Cylindrical Bed Configuration Shell Catalyst
292-I	7.3	50.4			103	313	.00217	.985	11.8	No	
292-M	9.3	64.1			116	320	.00217	.985	11.8	No	
292-S	9.3	64.1			147	337	.00217	.985	11.8	No	
292-W	9.4	64.8			161	345	.00217	.985	11.8	No	
292-X	7.2	49.6			213	374	.00167	.759	8.8	No	
292-Y	6.4	44.1			142	335	.00117	.532	5.9	No	
293-J	8.9	61.4			121	323	.00417	1.89	23.4	No	
294-A	7.1	48.9			130	328	.00413	1.88	30.8	Yes	
294-B	7.1	48.9			121	323	.00413	1.88	30.8	Yes	
295-A	7.0	48.3	Amb	Amb	108	316	.00409	1.86	44.4	Yes	
296-A	21.8	149	-108	196	-97	202	.00387	1.76	21.8	Yes	
296-B	36.5	252	-92	204	-87	207	.00267	1.21	14.7	Yes	
296-C	28.4	196	-92	204	-87	207	.00272	1.24	11.4	Yes	
296-D	26.6	183	-97	202	-87	207	.00409	1.86	44.4	Yes	
283-A	108	745	Amb	Amb	80	300	.01157	5.25	19.8	Yes	High Pressure Reactor Cylindrical Bed Configuration Engelhard Catalyst
283-J	180	1240			113	318	.01151	5.25	22.9	No	
283-K	164	1130			100	311	.00451	2.05	9.1	No	
285-Z	155	1068			253	396	.00130	.591	29.0	No	High Pressure Reactor Cylindrical Bed Configuration Shell Catalyst
286-I	58	400			195	364	.00130	.591	40.0	Yes	
287-H	44	303			217	376	.00098	.445	50.0	Yes	
287-J	44	303			230	383	.00098	.445	50.0	Yes	
288-K	58	400	Amb	Amb	156	342	.00196	.891	20.6	Yes	

[1] Propellant temperature measured just upstream of catalyst bed and includes effect of hardware heating on propellant temperatures.

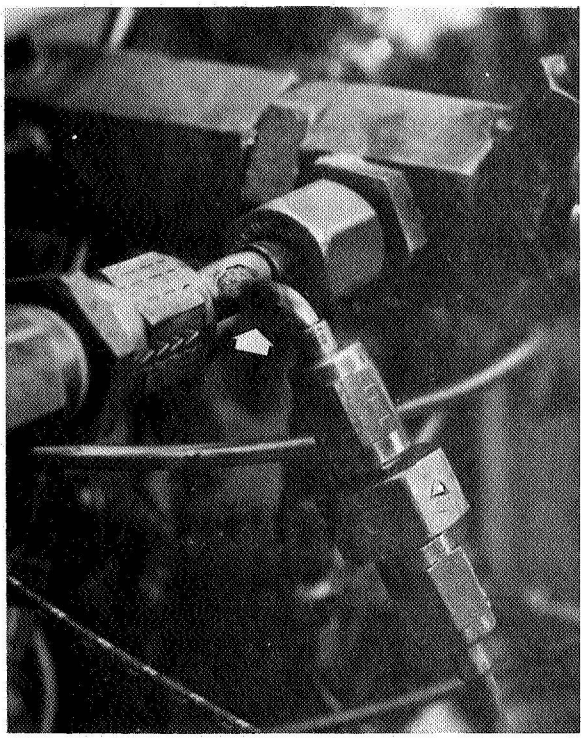

Figure 53. Transducer Line Rupture

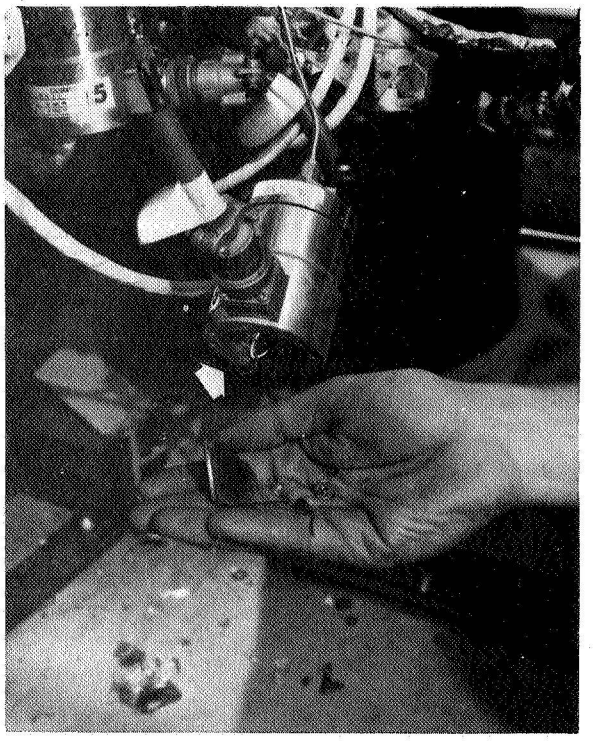

Figure 54. GOX Transducer

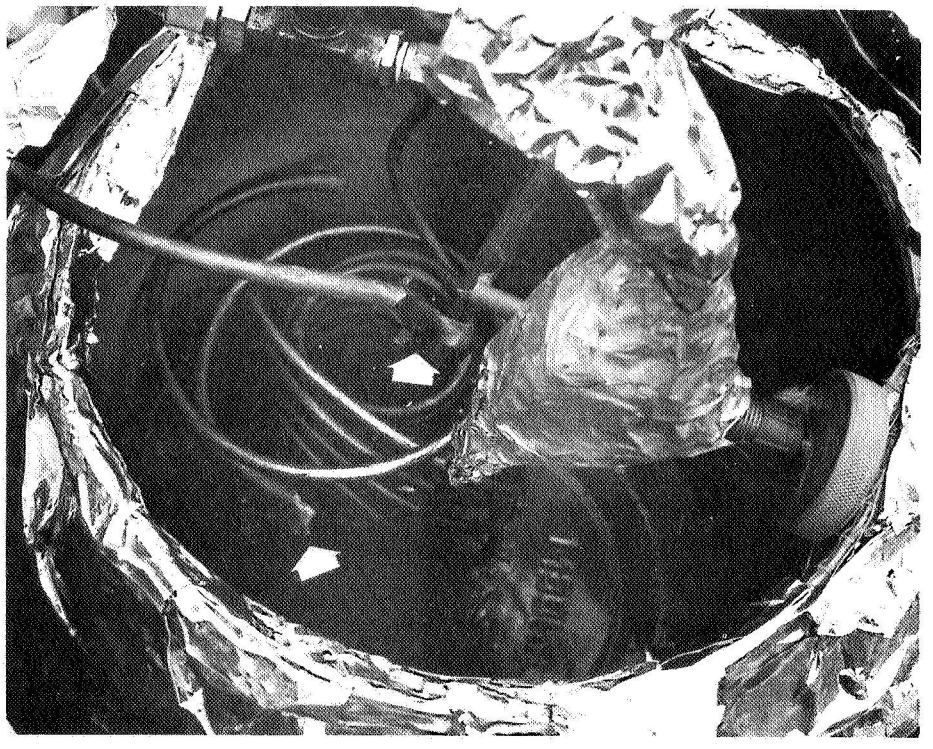

Figure 55. Heat Exchanger Rupture

3.2.2.4 Conclusions From Experimental Results

A significant achievement of the response enhancement task effort was the 100:1 reduction of the catalytic igniter overall response time, defined as the time required for the effluent gases to reach a temperature sufficient for ignition of the main thruster, approximately 1200°F (920°K). The major conclusions resulting from these tests were:

- Response times of less than 25 milliseconds can be attained with either the high or low pressure igniter by injecting oxygen downstream of the catalyst bed.
- Overall response times may be reduced by up to 20% by thermally insulating the catalyst bed to minimize heat loss to the reactor wall.
- Preheating the catalyst bed to temperatures as high as 1200°F (920°K) can reduce response times by one-half compared to ambient bed tests without downstream oxygen injection, but does not significantly improve response with the downstream injection igniter configuration.
- High initial mixture ratio propellants injected upstream of the catalyst bed during the ignition transient resulted in flashback before any noticeable reduction in response time was achieved.

3.2.3 Igniter Scaling Analysis

During this task all igniter data obtained from the catalyst life, flashback, and response tests, as well as related data from NAS 3-11227 (Reference 1), were correlated for use in establishing generalized design criteria for catalytic pilot bed igniters. Geometrical requirements were determined for pilot bed igniters for hydrogen-oxygen thrusters operating over a wide range of thrust levels, chamber pressures, and temperatures. Particular emphasis was given to mapping the design requirements for propellant mixture ratio and flashback control, response, bed loading and propellant flowrate limitations, and overall operational requirements for optimum life and reliability.

Correlation of the flashback data utilized computer modeling techniques for mapping flashback limits over extended operating conditions. Overall igniter thermal response data was correlated and compared with previous results of NAS 3-11227. Generalized igniter design guidelines were established and applied in specific designs of both high and low chamber pressure igniters for high thrust gaseous hydrogen-oxygen thrusters.

3.2.3.1 Flashback Data Correlation

Results of the flashback test series (Section 3.2.1) were evaluated to determine igniter design guidelines that would insure against flashback occurring under all anticipated operating conditions. Tests of both high and low pressure igniters indicated that flashback could be controlled by

providing a hydrogen lead on startup to insure against high initial mixture ratios. To determine the limiting transient mixture ratio resulting in flashback, analysis of the test firing data (Table 13) was conducted, utilizing an analog computer dynamic model for mapping of flashback limits over a wide range of operating conditions. This computer model, shown schematically in Figure 56, was designed to simulate the dynamic flow characteristics of the feed system used for high initial mixture ratio tests (Figure 44).

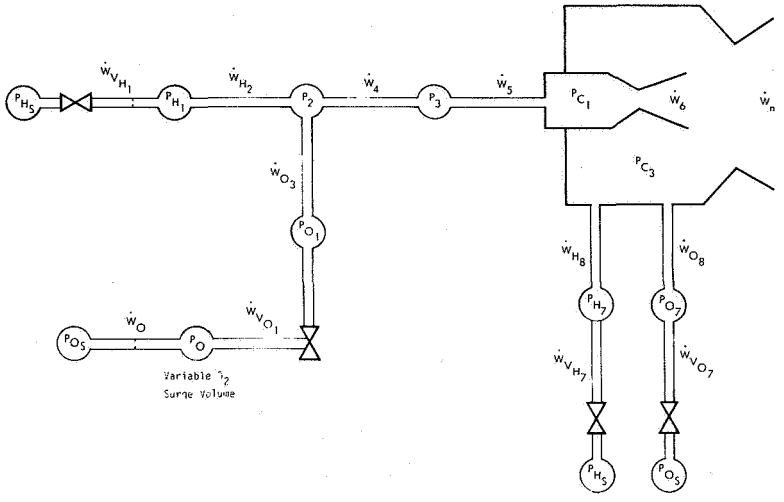

Figure 56. Computer Model Flow Schematic - Lumped Parameter Simulation of Test Correlation

Typical dynamic model simulations of actual test firing conditions are presented in Figures 57 through 59 (data from these tests were previously listed in Table 13). Comparison of the peak transient mixture ratio (upper left corner of each figure) between flashback/no flashback tests indicated that approximately 1.5 O/F was the limiting transient mixture ratio before flashback was initiated on start-up (computer runs were not automatically terminated when flashback occurred, as actual test firings were).

Correlation of both actual test firing and computer predicted flashback data is shown at the left in Figure 60. This plot indicates that the ratio of oxygen and fuel supply pressures has a secondary effect on the limiting flashback transient mixture ratio. The experimental apparatus design made it possible to very accurately determine the effects of upstream O_2 surge volume effects as shown in the right hand part of Figure 60. The overall assessment of the results indicates that the major design guideline to prevent flashback is to simply prevent mixture ratio excursions upstream of the catalyst fed from exceeding a 1.5 O/F.

Other design guidelines to prevent flashback occurrence were established after analysis of the effects of flow velocity (Section 3.2.1.2) and injector streaking (Section 3.2.1.4) on flashback. The results of the

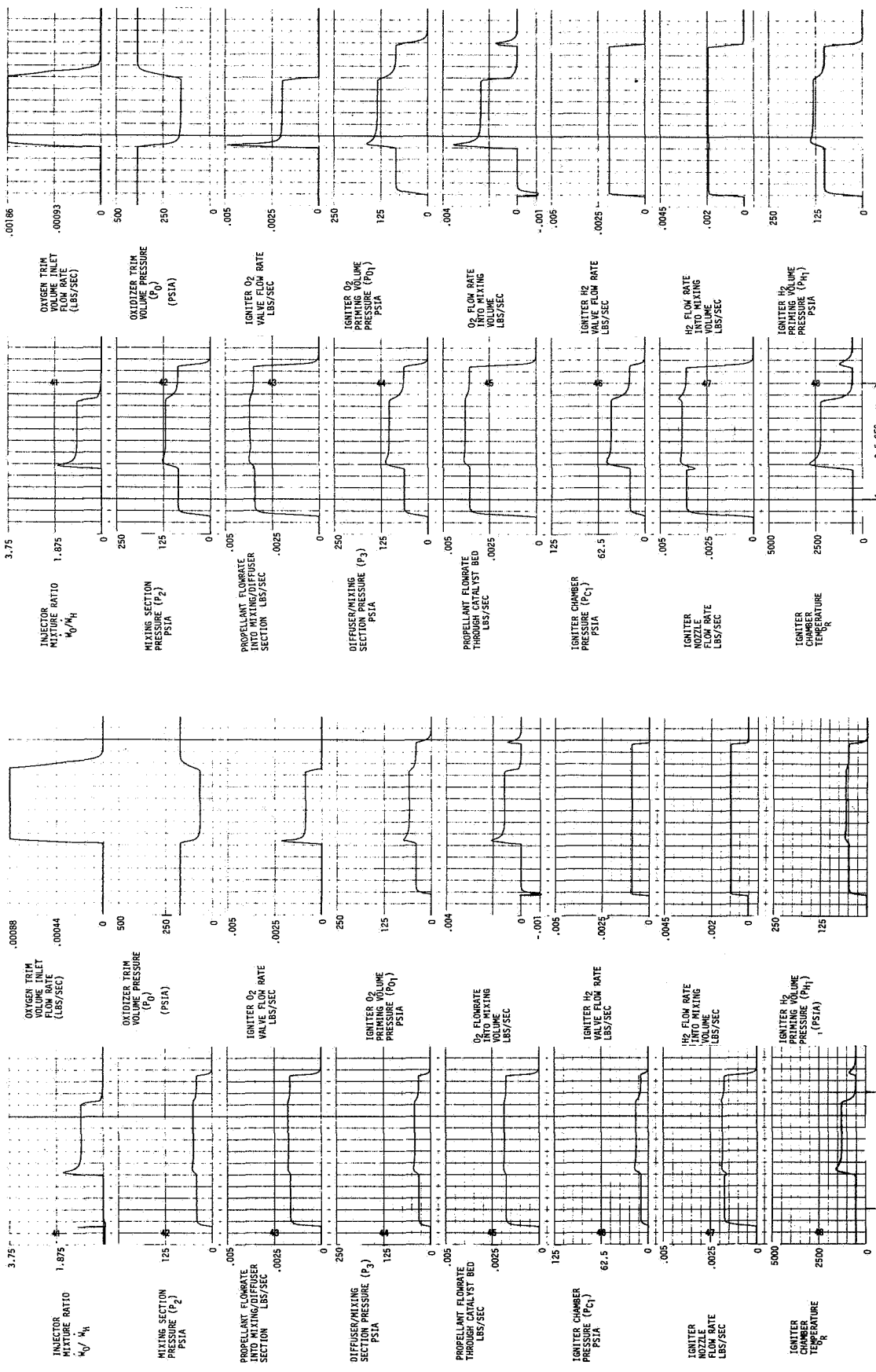

Figure 57. Computer Correlations of Test Firing Data - Variations in Oxygen and Hydrogen Feed Pressures

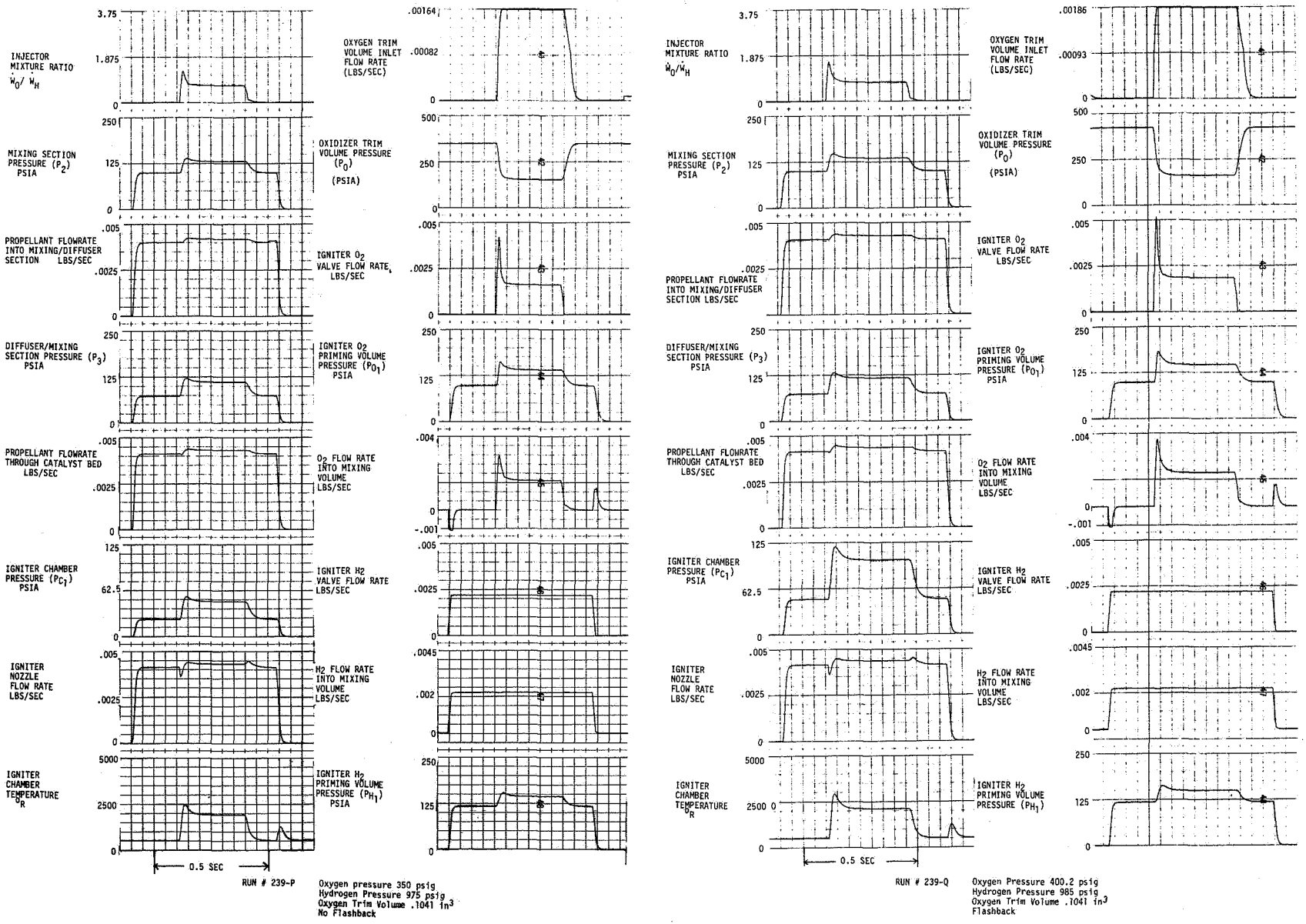

Figure 58. Computer Correlations of Test Firing Data - Variation in Oxygen Feed Pressure

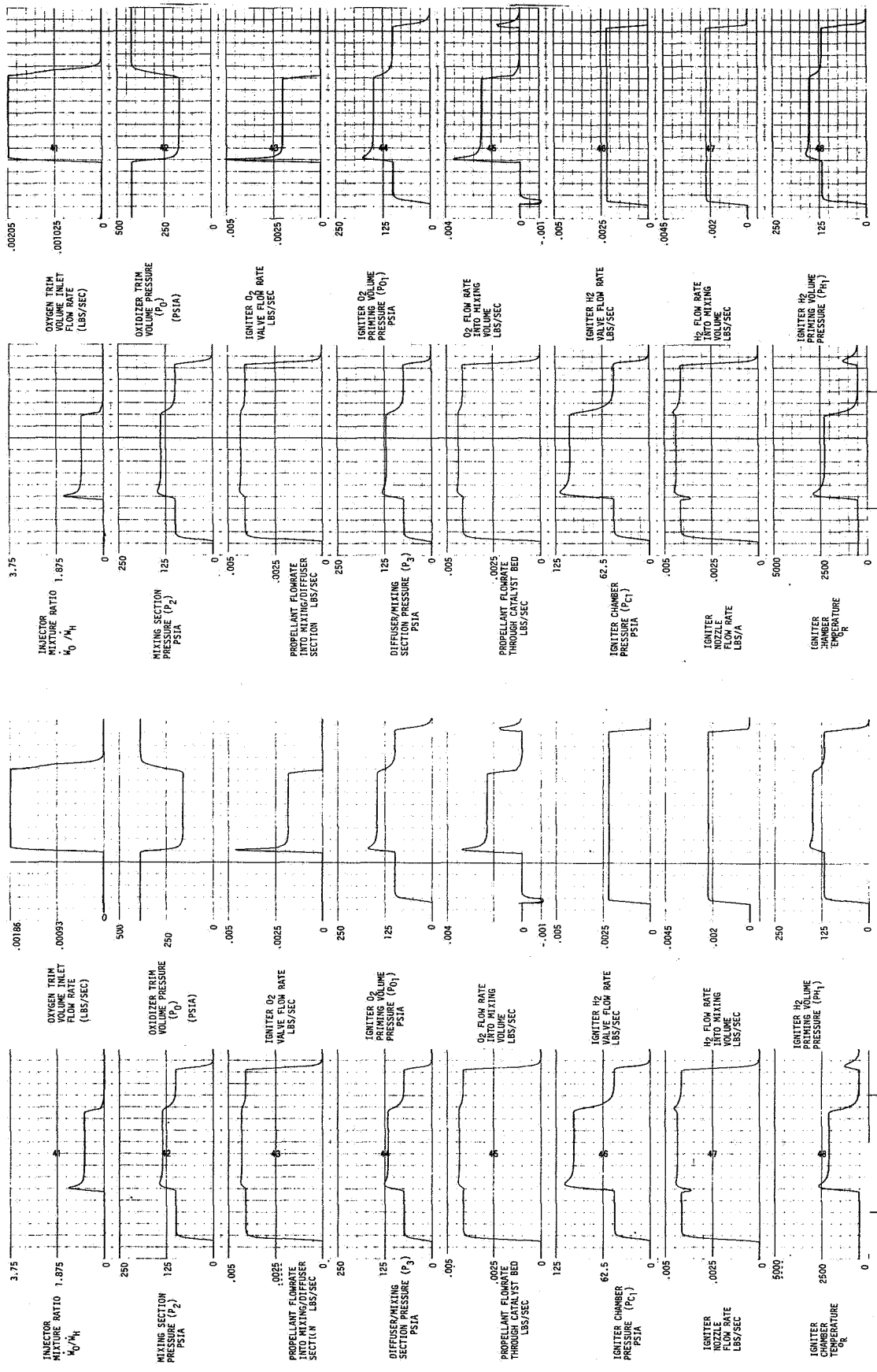

Figure 59. Computer Correlations of Test Firing Data - Variation in O_2 Feed Pressure, Reduced O_2 Trim Volume

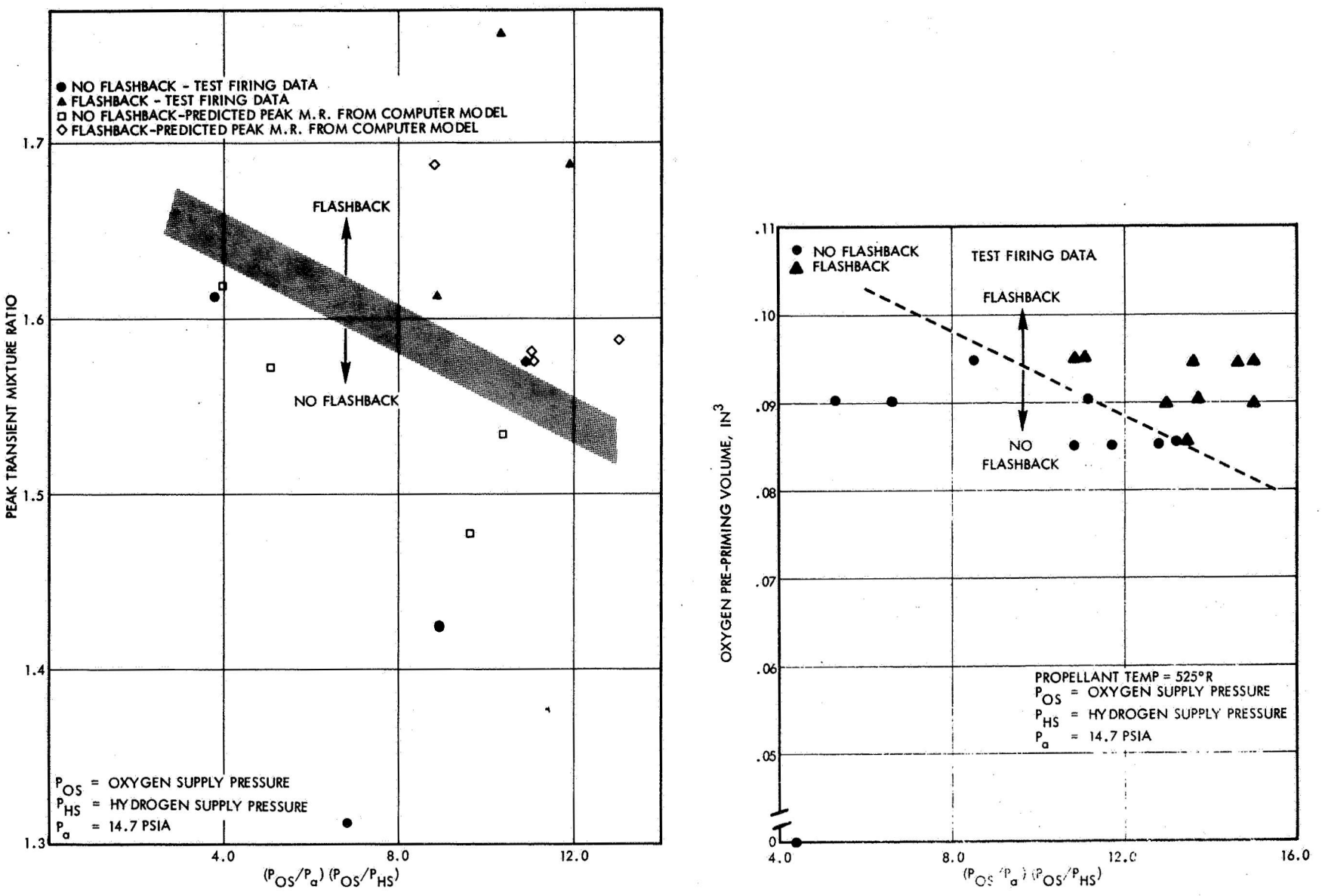

Figure 60. Catalytic Igniter Flashback Test Data Correlation

flow velocity effects tests (Table 12) are summarized in Figure 61. Based on this data, a minimum catalyst bed inlet velocity of 50 ft/sec (15 msec) was selected for both low and high pressure igniter operation. Flashbacks did occur at mix section velocities of 40 ft/sec (12 msec) with the low Pc igniter; however, this was only at chamber pressures over four times nominal Pc. Flashbacks were not induced with the high Pc igniter at velocities as low as 15 ft/sec (4.6 msec) and pressures up to 500 psia (3450 kN/m^2); however, 50 ft/sec (15 msec) was selected as a conservative minimum bed input velocity.

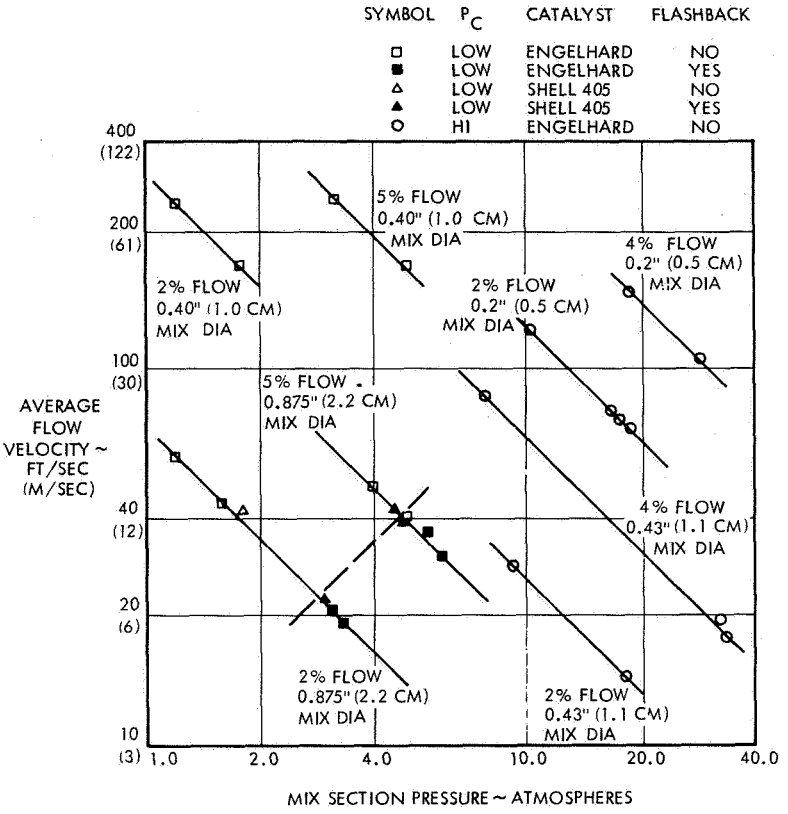

Figure 61. Igniter Flashback Test Data - Flow Velocity Effects

The induced streaking flashback tests (Table 14) indicated that only extremely non-uniform mixture ratio conditions would initiate flashback. Even a relatively inefficient mixing injector design should preclude this flashback mode. Diffusion ball beds may be utilized to further insure propellant mixing if their addition does not otherwise compromise the igniter design reliability. Diffusion beds of high conductivity, high heat capacity materials such as copper shot were not able to completely arrest flashback from the catalyst bed to the mixing injector. The type of catalyst, Shell 405-ABSG or Engelhard MFSA, did not affect igniter flashback characteristics.

3.2.3.2 Response Data Correlation

Test firing data from the response enhancement investigation (Section 3.2.2.1, Tables 15 and 16) are correlated in Figure 62. Thermal response time to effluent temperatures of 1200°F (920°K) is plotted as a function of igniter flow rate for plain cylindrical catalyst beds (without downstream oxygen injection) at each pressure level. Response time of the Engelhard catalyst beds is less than for the Shell catalyst at each pressure level because of the lower thermal mass of the Engelhard catalyst bed. This response time reduction with the Engelhard catalyst is of considerable magnitude for the low Pc tests, where the bed loads are over four times the mass of the high Pc beds.

Thermal response data from NAS 3-11227 (Reference 1) is presented in Figure 63. The response time for this correlation is defined as time to 95% of steady-state effluent temperature, and the times are correspondingly longer compared to the response times to 1200°F (920°K) in Figure 62. Also, the slopes of the lines in Figure 62 are steeper, indicating nearly a linear inverse relationship between response time and flow rate, compared to Figure 63 data, where response time decreased as the square root of the igniter flow rate for each bed configuration.

Results of the heat transfer effects (Section 3.2.2.2) and the mixture ratio effects (Section 3.2.2.3) response tests indicated no major improvement in overall igniter response time could be achieved by these methods. However, a 100:1 reduction in response was attained with each pressure level igniter by injecting oxygen downstream of the catalyst bed, as described in detail in Section 3.2.2.1. Overall response times of 25 milliseconds were measured at each chamber pressure level with downstream oxygen injection (Tables 15 and 16). These response data supersede all previous igniter response criteria established during this program and NAS 3-11227 (Reference 1). Based on these test results, the downstream injection igniter design was selected for all further igniter testing and evaluations.

3.2.3.3 Generalized Igniter Design Guidelines

Analysis and correlation of all igniter test data generated during this program and NAS 3-11227 has resulted in the following generalized design guidelines for catalytic igniters:

- Catalyst life can be maximized by operating the bed at as low a temperature as possible and still provide an effluent temperature above 1200°F (920°K) to insure main thruster ignition. Downstream oxygen injection provides a high temperature effluent with low catalyst bed operating temperatures.

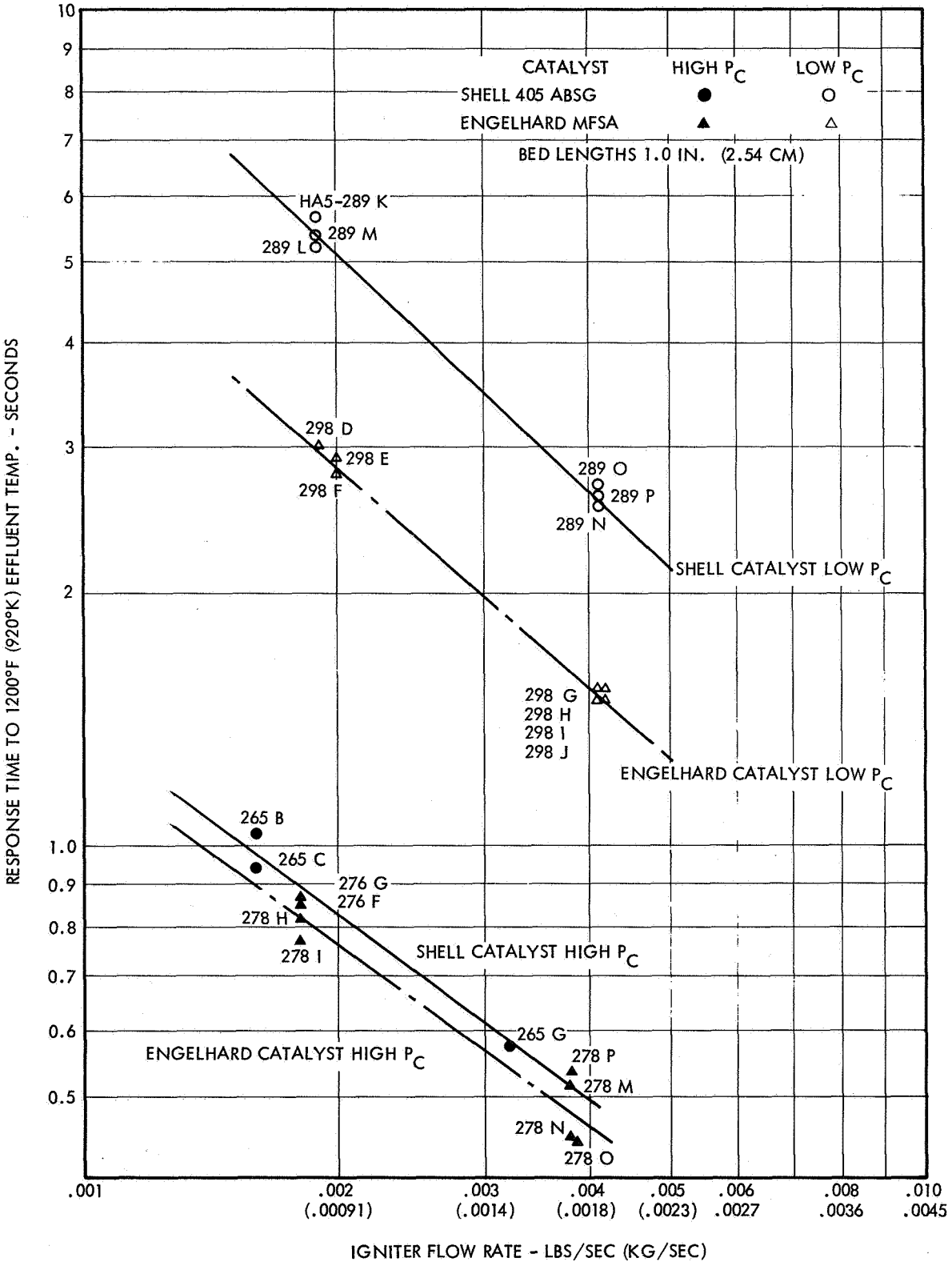

Figure 62. Correlation of Igniter Bed Response Data - Thermal Response to 1200°F (920°K) Versus Flow Rate

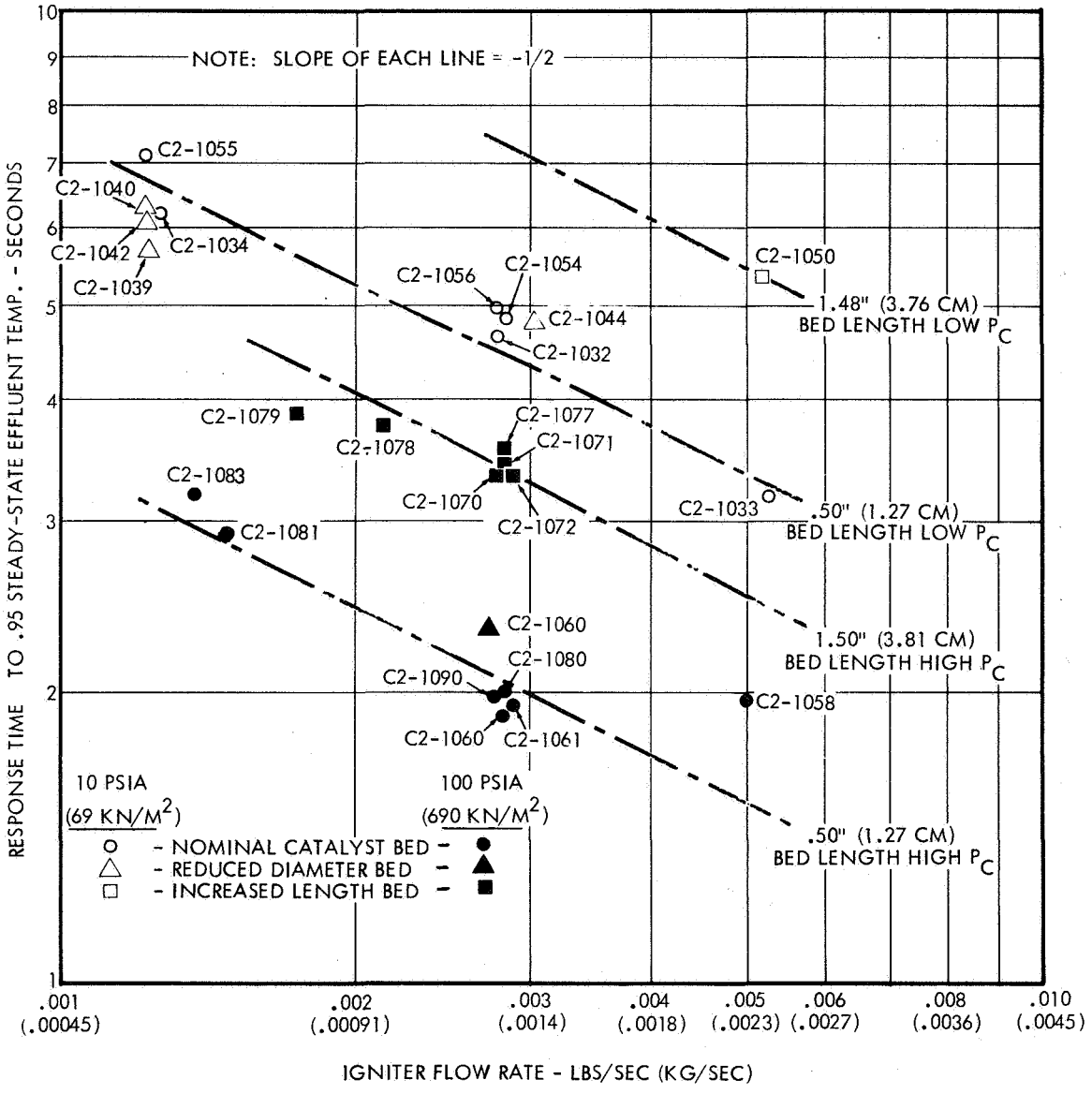

Figure 63. Correlation of Igniter Bed Optimization Data — Thermal Response to 0.95 Steady-State Effluent Temperature Versus Flow Rate (NAS 3-11227)

- Flashback from the catalyst bed to the mixing injector can be precluded by insuring hydrogen leads on startup, keeping mixture ratios upstream of the catalyst bed below 1.5 O/F during transients as well as steady-state operation, maintaining mixing section velocities above 50 ft/sec (15 msec), and avoiding oxidizer-rich streaks by adequate injector mixing and/or diffusion ball beds upstream of the catalyst bed.

- The downstream oxidizer injection igniter configuration was selected after exhibiting a 100:1 improvement over previous catalytic reactor thermal response. Overall response times of 25 milliseconds were attained over a wide range of igniter pressure levels and flow rates.

- Igniter flow rates of 2 percent of nominal thruster flows were selected as baseline design conditions. High response thruster ignitions have been attained with igniter flows as low as one-half of one percent of thruster flows, and no minimum flow requirement has been experimentally determined. The conclusion from NAS 3-11227 (Reference 1) that the primary requirement for thruster ignition was a minimum igniter effluent temperature rather than an energy limit appears to be substantiated by the results of this experimental program as well.

These basic design guidelines were incorporated in the design of two specific igniters for high thrust hydrogen-oxygen thrusters at widely varied operating pressures. Selection of these example cases was approved by the NASA/LeRC Project Manager. Figure 64 shows the basic catalytic igniter designed for a 1500 lbf (6672 N) thrust, 300 psia (2068 kN/m^2) thruster. Overall propellant mixture ratio is 1:1, with 90% of the total igniter hydrogen flow used for cooling the reactor combustion chamber. Ten percent of the igniter hydrogen and oxygen pass through the catalyst bed at a mixture ratio of 1:1 or lower. The remaining 90% of the oxygen is injected downstream of the catalyst bed to provide high response downstream bed ignition and to raise the local mixture ratio to 10 O/F to provide a high temperature effluent for reliable thruster ignition. The high pressure catalytic reactor in Figure 64 was fabricated and tested, with a high thrust, high chamber pressure hydrogen-oxygen thruster, as described in Volume II of this contract report.

A second design case was for an igniter for a low pressure thruster igniter, 15 psia (103.4 kN/m^2) chamber pressure, also at the 1500 lbf (6672 N) thrust level. The basic design of this reactor is shown in Figure 65. This all-welded design represents a flight-type igniter configuration, compared to the threaded assembly test igniter design in Figure 64. Downstream oxygen injection and an overall mixture ratio of 1:1 with 10:1 O/F downstream of the catalyst bed were also selected for the low pressure high thrust igniter design.

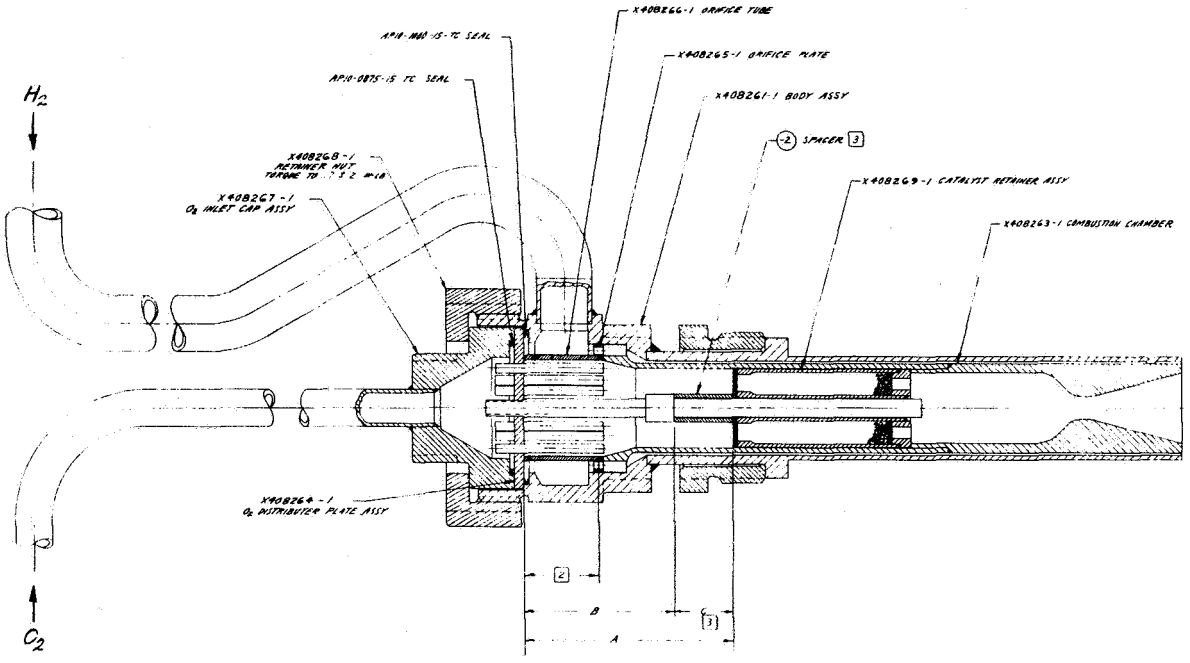

Figure 64. Catalytic Reactor — Downstream O_2 Injection, High Chamber Pressure

Design Features -

1. Combustion Chamber ID = .470" (1.19 cm)
2. Copper Combustion Chamber, Cooled by 90% of H_2.
3. O_2 Downstream Injection Tube, .090" (.229 cm), I.D. 90% of O_2 through Injection Tube.
4. Axial Diffusion Pre-Mix Section
   - o 36 O_2 tubes, .007" (.018 cm), I.D. by .720" (1.84 cm) long.
   - o Diffusion Distance = 3.4" (8.6 cm).

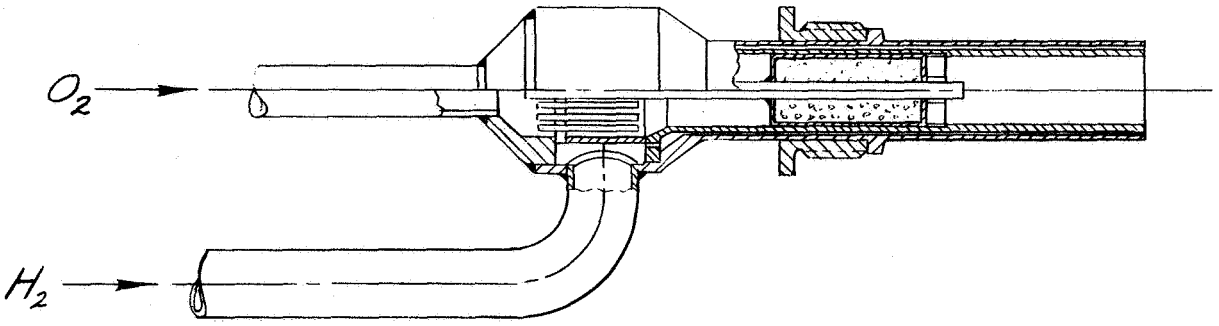

Figure 65. Catalytic Reactor-Downstream O_2 Injection - Low Chamber Pressure

3.3 ENVIRONMENTAL EFFECTS DETERMINATION

Both laboratory evaluations and igniter firing tests were conducted to determine the effects of various potentially degrading environmental conditions on the performance of catalytic hydrogen-oxygen igniters. The objectives of this experimental task were:

- Perform laboratory evaluations to identify the environmental conditions which most severely affect catalyst activity, as determined by chemisorption tests measuring the active surface areas of catalyst samples before and after exposure.
- Simulate typical space shuttle flight profiles, including exposure to potentially degrading environments such as salt spray, humidified and polluted air, and reentry heating.
- Determine the effects of these simulated flight profiles on hydrogen-oxygen ignition characteristics by conducting igniter test firings after each change of environmental exposure conditions.

These investigations were performed to determine catalyst environmental effects during shuttle vehicle earth residence (earth stay simulation) and reentry (reentry simulation), and to indicate effective catalyst protection methods, if necessary.

3.3.1 Earth Stay Effects

The effects on catalyst activity of the following simulated earth stay environmental exposures were investigated for both the Shell 405-ABSG and Engelhard MFSA catalysts.

- Oxygen during earth stay (thirty day clean, dry air soak under ambient conditions)
- Polluted humid air during earth stay (30 minutes, 24 hours, 30- and 50-day soaks at ambient conditions)

- Salt spray at ambient conditions (24-hour earth stay)

Laboratory screening tests were first performed to identify the soak conditions having the most effect on catalyst activity. Catalyst loads were then exposed to these selected environmental conditions and evaluated during full scale igniter firing tests at both high and low chamber pressure levels.

3.3.1.1 Laboratory Evaluations

All catalyst samples tested were pretreated in accordance with the standard procedure (Section 3.1.1.3) established during previous programs. The catalytic activity of each sample was measured immediately after each exposure (soak) and compared to that obtained from samples not exposed to any environment (no soak tests). Sample size varied from 0.5 to 2 grams.

Catalytic activity was determined by low temperature, low pressure hydrogen adsorption rate measurements [-78°C (195°K), 1 torr hydrogen pressure] and by maximum adsorption capacity at 200°C (473°K) (equilibrium hydrogen adsorption as a function of pressure). A BET (Reference 2) type apparatus was used for controlled exposures and activity determinations, and was previously described in Section 3.1.1.3 of this report.

The polluted-humid air was synthetically prepared at TRW Systems from VW engine exhaust and sulfur dioxide-nitrogen cylinder gas mixture. The stock gas mixture was diluted with clean air and analyzed chromatographically as well as by Beckman NDIR and flame ionization analyzers. The final composition was as follows (dry): oxygen = 20.5%, CO_2 = 1500 ppm, CO = 20 ppm, SO_2 = 20 ppm, hydrocarbons 19 ppm (as propane), NO_2 = 17 ppm, balance nitrogen. The water vapor was estimated at 1.5% $\pm$ 0.5 by volume (approximately 50% saturated).

The above composition simulates severely polluted atmosphere. For comparison purposes, one sample of each catalyst was exposed to Redondo Beach, California air for 30 days. Two samples (one Shell and one Engelhard) were exposed for 24 hours to 5% sodium chloride spray in a salt spray chamber (salt spray soak).

The data presented in Figures 66 and 67 indicate the effects of oxygen, water vapor and pollutants, salt spray, and exposure time during earth residence of the spacecraft on the catalytic activity of the thruster igniters. All soaks were performed at ambient temperature and pressure. The pretreated catalyst samples were soaked in the environments and for the duration indicated, evacuated for 4 hours (ascent simulation), and cooled to -78°C (195°K) for hydrogen adsorption measurements. Subsequent to rate measurements the samples were heated to 200°C (473°K) for the equilibrium hydrogen adsorption determinations.

The three 30-day soaks were performed in order to furnish information on the effects of oxygen, water vapor and pollutants, and pollutant concentrations on catalytic activity (Redondo Beach air pollutant concentrations are on the average lower than those of the synthetic polluted air used by at least a factor of two). The 30 minutes, 24 hour, 30 and 50 day soaks were employed to study the effect of exposure duration on catalytic activity; highly polluted air was utilized to furnish the most severe test.

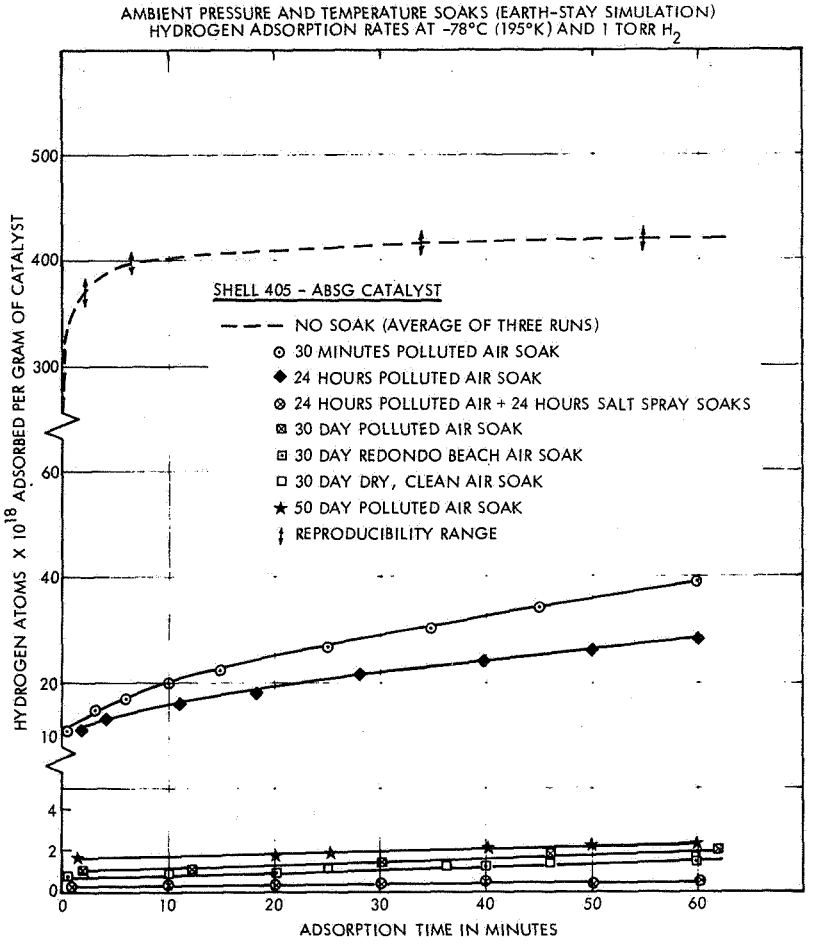

(a)

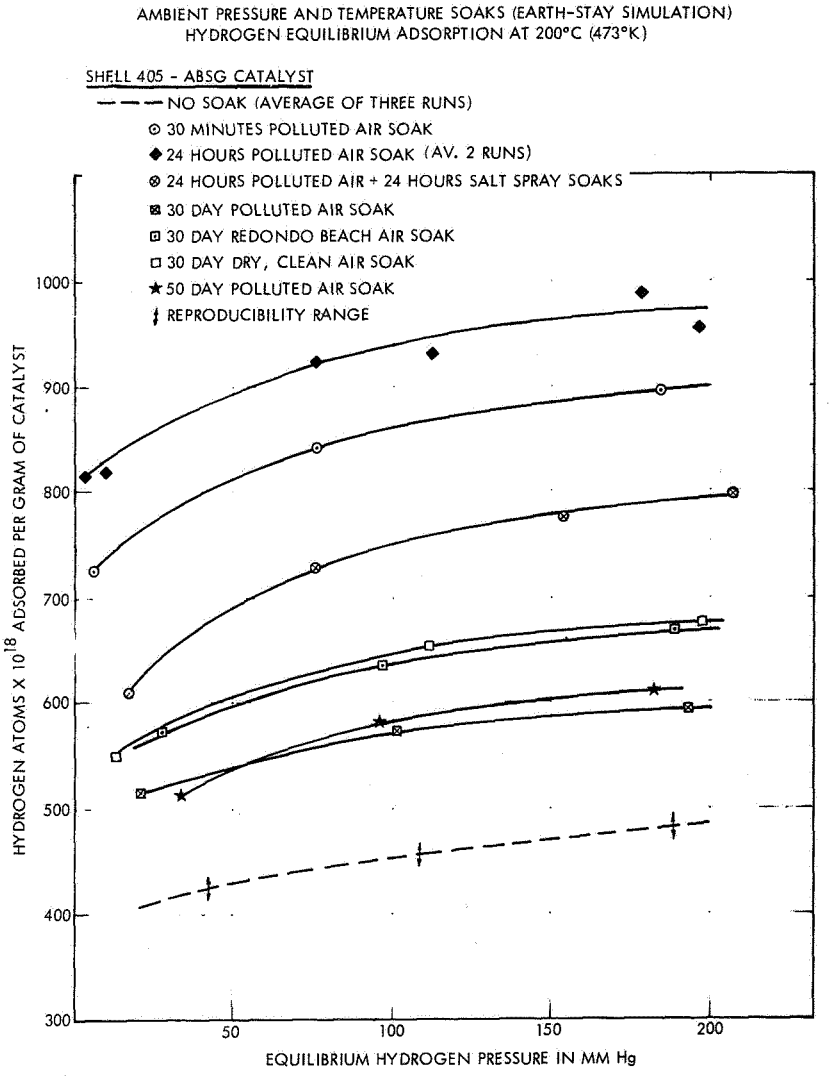

(b)

Figure 66. Effects of Earth Stay Simulations on Activity of Shell Catalyst

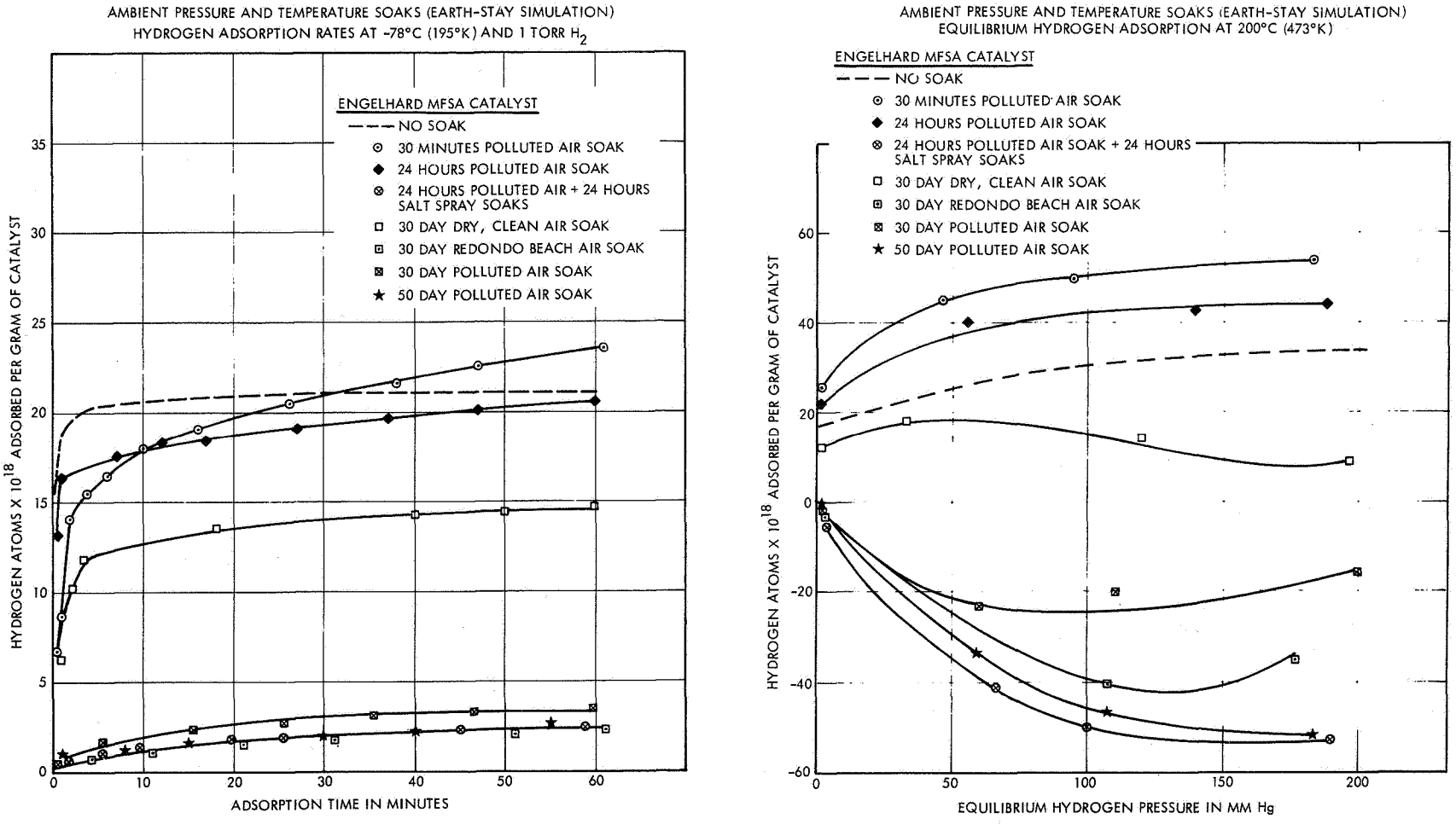

(a) (b)

Figure 67. Effects of Earth Stay Simulations on Activity of Engelhard Catalyst

These tests were also designed to furnish data on the need for protective measures against catalyst poisoning during prolonged earth residence of the space shuttle vehicle. The salt spray soak exaggerates spacecraft residence near sea coasts.

Shell 405-ABSG Catalyst. Figure 66a illustrates the effects of the various environmental soaks on low temperature hydrogen adsorption rates on Shell 405 catalyst:

- All seven soaks had a pronounced effect on the catalytic activity at low temperatures.
- The rate of adsorption dropped by a factor of approximately 20 when soaks in polluted air were restricted to 30 minutes and 24 hours and by at least an additional order of magnitude for all other soaks. Increase in exposure duration appeared to increase catalytic activity deterioration; this increase leveled off sometime prior to 30 days.
- Pollutants and normal humidity did not affect catalytic activity when present in air (compare 30-day soaks in dry, clean air and humidified, polluted air).
- Salt spray affected catalytic activity approximately as much as a 30-day exposure to air. Prior to salt spray soak, the same sample was soaked in polluted air for 24 hours. Comparison of the two sets of data (24 hours in polluted air versus 24 hours in salt spray chamber) indicated that salt spray treatment reduced the adsorption rate by a factor of 100. Whether sodium chloride was responsible for the excessive deterioration or not is not clear. During this soak the catalyst samples were flooded with the solution; therefore, water, frozen at -78°C (195°K) could be principally responsible for the observed low hydrogen adsorption rates. The sample was partially dried and evacuated for four hours prior to the rate measurements, but water in the pores cannot be driven off by evacuation at room temperature. If NaCl caused the activity deterioration, the poisoning of the catalyst would have been permanent. The equilibrium adsorption measurements on the same sample (Figure 66b) indicate that this is not the case. The principal culprit appears to be the water. Normal water vapor in the air does not affect catalytic activity (beyond the oxygen effect), but if water is allowed to condense in the pores of the catalyst its effect in low temperature reaction rates is severe.

Figure 66b presents the equilibrium hydrogen adsorption data on Shell 405 catalyst samples soaked in the environments described above. The following observations were made:

- All seven soaks affected the maximum hydrogen adsorption capacity of the catalyst, but in all cases the effect was positive.

- The volume of hydrogen adsorbed decreased with increase in exposure time, but in all cases it was greater than that absorbed by the unexposed (not soaked) samples.

- Pollutants or water vapor or both appear to have had some effect on the quantity of hydrogen adsorbed, but it was minor. The same was true of salt spray.

- Extension of exposure time from 24 hours to 30 days reduced the catalyst's hydrogen capacity by 30%.

Engelhard MFSA Catalyst. Figure 67a presents the data on the effects of ambient air (clean and polluted) and salt spray for hydrogen adsorption rates on Engelhard MFSA catalyst. The following observations were made:

- Soaks of 24 hours or less in humid polluted air had no appreciable effect on hydrogen adsorption rates at -78°C (195°K).

- Thirty day clean, dry air soaks caused an average 30% reduction on hydrogen adsorption rates.

- Soaks of 30 or more days in polluted air and 24 hours in salt spray reduced low temperature hydrogen adsorption rates by 90%. Thus, humidity and/or pollutants have an effect on this catalyst at low temperatures.

Figure 67b summarizes the equilibrium hydrogen adsorption data on Engelhard MFSA catalyst samples soaked with air and salt spray under ambient conditions. The data indicated the following:

- Ambient polluted air soaks of 24 hours or less had a small positive effect on the hydrogen adsorption capacity of the catalyst.

- Thirty day dry, clean air soaks affected only slightly the capacity of the catalyst for hydrogen at pressures below 50 torr. At higher pressures (up to 200 torr) limited desorption was observed. However, in the entire pressure range investigated hydrogen adsorption remained positive.

- Lengthy ambient soaks in humid polluted air and the 24 hour salt spray soak caused the catalyst to exhibit negative adsorption (net desorption) when treated with hydrogen at 200°C (473°K). The number of molecules desorbed from the catalyst surface exceeded the number of hydrogen molecules adsorbed on it. Comparison of the thirty day dry and humid air curves and the salt spray curve with the 24-hour polluted air curve indicated that water vapor desorbs from the catalyst at this temperature.

Data Reproducibility. A number of experimental tests were performed twice in order to verify the validity of the observed effects; in almost all cases reproducibility of results was better than ±2%. Figure 68 illustrates the reproducibility obtained with both catalysts at the start and end of the program. Low temperature rate data was chosen for these tests because it is the most sensitive to contamination, catalyst composition changes, or experimental procedure variations.

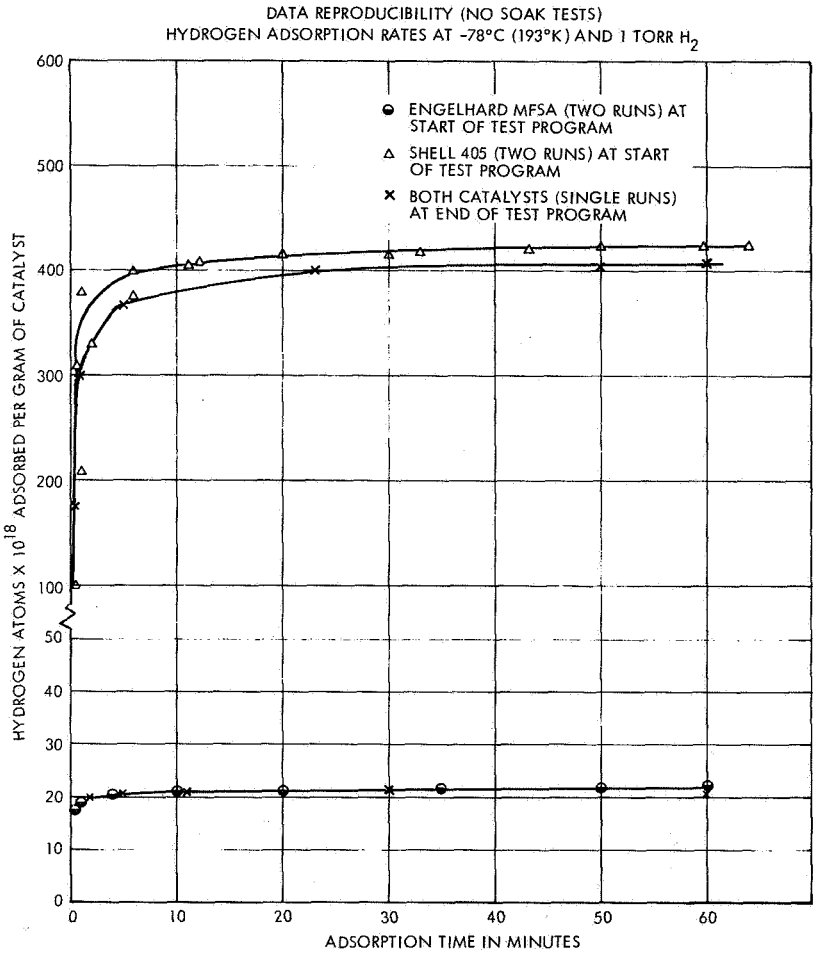

Figure 68. Reproducibility of Catalyst Activity Experimental Data

Data Interpretation. The Shell 405-ABSG catalyst is heavily loaded with iridium (approximately 30% by weight) which totally covers the alumina surface. Therefore, the various soaks performed on the catalyst should only affect the noble metal. The hydroscopic properties of alumina should only play a minor role in the behavior of this catalyst subsequent to humid air soaks. The data verified this conclusion, the only exception being the 24-hour salt spray soak during which the catalyst was literally soaked in liquid water. The data also indicated that air pollutants had no appreciable effects on the ability of this catalyst to catalyze the H_2-O_2 reaction in the temperature and pressure ranges investigated. It is oxygen that principally affects the catalytic activity.

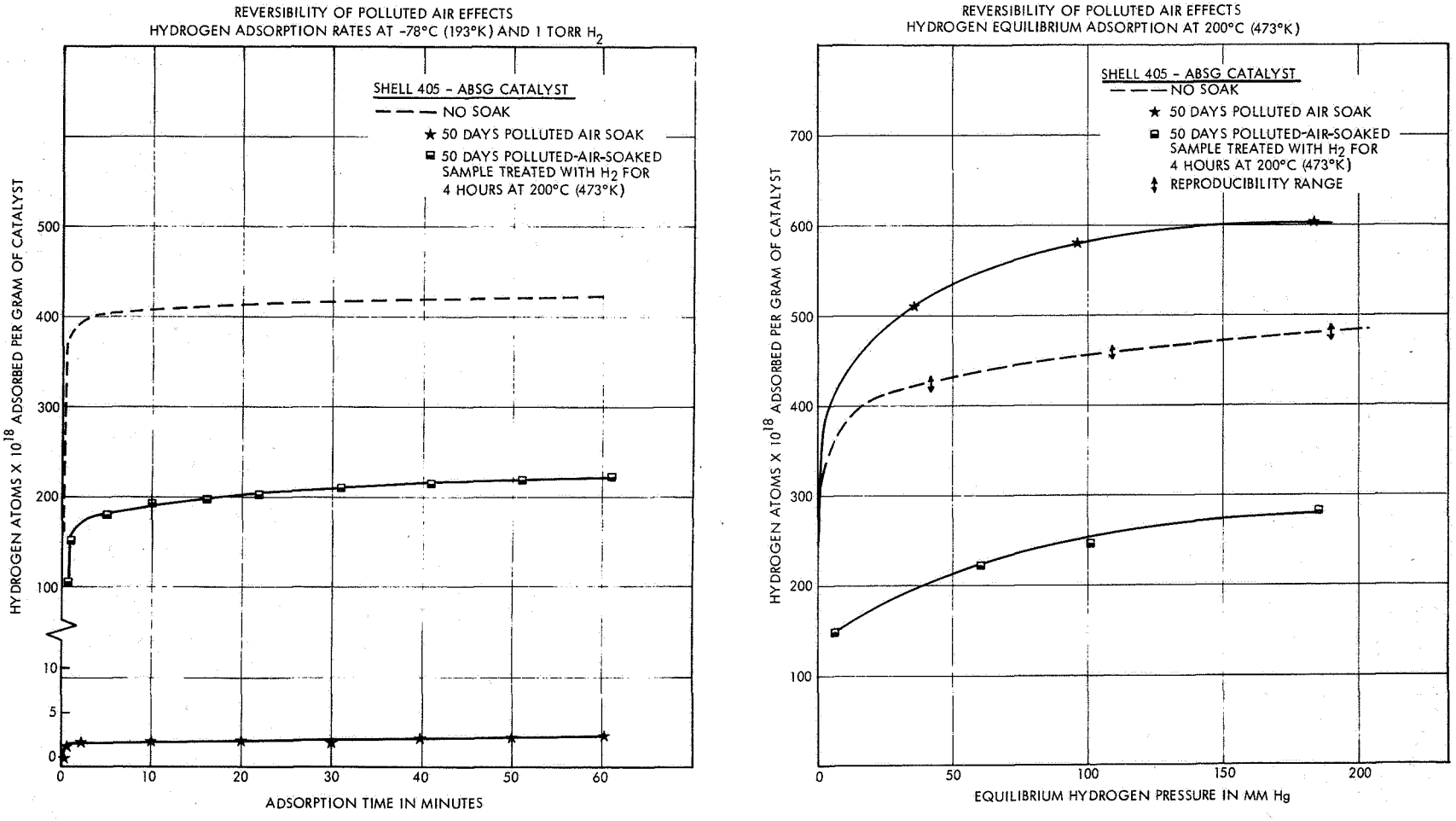

(a) (b)

Figure 69. Reversibility of Polluted Air Effects on Activity of Shell Catalyst

During ambient soaks with the Shell catalyst, oxygen adsorbs on the noble metal, blocking the sites to hydrogen adsorption at low temperatures. The amount of adsorbed oxygen increases with time until all easily accessible sites are saturated with oxygen (this occurs sometime between 24 hours and 30 days and involves over 90% of the active sites). Further reduction in the number of sites available to hydrogen become immeasurably slow. The chemisorbed oxygen cannot be removed by room temperature evacuation (ascent simulation); on the other hand, most adsorbed water vapor is removed from the noble metal during the four-hour evacuation. The water adsorbed during the salt spray soak is only partially removed (it either penetrates into the alumina, or four hours evacuation is not quite enough). When the sample is heated to 200°C (473°K) and hydrogen is added to it, the latter reacts with the adsorbed oxygen to form water, which remains attached to the site by its oxygen. If single site attachment for oxygen is assumed (one oxygen atom per iridium active site), the atoms of hydrogen adsorbed can be as high as twice the number of active sites. Indeed the data of Figure 66b indicates higher hydrogen adsorption for samples presoaked with ambient air; the increase approaches the 100% level for the short soaks (30 minutes and 24 hours). The fact that the 30-day soaks do not exhibit 100% increase in hydrogen adsorption must be due to excessive oxygen presence. It is possible that hydrogen cannot react with the adsorbed oxygen unless itself adsorbs next to it. This would necessitate the partial desorption of oxygen, or formed water, giving rise to a lower "apparent" hydrogen adsorption (the pressure above the sample will not drop as much, which would indicate lower hydrogen adsorption capacity). Another explanation can be that some association occurs between oxygen atoms on the catalyst surface during the long soaks which makes them less reactive with hydrogen and also easier to desorb.

The above interpretation of the Shell catalyst data is consistent with the results from the various soaks. To further confirm the conclusions concerning the behavior of the catalyst during the described soaks, the additional data presented in Figure 69 was obtained. A sample soaked in polluted air for 50 days was evacuated for four hours at room temperature and, as previously, its hydrogen adsorption and equilibrium rates were measured. Subsequently, the sample was evacuated for 4 hours at room temperature and its hydrogen adsorption rate and equilibrium capacity were measured again. The data indicates that the second measurements approached those obtained from samples that were never soaked in air (no soak tests). This confirms that whatever adsorbed on the catalyst surface during the air soak (believed to be oxygen), and could not be removed by ambient temperature evacuation, reacted with hydrogen during the equilibrium adsorption measurements and converted in a species (water) that could be removed by ambient temperature evacuation. This data allows the conclusion that normal humidity does not appreciably affect the intended function of the catalyst igniter.

The environmental soaks affect the active metal of the Engelhard MFSA catalyst in the same manner as described for Shell 405-ABSG. The macroscopic differences observed in the data obtained from the two catalysts are principally due to the gross difference in noble metal loading. The Engelhard catalyst is loaded with approximately 1% noble metal versus 30% for the Shell catalyst. The difference in active metals appears only to have an effect on the rate of oxygen adsorption and/or the strength of the bond

between the noble metal and oxygen. Platinum and rhodium appear to adsorb less oxygen and less strongly than does iridium. Thus, oxygen has a less pronounced effect on the Engelhard catalyst in general and water a greater effect than on the Shell catalyst. The following paragraphs present the interpretation of the data obtained with the Engelhard catalyst:

The assumption that oxygen is not held as strongly on platinum as on iridium is consistent with the data in Figure 67a. Short duration exposures to air (30 minutes and 24 hours) had no effect on hydrogen adsorption rates and very little effect on the hydrogen adsorption capacity of the catalyst. Obviously, the 4 hour ambient temperature evacuation (ascent simulation) was sufficient to desorb most adsorbent from the active sites.

Long duration polluted, humid air exposures (30 days or more) have a pronounced effect on hydrogen adsorption rates with the Engelhard catalyst. This is not true for the exposure to dry air. Again there is verification that oxygen is not strongly held by platinum and rhodium. Water vapor must be the culprit. This catalyst, being lightly loaded with noble metal, has an extensive alumina surface in contact with the humid air. Since alumina is a dehydrating agent, it adsorbs all the water vapor from the air during long exposures. At -78°C (195°K) the water freezes, expands and blocks the active sites. At 200°C (473°K) this water desorbs from the alumina, raising the pressure above the sample. Since alumina does not adsorb hydrogen, any pressure drop due to hydrogen adsorption on the active metal is masked by the increase in pressure due to desorbed water vapor. The net effect is negative adsorption (Figure 67b). The salt spray soak data verifies further this mechanism. The small "dip" in the dry air exposure curve of Figure 67b can be attributed to oxygen desorption.

In order to verify the contention that it is water (or some other desorbable species) which causes the temporary reduction in catalytic activity at low temperatures, and not permanent poisoning of the catalyst by pollutants or non-desorbable oxygen, the data shown in Figure 70 was obtained. This data is identical to that on Shell 405-ABSG presented in Figure 69 and it was obtained as described there. It is seen that four hours ambient temperature evacuation is sufficient to remove a substantial portion of the activity-inhibiting species (water according to our theory). Higher temperature evacuation or a single catalyst firing should restore the catalytic activity completely.

The results of the earth stay simulation laboratory tests indicated that exposure to air pollutants,normal humidity, and salt spray had no major effect on the activity of the Shell 405-ABSG catalyst. However, extended exposure to ambient air severely reduced the low temperature ignition capability of this catalyst, due to strongly adsorbed oxygen. Full scale igniter firing evaluation of the Shell catalyst subsequent to 30-day air exposure was recommended to determine low temperature ignition capability.

The Engelhard catalyst activity was not seriously affected by dry air soaks, but low temperature activity was substantially reduced by humidity during long exposures. Igniter firing tests after 30-day air exposures

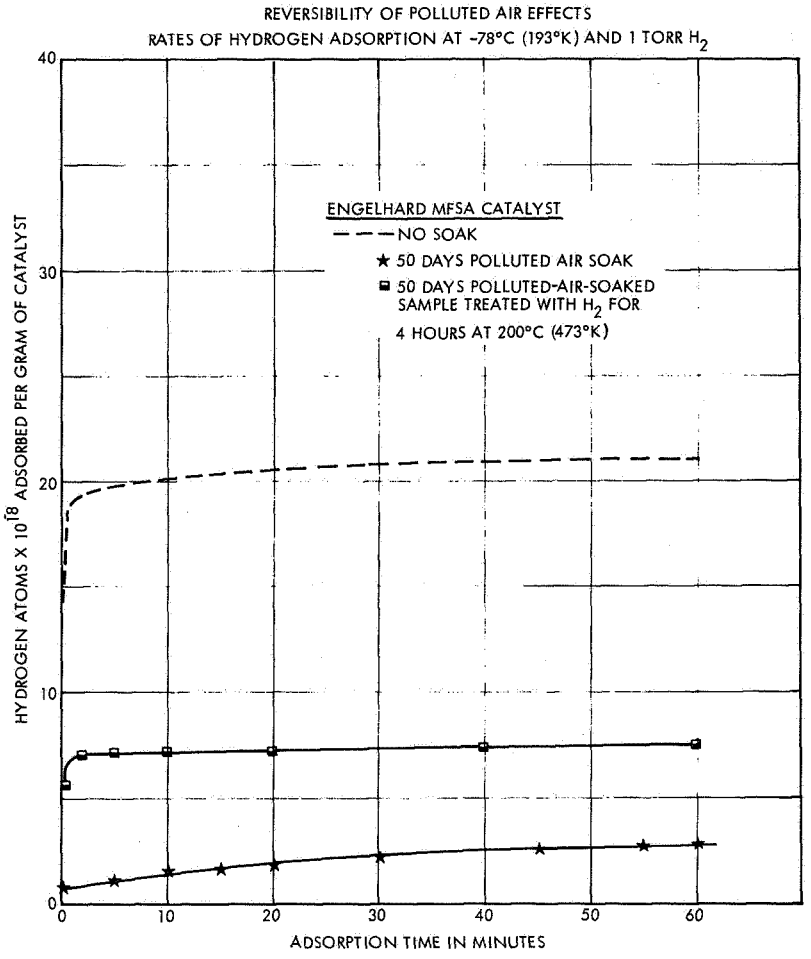

(a)

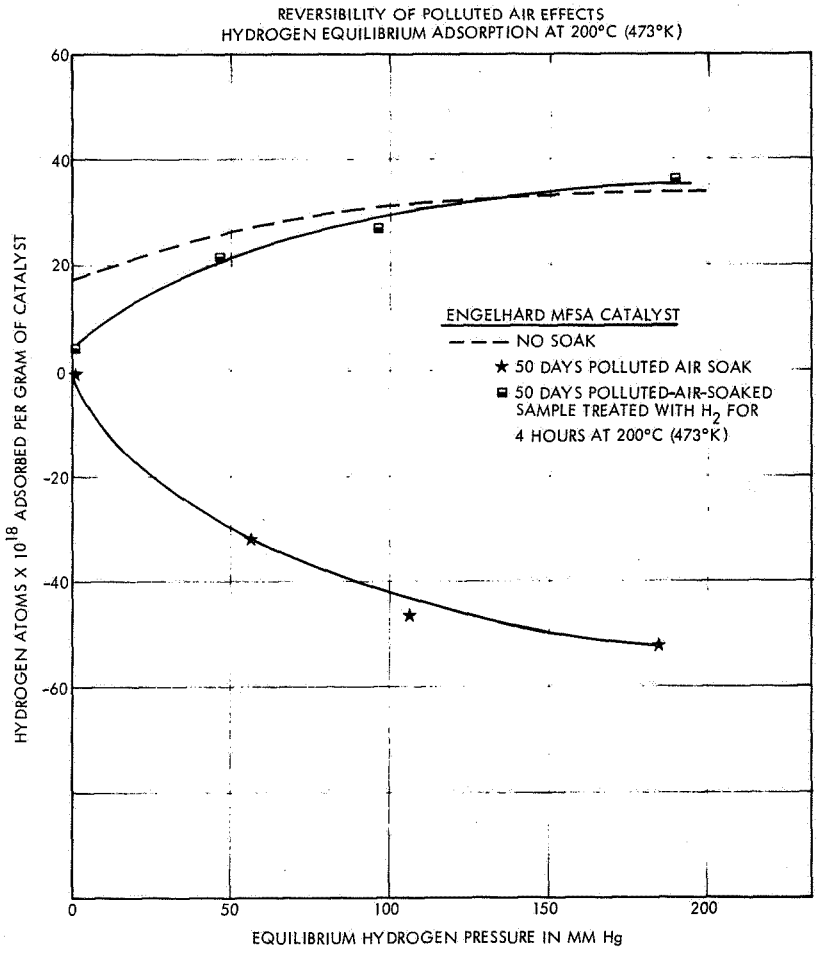

(b)

Figure 70. Reversibility of Polluted Air Effects on Activity of Engelhard Catalyst

were also recommended, in this case to investigate humidity effects, rather than oxygen adsorption, as with the Shell catalyst.

3.3.1.2 Igniter Firing Tests

A series of igniter test firings were conducted to determine the effects of simulated earth stay environments on the ignition characteristics of the Shell and Engelhard catalysts. The procedures followed for the environmental effects tests were:

(1) Each catalyst load was exposed to humid, polluted air (at Redondo Beach, California) for thirty continuous days.

(2) Each catalyst bed was loaded into the igniter and held overnight at vacuum prior to testing.

(3) The catalyst beds were externally conditioned to 250°R (139°K) and firings were attempted with 250°R hydrogen and 375°R (208°K) oxygen.

(4) If ignition did not occur, catalyst bed and/or propellant temperatures were increased until ignition was attained, and low temperature ignition attempts were then repeated.

The igniter hardware utilized for these tests was previously described in Sections 3.2.1 and 3.2.2. The downstream oxidizer injection configuration was selected for this test series. Data from the environmental effects test are listed in Table 20 for both the earth stay and reentry simulations. The results of the earth stay environment (30 days exposure to humid, polluted air) effects tests are described as follows:

Tests 344A, L: The initial high pressure reactor test with Shell catalyst after 30-day exposure resulted in no ignition with cold propellants and catalyst bed. Ignition was achieved after the bed was allowed to reach near ambient temperatures. Results of the reentry effects tests will be discussed later; however, it should be noted that the catalyst did ignite at reduced bed temperatures after a single ambient firing, indicating that no irreversible loss of activity resulted from the earth stay environment expsure.

Test 345A: Ignition was achieved on the first attempt with the Engelhard catalyst after earth stay exposure; however, initial response was increased compared to the baseline response tests for this catalyst (Table 15). It may be noted, however, that response decreased as additional tests were performed, even after the exposure to simulated reentry environments was added (Tests 345 C-G).

Tests 351A-E: Low pressure tests of Shell catalyst after earth stay exposure resulted in no ignition on the first two attempts. After one ignition was achieved on test 351D after allowing the catalyst bed to warm to ambient temperature, further ignitions were then attained at low bed temperatures, indicating a recovery of catalyst activity.

Table 20. Igniter Environmental Effects - Earth Stay and Reentry Simulations[1]

Test No. (HA5-)	P_{CD} (lbf/in^2)	P_{CD} (kN/m^2)	O_2 Temp. (°R)	O_2 Temp. (°K)	H_2 Temp. (°R)	H_2 Temp. (°K)	Initial Bed Temp. (°R)	Initial Bed Temp. (°K)	Environ. Exposure (ES,R)[2]	Time To 1200°F(920°K) (sec)	Comments	
344A	-	-	368	204	199	111	249	138	ES	-	no ignition	
344L	192	1324	391	217	192	107	497	276	ES	0.031	ambient bed	
344N	-	-	384	213	203	113	241	134	ES+R	-	no ignition	
344O	242	1669	382	212	205	114	385	214	ES+R	0.027	cold bed	High P_c
344P	219	1510	389	216	208	116	345	192	ES+R	0.025	cold bed	Shell
344R	249	1717	394	219	215	119	272	151	ES+R	0.055	cold bed	Catalyst
344S	220	1517	385	214	214	119	257	143	ES+R	0.040	cold bed	
345A	228	1572	384	213	231	128	215	119	ES	0.076	cold bed	
345C	207	1427	381	212	258	143	346	192	ES+R	0.071	cold bed	High P_c
345D	245	1689	375	208	203	113	352	196	ES+R	0.045	cold bed	Engelhard
345E	231	1593	377	209	192	107	268	149	ES+R	0.048	cold bed	Catalyst
345F	214	1475	380	211	187	104	239	133	ES+R	0.054	cold bed	
345G	223	1538	372	207	189	105	214	119	ES+R	0.052	cold bed	
351A	-	-	380	211	206	114	267	148	ES	-	no ignition	
351B	-	-	377	209	208	116	260	144	ES	-	no ignition	
351D	18.7	129	379	211	203	113	505	281	ES	0.097	ambient bed	
351E	16.9	117	381	212	192	107	368	204	ES	0.062	cold bed	Low P_c
351I	16.2	112	382	212	207	115	264	147	ES+R	1.88	cold bed	Shell
351J	17.1	118	378	210	206	114	508	282	ES+R	0.080	ambient bed	Catalyst
351Z8	16.9	117	390	217	215	119	280	156	ES+R	0.087	cold bed	
351Z9	17.4	120	39]	218	252	140	262	146	ES+R	0.090	cold bed	
351Z10	16.8	116	390	217	273	152	252	140	ES+R	0.060	cold bed	
352A	11.7	81	376	209	208	116	275	153	ES	-	partial ignit.	
352B	16.2	112	375	208	242	134	335	186	ES	0.070	cold bed	
352D	15.9	110	375	208	249	138	310	172	ES	0.093	cold bed	Low P_c
352M	13.1	90	381	212	207	115	250	139	ES+R	-	partial ignit.	Engelhard
352N	16.3	112	374	208	199	111	357	198	ES+R	0.067	cold bed	Catalyst
352O	16.5	114	375	208	205	114	318	177	ES+R	0.065	cold bed	

[1] Earth stay simulation was 30 days exposure to humid, polluted air; reentry simulation was exposure at 1500°F (1089°K) for one hour in 3.5 psia (24 kN/m^2) air.

[2] ES = earth stay simulation, R = reentry simulation

Tests 352A-D: Low pressure Engelhard catalyst tests after earth stay exposure resulted in a partial ignition on the first attempt. Full high response ignition was attained on the next two firings at low bed temperatures.

The results of the igniter firing tests with catalyst exposed to simulated earth stay environmental exposures indicated that low temperature ignitions could not be attained with the Shell catalyst until the bed was allowed to reach near ambient temperatures for the first firing, after which initial catalyst activity was recovered and low temperature ignitions could be achieved.

Although at least a partial ignition resulted on the first firing of the Engelhard catalyst at each pressure level after earth stay exposure, ignition was more consistent and response improved for subsequent firings. The full-scale test data was entirely consistent with the subscale laboratory tests.

3.3.1.3 Conclusions From Experimental Results

The results of the laboratory investigations of earth stay environmental effects on catalyst activity led to the following conclusions:

- Pollutants and normal humidity have no appreciable effect on Shell 405-ABSG catalyst. Humidity during long exposures (more than 24 hours) at ambient conditions reduces substantially the low temperature catalytic activity of the Engelhard catalyst. Both catalysts, if soaked in liquid water and not thoroughly dried, lose their ability to ignite the H_2-O_2 reaction at -78°C (195°K).

- Normal salt spray concentration of coastal areas should not have any effect on Shell catalyst and only a possible minor effect on Engelhard catalyst.

- Long exposures to ambient air appears to hinder severely the low temperature H_2-O_2 ignition capability of Shell 405. Full scale testing of this catalyst subsequent to 30 day air soaks is recommended. It is possible that catalyst reactivation would be required during long term earth residence of the shuttle vehicle.

Full-scale igniter test firings with catalysts exposed to simulated earth stay environments (30 days in polluted, humid air) tended to substantiate the results and conclusions of the laboratory activity evaluations. The following conclusions were suggested by the test firing results:

- Low temperature ignition capability of both the Shell and Engelhard catalysts was initially reduced by simulated earth stay environments for 30 day periods. However, in each case, the original catalyst activity level was recovered after a hot firing. These results verify the laboratory test data indicating that polluted air effects are reversible (Figures 69 and 70).

- High response on the first ignition with either catalyst after extended earth stay can be assured by heating and/or hydrogen purging of the catalyst bed.

3.3.2 Reentry Effects

Both laboratory investigations and full-scale igniter test firings were conducted to determine the effects of reentry on catalyst activity, including the following environmental conditions:

- Heat during reentry (vacuum soak)
- Oxygen during reentry (clean, dry air soak)
- Polluted humid air during reentry (polluted air soak)
- Exposure time during reentry (1- and 60-minute reentry simulations)

As previously described for the earth stay effects determination, laboratory experiments were performed to identify significant reentry effects on catalyst activity to be investigated by igniter tests with both the Shell and Engelhard catalysts at each pressure level.

3.3.2.1 Laboratory Evaluations

The laboratory reentry simulations were divided into two groups:

- One-minute soaks at 1500°F (1089°K)
- Sixty-minute soaks at 1500°F (1089°K)

The pretreated catalyst samples were heated under vacuum to 1500°F (1089°K), soaked for the duration and in the environment indicated [vacuum or 3.5 (24 kN/m^2) psia air], cooled to ambient temperature under vacuum or by the addition of the appropriate type of air, kept at ambient conditions for 30 minutes (earth stay simulation), evacuated for four hours at ambient temperature (ascent simulation), and cooled to -78°C (195°K) for hydrogen adsorption measurements. Subsequent to rate measurements the sample was heated to 200°C (473°K) for the equilibrium adsorption determinations.

Figures 71 through 74 present all the data on the combined reentry and 30 minutes earth stay effects on catalytic activity.

Shell 405-ABSG Catalyst. Figures 71 and 72 show data obtained during short and normal reentry exposures of Shell catalyst samples. The data indicates that:

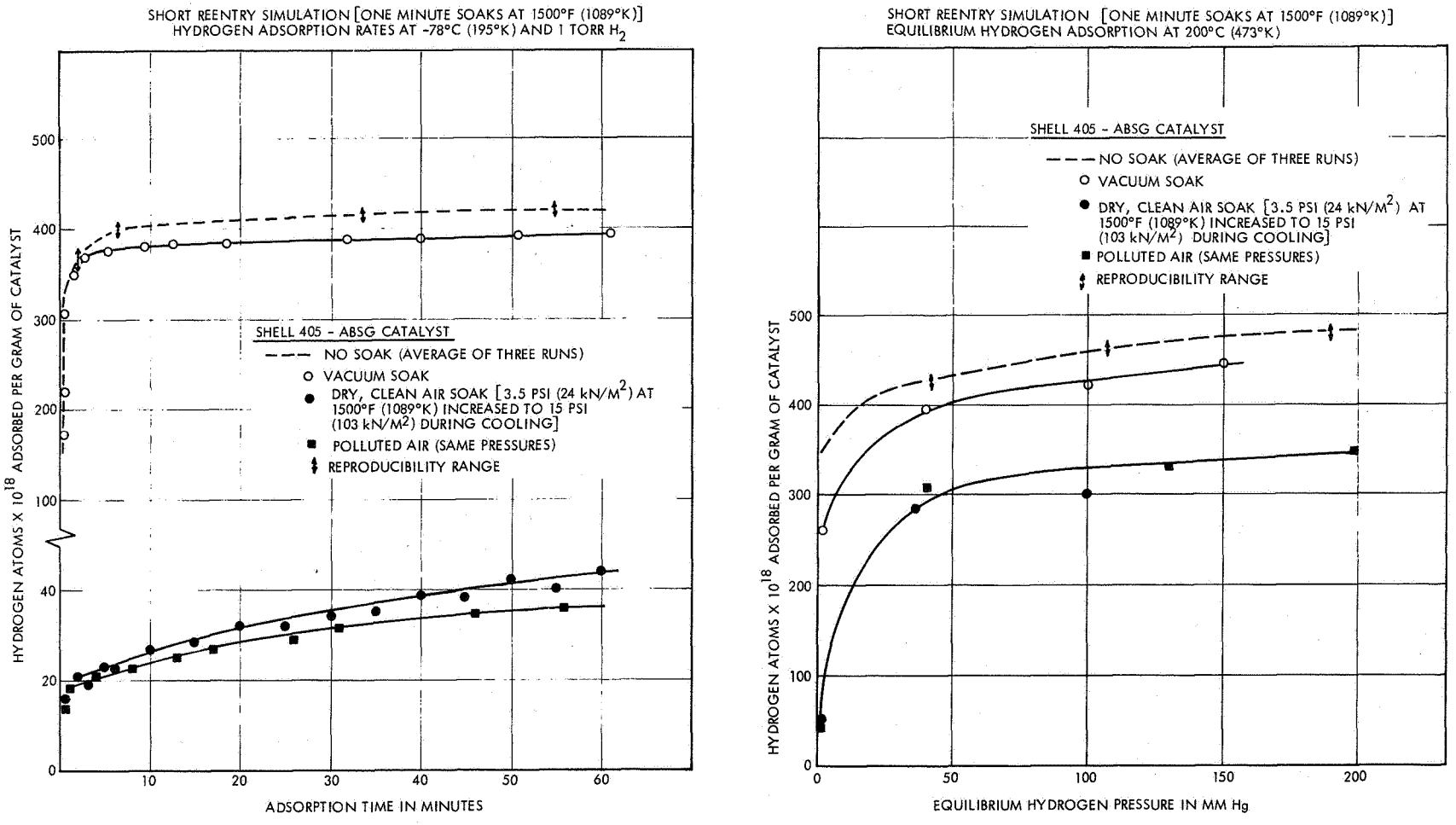

Figure 71. Effects of Short Reentry Simulations on Activity of Shell Catalyst

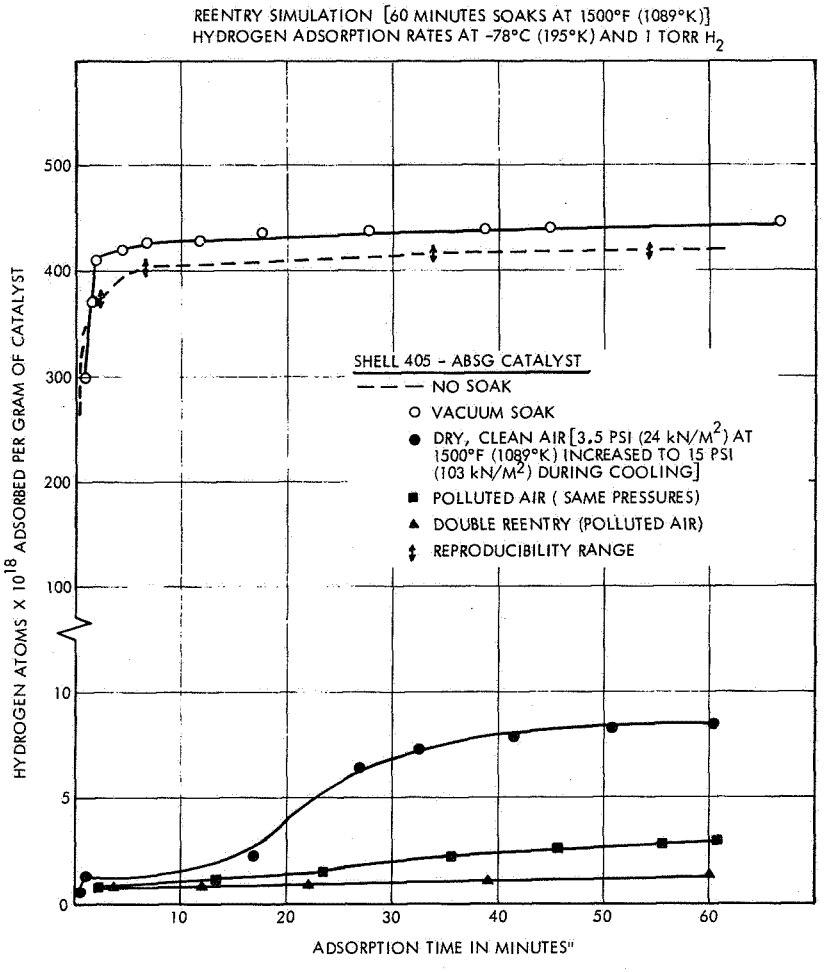

(a)

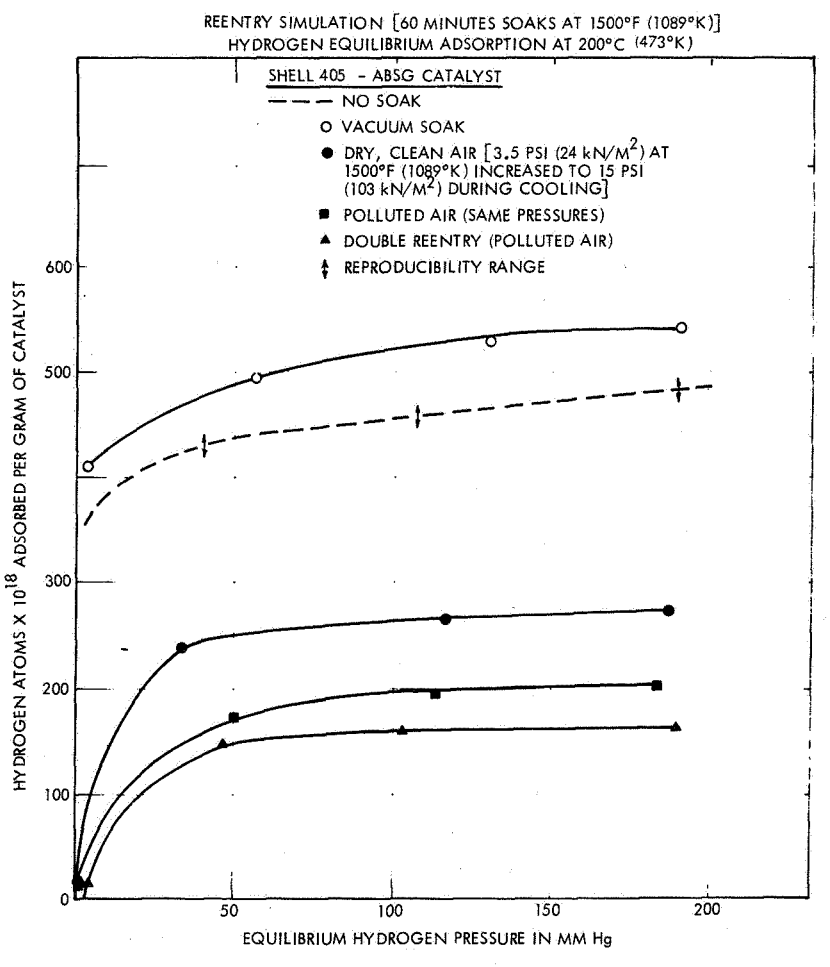

(b)

Figure 72. Effects of Longer Reentry Simulations on Activity of Shell Catalyst

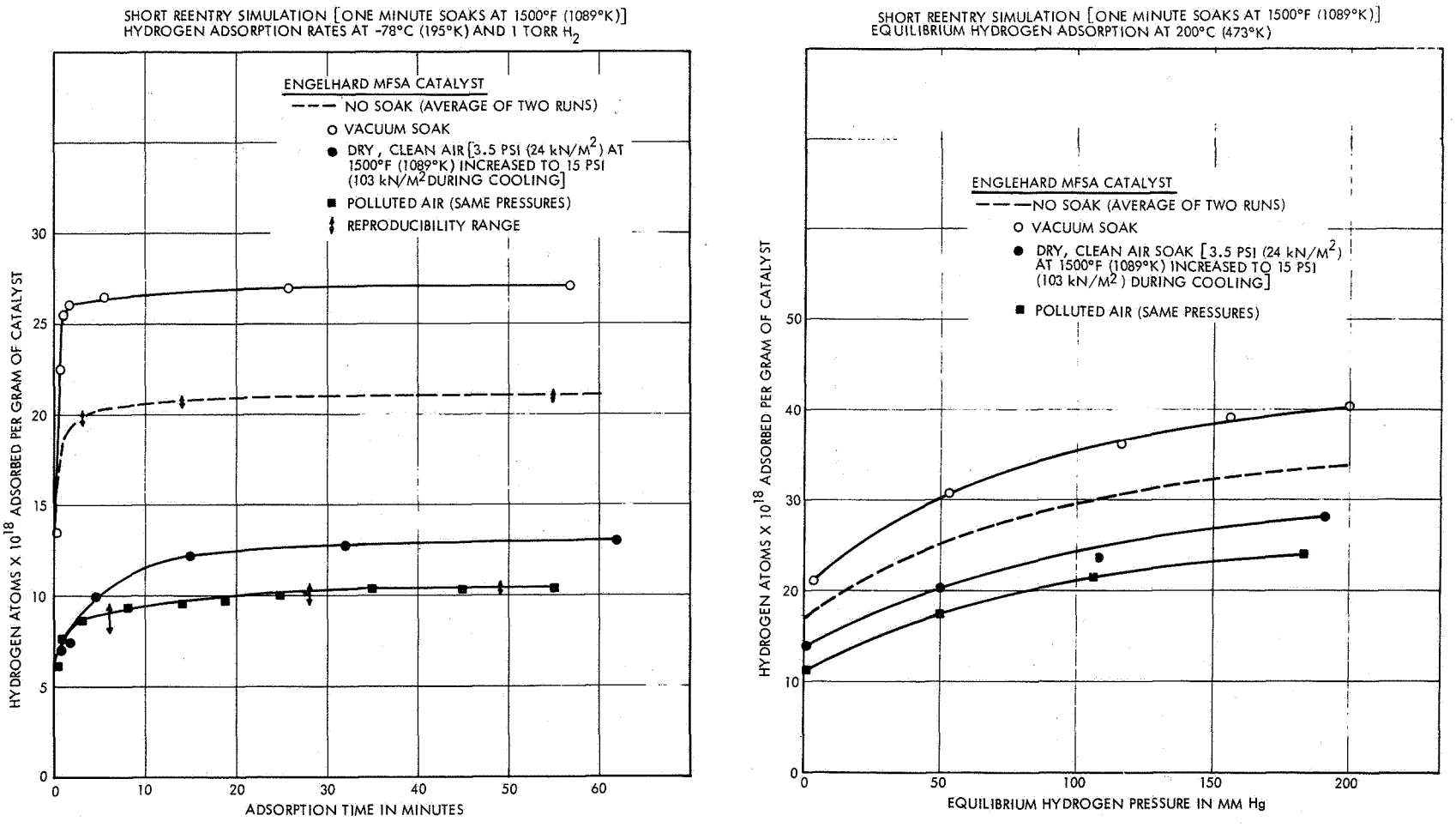

Figure 73. Effects of Short Reentry Simulations on Activity of Engelhard Catalyst

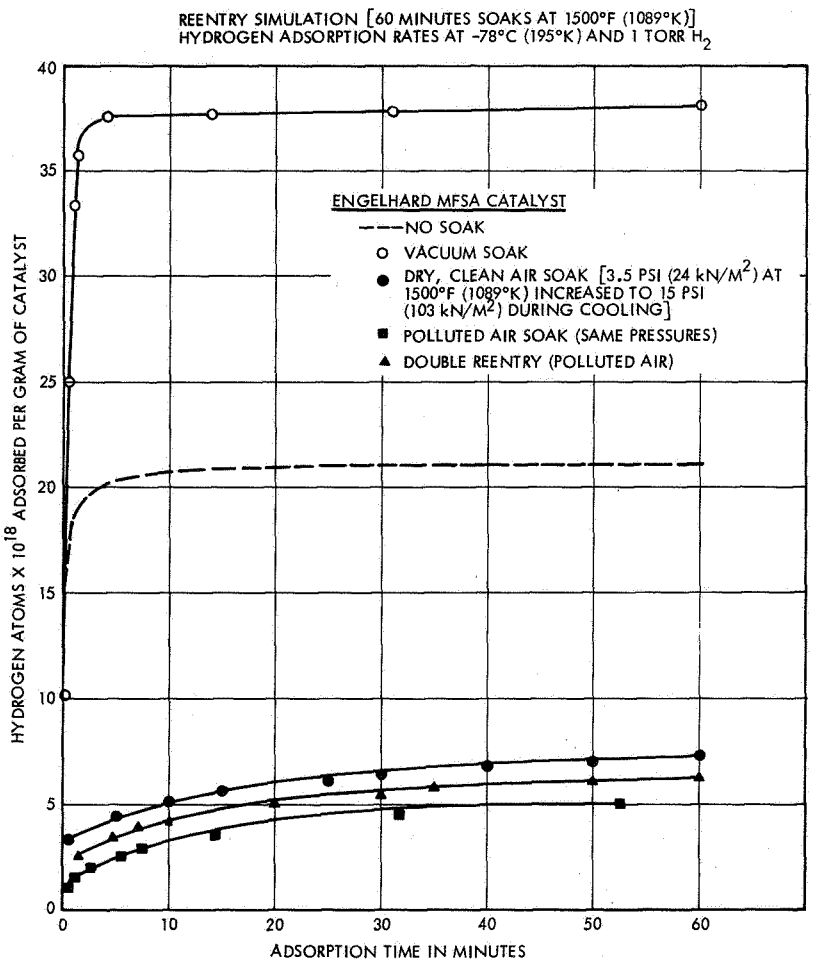

(a)

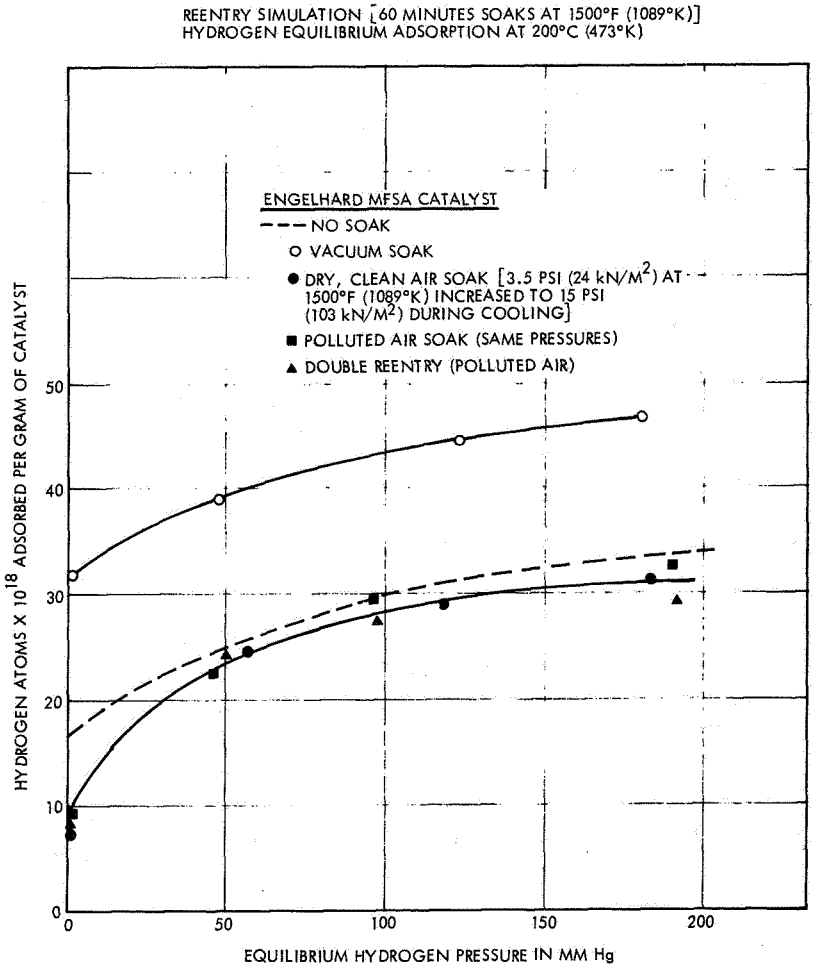

(b)

Figure 74. Effects of Longer Reentry Simulations on Activity of Engelhard Catalyst

- Reentry heat only (vacuum soaks) has no effect on the activity of this catalyst; if anything, the 60 minutes vacuum soak at 1500°F (1089°K) tends to increase the maximum hydrogen adsorption on the catalyst. In all probability, prolonged high temperature evacuation removes strongly adsorbed species from the catalyst surface which were not removed during pretreatment.

- The presence of oxygen during reentry has a pronounced effect on low temperature hydrogen adsorption rates on this catalyst; in addition, the effect increases with increase in exposure time (Figures 71a and 72a). Adsorption rates decrease by an order of magnitude after one minute soaks and by two orders of magnitude after 60 minute soaks. The effect on equilibrium hydrogen adsorption is mild by comparison; the maximum hydrogen adsorption is reduced by less than a factor of two (Figures 71b and 72b). Since heat alone (vacuum soaks) had no effect on catalytic activity, the deterioration in adsorption rates observed in this data must be due to catalyst-active-site "poisoning" by oxygen; some sintering, however, cannot be ruled out.

- The presence of polluted air during reentry has no significant effect on catalytic activity beyond that observed for oxygen. Thus, water vapor and pollutants in air do not affect catalytic activity appreciably. Oxygen appears to be the primary culprit.

- Repeated reentry simulations in polluted air on the same catalyst sample did not affect catalytic activity beyond the effects of the first reentry. Since the sample was hydrogen treated between reentries (rate and equilibrium measurements were made on it) it would appear that the oxygen effect is reversible, otherwise, further activity deterioration would have been observed with each successive reentry.

Engelhard MFSA Catalyst. Figures 73 and 74 represent the simulated reentry effects on the activity of Engelhard MFSA catalyst. The effects of temperature, oxygen, water vapor and air pollutants, exposure duration, and repeated reentries are discussed below:

- Reentry temperatures up to 1500°F (1089°K) appear to have a positive effect on catalytic activity. This increase in activity is significant only for low temperature adsorption rates. This effect was not observed with the Shell catalyst (it was not as pronounced).

- The presence of oxygen during reentry influences the catalytic activity of Engelhard catalyst in similar fashion but smaller in extent than that of Shell 405-ABSG. This discrepancy in extent of deterioration must be due to the lower per unit weight activity of Engelhard catalyst (less active sites per gram). Increase in exposure time increases the deterioration of adsorption rates (Figures 73 and 74).

- Water vapor, pollutants, and multiple reentries do not affect catalytic activity appreciably. The catalyst exhibits approximately the same adsorption rate deterioration with clean, dry air as with humid, polluted air.

Data Interpretation. The data obtained for the Shell catalyst indicates that oxygen at 1500°F (1089°K) reacts with iridium and in the process releases heat which "spot sinters" the active metal of the catalyst. One hour soak at 1500°F and 3.5 psia (24.1 kN/m^2) air can reduce the active sites of the catalyst to one third the original number. Upon prolonged treatment with hydrogen at 200°C (473°K), the formed oxide reduces to the metal, but the sintering effect is permanent. A second treatment with oxygen at 1500°F does not sinter the catalyst further; at least not appreciably. The above statements are supported by the data on Figures 66 and 72. The data shows that 1 hour vacuum soaks at 1500°F has no effect on either the rate or equilibrium adsorption of the catalyst. Soaks of the same duration with air have a pronounced negative effect on both rate and equilibrium adsorption which is much greater than that observed with 30 minute ambient air soaks. As expected, the sintering effect increases with exposure time, but not severely (compare Figure 71 with Figure 72).

During reentry, the active metal of the Engelhard MFSA catalyst reacts with oxygen, if present, but the heat generated is small (the noble metal loading of the support is low) and no appreciable sintering takes place. The reacted oxygen does not, of course, desorb during ambient temperature evacuation and by remaining on the surface it causes severe reduction in low temperature adsorption rates. At 200°C (473°K), the "oxide" reduces to the metal by hydrogen, and the catalyst behaves as if it had never been soaked in air. Just as with the Shell catalyst, the assumption is made that oxygen atoms adsorb on single sites, but the product of the reaction with hydrogen (water) desorbs at 200°C. Thus, the net effect on pressure above the sample from the reaction of hydrogen with oxygen is zero (one mole of hydrogen is used up but one mole of H_2O is desorbed); any change in pressure reflects the adsorption of hydrogen on the freed sites. As expected, hydrogen adsorption is equal to that of "no soak" samples (Figure 74b).

The results of the reentry environment simulation laboratory tests indicated that heating alone (in vacuum) tends to increase the catalyst activity by further pretreating of the catalyst surface. Heating of the Shell 405-ABSG to 1500°F (1089°K) in an air environment (oxygen exposure) decreased catalyst activity; however, the effects appear to be reversible.

The Engelhard MFSA catalyst was affected to a lesser extent by oxygen during reentry than the Shell catalyst. No additional activity losses resulted from polluted air reentry simulations with either catalyst. Repeated aerated reentries with both the Shell and Engelhard catalysts did not further reduce activity, again indicating that the oxygen effect is reversible.

Based on the results of the laboratory reentry effects experiments, full-scale igniter firing tests of each catalyst after reentry heating in air were recommended. These tests were to be conducted with catalyst loads previously exposed to 30-day earth stay environments (polluted, humid air)

to determine the combined environmental effects on low temperature catalytic ignition of hydrogen-oxygen.

3.3.2.2 Igniter Firing Tests

Full-scale igniter test firings were performed to investigate the effects of simulated reentry environmental exposure on the ignition capability of the Shell 405-ABSG and Engelhard MFSA catalysts. These firings were conducted after aerated reentry heating of the same catalyst loads exposed to 30-day earth stay environments (polluted, humid air) as described in Section 3.3.1. The proceedures followed for these tests were:

(1) Each catalyst bed was externally heated and held at 1500°F (1089°K) for 1 hour in a 3.5 psia (24 kN/m^2) air environment, then gradually cooled as pressure was increased to 1 atmosphere, simulating anticipated shuttle vehicle reentry.

(2) The catalyst beds were then returned to a vacuum environment and cooled to 250°R (139°K) and firings attempted with 250°R hydrogen and 375°R (208°K) oxygen.

(3) If ignition did not occur, catalyst bed and/or propellant temperatures were increased until ignition was attained, and low temperature ignition attempts were then repeated.

The igniter stand installation for the reentry effects tests is shown in Figure 75. An electrical heater was utilized to heat gaseous

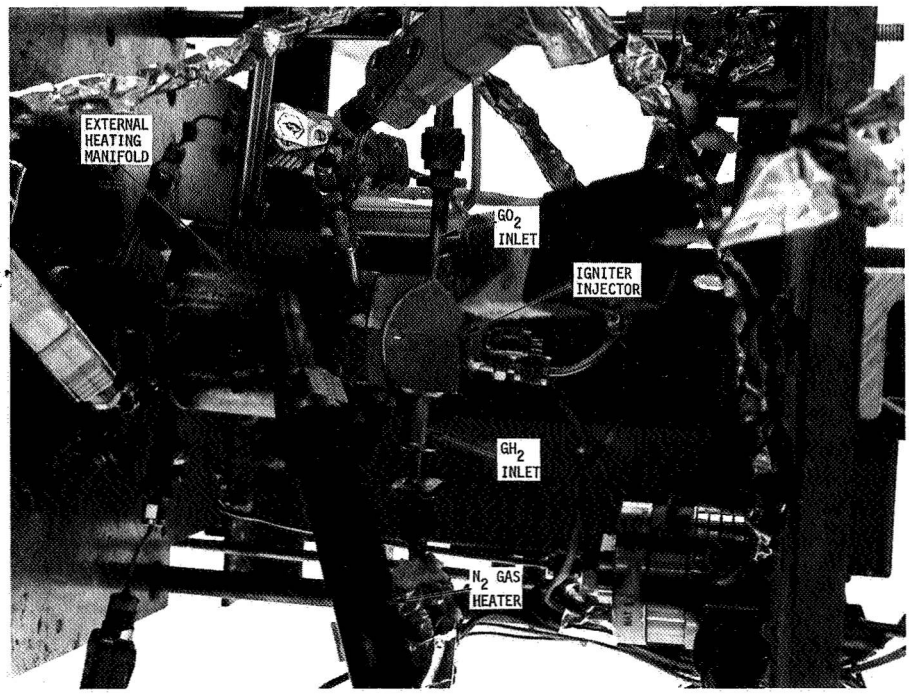

Figure 75. Reentry Effects Test Stand Installation

nitrogen, which was ducted around the igniter body to maintain a catalyst bed temperature of 1500°F (1089°K) for 1 hour. Simulated reentry atmospheric pressures of 3.5 psia (24 kN/m^2) were maintained by controlled bleeding of air into the vacuum chamber while a small mechanical pump was operating. Catalyst bed temperatures and pressures were held within 5 percent of nominal values during the 1-hour reentry simulations.

The data from the combined earth stay and reentry (ES+R) tests are listed in Table 20 (along with the earth stay only tests described in Section 3.3.1.2). Results of thest tests are described as follows:

Tests 344 N-S: The first test, 344N, after combined earth stay and reentry (ES+R) exposure resulted in no ignition with the Shell catalyst and the high Pc igniter. Ignition was achieved on test 344 "O" after catalyst bed temperature was allowed to increase. Subsequent ignitions were then attained with reduced catalyst bed temperatures.

Tests 345 C-G: High Pc igniter tests of the Engelhard catalyst following combined environmental exposure resulted in ignition on the first attempt (Test 345C); however, response times were reduced on following tests, even at lower initial catalyst bed temperatures.

Tests 351 I-Z10: The initial low Pc Shell catalyst test resulted in a very long ignition delay after reentry exposure, but repeatable high response ignitions were attained after a single firing was performed at ambient catalyst bed temperatures.

Tests 352 M-O: Low Pc Engelhard catalyst tests also indicated that erratic low temperature first ignitions may occur after aerated reentry heating of the catalyst. Subsequent ignitions were attained with repeatable response times.

Typical oscillograph traces from the environmental effects tests (Table 20) are presented in Figures 76 through 79. High pressure igniter response with the Shell and Engelhard catalysts is shown in Figures 76 and 77, respectively. Figure 76 indicates that the overall igniter response [time for the effluent to reach a temperature of 1200°F (1089°K), sufficient for main thruster ignition] for the Shell catalyst was 40 milliseconds after oxygen valve opening. This response is identical to results of the baseline response tests (Section 3.2.2.1) with "new" catalyst at reduced bed and propellant temperatures (Figure 51).

Figure 77 is a similar oscillograph record for a high pressure igniter firing with Engelhard catalyst, also exposed to simulated earth stay and reentry environments. Low temperature ignitions were attained with this catalyst immediately following the environmental exposures, but were erratic in response. After an ambient propellant temperature firing, low temperature response times of 45 milliseconds were attained, as shown in Figure 77.

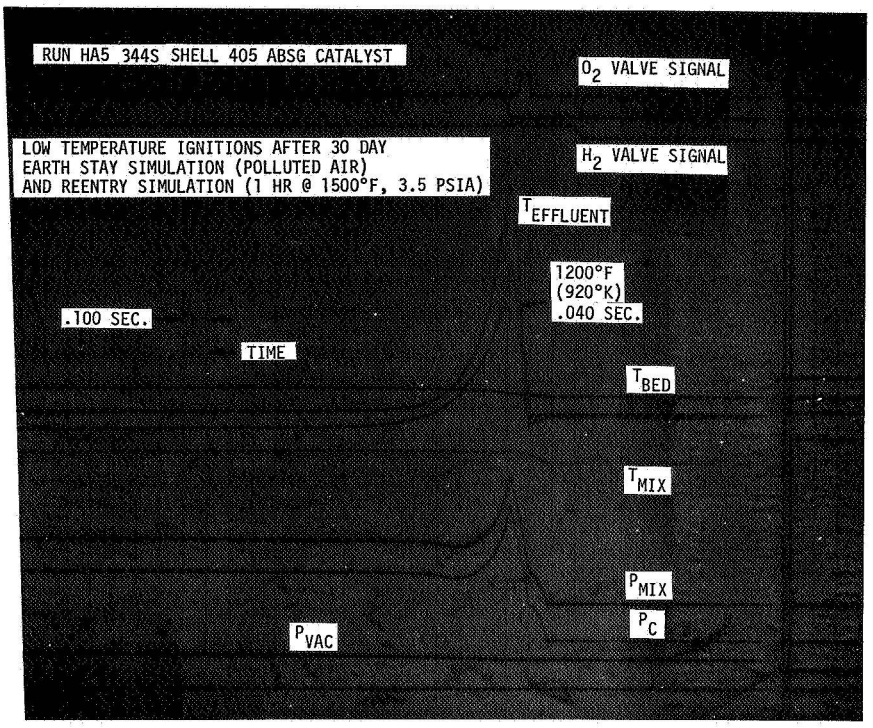

Figure 76. Shell Catalyst High P_C Response After Earth Stay and Reentry Simulation

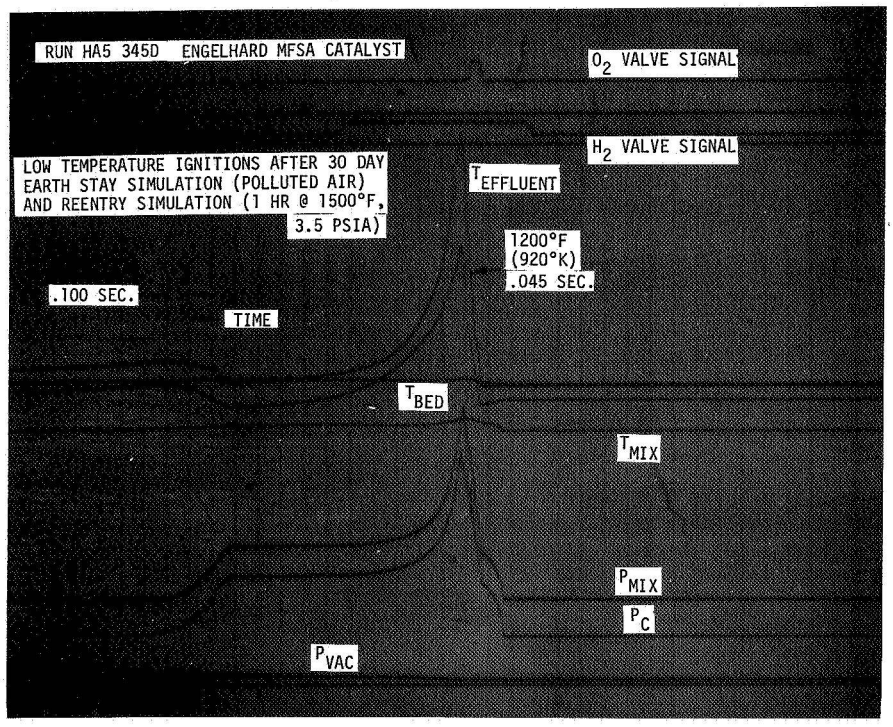

Figure 77. Engelhard Catalyst High P_C Response After Earth Stay and Reentry Simulation

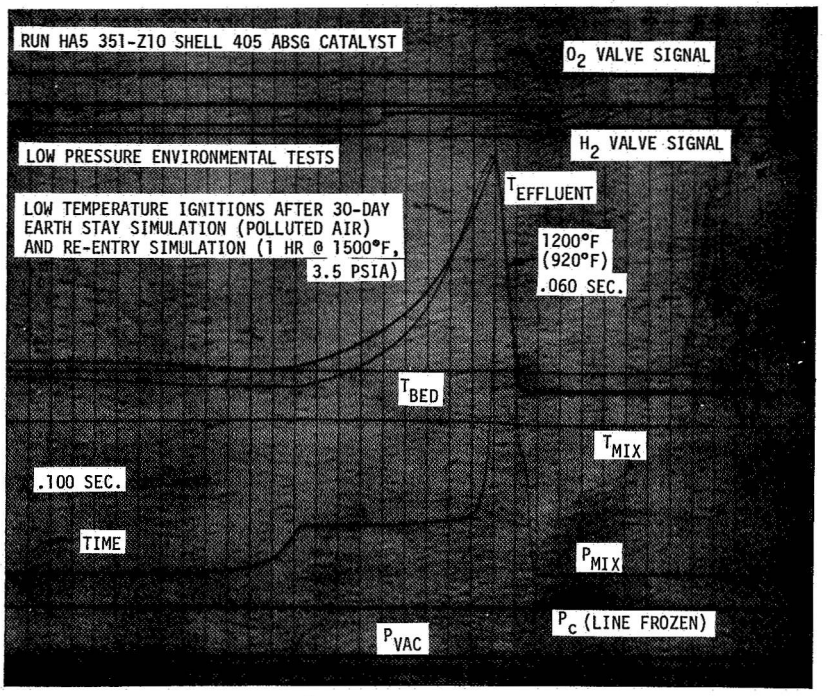

Figure 78. Shell Catalyst Low P_c Response After Earth Stay and Reentry Simulation

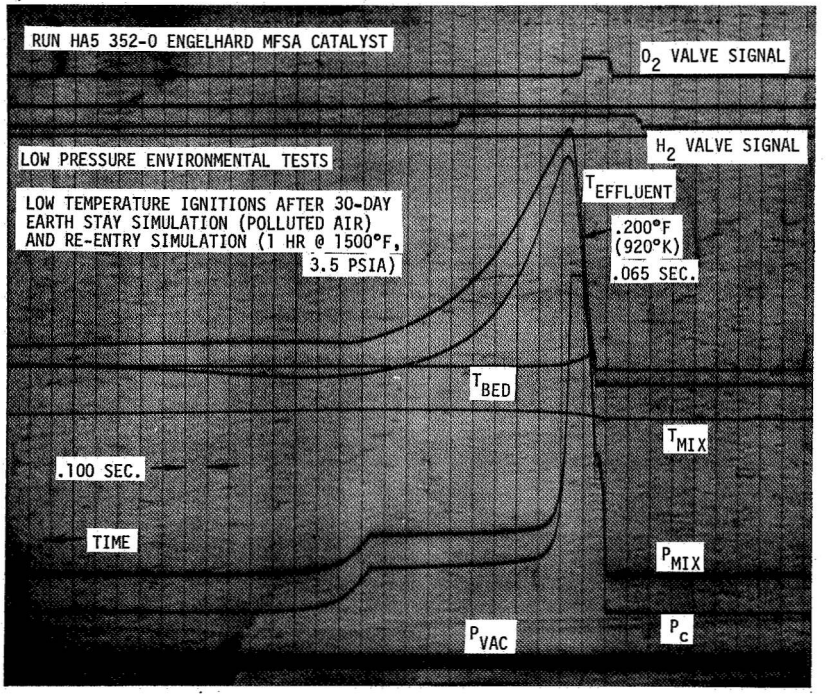

Figure 79. Engelhard Catalyst Low P_c Response After Earth Stay and Reentry Simulation

Typical oscillograph traces of low pressure igniter environmental test firings with the Shell and Engelhard catalysts are presented in Figures 78 and 79, respectively. Each of these catalyst loads had been subjected to both the 30-day polluted air soak and reentry simulation prior to these ignitions. Figure 78 indicates that the overall igniter response for Shell catalyst was 60 milliseconds after oxygen valve opening.

Figure 79 is a similar oscillograph record for a low pressure igniter firing with Engelhard catalyst, also exposed to simulated earth stay and reentry environments. After an ambient propellant temperature firing, low temperature response times of 65 milliseconds were attained, as shown in Figure 79.

The igniter firing tests of reentry exposed Shell and Engelhard catalysts strongly substantiated the laboratory investigation conclusion that oxygen effects on catalyst activity are reversible. At each igniter pressure level, ignitions were not achieved (or response times were erratic) on the first attempt with low catalyst bed and propellant temperatures; however, once a single ignition had been attained by allowing the catalyst bed temperature to increase, subsequent low bed temperature ignitions were repeatable and consistent in response times.

3.3.2.3 Conclusions From Experimental Results

The conclusions resulting from the laboratory investigations of reentry environmental effects on catalyst activity were:

- Reentry heat alone (at vacuum) has no adverse effect on the catalytic activity of either catalyst at temperatures up to 1500°F (1089°K).

- Prolonged reentry heat on air exposed Shell 405-ABSG catalyst [one hour at 1500°F (1089°K)] reduces its activity by as much as 70 percent. Repeated reentries do not further affect the catalytic activity. This activity deterioration is equivalent to that observed after several hundred firings of catalysts not exposed to reentry heat and is not sufficient to cause great concern, because the catalyst appears to stabilize after the first reentry and additional reentries and/or multiple firings should not alter its activity further.

- Engelhard MFSA was not as strongly affected by aerated reentries as the Shell catalyst; however, full-scale testing of both catalysts subsequent to reentry exposures is recommended to verify low temperature ignition capability.

The results of the igniter test firings at each pressure level of catalysts exposed to both simulated earth stay (30 days in polluted, humid air) and reentry [one hour at 1500°F (1089°K) in 3.5 psia (24 kN/m^2) air] environments led to the following conclusions:

- Low temperature ignition capability of the Shell and Engelhard catalysts was severely reduced on the initial firing after combined earth stay and reentry environmental exposures. However, "new" catalyst response times were achieved after a single hot firing at increased catalyst bed temperatures, again indicating that oxygen effects are reversible.

- Hydrogen purging and/or heating of the catalyst bed will restore high response, low temperature ignition capability of either catalyst after exposure to combined earth stay and reentry environments.

- The full scale igniter test results were entirely consistent with the corresponding laboratory experimental results. This allows extrapolation of laboratory obtained data with substantial confidence.

4. LOW PRESSURE THRUSTER INVESTIGATIONS

4. LOW PRESSURE THRUSTER INVESTIGATIONS

This analysis, design, and experimental task was conducted to evaluate the overall performance, operating characteristics, and durability of a cooled, flightweight gaseous hydrogen-oxygen thruster. The specific objectives of these investigations were:

- Perform design and cooling analyses for a 30 lbf (133N) thrust, 15 psia (103 kN/m^2) chamber pressure flightweight reaction control type thruster.
- Conduct a series of injector screening tests (including cold flows) with the thruster injector designed above and the residual injector from NAS 3-11227 (Reference 1).
- Determine delivered altitude performance and operational characteristics of the cooled thruster assembly, and demonstrate durability by performing an 1800 second continuous firing.

The low chamber pressure thruster assembly was designed, fabricated, and test evaluated as described in the following report sections.

4.1 THRUSTER ANALYSIS AND DESIGN

The nominal design conditions for the low pressure flightweight cooled thruster were:

• Vacuum thrust	30 lbf (133N)
• Chamber pressure	15 psia (103 kN/m^2)
• Overall mixture ratio	2.5 (1.5-3.0 test range)
• Nozzle expansion ratio	5:1
• Propellant inlet temperatures	Ambient and -250°F (117°K)
• Duty cycle	Steady state/pulse mode

The thruster was designed to operate with gaseous hydrogen-oxygen and to employ a pilot bed catalytic igniter utilizing the reactor design criteria previously described in Section 3.2.3.3.

4.1.1 Injector/Igniter Design

The injector design selected for this program was based largely upon a triplet impingement gaseous hydrogen-oxygen injector concept which had been recently developed by TRW Systems and had delivered high combustion efficiencies with a cooled thrust chamber. The pilot bed catalytic reactor design was a modification of the NAS 3-11227 low pressure igniter to include downstream oxygen injection to enhance overall thermal response.

4.1.1.1 Triplet Injector

The low pressure injector, shown in Figure 80, is a raised post triplet design with 96 triplet elements (2 oxidizer on 1 fuel) located symmetrically about a central igniter port, plus 48 non-impinging hydrogen orifices to provide a lower mixture ratio environment at the thrust chamber wall. Nominal injection pressure drops were 3 psia (21 kN/m^2) for both propellants.

A simple but highly effective engineering design model has been formulated and proven for basic injector patterns of interest in GH_2/GO_2 injector design. This analysis is summarized below.

- Basic model employed assumes combustion efficiency governed by turbulent mixing of propellant streams
- Model applicable to all basic injection elements - empirically accounts for degree of initial mixing and overall element (pattern) fineness
- Stream reaction/combustion has minor effect on resulting axial mixing profiles
- Injection geometry selected to minimize recirculation induced injector face heat transfer
- Model applies to symmetrical injection elements

A completely generalized mixing model is used for the design as shown in Figure 81. It has been found from a large number of cold flow tests that the model empirical coefficients are given as shown in Figure 81 for all of the configurations evaluated. The required number of elements for a given normalized combustor length of $\bar{x}$ ($\bar{x} \sim x/r_j$, r_j = reference dimension in injector element) and contraction ratio ε_c, is then readily determined from the η_{C^*} relation. The performance of the 96 triplet element low pressure injector (Figure 80) was predicted to be over 99% of theoretical combustion efficiency using this generalized mixing model. Cold flow measurements performed with the low pressure triplet injector also indicated excellent mixing characteristics resulting in predicted combustion efficiency of over 99% (Section 4.2.1.1).

Injector design analyses also included computer optimization of oxidizer and fuel manifold sizing. Manifold sizing was not significant in affecting pulse response, as indicated in Figure 82. Instead, pulse pressure rise rate was found to be essentially a function of valve response capability. The ratios of the manifold volumes are important, however. Figure 83 indicates the wide variations in mixture ratio on startup and shutdown when volume ratios are not optimized (hydrogen to oxygen manifold volume ratio 6.4 for mixture ratio 2.5), resulting in reduced pulse performance.

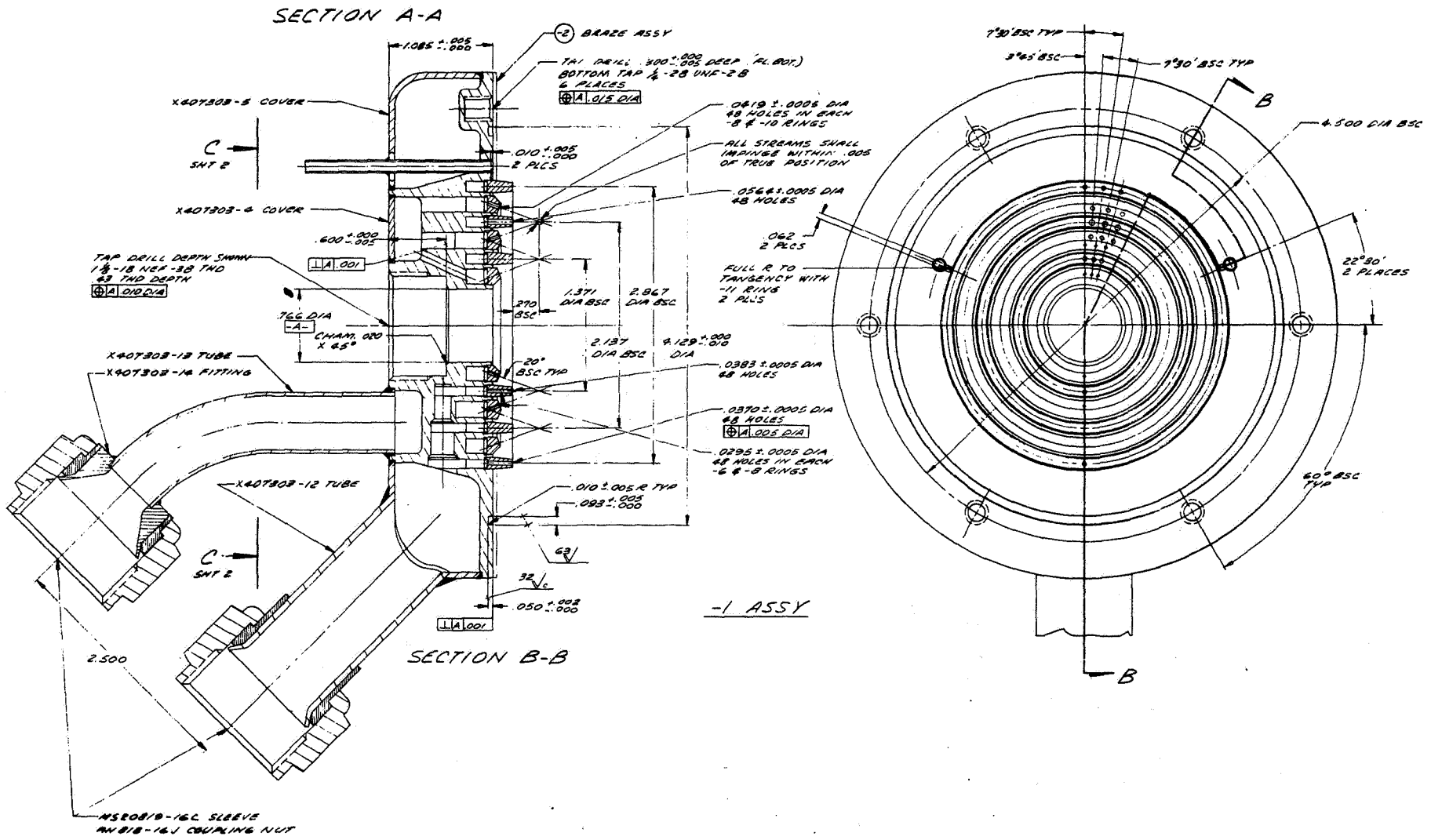

Figure 80. Injector Assembly, H_2/O_2 Thruster. Thre Raised Posts are OFHC Copper, and the Remaining Body is 347 S.S.

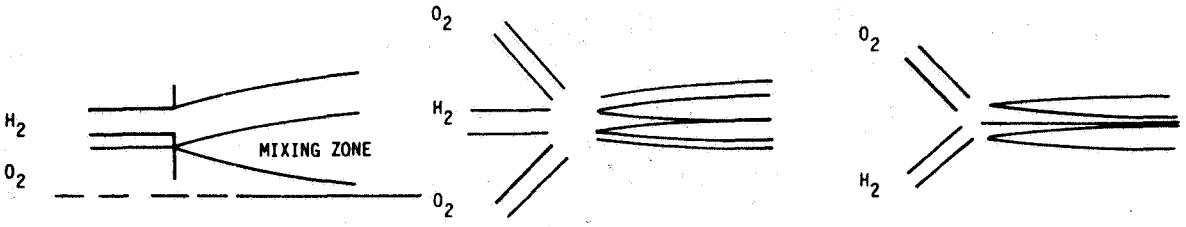

NOTE: H_2 VELOCITY ALWAYS ~5-8 O_2 VELOCITY ASSUMING AXISYMMETRIC SYMMETRY, CENTER LINE CONCENTRATIONS FOLLOW FOR:

$$Y_0 = 1 - \exp\left[\frac{K_0}{K_1 \bar{X} \bar{\rho}_e^{1/2} - K_2}\right]$$

COMBUSTION PERFORMANCE POSTULATED TO BE:

$$\eta_C^* = 1 - Y_0$$

$$\left.\begin{aligned} \bar{X} &= X/r_j \\ \bar{\rho}_e &= \rho_e/\rho_j \end{aligned}\right\} \; j = \text{REFERENCE JET}$$

K_0 = MEASURE OF INTERACTION BETWEEN ADJACENT ELEMENTS

K_1 = MEASURE OF LOCAL TURBULENT MIXING

K_2 = KLEINSTEIN CONSTANT (FROM BASIC THEORY)

$$\bar{X} = C \frac{L^*}{\epsilon_C} \left(\eta_j \frac{P_C}{F}\right)^{1/2} - \eta_j^{1/2} \left(\frac{\epsilon_C^{1.5} - 1}{\epsilon_C}\right)$$

$$\eta_j = \eta_j \left[F, \Delta P_{INJ}/P_C\right]$$

EXAMINED DATA FOR TRIPLET, DOUBLET, SHOWERHEAD, COAXIAL INJECTORS. RANGE OF PARAMETERS:

$0.5 < K_0 < 3.0$

$0.03 < K_1 < 0.1$

$K_3 = 0.70$

← SHOWERHEAD IMPINGING JETS →

Figure 81. Generalized Mixing Model

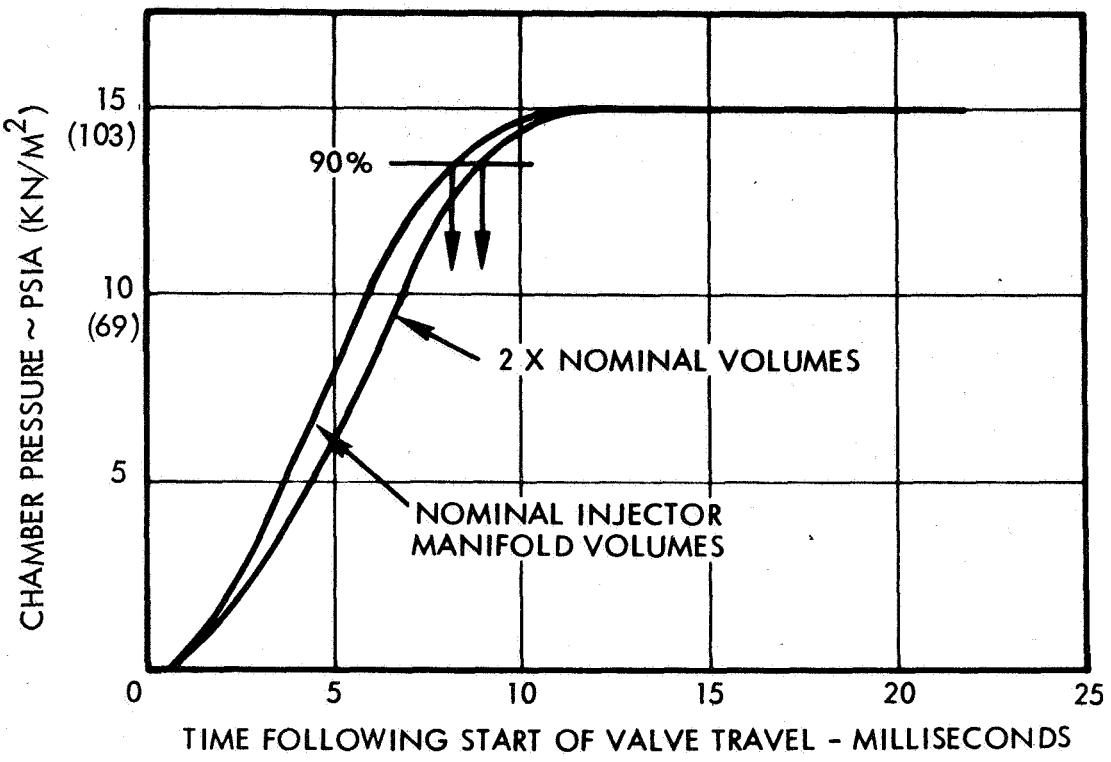

Figure 82. Effect of Injector Volumes on Thruster Start Transient - Low P_c Thruster

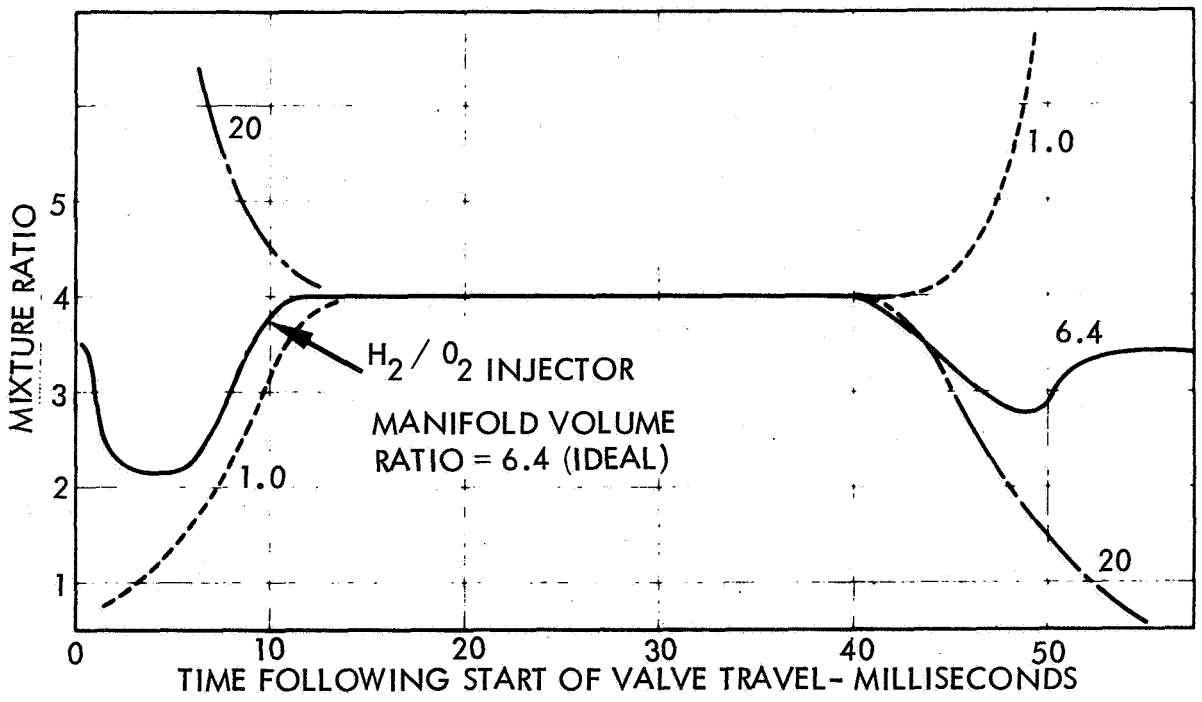

Figure 83. Variation in Pulse Mode Mixture Ratio With Injector Manifold Volume Ratio Low P_c Thruster

After final design approval by the NASA/LeRC Project Manager, the triplet injector shown in Figure 84 was fabricated. The injector body was machined from 347 stainless steel, and the injection rings were made of OFHC copper. All of the injection orifices were formed by electrical discharge machining as the final operation of the injector fabrication.

4.1.1.2 Catalytic Igniter

The catalytic igniter used for the low pressure thruster investigations was previously fabricated during the performance of NAS 3-11227, and is shown in Figure 85. A disassembled view of the same hardware is presented in Figure 86. A section view of this igniter was shown in Figure 40 (Section 3.2.1.1).

Modifications were performed to match this igniter to the low pressure triplet injector and to incorporate downstream oxygen injection, as shown in Figure 87, to achieve high overall igniter response (Section 3.2.2.1).

4.1.2 Thrust Chamber Design

Design and cooling analyses were performed to evaluate both ducted and film/conduction cooled thrust chambers. Based on these analytical results, duct cooling was selected for the flightweight thruster design. A heat sink copper chamber was also designed and fabricated for the injector screening tests.

4.1.2.1 Thrust Chamber Cooling Analysis

Detailed thermal analyses were performed to evaluate both ducted and film/conduction cooling concepts for a thruster capable of both steady-state and pulse mode operation. Existing TRW Systems thermal model and computer programs were utilized in performing these cooling analyses. Figure 88 presents a generalized flow chart of the program employed, which computes temperature distributions for either duct cooled or film cooled thrust chambers. The model is presented in detail in Vol. II.

The results of these computations are shown in Figures 89 through 95. The duct wall, coolant/film, and chamber wall temperatures for duct cooled thin wall chambers of varied duct lengths are shown in Figures 89 through 92. The results of the thin wall chamber calculations are summarized in Figure 93, where predicted chamber wall and throat temperatures are plotted as a function of duct length.

Analyses were also conducted for a thick wall chamber of high conductivity material to identify the effects of axial conduction on reducing maximum chamber temperatures. Figures 94 and 95 present the calculated data for copper chambers of varied thicknesses, and reveal that maximum chamber temperatures can be reduced by over 200°F (111°K) compared to a thin wall chamber with essentially no axial conduction.

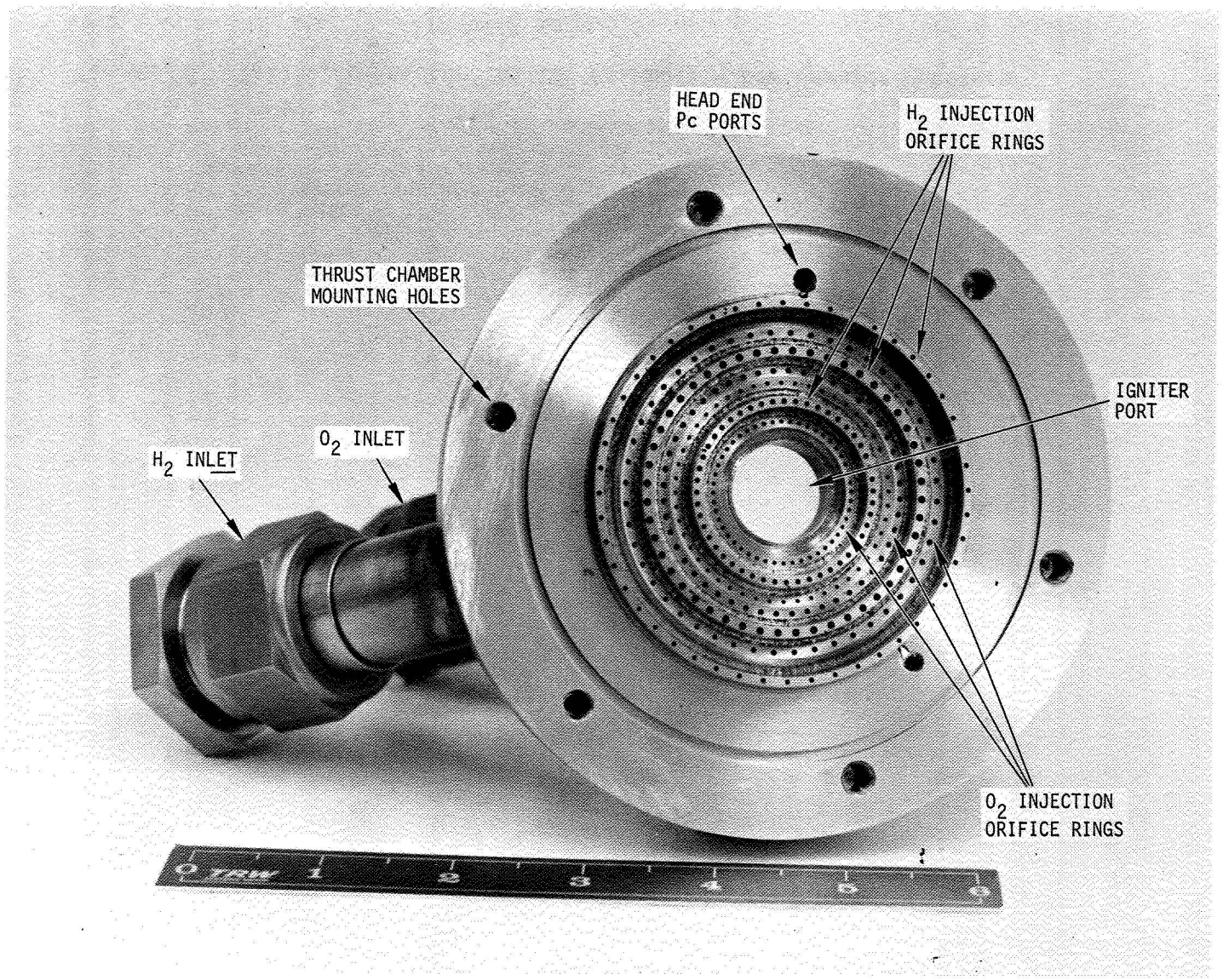

Figure 84. Flightweight Triplet Injector

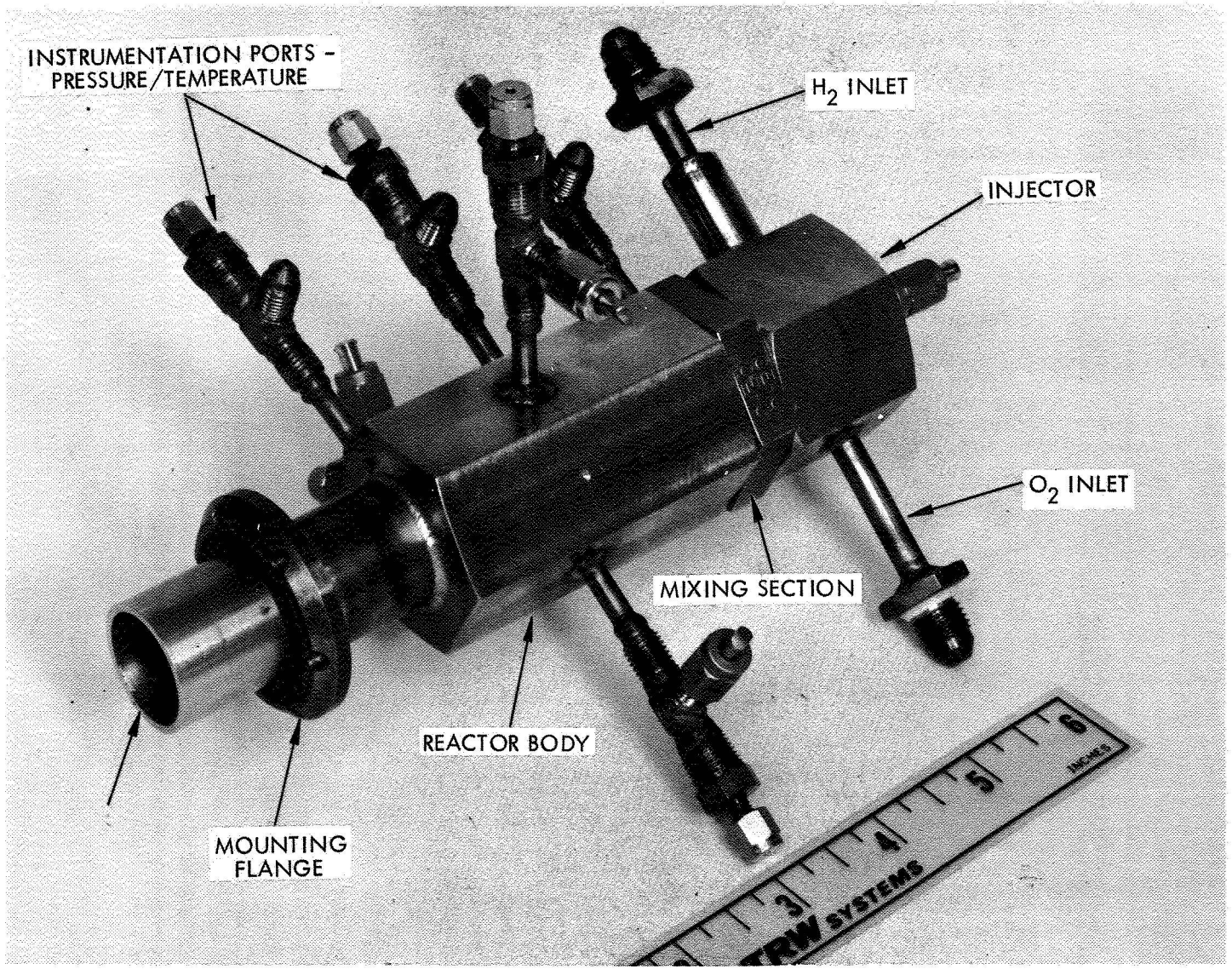

Figure 85. Catalytic Reactor Igniter Assembly - Low Chamber Pressure

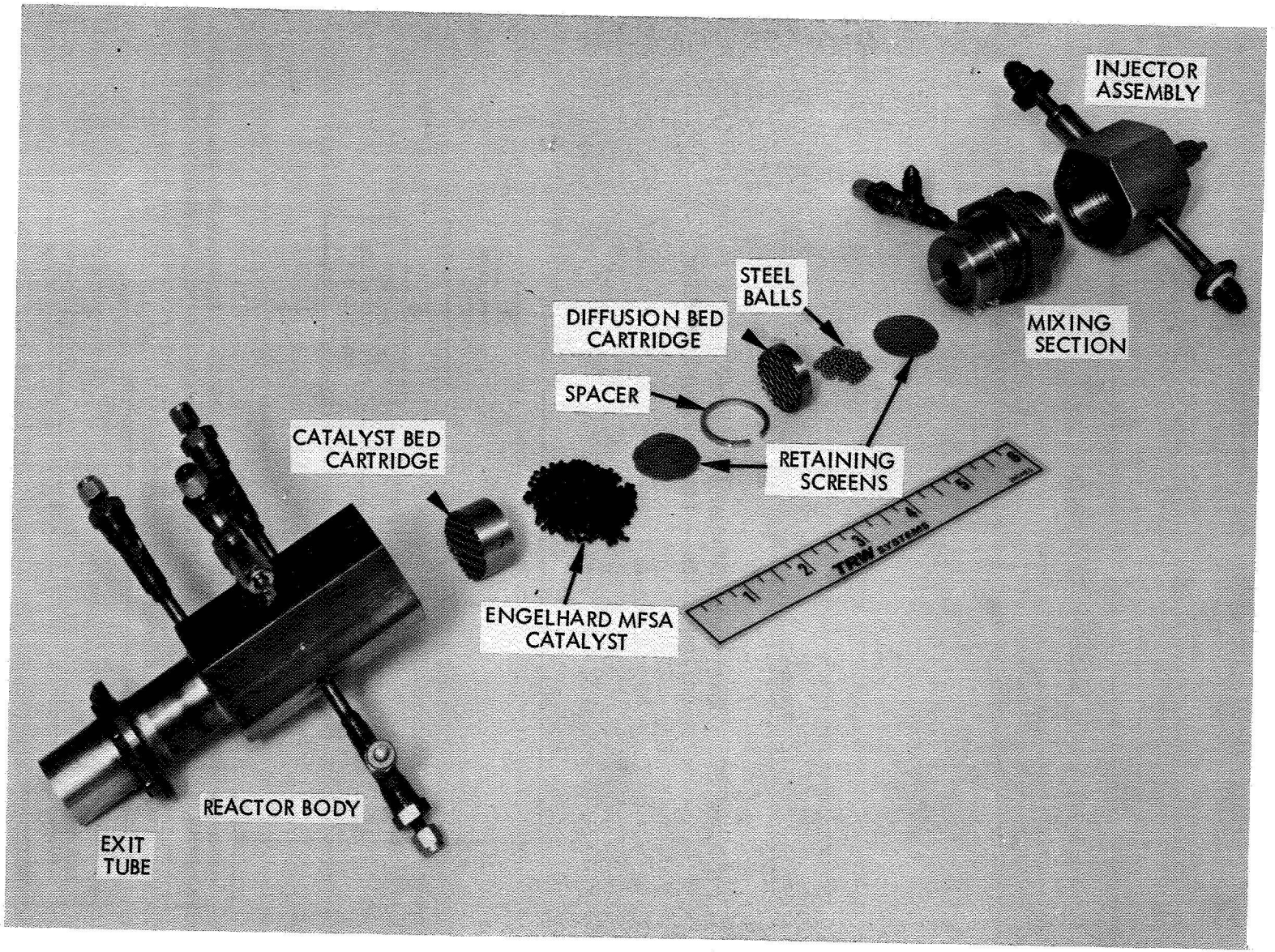

Figure 86. Disassembled Catalytic Reactor Igniter - Low Chamber Pressure

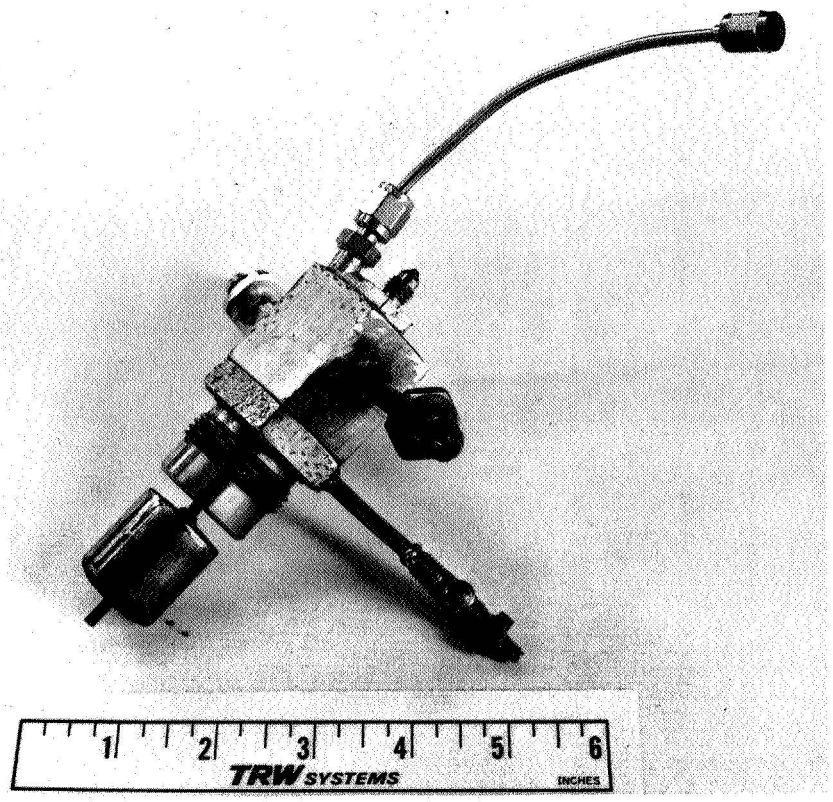

Figure 87. Downstream Oxygen Injection Test Configuration - Low Pressure Reactor

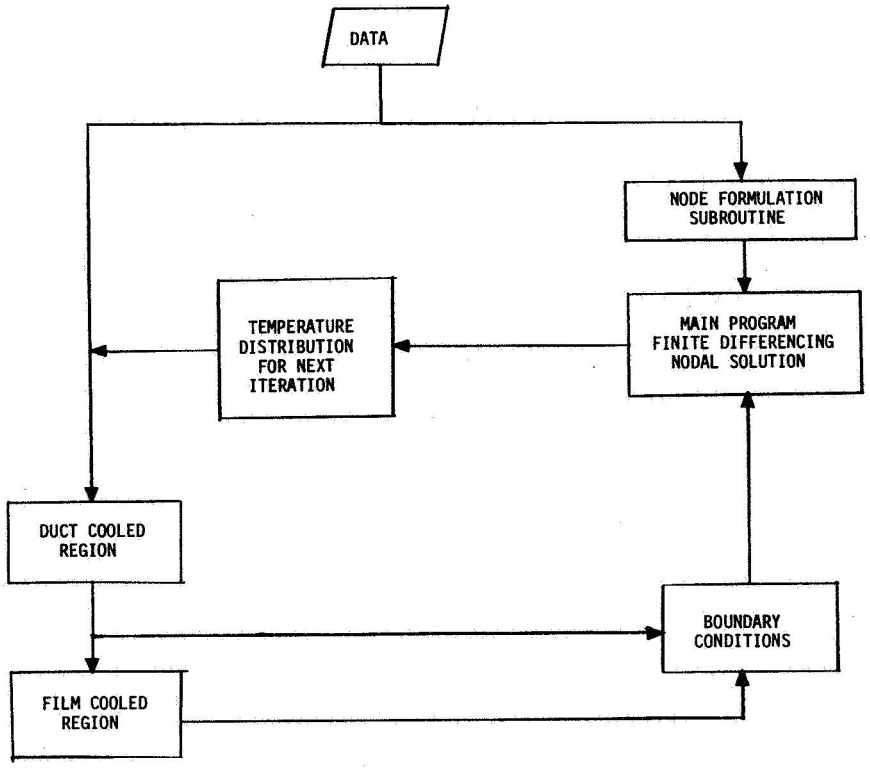

Figure 88. TRW Systems Generalized Duct Film Cooling Program Flow Chart

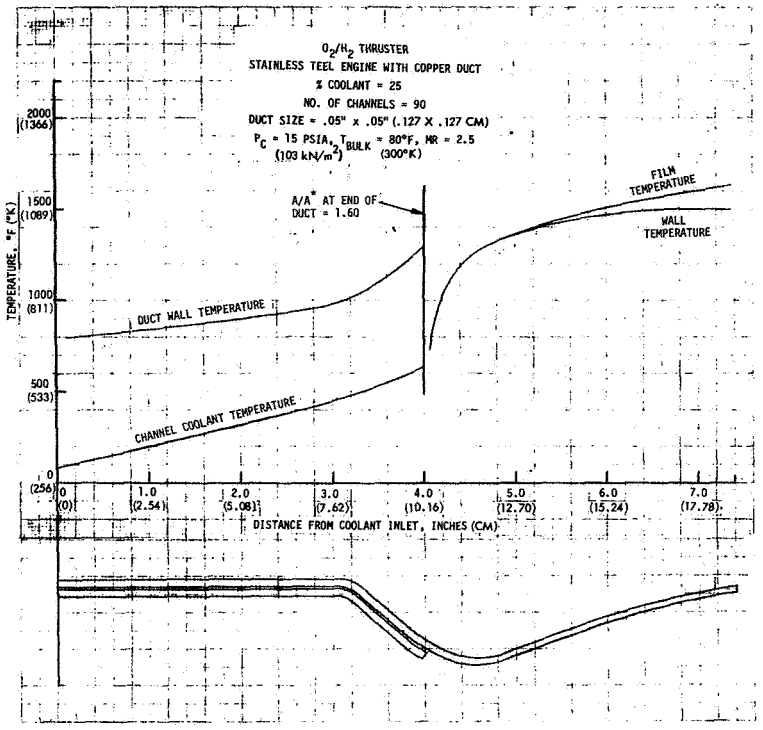

Figure 89. Predicted Thrust Chamber Temperatures, Thin Wall, Duct A/A* = 1.60

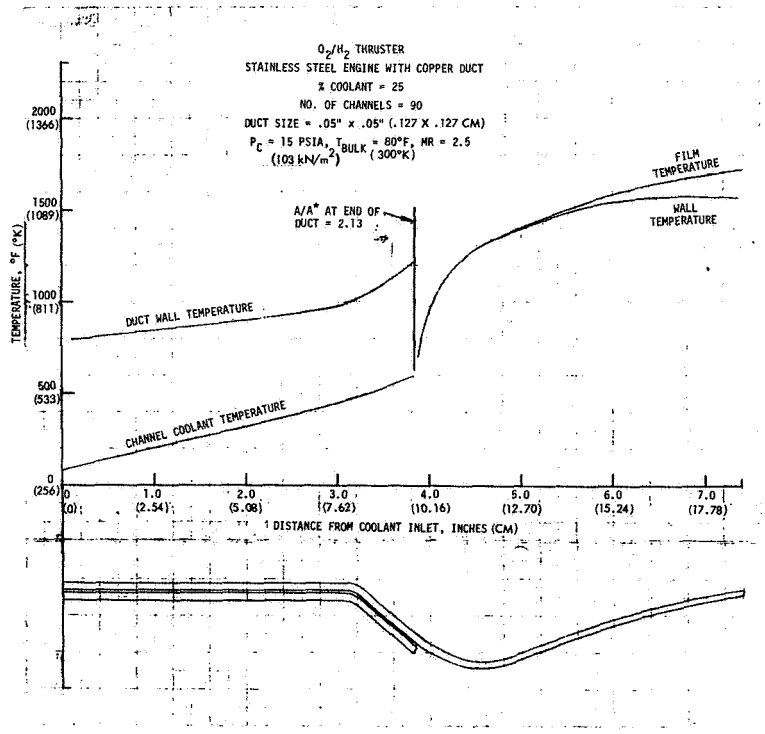

Figure 90. Predicted Thrust Chamber Temperatures, Thin Wall, Duct A/A* = 2.13

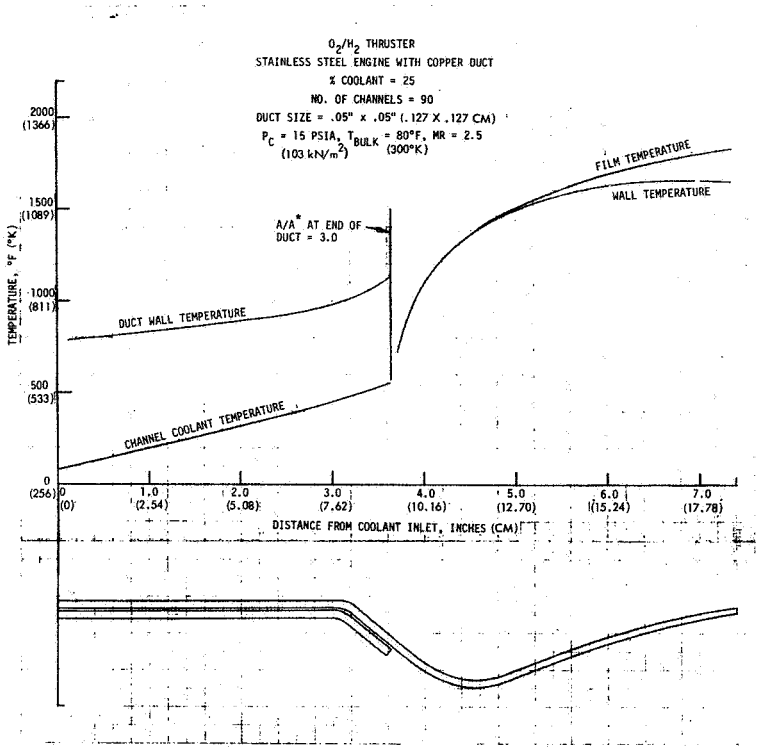

Figure 91. Predicted Thrust Chamber Temperatures, Thin Wall, Duct A/A* = 3.00

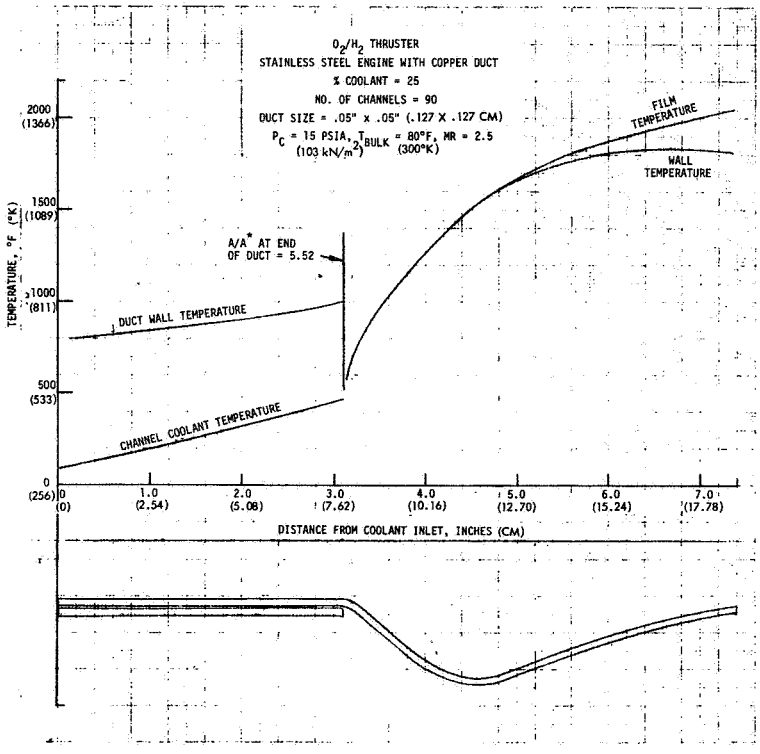

Figure 92. Predicted Thrust Chamber Temperatures, Thin Wall, Duct A/A* = 5.52

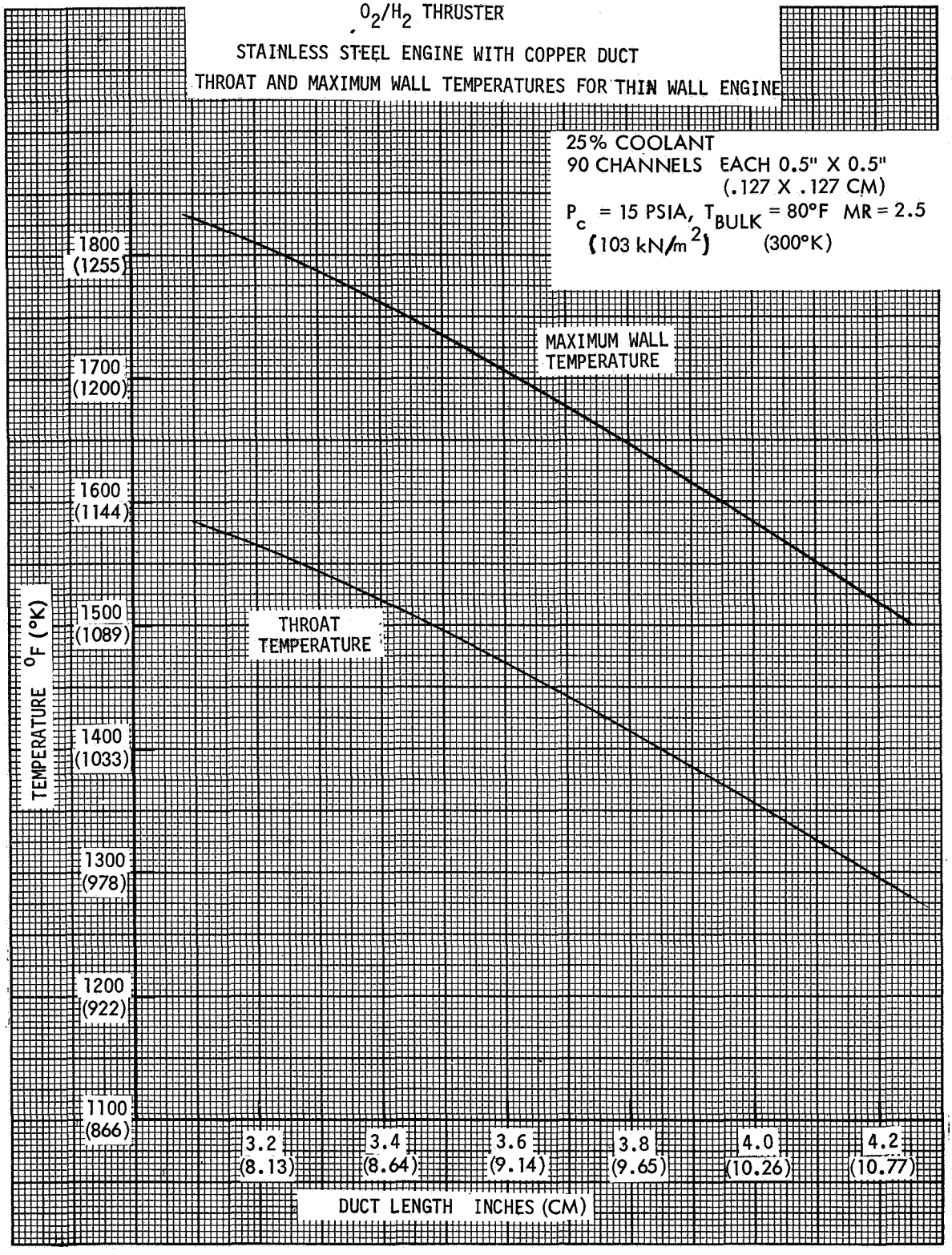

Figure 93. Thrust Chamber Temperatures Versus Duct Length, Thin Wall Chamber

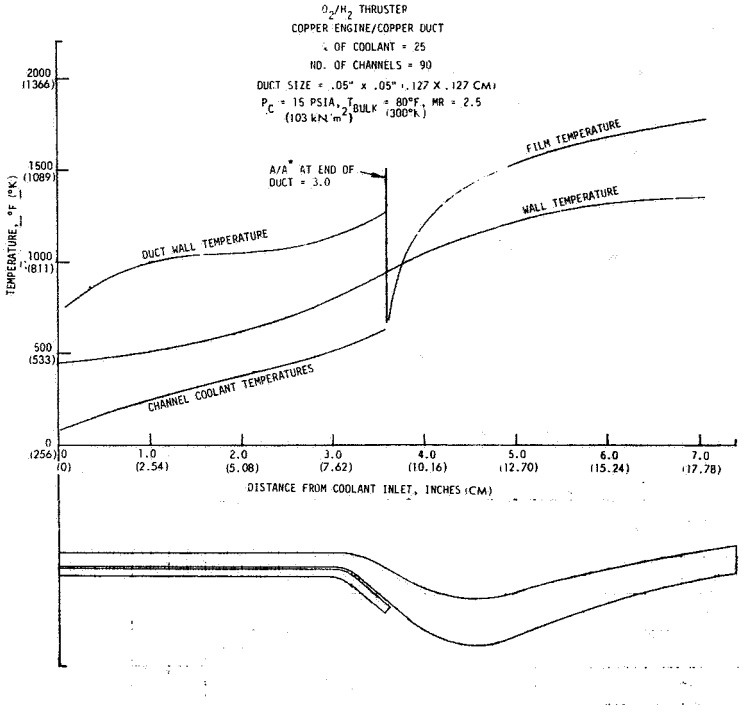

Figure 94. Predicted Thrust Chamber Temperatures, Thick Wall, Duct A/A* = 3.00

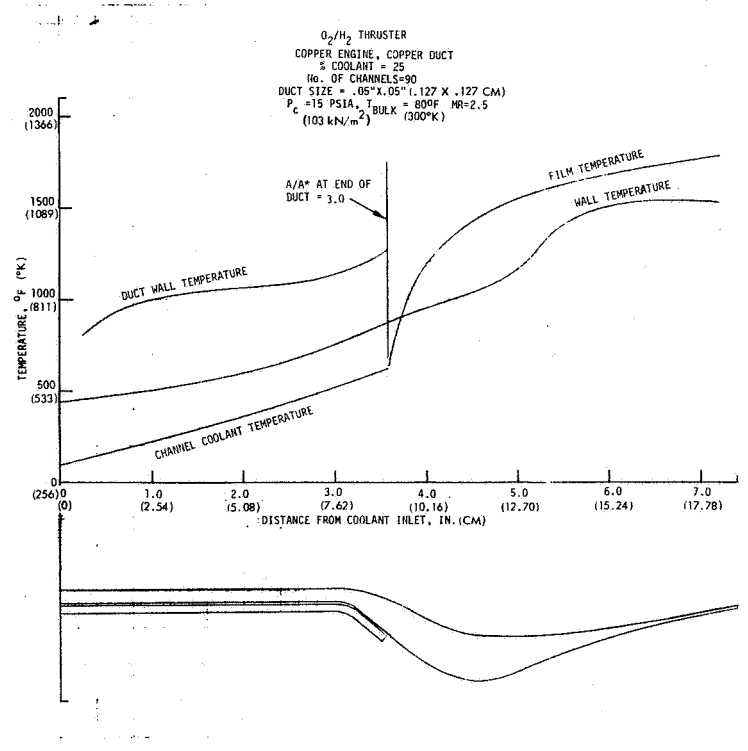

Figure 95. Predicted Thrust Chamber Temperatures, Thick Wall, Thin Exit, Duct A/A* = 3.00

The results of these analyses indicated that satisfactory thrust chamber temperatures for long duration steady-state operation could be attained by duct cooling of a thin walled thruster, with ducts extending beyond a convergent area ratio of 3:1. With thicker walls of a high conductivity material, the duct length could be shorter, but engine weight penalties would be incurred.

The duct/film cooling approach has previously been shown experimentally as well as theoretically to be an effective technique for thrusters of this type. The computed results for this specific application demonstrated the feasibility of attaining the required steady-state operational capability using this concept.

Predicted steady-state operating temperatures are presented in Figure 90 for the thrust chamber and duct design configuration selected. The cooling duct extends to a convergent area ratio (A/A*) of 2.13, as shown at the bottom of the figure. Maximum chamber temperature is slightly over 1500°F (1089°K) in the nozzle.

4.1.2.2 Heat Sink Thrust Chamber

An uncooled thrust chamber was designed and fabricated for injector screening tests of the triplet injector and the residual impinging sheet injector from NAS 3-11227. Figure 96 shows the heat sink thrust chamber design. Numerous thermocouple locations, as shown, provided capability of both axial and circumferential temperature measurements in the thrust chamber wall, throat, and exit areas.

Figure 97 is a photograph of the basic OFHC copper uncooled thrust chamber and additional stainless steel chamber sections used to investigate the effects of variation of chamber L* and length on thruster performance and chamber heat transfer characteristics.

The flightweight triplet injector and heat sink thrust chamber assembly is shown in Figure 98. This assembly was test fired in the injector screening phase, prior to thruster tests with the duct cooled flightweight thrust chamber. The heat sink thrust chamber was also compatible with the NAS 3-11227 impinging sheet injector for screening tests, as illustrated in Figure 99.

4.1.2.3 Duct Cooled Thrust Chamber

Based upon the cooling analysis results, the low pressure duct and cooled thrust chamber designs shown in Figures 100 and 101 were completed. Predicted operating temperatures for this selected cooled chamber design were presented in Figure 90.

In order to vary the duct coolant flow rate during thruster evaluations, the coolant entered the thrust chamber through a hydrogen distribution ring with propellant inlets supplied independently of the thruster injector. The duct hydrogen distribution ring is shown in Figure 102.

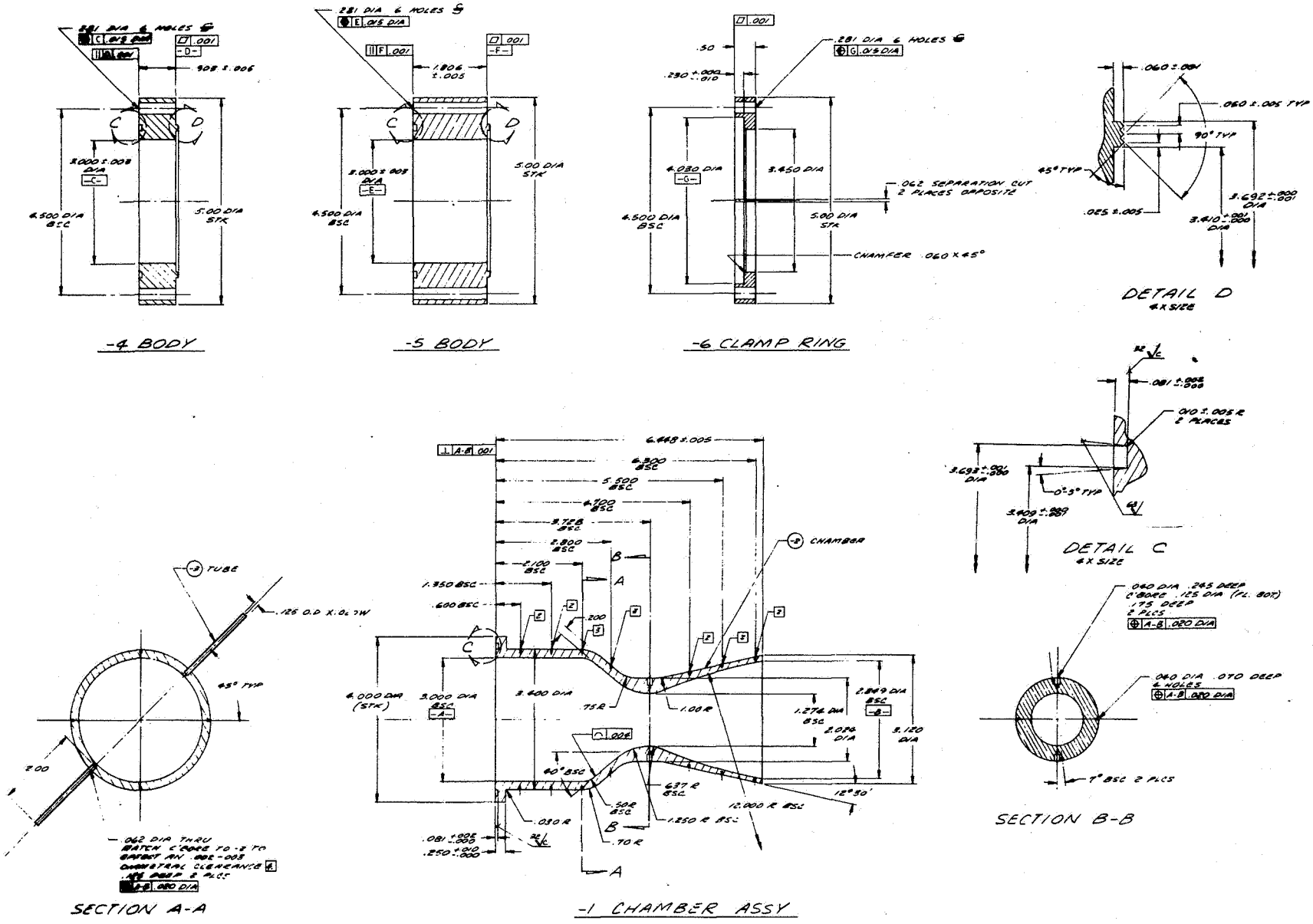

Figure 96. H_2/O_2 Heat Sink Thrust Chamber Components

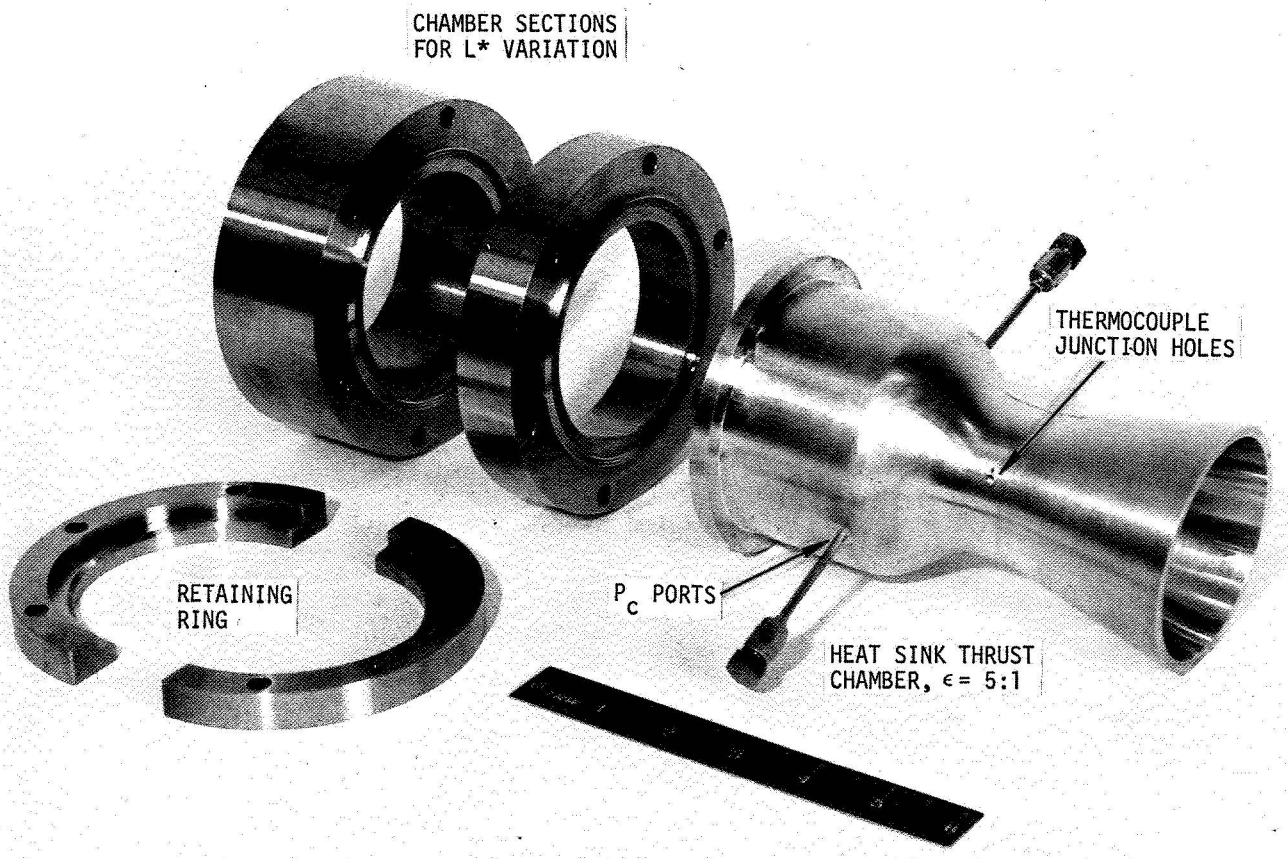

Figure 97. Heat Sink Thrust Chamber Hardware

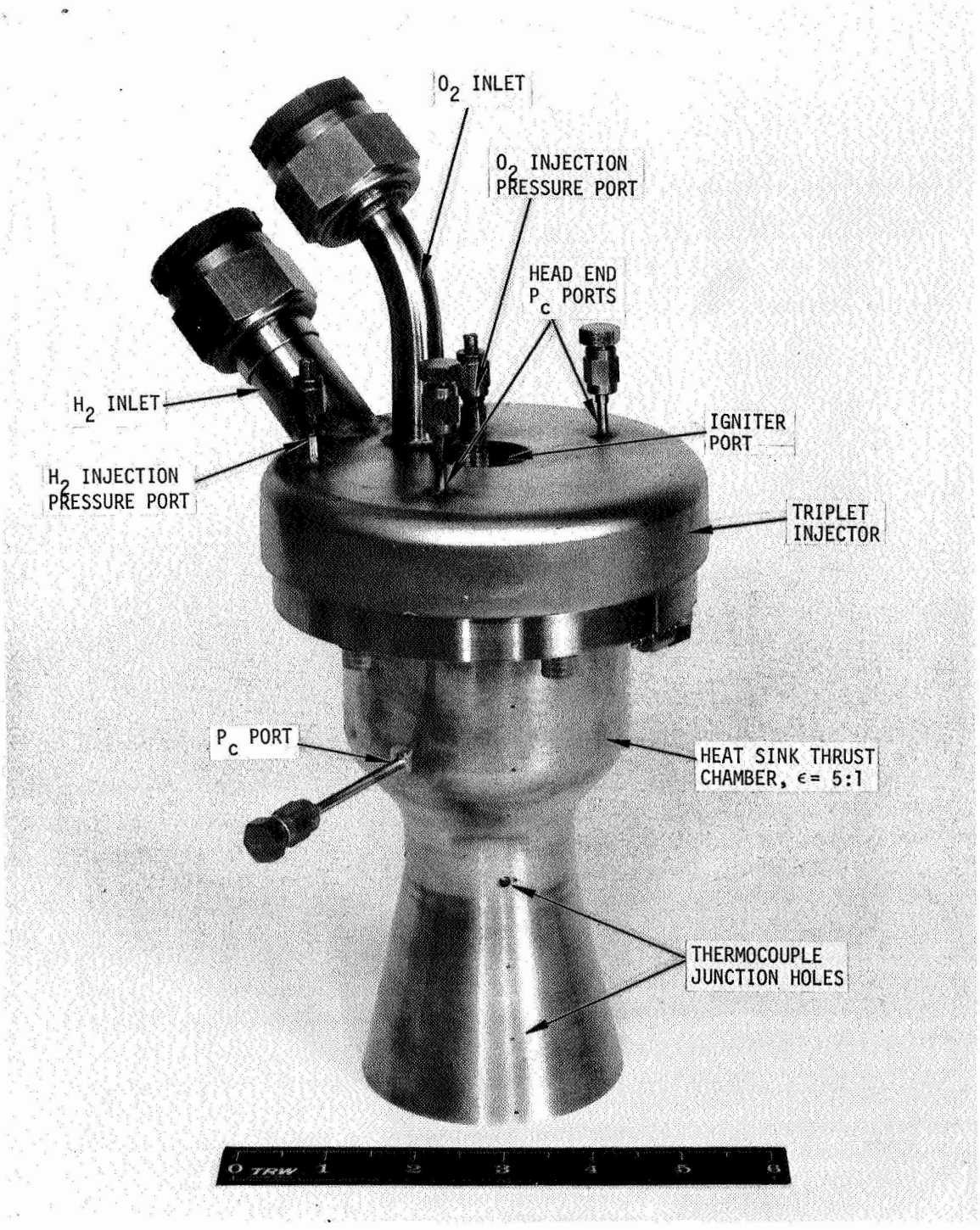

Figure 98. Assembly of Flightweight Triplet Injector and Heat Sink Thrust Chamber

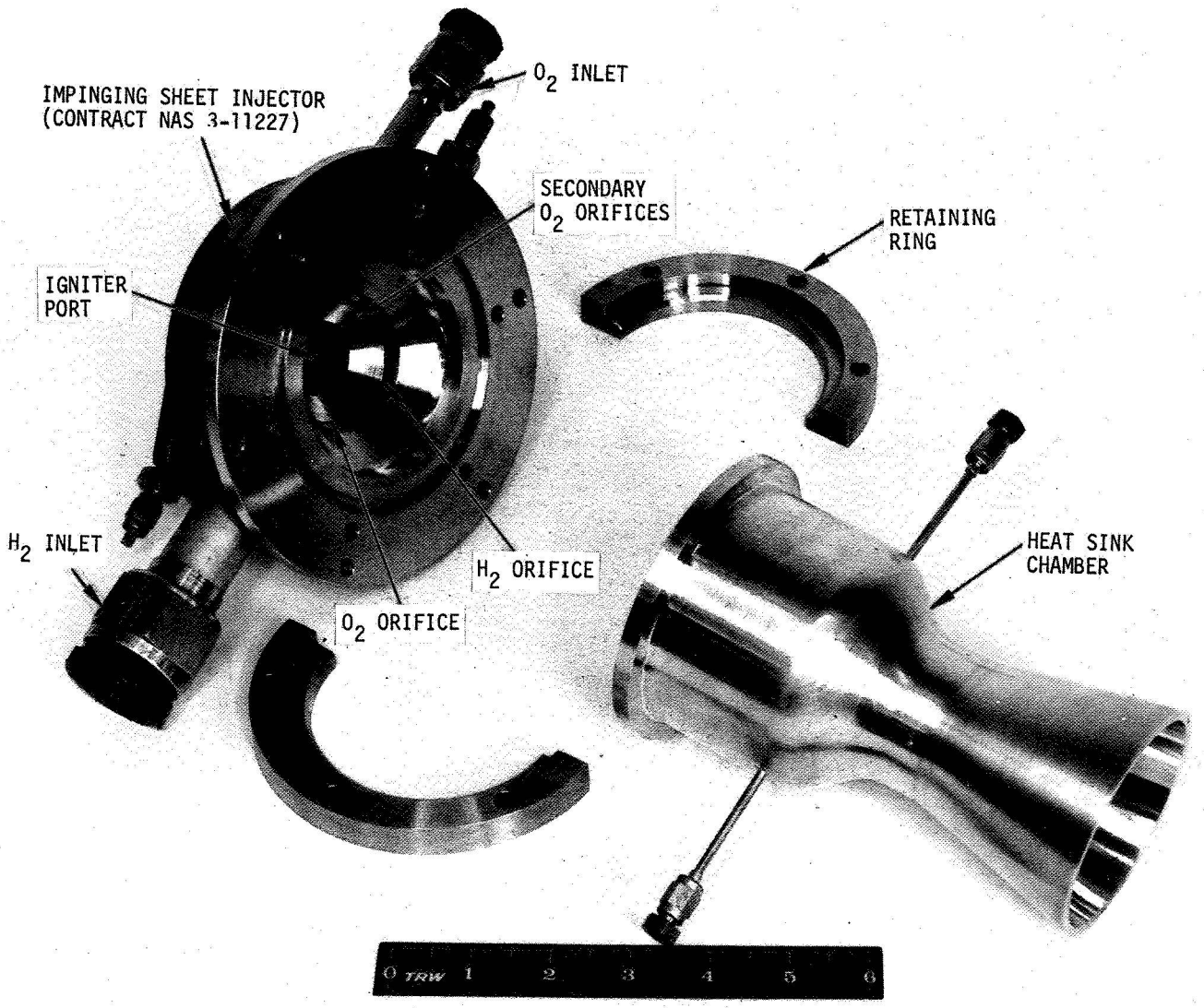

Figure 99. Impinging Sheet Injector (NAS 3-11227) and Heat Sink Thrust Chamber, Disassembled

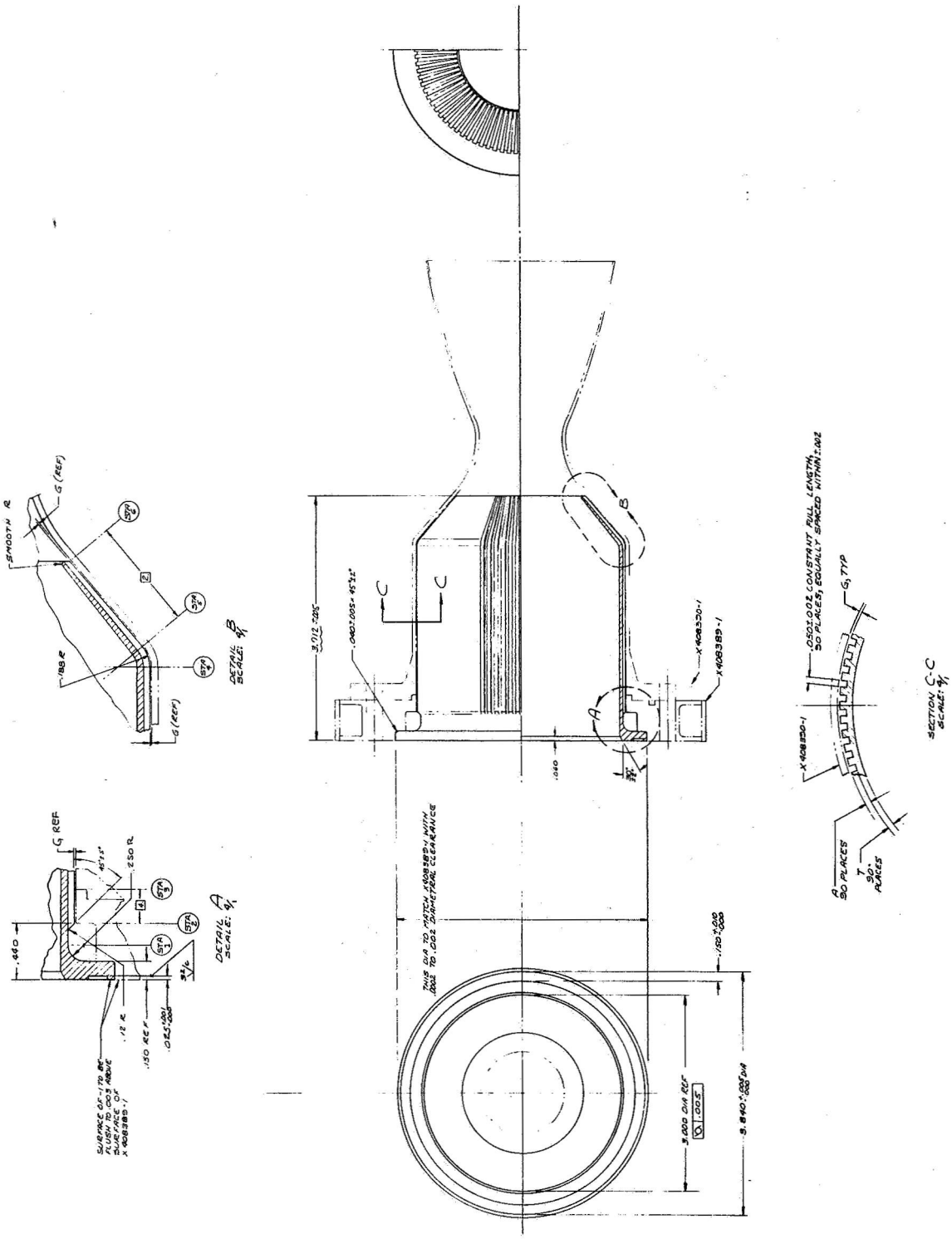

Figure 100. Low Pressure Duct, H_2/O_2 Thruster

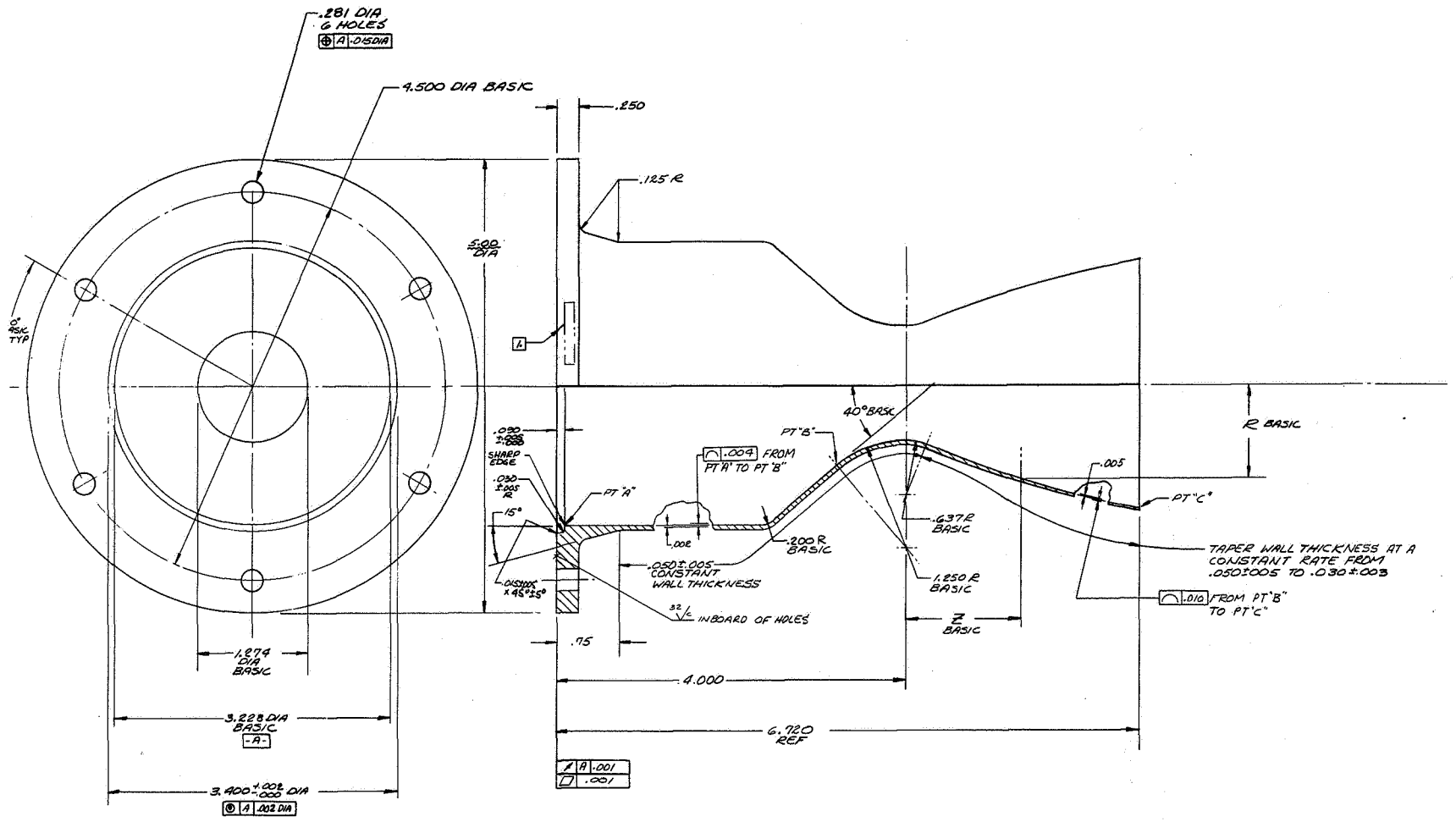

Figure 101. Low Pressure Thrust Chamber and Nozzle, H_2/O_2 Thruster

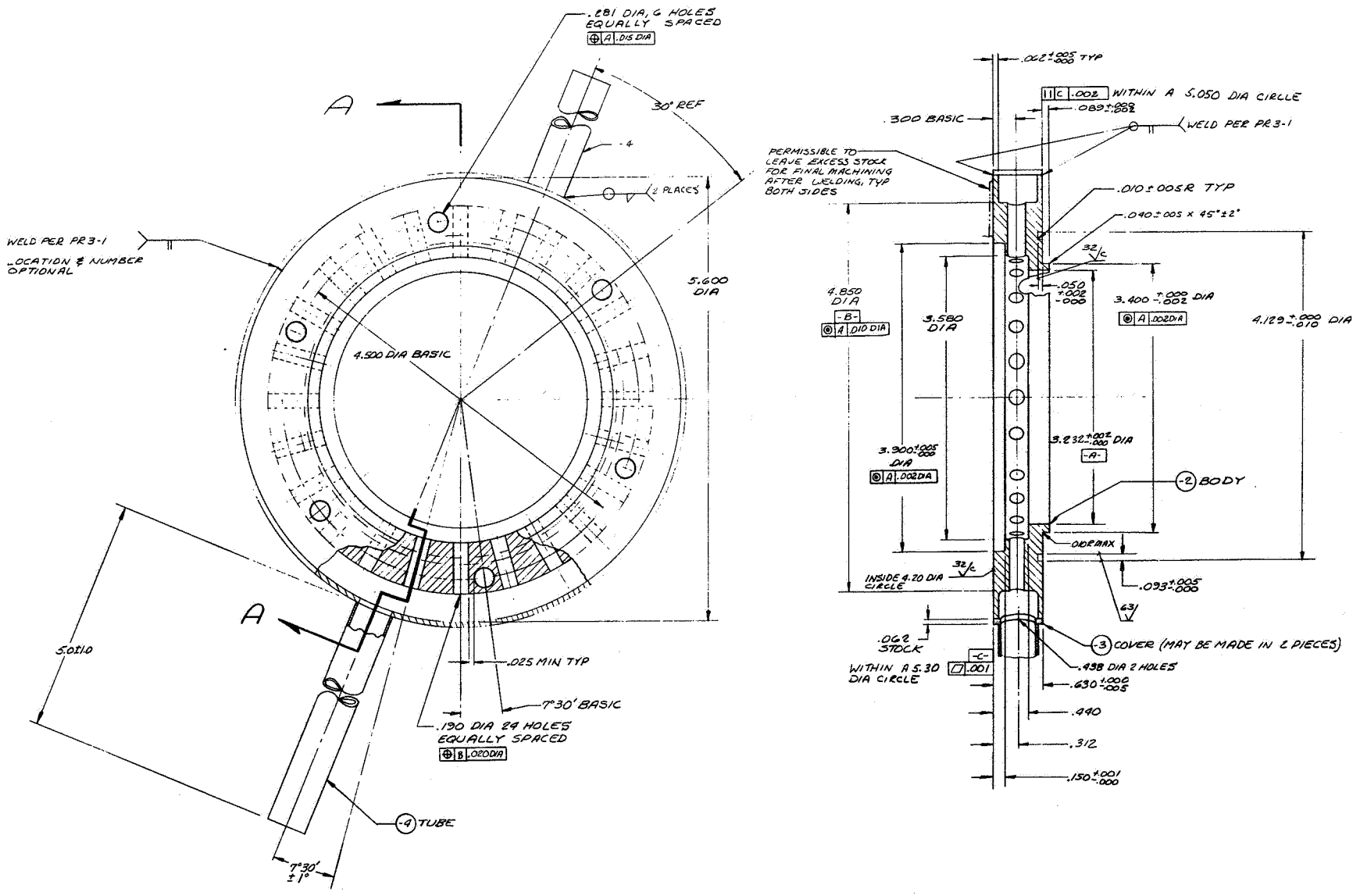

Figure 102. Low Pressure Duct Coolant Distribution Ring, H_2/O_2 Thruster

Fabrication of the low thrust flightweight thrust chamber, cooling ducts, and coolant flow distribution manifold was performed after design approval by the NASA/LeRC Project Manager. Figure 103 shows the A-286 thrust chamber and nozzle with the 5:1 exit ratio specified for this program. Figure 104 is a closeup view of the copper/beryllium alloy (Berylco 10) duct, showing the coolant flow passages. A second duct was fabricated from OFHC copper.

Figure 105 is a disassembled view of the thrust chamber, duct, coolant flow manifold, and the flightweight triplet injector. Figure 106 illustrates the complete assembly of the flightweight duct cooled thruster.

4.2 INJECTOR SCREENING TESTS

A series of injector evaluation tests, including both cold flows and thruster firings, was conducted with the triplet injector designed and built during this program and the residual low chamber pressure injector from NAS 3-11227. The objectives of these screening tests were:

- Conduct cold flow evaluations of both the triplet and impinging sheet injectors in order to make performance predictions
- Perform uncooled thrust chamber tests with each injector to determine baseline injector performance and heat transfer characteristics.

Based on these test results, one injector was selected by the NASA/LeRC Project Manager for the flightweight thruster performance and durability tests.

4.2.1 Injector Cold Flows

TRW has developed and evaluated several diagnostic tools for use in injector cold flow evaluations. For analysis purposes, it is necessary at a minimum to obtain a mapping of the local mass flux and mixture ratio. An evaluation of existing methods for MR determination shows that only the direct chemical analysis method is reliable. Other investigators have used temperature rakes with heated and cooled streams to determine local MR. It has been our experience that this technique is fraught with error inherent to the technique. Figure 107 shows the results of a calculus of error analysis. It indicates that in the zone of MR of interest the error can be so large as to render the data meaningless for combustion performance prediction. As a consequence, chemical analysis has been selected as the best method of analysis for cold flow interpretation.

A review of mixing profile analytical results also indicates that absolute pressure has very little effect on low Mach number stream mixing. As a result, mixing measurements can be made at low pressure as long as the density and velocity ratios are simulated for the actual flows. The TRW chemical sampling apparatus and setup is shown in Figure 108. The sampling rake and locations are shown in Figure 109. Data from this rig

Figure 103. Thrust Chamber and Nozzle-Low Pressure Thruster

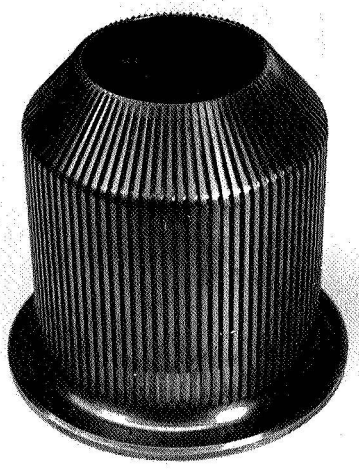

Figure 104. Duct - Low Pressure Thruster

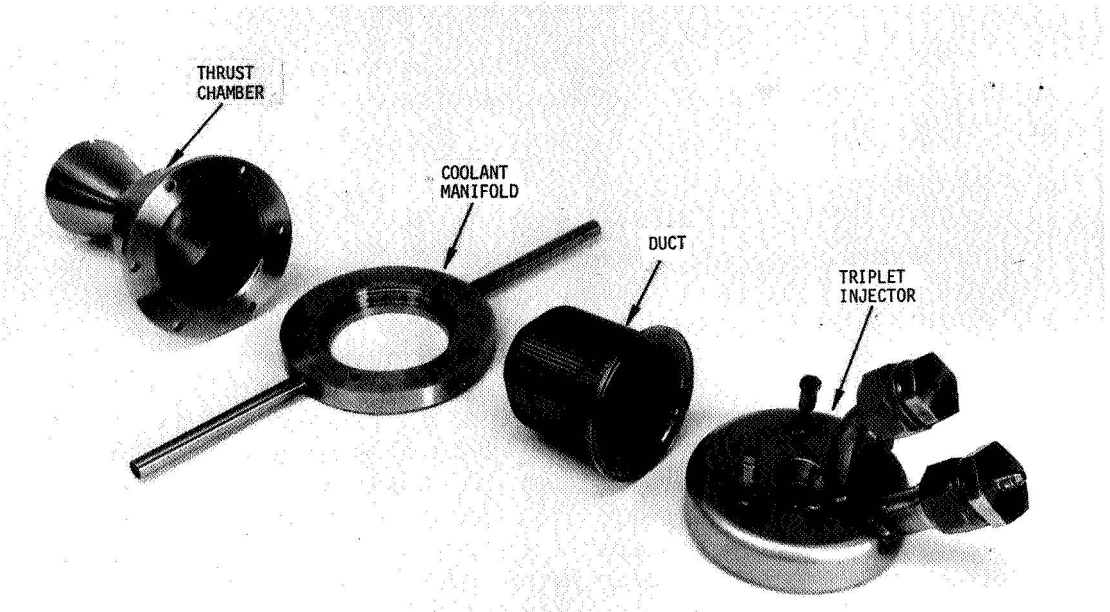

Figure 105. Low Pressure Duct Cooled Thruster Components

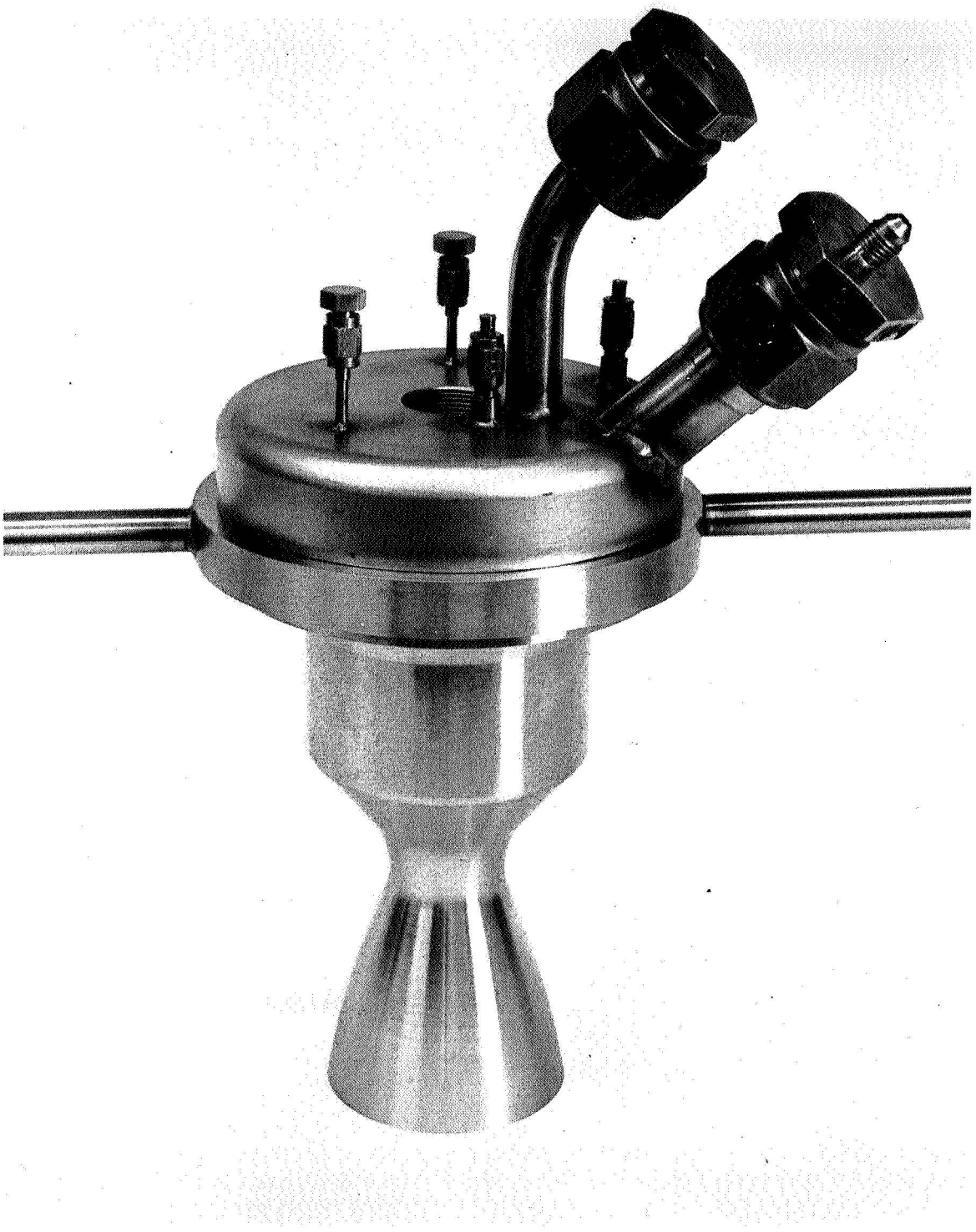

Figure 106. Assembly of Flightweight Triplet Injector and Duct Cooled Thrust Chamber

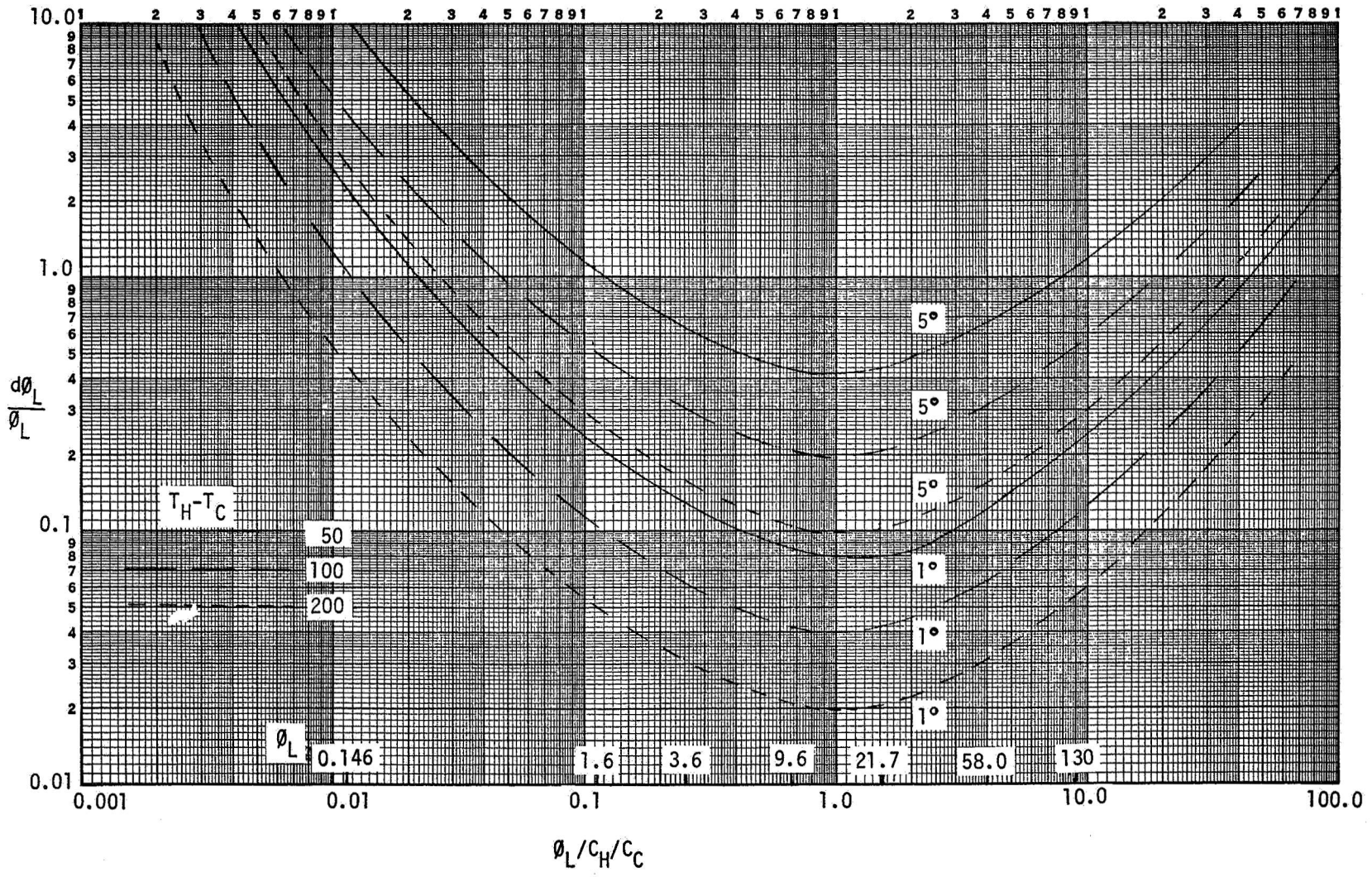

Figure 107. Error Analysis for Temperature Measuring System for ϕ

Figure 108. Injector Cold Flow Characterization - Chemical Analysis for Mixture Ratio

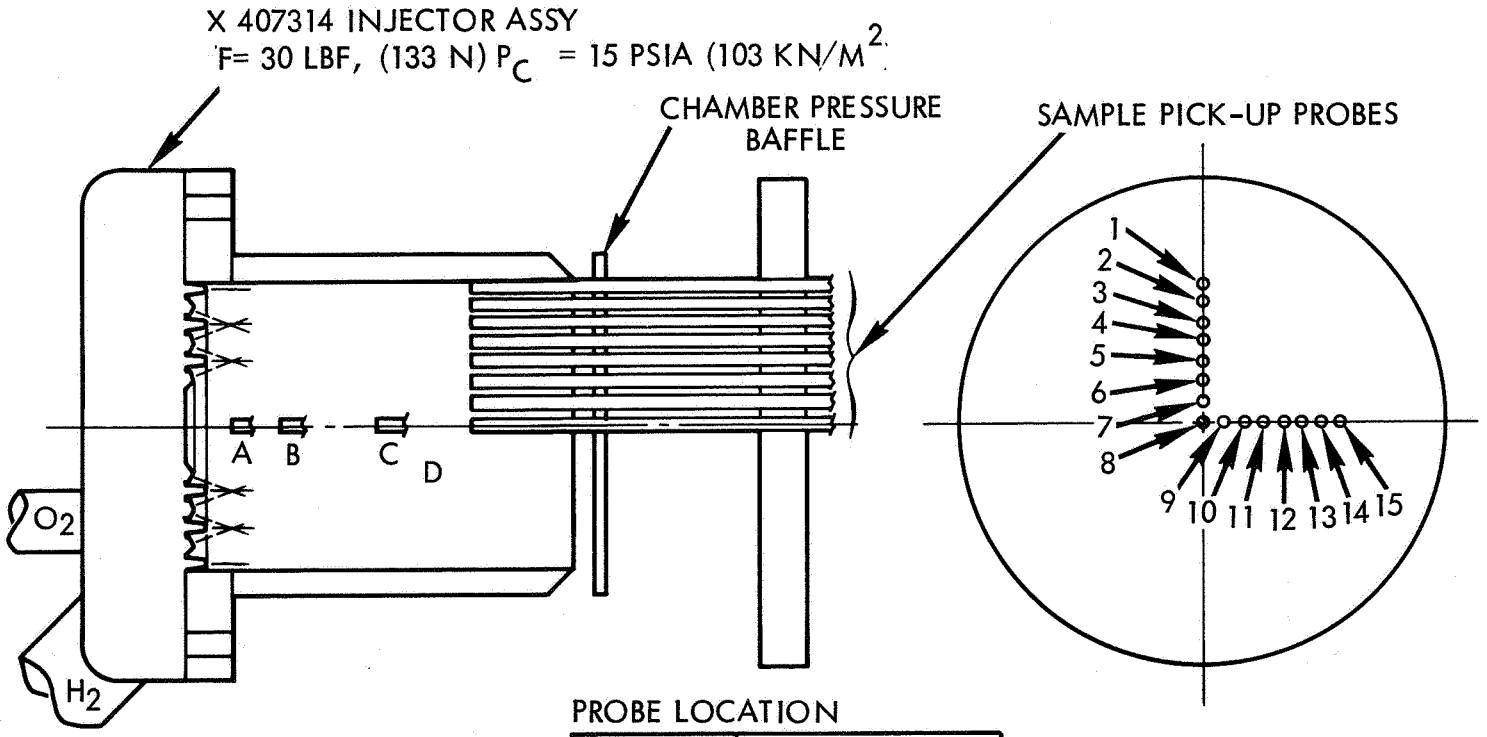

PROBE LOCATION

POSITION	DISTANCE FROM H_2 POST
A	0.25" (.64 CM)
B	0.75 (1.90 CM)
C	1.75 (4.45CM)
D	2.75 (6.98 CM)

Figure 109. Cold Flow Sample Probe Location

provide local MR mapping. The mass flux is determined through use of the total pressure probe shown in Figure 110.

Typical results are given in Figures 111 and 112 for the 30 lbf (133N) triplet injector. The η_{C^*} is determinable as a function of chamber length. As shown in Figure 112, the excellent mixing character of this injector predicts over 99% of theoretical C* performance for a 2 inch (5.08 cm) chamber length.

Cold flow tests were next conducted with the impinging sheet injector from NAS 3-11227 (Figure 99), using the same test apparatus and procedures employed in the triplet injector flows.

Concentric Sheet Injector Cold Flow

Test No. 5
Nominal MR = 2.5
1.5 Inches From Impingement Plane

Probe Number Probe Number	Radius (in)	Local MR Local MR
1	1.43	2.44
2	1.25	2.38
3	1.07	2.31
4	.88	2.24
5	.69	2.24
6	.46	3.66
7	.23	4.06
8	0	5.10
9	.23	4.00
10	.46	2.52
11	.69	2.17
12	.88	2.26
13	1.07	2.30
14	1.25	2.72
15	1.43	2.52

- TOTAL PRESSURE FOR MASS FLUX

$$\frac{\dot{W}}{A} = P_o \left(\frac{P_s}{P_o}\right)^{1/2} \sqrt{\frac{2g}{RT_o}} \left[\left(\frac{\gamma}{\gamma-1}\right)\left(1 - \left(\frac{P_s}{P_o}\right)^{\frac{\gamma-1}{\gamma}}\right)\right]^{1/2}$$

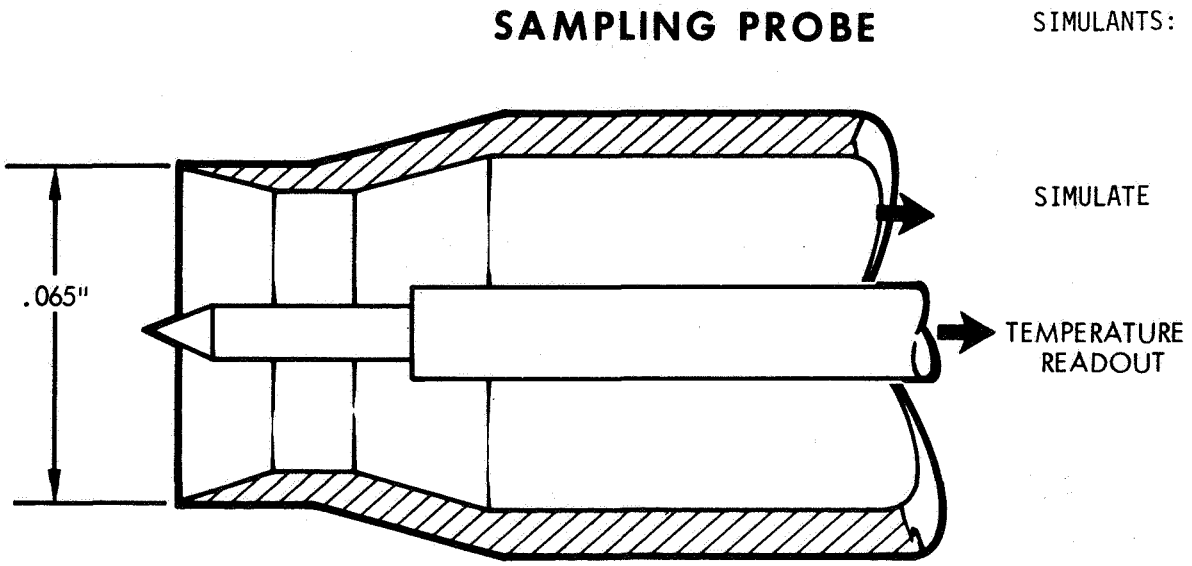

SIMULANTS: He or H_2 FOR H_2

N_2 FOR O_2

SIMULATE ρV , MR.

Figure 110. Injector Cold Flow Characterization

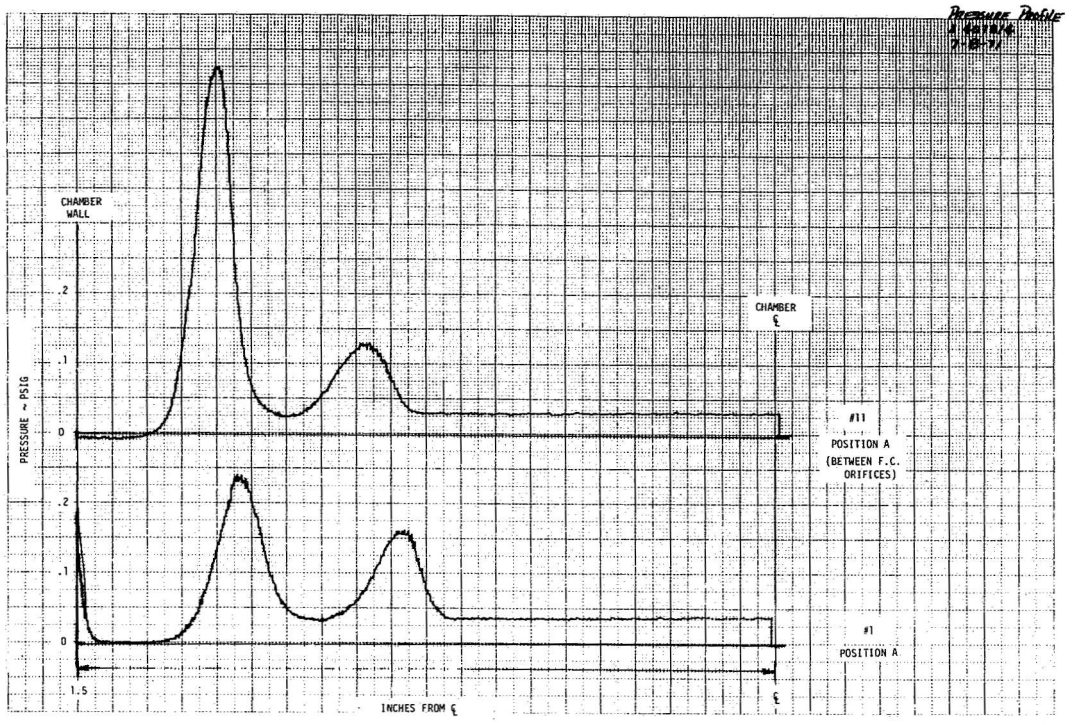

(a)

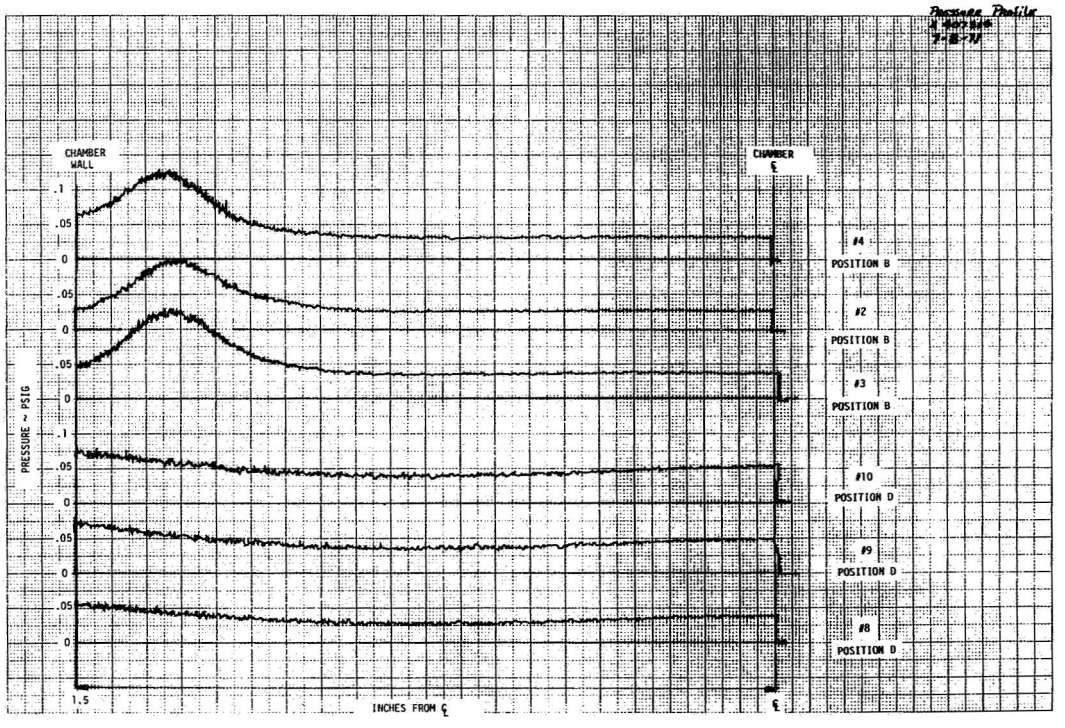

(b)

Figure 111. Typical Total Pressure Results

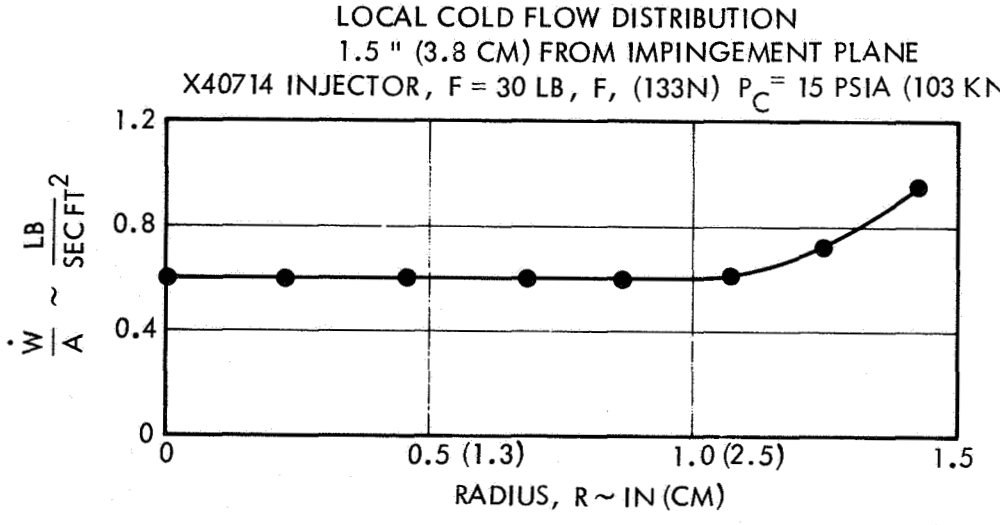

$$C^*(X) = \frac{\Sigma \frac{\dot{W}}{A} \Delta A\, C^*}{\Sigma \frac{\dot{W}}{A} \Delta A} \quad \text{LOCAL}$$

$$MR_{CALC} = \frac{\Sigma MR \frac{\dot{W}}{A} \Delta A}{\Sigma \frac{\dot{W}}{A} \Delta A}$$

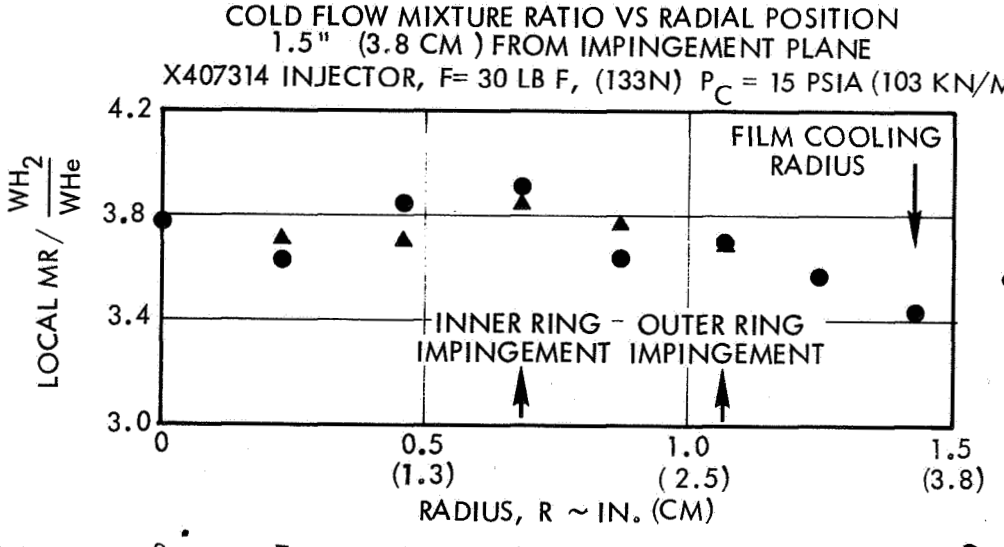

RESULTS:

η_{C^*} ~ 99.7 AT X = 1.5 IN(3.8 CM)

~ 99.0 AT X = 0.5 IN (1.3 CM)

X MEASURED FROM IMPINGEMENT

● INDICATES EXCELLENT MIXING EFFICIENCY OF TRIPLET DESIGN

SAMPLE NO. 8 7 6 5 4 3 2 1 ●
9 10 11 12 13 ▲

$\frac{LB}{SEC\,FT^2}$ $\frac{KG}{SEC\,M^2}$ $\frac{.453}{.0929}$

Figure 112. Combustion Performance Prediction, Triplet Injector Cold Flow

4.2.2 Uncooled Thruster Firings

Low pressure injector screening tests were performed with the triplet and impinging sheet injectors using the heat sink thrust chamber hardware described in Section 4.1.2.2. The initial injector screening tests were performed with the residual low chamber pressure concentric sheet injector from NAS 3-11227. Figure 113 shows the basic design of this injector. Test stand installation of the impinging sheet injector is illustrated in Figure 114; the triplet injector was tested in the same setup.

Data from the low pressure injector screening tests are listed in Table 21, and the results are described as follows:

Tests 319A-321H: Baseline injector performance for the concentric sheet injector was determined over a range of mixture ratios from 1.4 to 4.0 (an injector MR of 4.0 results at an overall MR of 3.0 when 25% of the hydrogen is used for chamber cooling of the flightweight thruster). These tests were performed with ambient temperature propellants, and firings were repeated at each mixture ratio.

Tests 325L-O: Concentric sheet injector evaluations were also conducted with propellants conditioned to a nominal inlet temperature of -250°F (117°K), using a liquid nitrogen heat exchanger to cool the gaseous hydrogen and oxygen. Approximately the same performance levels were attained with cold propellants, based on reduced theoretical C* values for these inlet temperatures.

Tests 331A-H: Ambient propellant tests performed with the triplet injector resulted in performance increases from 2 to 7%, depending on mixture ratio, compared to the concentric sheet injector.

Tests 333E-J: Low temperature propellant tests with the triplet injector over a mixture ratio range of 1.8 to 4.4 indicated a decrease of approximately 2% in combustion efficiency compared to ambient temperature propellant tests.

Performance results of the screening tests with each injector are compared in Figure 115. C* performance data points were very repeatable over a propellant mixture ratio survey from 1.5 to 4.0 O/F. The data point at exactly 2.5 mixture ratio in Figure is from previous tests of the impinging sheet injector under Contract NAS 3-11227, and shows excellent agreement with the recent test results.

Although lower in performance than originally predicted from injector cold flow analysis, the triplet injector delivered at least 2% higher C* than the impinging sheet injector, and was significantly higher in performance at the mixture ratio extremes. Performance of the triplet injector closely follows the theoretical C* over the entire mixture ratio range tested, indicating that the triplet design delivers consistent C* efficiency over wide mixture ratio varations. Post-firing condition of the triplet injector is shown in Figure 116. The injector face experienced no erosion or other damage during hot firings, and remained in excellent condition.

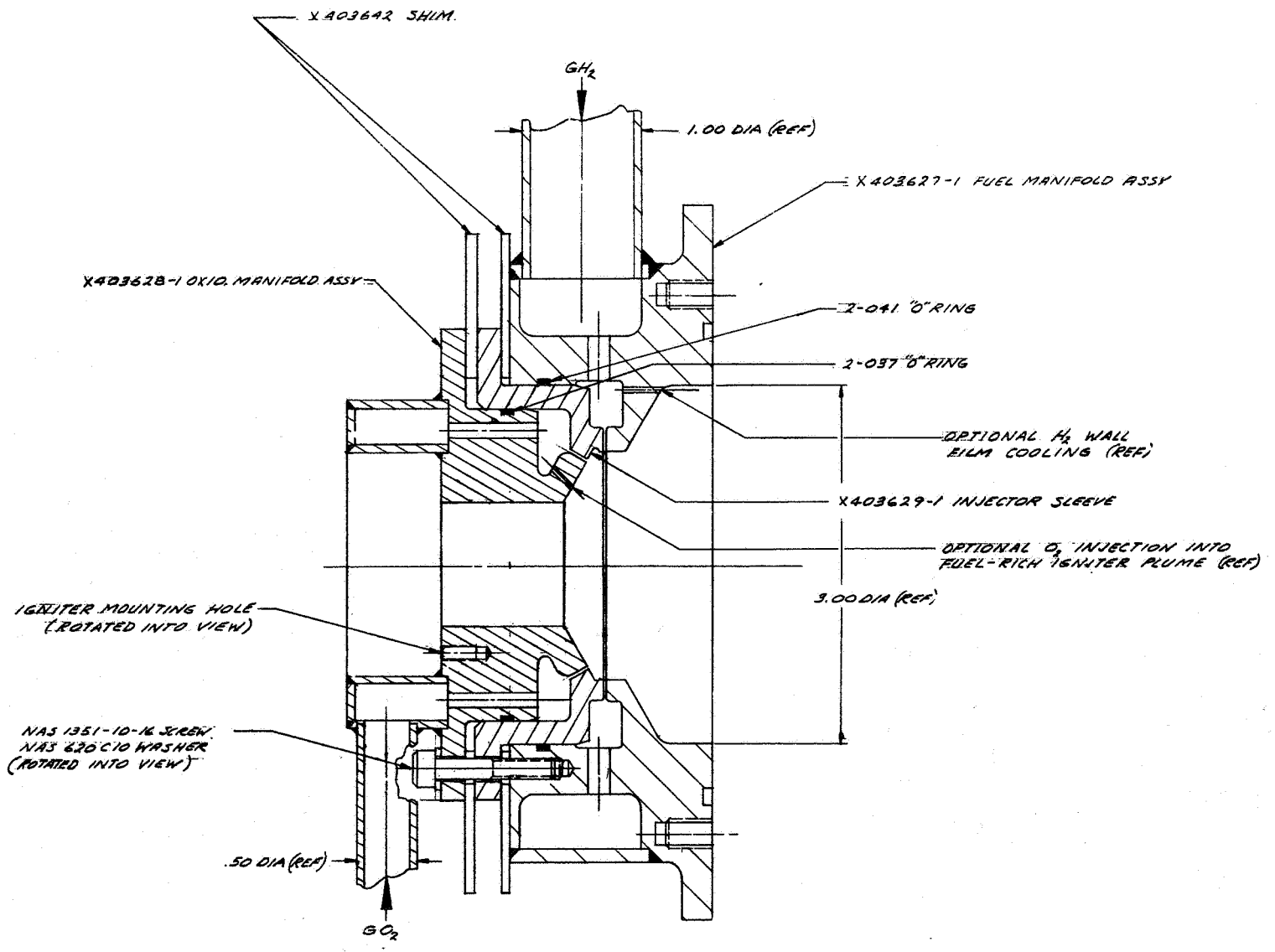

Figure 113. Impinging Sheet Injector (Contract NAS 3-11227)

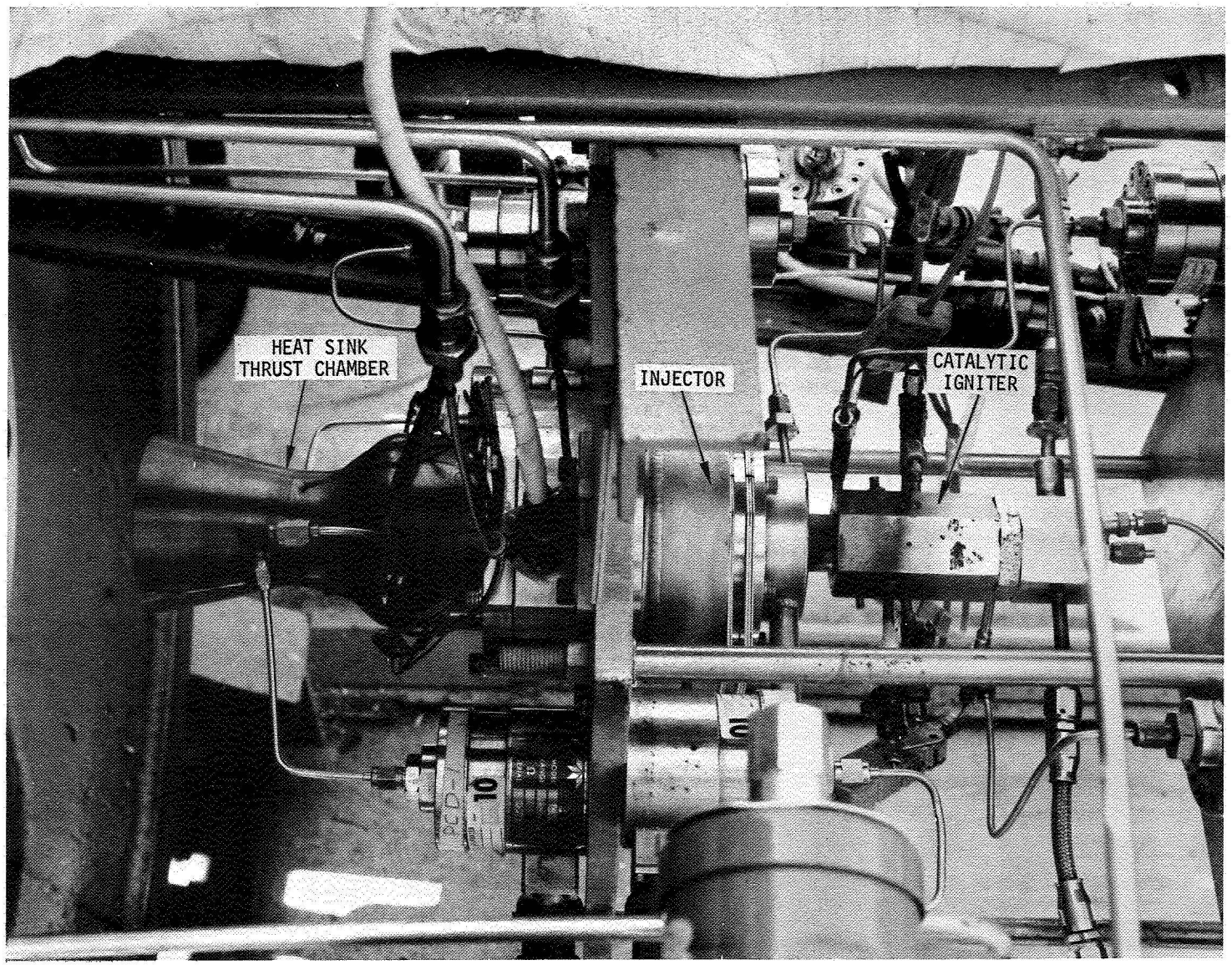

Figure 114. Test Stand Installation - Impinging Sheet Injector and Heat Sink Chamber

Table 21. Low Pressure Injector Screening Tests - Uncooled Thrust Chamber

Test No. (HA5-)	P_{CD} (lbf/in^2)	P_{CD} (kN/m^2)	$\dot{W}_{total}$ (lb/sec)	$\dot{W}_{total}$ (kg/sec)	Mixture Ratio (O/F)	$C^*_{corrected}$ (ft/sec)	$C^*_{corrected}$ (m/sec)	η_{C^*} (%)	Comments
319A	14.30	98.6	0.0772	0.0350	2.385	7717	2352	91.9	
319B	14.88	102.6	0.0801	0.0363	2.356	7636	2327	90.9	
319C	14.21	98.0	0.0806	0.0454	1.414	7252	2210	87.5	
319D	14.91	102.8	0.0802	0.0364	2.766	7642	2329	91.4	
319E	15.30	105.5	0.0822	0.0373	2.813	7649	2331	91.6	
319F	15.22	104.9	0.0816	0.0370	2.423	7665	2336	91.3	Concentric sheet injector
319G	14.96	103.1	0.0827	0.0375	1.430	7432	2265	89.6	(NAS 3-11227)
319H	14.80	102.0	0.0830	0.0376	1.428	7335	2236	88.6	Ambient propellant temperature
321D	14.91	102.8	0.0833	0.0378	1.547	7353	2241	88.7	
321E	15.48	106.7	0.0829	0.0376	2.542	7676	2340	91.4	
321F	15.15	104.5	0.0820	0.0372	3.046	7593	2314	91.5	
321G	13.92	96.0	0.0822	0.0373	3.993	6963	2122	86.0	
321H	14.26	98.3	0.0840	0.0381	3.930	7029	2142	86.8	
325L	14.03	96.7	0.0771	0.0350	1.941	7478	2279	91.6	
325M	14.36	99.0	0.0807	0.0366	1.557	7312	2229	90.4	Concentric sheet injector
325N	14.81	102.1	0.0839	0.0381	1.375	7254	2211	89.9	-250°F (117°K) propellant
3250	11.95	82.4	0.0669	0.0303	2.553	7331	2234	89.6	
331A	14.35	98.9	0.0763	0.0346	1.584	7726	2355	93.1	
331B	14.73	101.6	0.0783	0.0355	1.600	7735	2358	93.1	
331C	14.86	102.5	0.0778	0.0353	2.662	7844	2391	93.5	
331D	14.78	101.9	0.0785	0.0356	3.254	7741	2359	93.5	Triplet injector
331E	14.61	100.7	0.0800	0.0363	3.963	7504	2287	92.6	Ambient propellant temperature
331F	15.05	103.8	0.0828	0.0376	4.136	7474	2278	93.4	
331G	15.15	104.5	0.0807	0.0366	3.226	7712	2351	93.1	
331H	15.09	104.0	0.0791	0.0359	2.655	7845	2391	93.6	
333E	14.73	101.6	0.0852	0.0386	1.830	7114	2168	87.9	
333F	14.70	101.3	0.0812	0.0368	2.517	7437	2267	90.6	
333G	15.08	104.0	0.0881	0.0400	4.408	7032	2143	91.3	Triplet injector
333H	14.42	99.4	0.0835	0.0379	4.150	7101	2164	92.4	-250°F (117°K) propellant
333I	16.08	110.9	0.0880	0.0399	2.403	7508	2288	91.6	
333J	14.83	102.2	0.0833	0.0378	1.829	7321	2231	90.0	

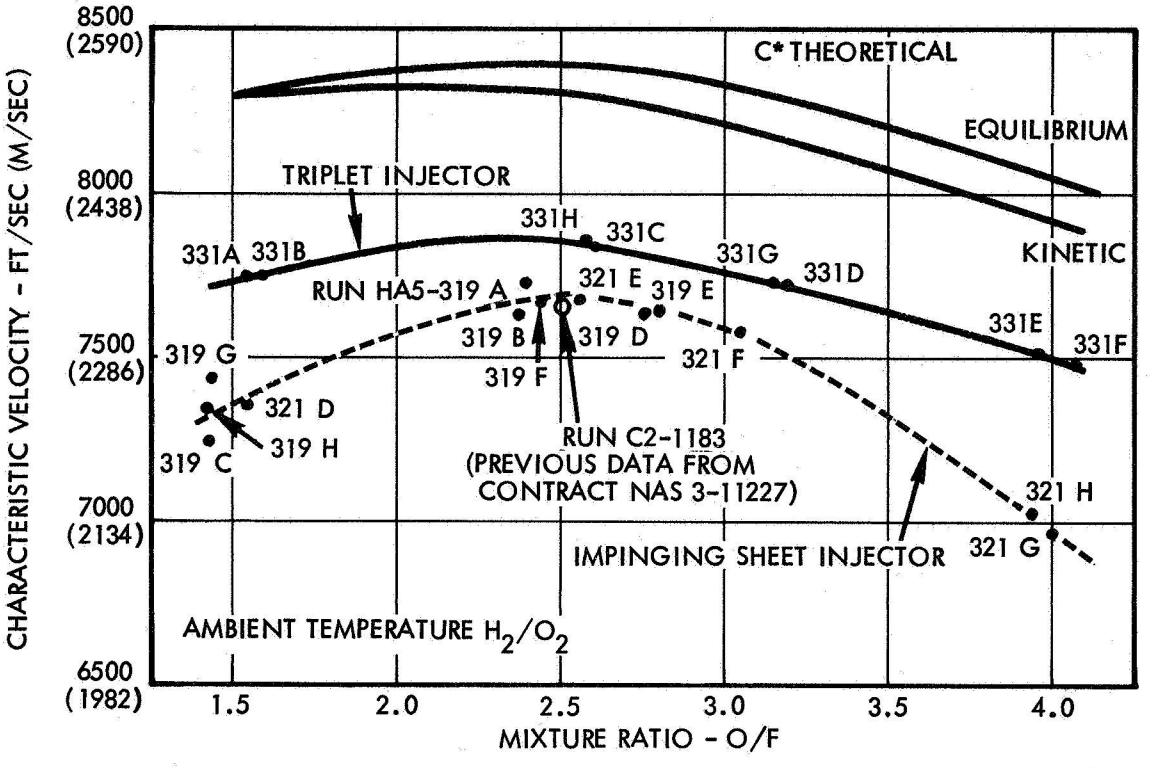

Figure 115. Injector Screening Test Performance - Heat Sink Chamber

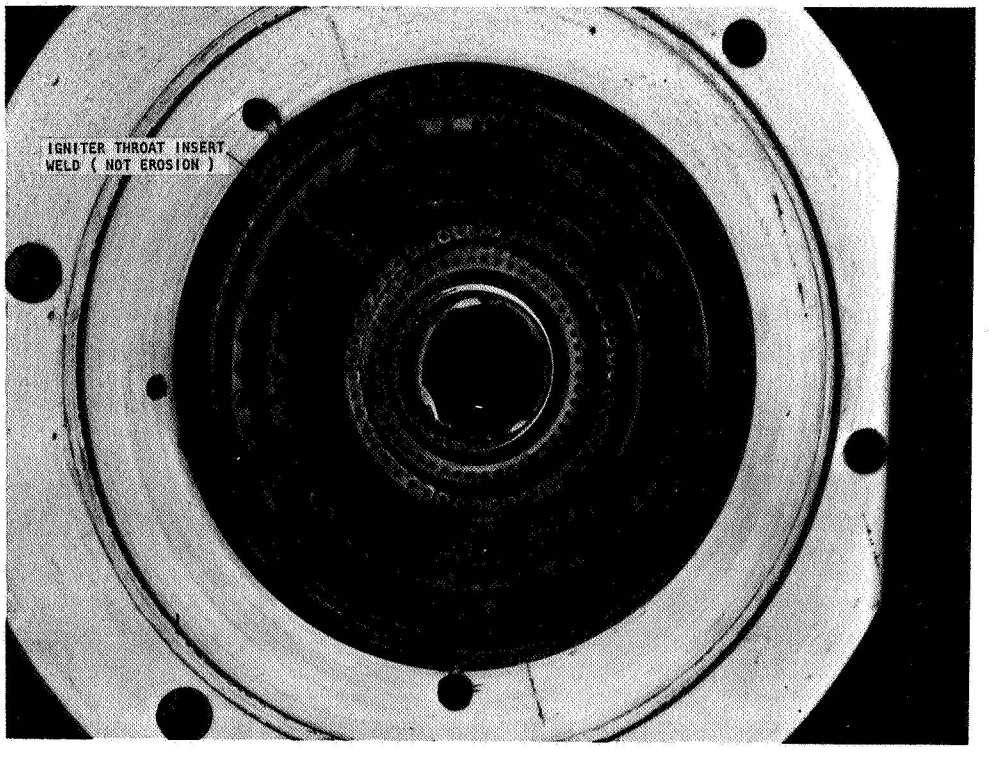

Figure 116. Low Pressure Triplet Injector After Screening Tests

Based upon the higher performance of the triplet injector compared to the impinging sheet injector, as indicated in Figure 115, the triplet injector was recommended for the cooled thruster evaluation tests. Selection of this injector was approved by the NASA/LeRC Project Manager.

4.3 COOLED THRUSTER EVALUATIONS

The purpose of this test series was to determine cooled thruster durability, effects of propellant feed system pressures and temperature, and overall impulse performance of the flightweight thruster assembly described in Section 4.1. The specific objectives of the cooled thruster evaluations were:

- Demonstrate the thrust chamber cooling capability and overall durability of the thruster design
- Determine the effect of propellant feed system pressure and temperature on thruster performance
- Determine the actual delivered thruster performance under simulated altitude conditions

The triplet injector was selected for the cooled thruster evaluations, based upon the performance results of the injector screening tests.

4.3.1 Test Description

Altitude test stand installation of the low pressure cooled thruster is shown in Figure 117. Both vacuum specific impulse and characteristic velocity performance determinations were made over a range of overall propellant mixture ratios and for different duct coolant flow rates. The flightweight triplet injector and duct cooled thrust chamber hardware were previously described in Section 4.1.

Thruster performance and cooling evaluation tests were conducted at a nominal chamber pressure of 15 psia (103 kN/m^2) and overall mixture ratios between 1.5 and 3.0. Performance and thruster operating temperatures were determined for both steady-state and pulse mode firings. Durability tests included hot firings of up to 1800 seconds duration.

4.3.2 Discussion of Results

Data from the cooled thruster evaluation tests are presented in Table 22. The methods used to calculate performance and combustion efficiencies are described in detail in Appendix A. The test results are described as follows:

Tests 355A-356A: A survey was made of mixture ratio and duct coolant flow effects on thruster performance and chamber cooling. C* efficiencies remained fairly constant, with lower $\eta_{C^*P_C}$ percentages at higher mixture ratios (Tests 355B, 355E). Tests 355C and 355F were extended duration test firings performed to establish steady-state cooled thrust chamber temperatures for different duct coolant flow rates. Chamber temperatures versus

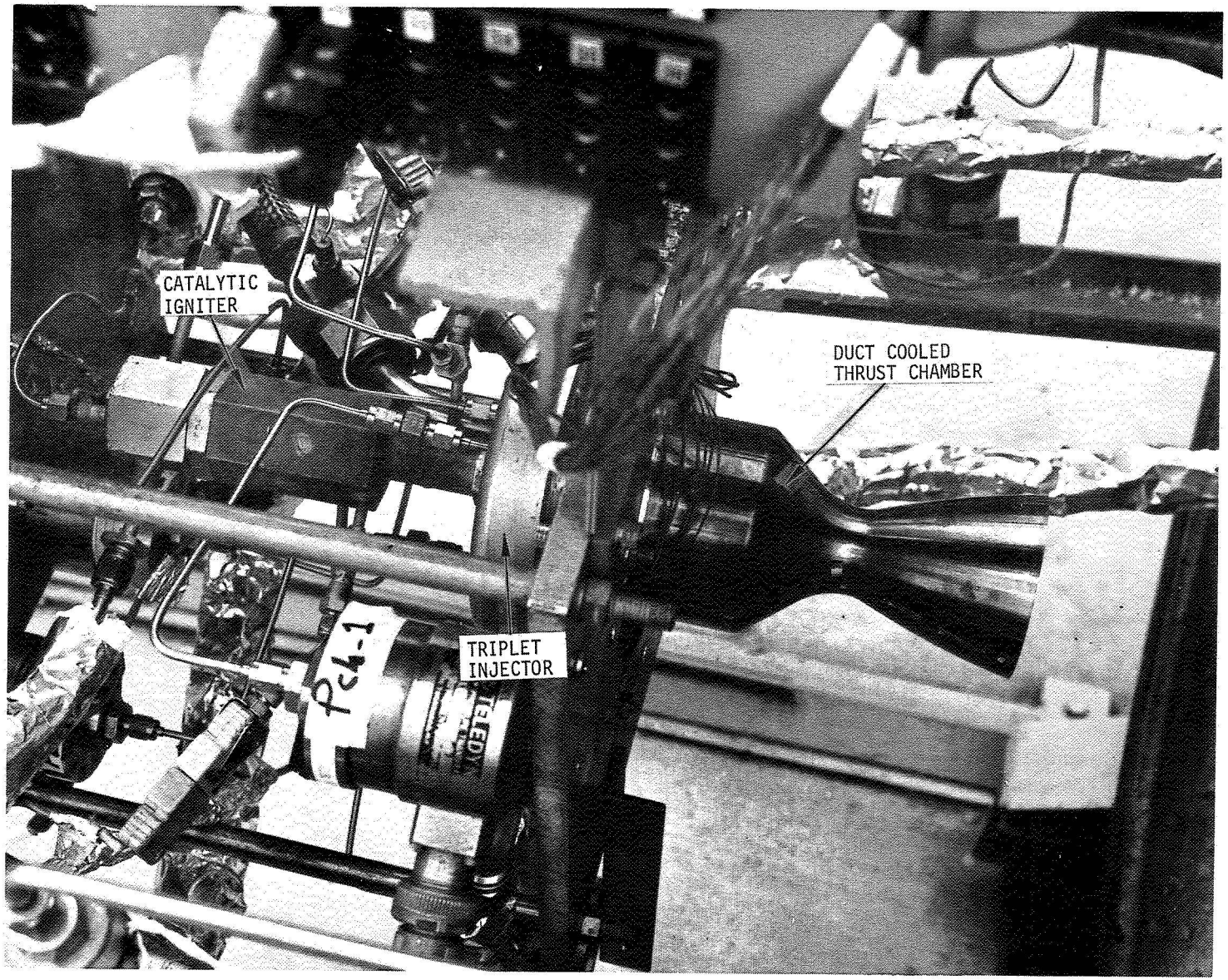

Figure 117. Test Stand Installation - Low Pressure Triplet Injector and Duct Cooled Thrust Chamber

Table 22. Low Pressure Cooled Thruster Tests

Run No. (HA-5)	P_{CD} (lbf/in^2)	P_{CD} (kN/m^2)	$\dot{W}_{Total}$ (lb/sec)	$\dot{W}_{Total}$ (kg/sec)	Mixture Ratio (O/F)	$C^*_{Measured}$ (ft/sec)	$C^*_{Measured}$ (m/sec)	F_{Vacuum} (lbf)	F_{Vacuum} (N)	Isp_{Vacuum} (lbf $\frac{sec}{lbm}$)	Isp_{Vacuum} (Nsec/kg)	η_{C^*F} (%)	η_{C^*Pc} (%)	Run Duration (sec)	Duct Coolant (% W_{H_2})	Comments
355A	14.34	98.9	0.0765	0.0347	1.781	7708	2349	28.52	126.9	327.7	3655	90.1	93.3	5	30	Mixture ratio and duct coolant flow rate effects survey, ambient temperature propellants
355B	14.15	97.6	0.0803	0.0364	3.734	7257	2212	28.09	125.0	349.2	3424	86.5	90.1	10	30	
355C	14.66	101.1	0.0803	0.0364	2.968	7509	2289	29.71	132.2	371.1	3639	89.7	91.0	50	30	
355D	14.37	99.1	0.0770	0.0349	1.695	7678	2340	28.66	127.5	372.2	3650	90.0	93.1	10	20	
355E	14.77	101.8	0.0638	0.0289	3.526	7423	2263	29.76	132.4	363.3	3563	89.4	91.6	10	20	
355F	14.95	103.1	0.0810	0.0367	2.873	7602	2317	30.52	135.8	375.7	3694	91.1	92.1	30	20	
356A	14.75	101.7	0.0802	0.0364	2.927	7572	2308	29.88	132.9	373.1	3659	90.2	91.8	10	25	
356B	15.01	103.5	0.0821	0.0372	2.874	7528	2295	30.65	136.3	373.5	3663	90.2	91.3	0.5	25	1 pulse
356C	15.06	103.8	0.0823	0.0373	2.873	7531	2295	30.79	137.0	374.2	3670	90.5	91.3	0.5	25	3 pulses
356D	15.01	103.5	0.0813	0.0369	2.985	7594	2315	30.18	134.2	371.0	3638	89.7	92.0	0.5	25	5 pulses
356E	15.03	103.6	0.0819	0.0371	2.910	7554	2302	30.14	134.1	369.1	3610	89.0	91.6	0.5	25	25 pulses
356L	13.20	91.0	0.0747	0.0339	3.012	7488	2282	27.31	121.5	364.2	3572	88.1	90.6	0.08	25	62 pulses
361G	15.06	103.8	0.0838	0.0380	2.697	7395	2254	30.39	135.2	362.0	3550	89.2	91.4	10	25	Steady state performance survey, -250°F (117°K) propellants
361H	14.28	98.5	0.0843	0.0382	4.322	7006	2135	28.46	126.6	338.2	3317	88.1	91.5	10	25	
361I	13.63	94.0	0.0781	0.0354	3.784	7180	2188	27.12	120.6	347.2	3405	88.2	91.4	10	25	
361J	14.60	100.7	0.0837	0.0380	3.777	7167	2185	29.01	129.0	346.5	3398	88.0	91.3	0.5	25	1 pulse
361K	14.96	103.1	0.0846	0.0384	3.803	7182	2189	28.89	128.5	341.8	3352	86.8	91.4	0.5	25	5 pulses — Pulse mode performance, -250°F (117°K) propellants
362B	14.95	103.1	0.0794	0.0360	2.322	7747	2361	29.54	131.4	372.4	3652	89.5	93.3	2	25	Checkout for durability test
363	15.43	106.3	0.0817	0.0371	2.420	7765	2367	30.64	136.3	374.8	3676	90.1	93.6	1800	25	Thruster durability test - continuous firing

Pulse mode performance and cooling effects survey, ambient temperature propellants

time for Test 355C, a 50 second single firing at 30% duct flow, are presented in Figure 118. A steady-state temperature of 1169°F (905°K) was measured at the chamber throat for the final 10 seconds of firing. Temperatures at the nozzle expansion ratios of 3.5 and 5 (exit) were 1249°F (950°K) and 1224°F (936°K), respectively, and were essentially stabilized, as shown in Figure 118.

Measured chamber temperatures from Test 355F, 20% duct coolant, are plotted in Figure 119. This test was terminated after 30 seconds of firing when chamber throat temperatures reached 1500°F (1089°K), indicating that duct temperatures might have been excessive. However, inspection of the duct after this test revealed no erosion or distortion of the duct, which remained in excellent condition, as shown in Figure 120. The photograph was taken on the altitude test stand, using a mirror to show the exit of the duct and the injector face. The injector face is shown in Figure 121, after removal of the thruster from the test stand. No erosion of the injector face was observed after the long duration (up to 50 seconds) steady-state firings. The center oxidizer ring and segments of the outer oxidizer ring were very bright, clean copper, while the remainder of the injector face was covered with a light oxide coating. No erosion or distortion was observed, and testing was continued.

Tests 356B - 356L: Pulse mode tests with on times of 500 and 80 milliseconds were conducted with ambient temperature propellants. Figure 122 is an oscillograph recording of the 10th pulse in a series of 25 pulse of 50 milliseconds on and 500 milliseconds off. Performance for this pulse (test 356E) was nearly identical to the steady-state firing performance. Figure 123 shows two pulses of an 80-milliseconds on and 500-milliseconds off duty cycle. Comparing these pulses to the 500-millisecond pulse of Figure 122, it is evident that full thrust and chamber pressure were not attained during the 80-millisecond pulses. This occurred because the test propellant valves (not flight design) did not fully open during the shorter pulses, and full flows were not established, as also indicated in Table 22, test 356L. Rapidly increasing chamber temperatures also indicated that full duct coolant flow was not attained, and the test was terminated after 62 pules.

Disassembly of the thruster revealed that minor melting of the duct tip occurred at two locations, as shown in Figure 124. The pulse duty cycle apparently caused a phase shift between the coolant flow and the combustion temperature heating of the duct. This condition would be corrected by feeding the duct directly from the injector hydrogen manifold and by the use of faster opening propellant valves, both of which would be incorporated in a flight type design. The Berylco 10 duct was repaired by machining the tip back to clean up the eroded area; however, the OFHC copper duct was utilized for the remainder of the cooled thruster tests.

The triplet injector remained in excellent condition after completion of the pulsing tests, as shown in Figures 125 and 126. Figure 125 indicates that darkening of the center oxidizer ring occurred, compared to Figure 116 (prior to pulse tests), except for one bright spot, as identified in the photo.

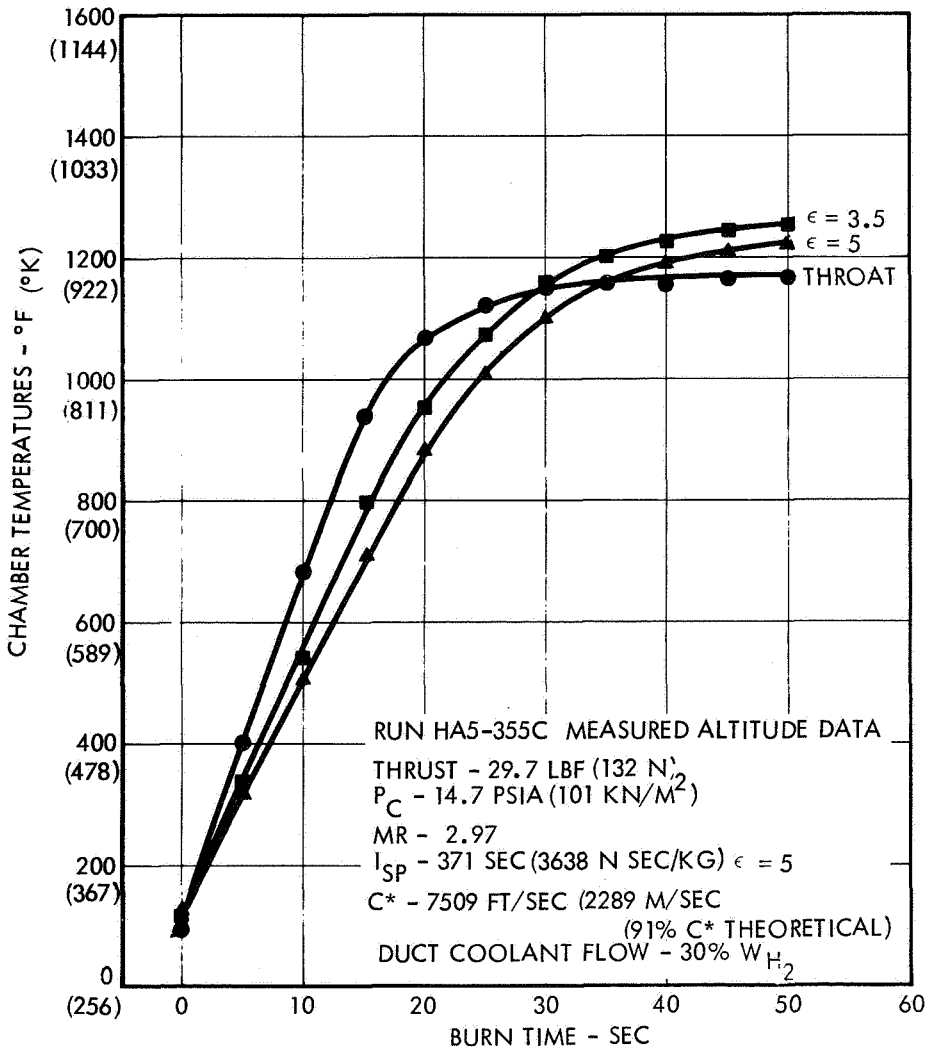

Figure 118. Low Pressure Thruster Chamber Temperatures - 30% Duct Coolant Flow

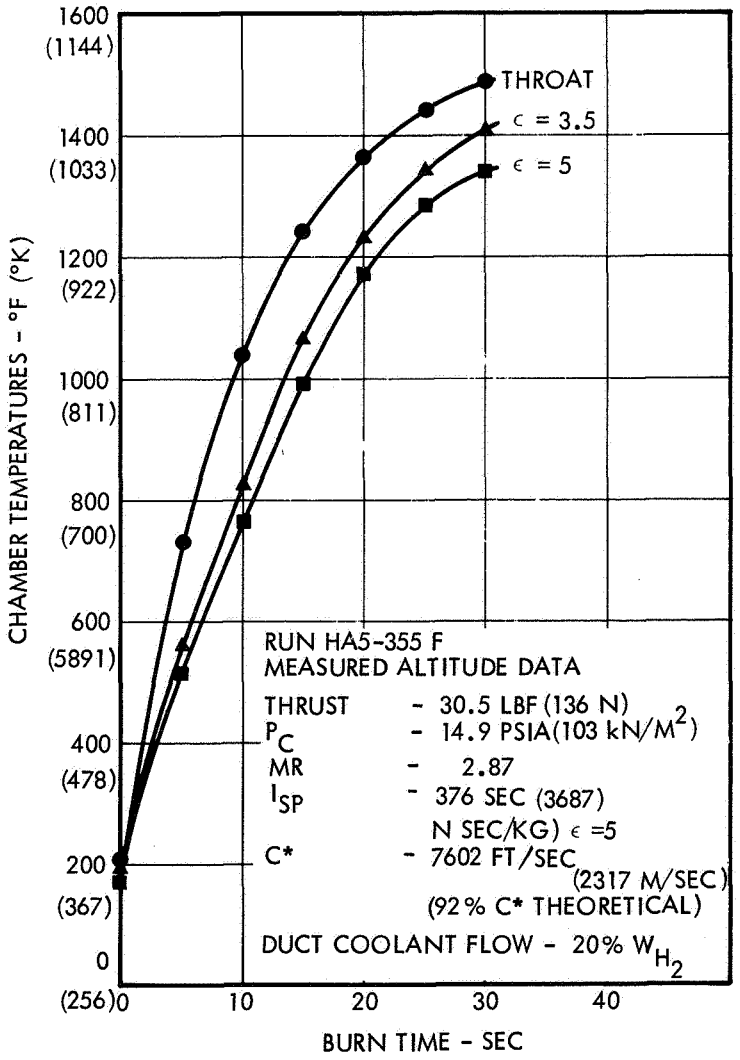

Figure 119. Low Pressure Thruster Chamber Temperatures - 20% Duct Coolant Flow

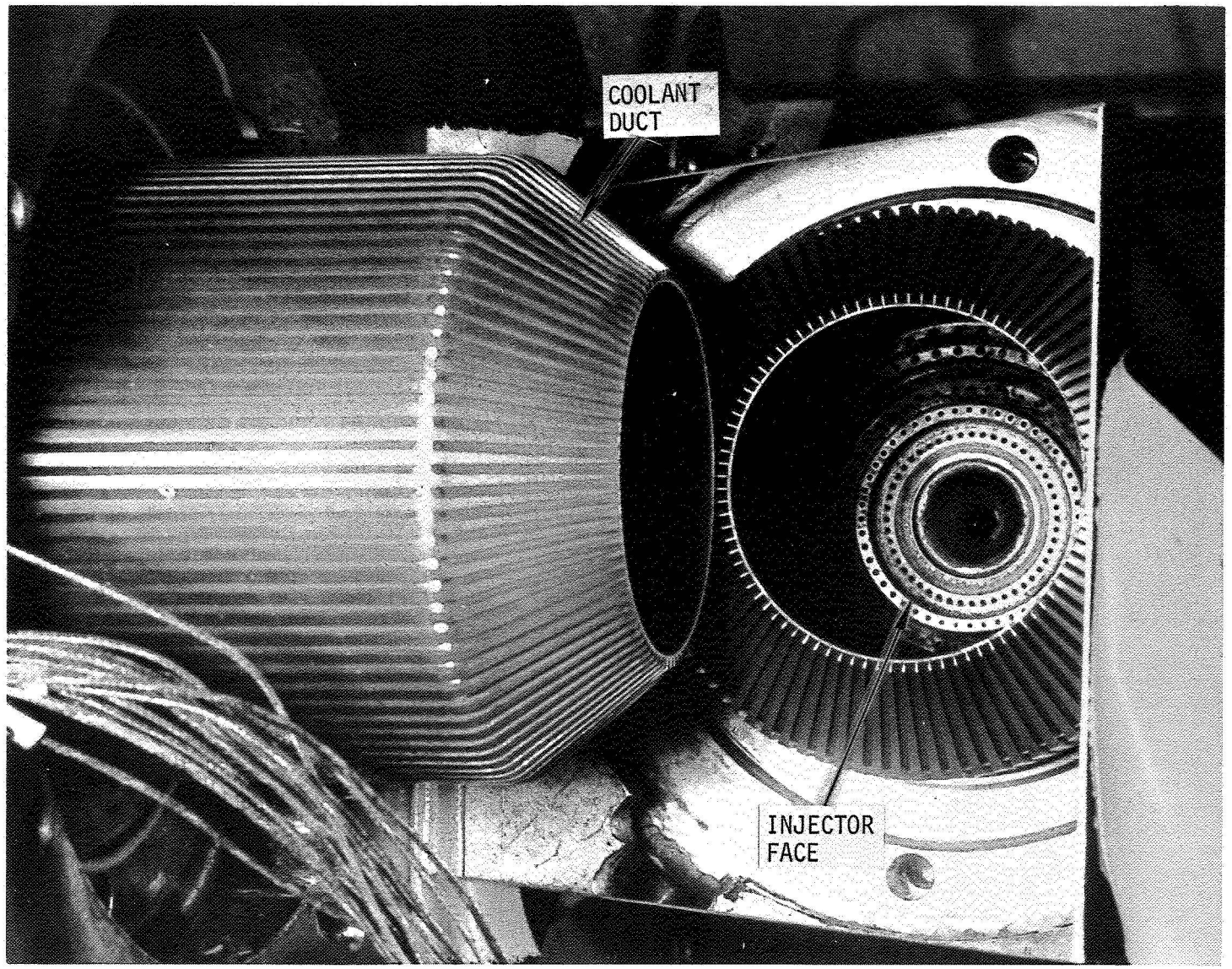

Figure 120. Low Pressure Duct After Steady-State Firings Up to 50 Sec Duration

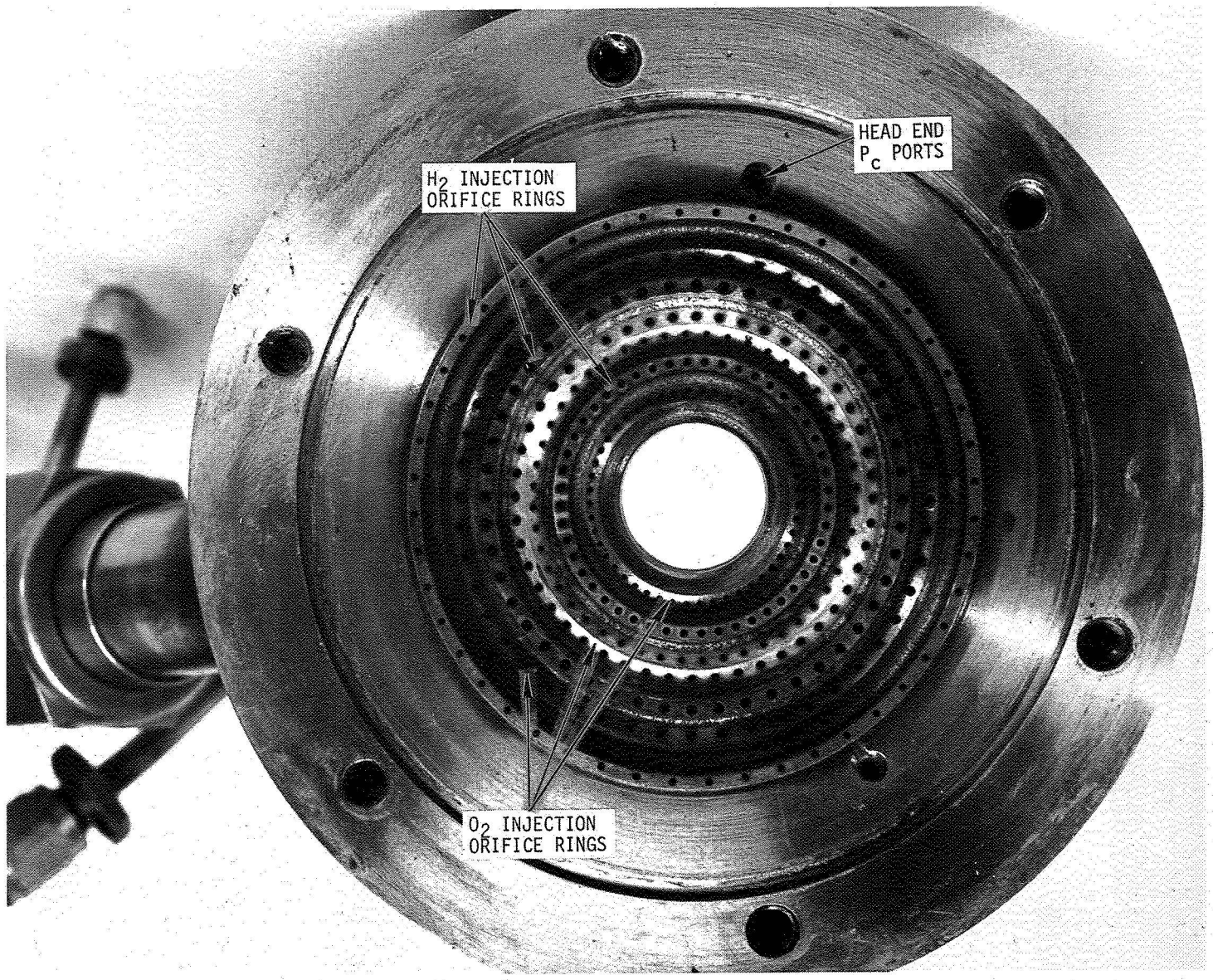

Figure 121. Low Pressure Triplet Injector Face After Steady-State Firings Up to 50 Sec Duration

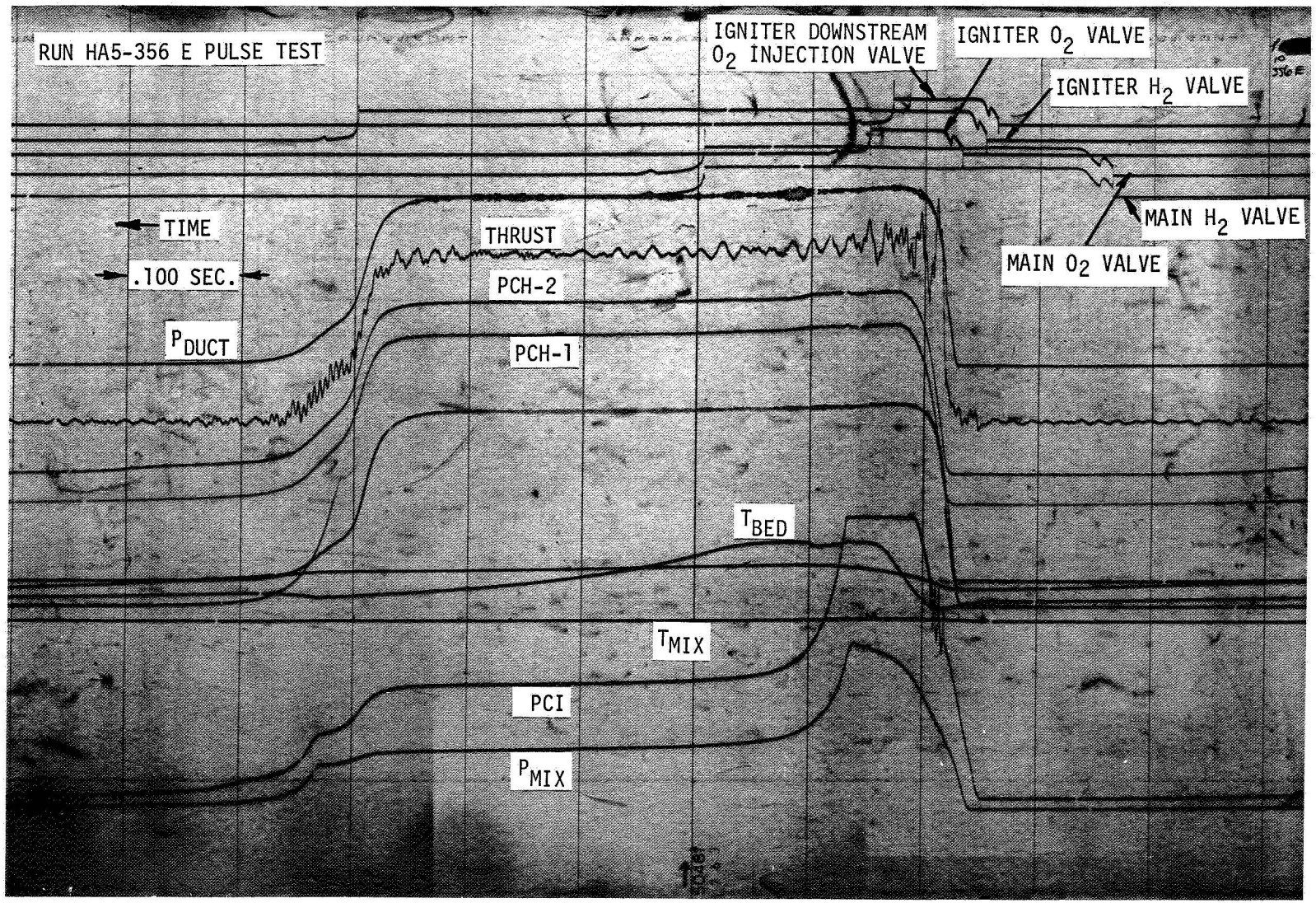

Figure 122. Run HA5-356E - Low P_c Thruster - 500 msec Pulse (#10 of 25)

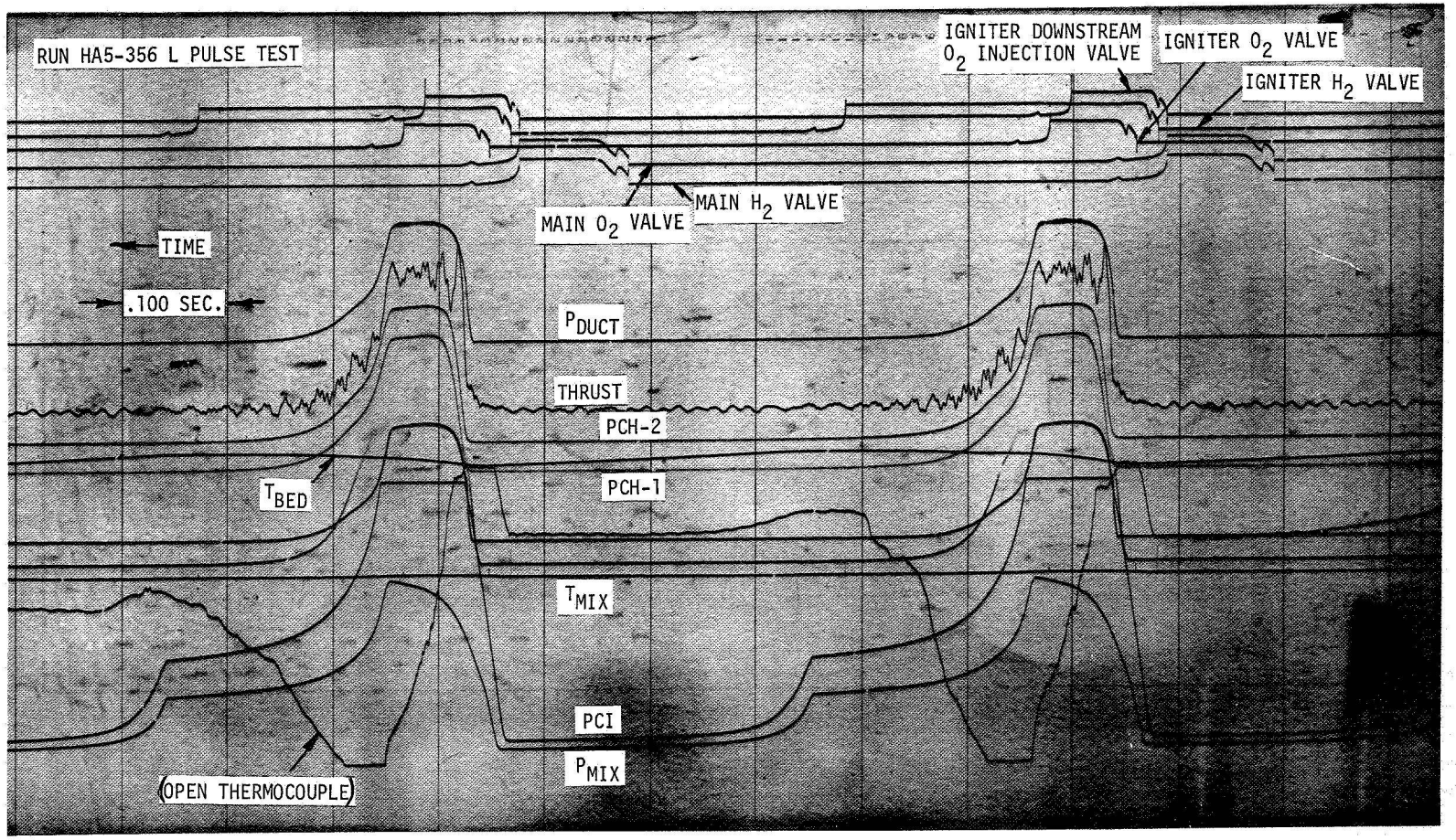

Figure 123. Run HA5-356L - Low P_c Thruster - 80 msec Pulses (#45 and 46 of 62)

Figure 124. Low Pressure Duct After Pulse Mode Firings - 80 msec Pulses

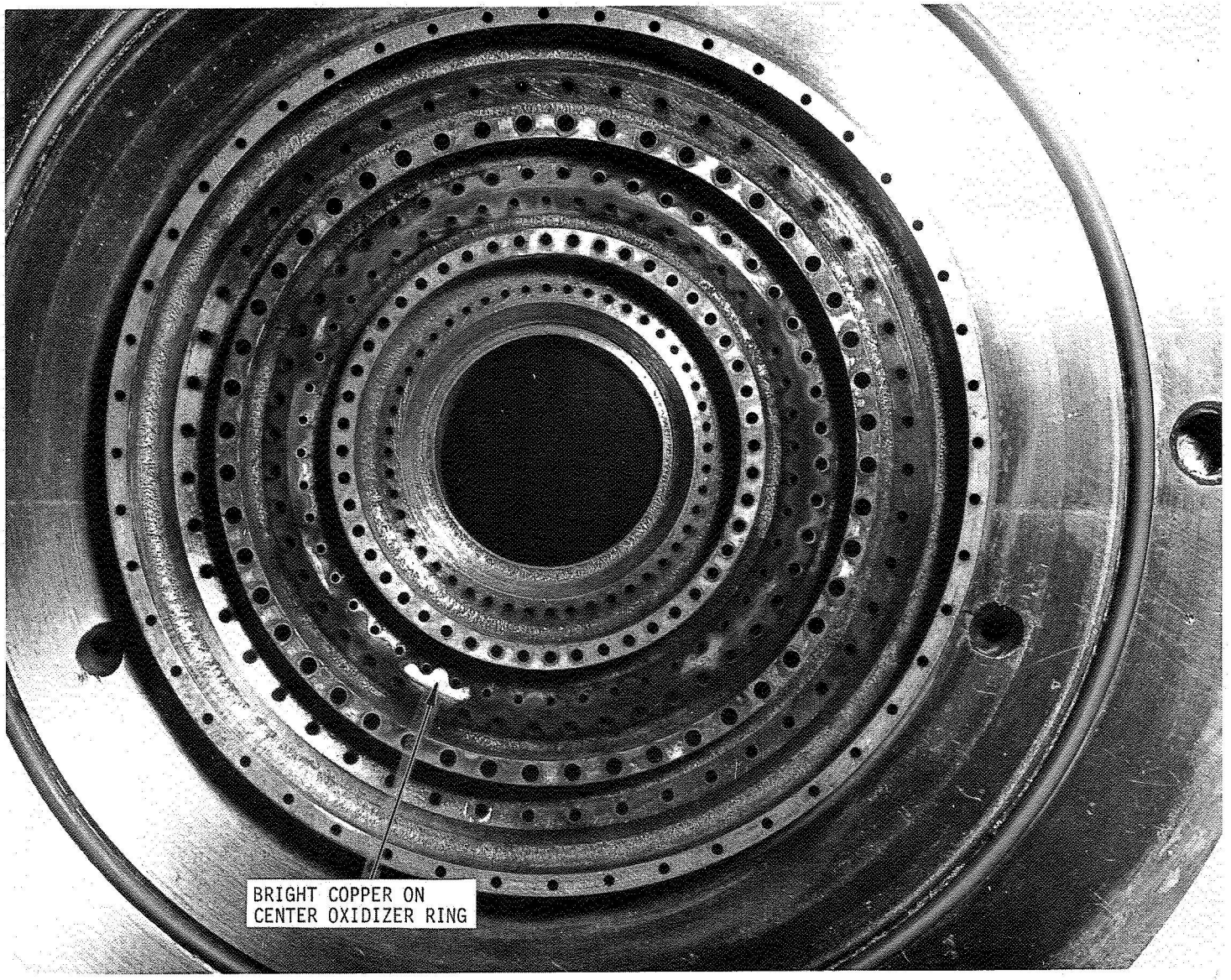

Figure 125. Low Pressure Triplet Injector Face After Pulse Mode Firings - Direct View

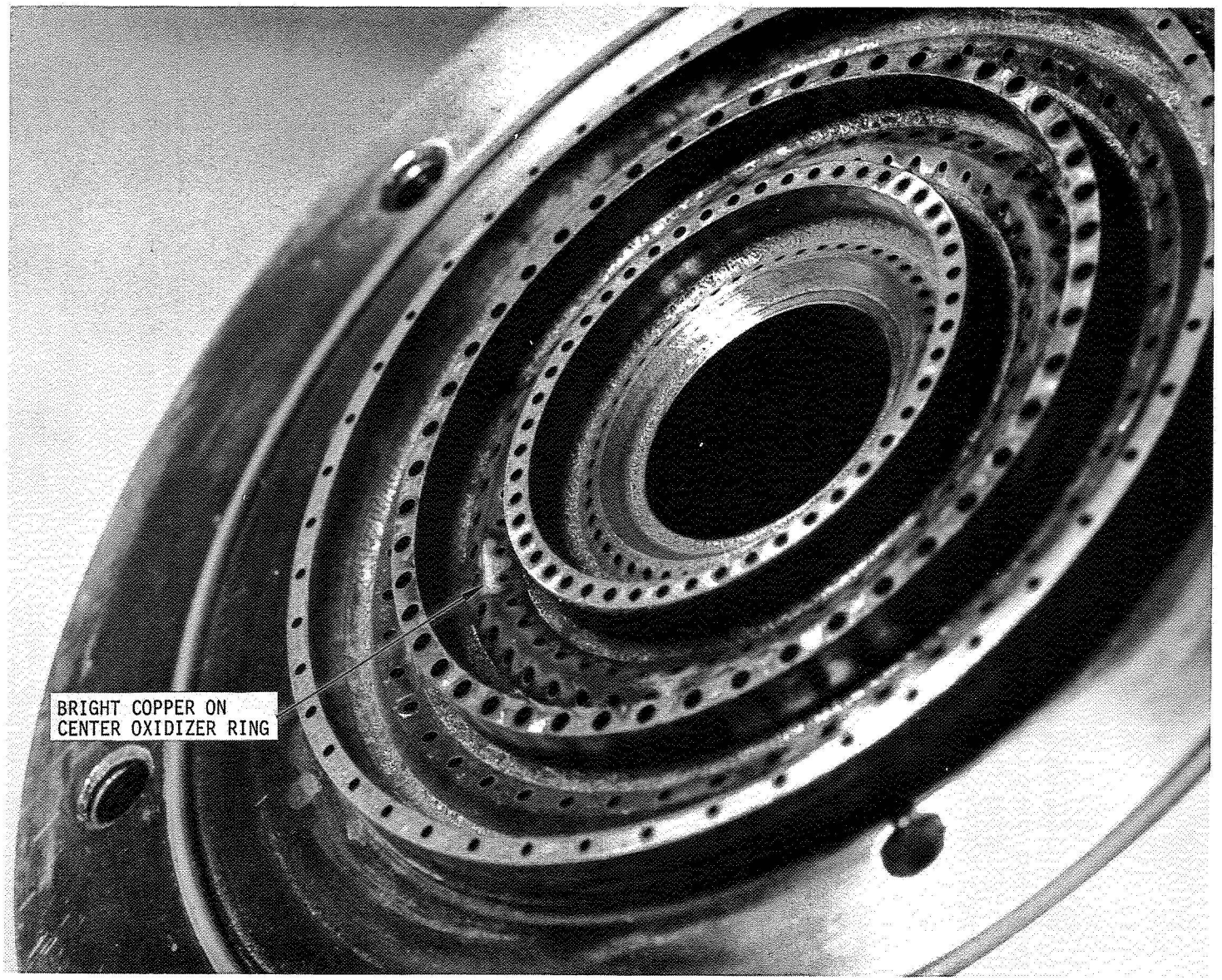

Figure 126. Low Pressure Triplet Injector Face After Pulse Mode Firings - Oblique View

Tests 361G - 361I: Steady-state performance and cooling evaluations were conducted with propellants conditioned to a nominal inlet temperature of -250°F (117°K). Performance ($\eta_{C^*P_C}$) was comparable to ambient propellant tests.

Tests 361J - 361K: Low temperature propellant pulsing tests were performed with consistent ignitions attained. A series of five 500-millisecond duration pulses was completed (Test 361K).

Tests 362B - 363: After a short checkout run, a single continuous firing of 1800 seconds duration was conducted to demonstrate the durability of the flightweight cooled thruster. Measured thrust chamber temperatures from this firing are presented in Figure 127, and are well within safe operating limits for unlimited chamber life.

The post-firing condition of the cooled low pressure thruster hardware is indicated in Figure 128. The injector, thrust chamber, and duct were all in excellent condition after the 1800 second firing, except for numerous minor pits on the inner surface of the exit of the copper cooling duct, shown in Figure 129. Hairline cracks were also observed in the duct exit, as indicated in Figure 130. Increased magnifications of metallographic specimens cut from the duct exit are shown in Figures 131 and 132. These photographs clearly reveal the pits and cracks in the copper, but do not indicate any interrelationship between them; i.e., cracks did not initiate within the surface pits, or vice versa.

A possible cause of the surface pitting of the copper duct exit could have been physical erosion by solid impurities in the gaseous propellants. Bombardment of the copper by these particles, heated to high temperatures, could have resulted in erosion of this type after long firing durations (over 2100 seconds with this duct). Inspection of the propellant feed system did not indicate any further evidence of erosion at propellant flow control orifices or elbows; however, the feed system was constructed from stainless steel, not relatively soft copper, and any particles would not be at the high temperatures and velocities of the impurities impacting the duct.

Stress analysis of the low pressure copper duct design indicated that the cracks resulted from combined creep-fatigue stress, which occurs after even low cycle operation with OFHC copper. Cyclic life analysis of coolant ducts for the high pressure GH_2/GO_2 thruster (described in Volume II of this contract report) indicated that Berylco BE-10 copper alloy was far superior to OFHC copper for this type of application. The use of Berylco BE-10 is recommended to eliminate fatigue cracking of the low pressure duct, and should also prevent or reduce pitting of the duct as well.

The effectiveness of the duct cooling concept was well demonstrated for the low pressure flightweight thruster during the 1800-second steady-state firing. Thrust chamber assembly durability for extended duration firing was proven to be feasible, with a change in duct material recommended to improve fatigue life.

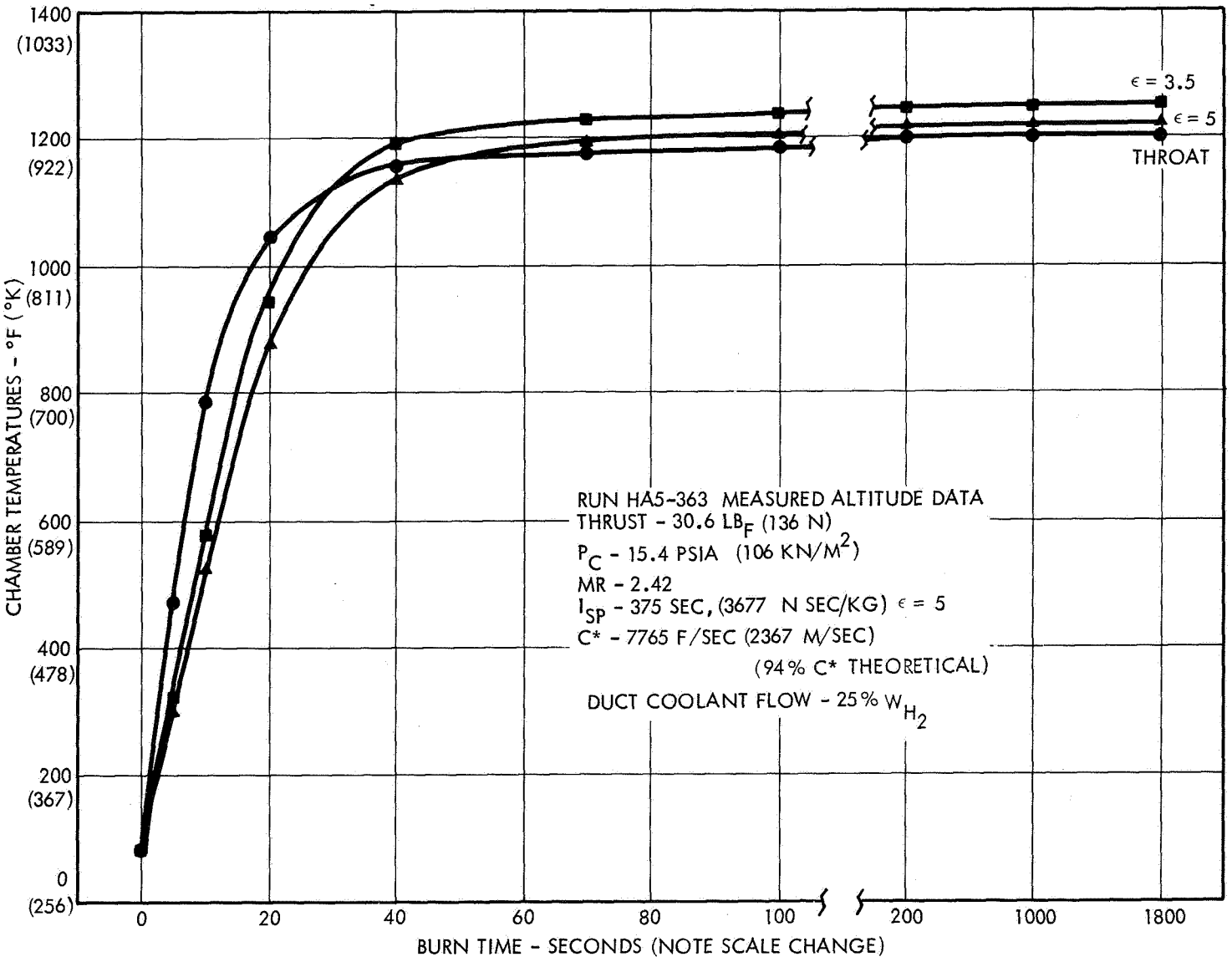

Figure 127. Low Pressure Thruster Chamber Temperatures - 1800-Second Firing

Figure 128. Low P_c Cooled Thruster After 1800-Second Firing

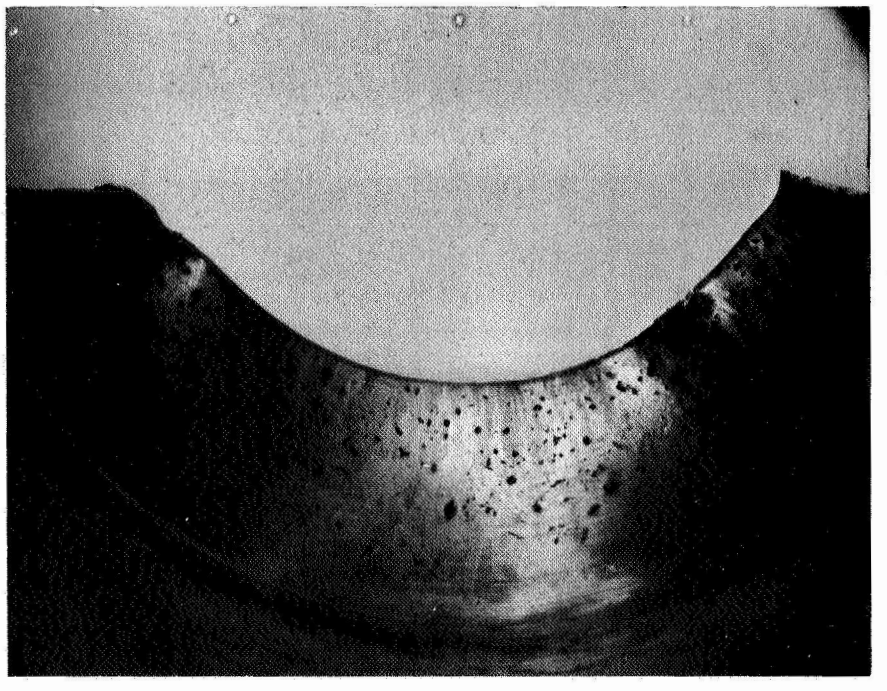

Figure 129. Low P_c Duct Exit 1800-Second Firing

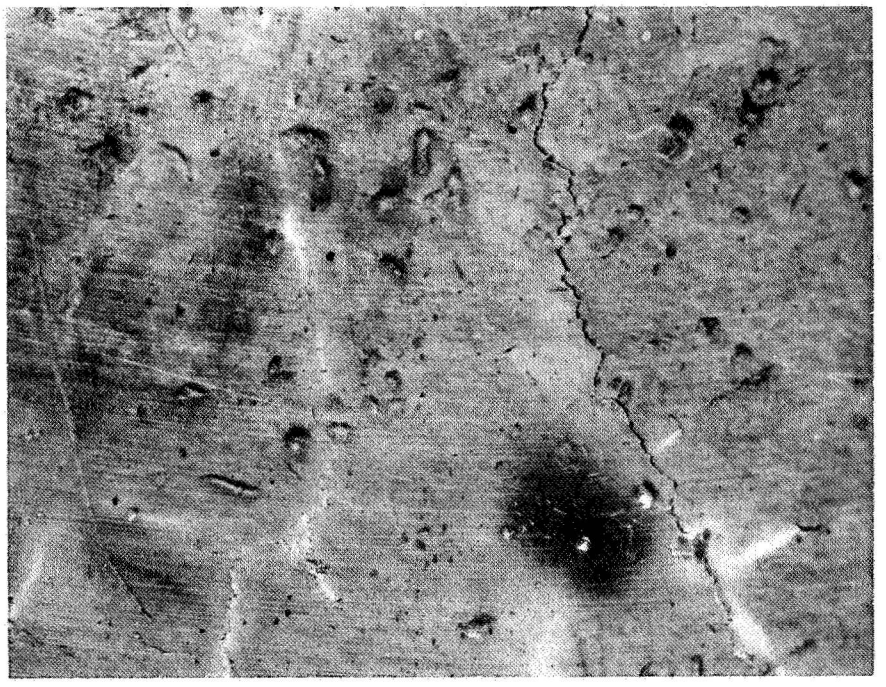

Figure 130. Duct Exit 7X Magnification

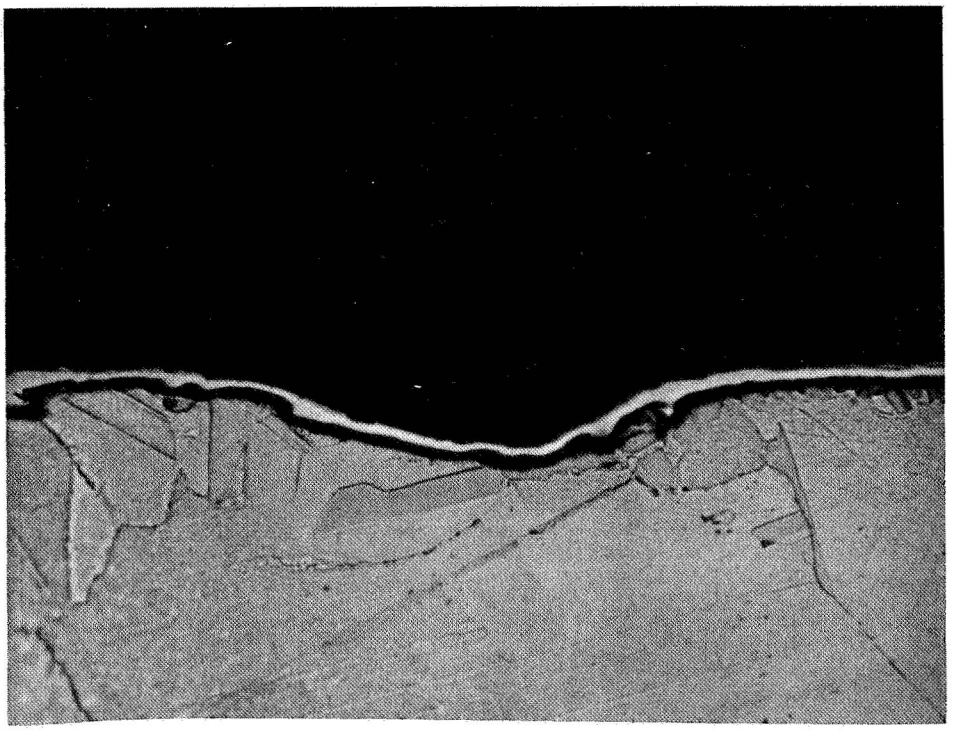

Figure 131 a. Surface Pitts in Copper Duct (440X)

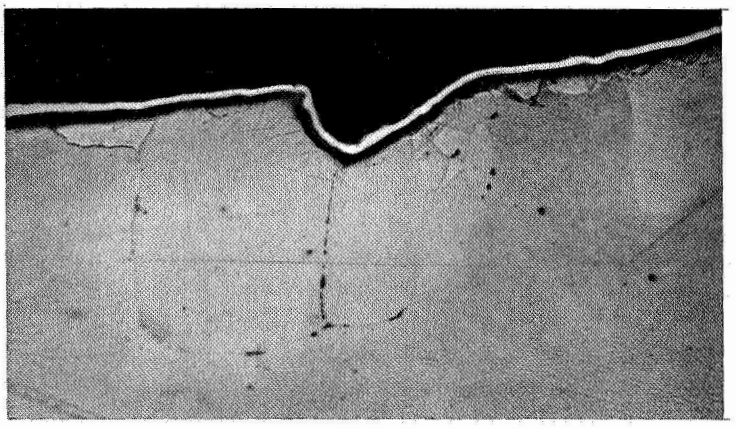

Figure 131 b. Surface Pits

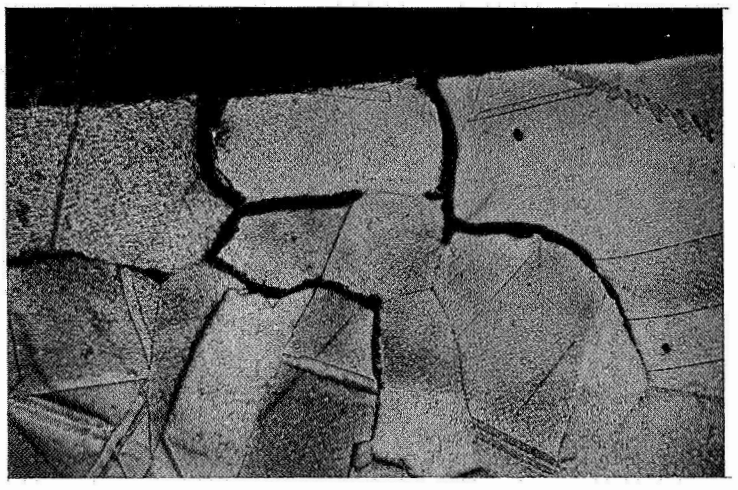

Figure 132 a. Surface Cracks in Copper Duct

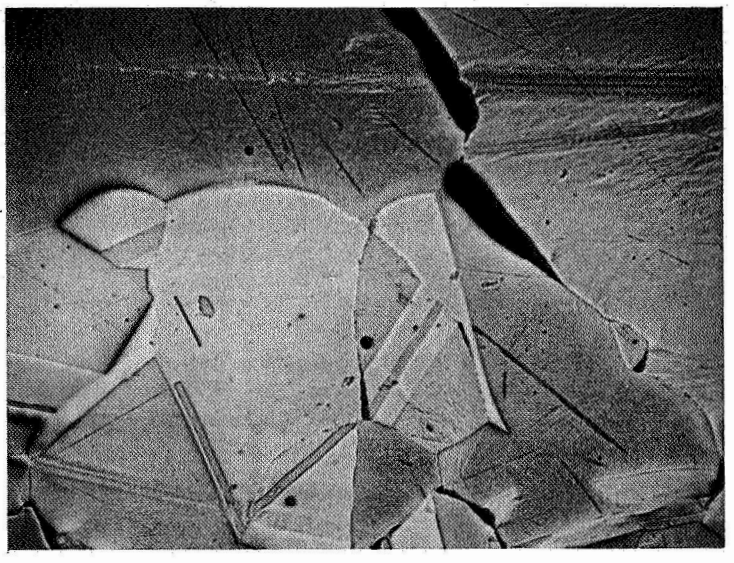

Figure 132 b. Surface Cracks Penetration in Copper Ducts

4.3.3 Performance Summary

Performance of the low pressure flightweight cooled thruster is summarized in Figures 133 and 134 for the range of test variables evaluated. Figure 133 presents the measured vacuum I_{sp} performance versus mixture ratio, which closely parallels the theoretical curves at the top of the figure. This indicates that the triplet injector delivers essentially a constant percentage of theoretical performance over the mixture ratio range of interest, as also observed during the injector screening tests. The effect of duct coolant flow rate variations on delivered I_{sp} is also shown in Figure 133. The tests performed with duct coolant flow rates of 30% of total hydrogen flow compared to 20% resulted in one percent lower performance at mixture ratios between 2.5 and 3.0 O/F. Performance loss increased at higher mixture ratios for 30% duct coolant, and was negligible at lower mixture ratios approaching 1.5, where the difference between 20 and 30% D.C. flow results in only minor variation of the injector core mixture ratio.

Measured C* performance for the same series of test firings is plotted in Figure 134 and also closely follows the theoretical C* performance trends over the entire mixture ratio range tested. Performance comparison of 20 and 30% duct coolant flow rate tests indicate no significant difference at mixture ratios below 2.0 O/F and one percent lower performance with 30% D.C. at mixture ratios approaching 3.0, consistent with the I_{sp} performance trends in Figure 133.

The predicted I_{sp} performance for the low pressure thruster of 375 lbf-sec/lbm (3677 N-sec/kg) with 25% duct coolant flow was verified by the data curves in Figure 133 and the results of the 1800-second firing (Figure 127).

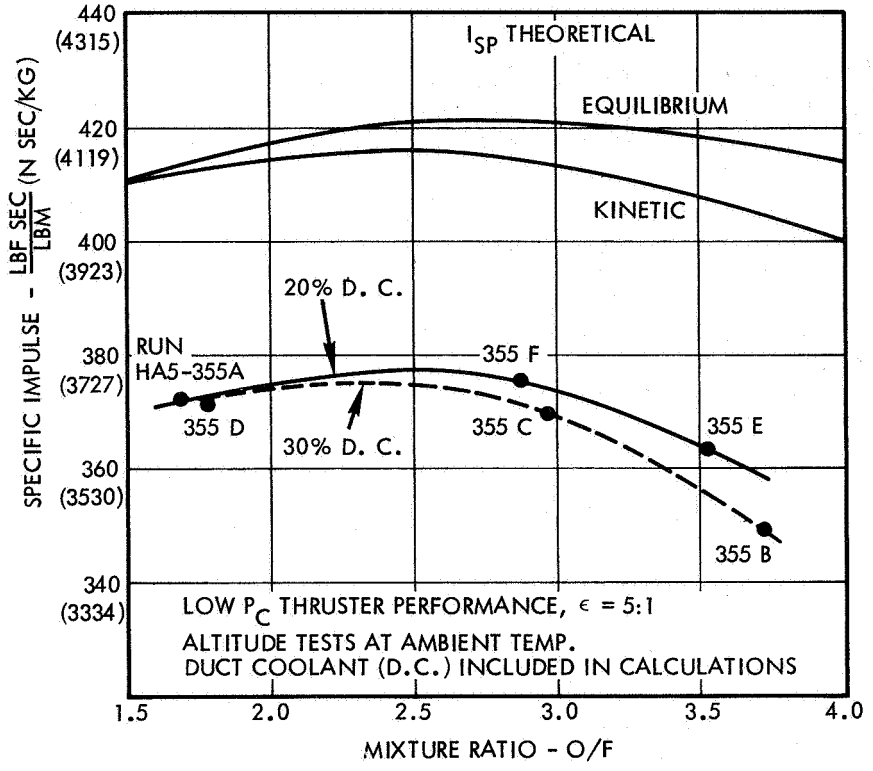

Figure 133. Low Pressure Duct Cooled Thruster Performance - Specific Impulse

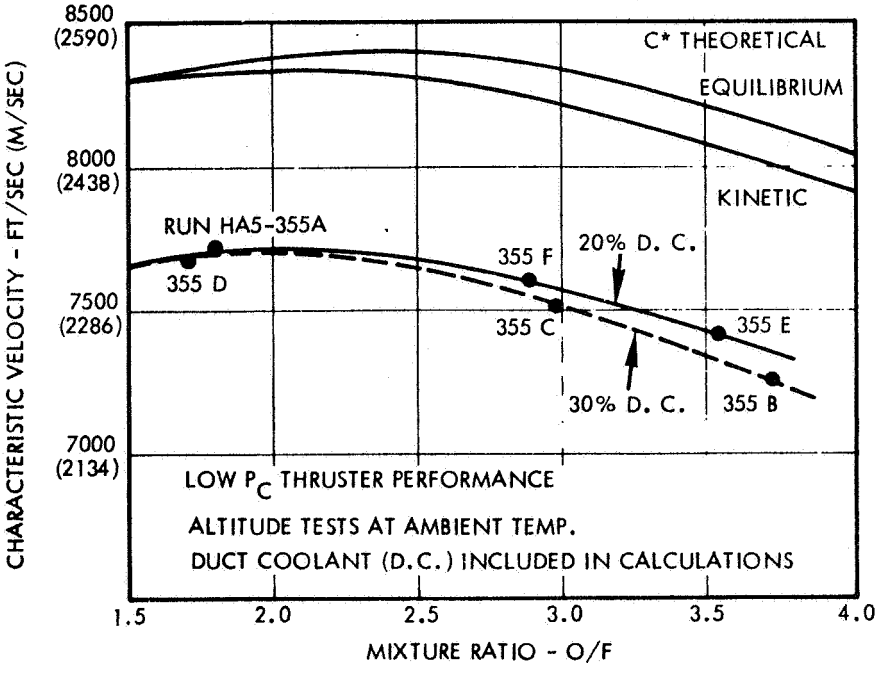

Figure 134. Low Pressure Duct Cooled Thruster Performance - Characteristic Velocity

5. CONCLUDING REMARKS

5. CONCLUDING REMARKS

The overall objectives of this program were to determine the performance and operating characteristics of cooled, flightweight GH_2/GO_2 thrusters and to provide generalized guidelines for reliable catalytic igniters. An extensive series of laboratory evaluations and test firings of igniters and thruster assemblies was conducted to establish operational limitations and delivered performance over a wide range of propellant inlet temperatures and pressures.

The major conclusions from the catalytic igniter investigations were:

- Both the Shell 405-ABSG and Engelhard MFSA catalysts are capable of extended duration firing, well beyond 4000 seconds steady-state or 5000 cycles of pulse-mode operation.

- Catalytic igniters can be designed to prevent flashback by reasonable control of the propellant velocities and startup start transient mixture ratio

- High overall ignition response (less than 25 msec) can be attained by injection of oxygen downstream of the catalyst bed. Catalyst life is also enhanced by this igniter configuration, which allows reduced bed operating temperatures.

- Exposure of either the Shell or Engelhard catalysts to simulated shuttle vehicle earth stay and reentry environments does not preclude low temperature ignition; however, hydrogen purging and/or heating of the catalyst bed is recommended after these exposures.

The low pressure flightweight thruster experimental evaluation led to the following conclusions:

- The triplet injector designed for this program is capable of a delivered I_{sp} of 375 lbf-sec/lbm (3677 N-sec/kg) with a cooled, flightweight thrust chamber (e = 5).

- Durability of the duct cooled thrust chamber was demonstrated by an 1800-second duration single firing.

The experimental results of this contract have demonstrated the feasibility of reliable, high response catalytic ignition of gaseous hydrogen-oxygen thrusters. The effectiveness of the duct cooling concept was proven for a flightweight reaction control thruster capable of high performance, extended duration operation.

REFERENCES

REFERENCES

1. Final Report, "Investigation of Thrusters for Cryogenic Reaction Control Systems," Volume I, by R. J. Johnson.
2. Brunauer, S., Emmett, P. H., and Teller, E. J., J. American Chemical Society, 60, pp. 309, (1938).
3. "Space Environments (NASA Contract NAS 7-520) Operation of Experimental Hydrazine Reactors," by R. A. Carlson, J. L. Blumenthal, R. J. Grassi, June 1968.

APPENDICES

APPENDIX A

CALCULATION OF C* EFFICIENCY

The index of injector performance used in the experimental program was the corrected C* efficiency. This parameter was calculated by two independent methods, one based on measurement of chamber pressure and the other on measurement of thrust. Details of the computational procedures and of the applied corrections are given in the following sections. The procedures and nomenclature format are essentially those as developed in NASA sponsored programs at Rocketdyne.

1.0 CHAMBER PRESSURE TECHNIQUE

Characteristic velocity efficiency based on chamber pressure is defined by the following:

$$\eta_{C^*} = \frac{(P_c)_o \ (A_t)_{eff} \ g_c}{(\dot{w}_T) \ (C^*)_{theo}} \qquad \text{(A-1)}$$

where

$(P_c)_o$ = stagnation pressure at the throat

$(A_t)_{eff}$ = effective thermodynamic throat area

g_c = conversion factor (32.174 lbm-ft/lbf-sec^2)

$\dot{w}_T$ = total propellant weight flow rate

$(C^*)_{theo}$ = theoretical characteristic velocity based on shifting equilibrium

Values calculated from Equation (A-1) are referred to as "corrected" C* efficiencies, because the factors involved are obtained by application of suitable influence factor corrections to measured parameters. Stagnation pressure at the throat is obtained from measured static pressure at start of nozzle convergence by assumption of isentropic expansion, effective throat area is estimated from measured geometric area by allowing for geometrical radius changes during firing and for nonunity discharge coefficient, and chamber pressure is corrected to allow for energy losses from combustion

gases to the chamber wall by heat transfer and friction. Equation (A-1) may therefore be written as follows:

$$\eta_{C^*} = \frac{P_c\ A_t\ g_c\ f_p\ f_{TR}\ f_{DIS}\ f_{FR}\ f_{HL}\ f_{KE}}{(\dot{w}_o + \dot{w}_f)\ (C^*)_{theo}} \qquad \text{(A-2)}$$

where

P_c = measured static pressure at start of nozzle convergence, psia

A_t = measured geometric throat area, in^2

g_c = conversion factor (32.174 lbm-ft/lbf-sec^2)

$\dot{w}_o$ = oxidizer weight flow rate, lb/sec

$\dot{w}_f$ = fuel weight flow rate, lb/sec

$(C^*)_{theo}$ = theoretical C* based on shifting equilibrium calculations, ft/sec

f_p = influence factor correcting observed static pressure to throat stagnation pressure

f_{TR} = influence factor correcting for change in throat radius during firing

f_{DIS} = influence factor correcting throat area for effective discharge coefficient

f_{FR} = influence factor correcting measured chamber pressure for frictional drag of combustion gases at chamber wall

f_{HL} = influence factor correcting measured chamber pressure for heat losses from combustion gases to chamber wall

f_{KE} = influence factor correcting C* values to account for finite chemical reaction rates

Methods of estimation of the various correction factors are described in the following paragraphs.

1.1 PRESSURE INFLUENCE FACTOR (f_p)

Measured static pressure at start of nozzle convergence is converted to stagnation pressure at the throat by assumption of effectively no

combustion in the nozzle and application of the isentropic flow equations, with contraction ratio (A_c/A_t) and shifting-equilibrium specific heat ratios (γ). Frozen-equilibrium specific heat ratios usually make the influence correction factor about 1/2 percent larger. Hence the value employed with shifting-equilibrium is the more conservative. Figure A-1 shows the influence factor as a function of contraction ratio.

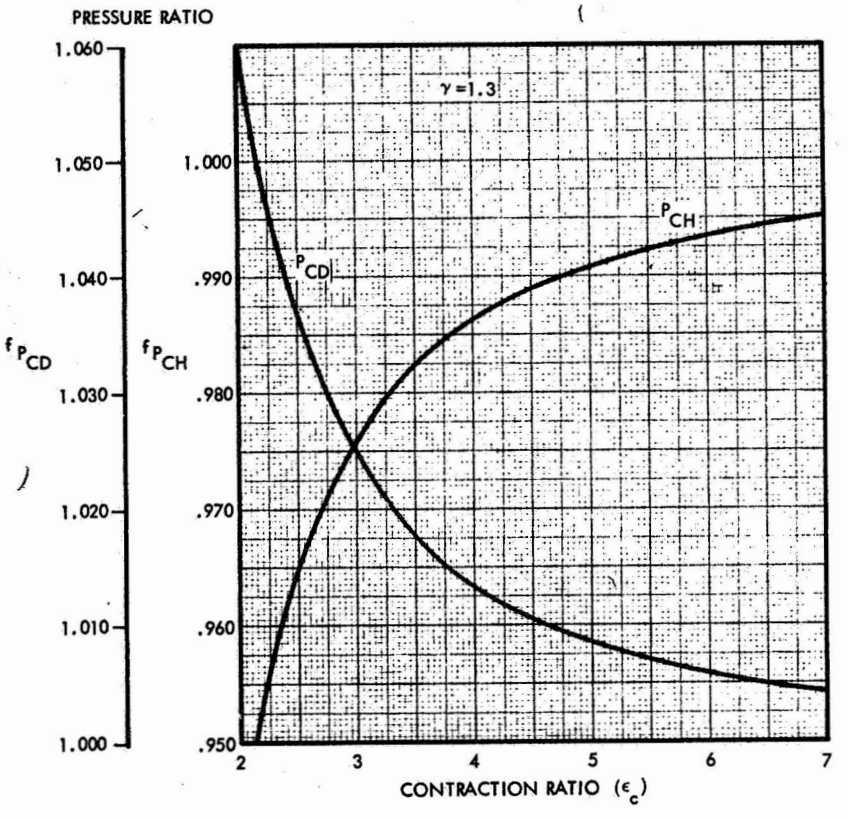

Figure A-1. Momentum Correction

1.2 THROAT RADIUS INFLUENCE FACTOR (f_{TR})

Temperature gradients produced in the solid metal nozzle wall result in thermal stresses which affect throat radius, with the result that the geometric throat diameter ambient measurement is not the same as that which exists during firing.

In the chamber type employed during the experimental effort (i.e. thin throat wall thickness), the throat area change is computed from the thermal growth of the throat based on temperature changes from ambient temperature. The change in throat area can be written as:

$$A_{th} = \frac{\pi}{4} (2 + \alpha\Delta T) (\alpha\Delta T) D^2 \qquad (A-3)$$

where

ΔA^* = change in throat area due to thermal growth

α = average thermal expansion coefficient

ΔT = temperature rise from ambient conditions

D = throat diameter at ambient conditions

The throat area correction factor is as follows:

$$f_{TR} = 1 + \frac{\Delta A_{th}}{A_{th}}$$

$$= [1 + \alpha\Delta T]^2 \qquad (A-4)$$

The thermal expansion coefficient for copper is $\alpha_{Cu} = 9.8 \times 10^{-6}$ in/in-°F, assuming an ambient temperature of 70°F, the throat area correction factor becomes

$$f_{TR} = [1 + 9.8 \times 10^{-6} (T_{th} - 70)]^2 \qquad (A-5)$$

This equation was used to generate the curve in Figure A-2.

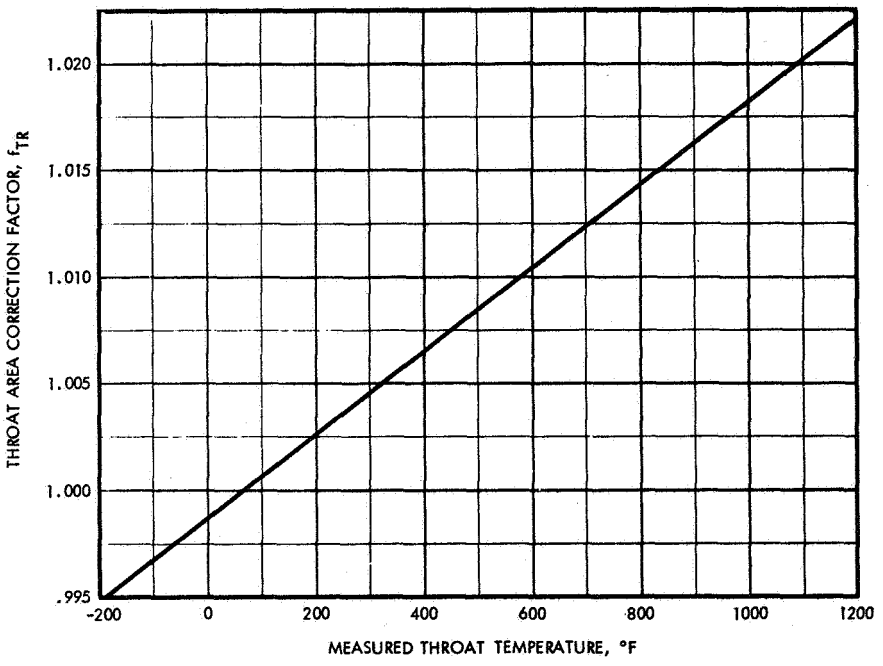

Figure A-2. Throat Area Correction Factor

1.3 THROAT DISCHARGE COEFFICIENT INFLUENCE FACTOR (f_{DIS})

The discharge coefficient is defined as the ratio of actual flow rate through the throat to the theoretical maximum, based on geometric throat area and ideal, uniform, one-dimensional flow with no boundary layer. The discharge influence coefficient may be estimated in two ways: one based on calculations made from a theoretical, inviscid flow model of combustion products, and the other based on a correlation of results obtained in various experimental study results of air flow through nozzles of similar geometry.

1.3.1 Theoretical Model

Total mass flow rate is given by

$$\dot{m} = \int_{o}^{A} \rho \, V \, dA \qquad \text{(A-6)}$$

where:

ρ = gas density
V = gas velocity
A = cross-sectional area

Theoretical maximum flow rate at the throat is

$$\dot{m}_{max} = \int_{o}^{A_t} \rho^* \, V^* \, dA \qquad \text{(A-7)}$$

where:

A_t = geometric area of the throat
ρ^* = sonic gas density
V^* = sonic gas velocity

For ideal, uniform, parallel flow, Equation (A-7) becomes

$$\dot{m}_{max} = \rho^* \, V^* \, A_t \qquad \text{(A-8)}$$

The discharge coefficient is then

$$C_D = \frac{\dot{m}}{\dot{m}_{max}} = \int_0^A \left(\frac{\rho}{\rho^*}\right)\left(\frac{V}{V^*}\right)\left(\frac{dA}{A_t}\right) \qquad \text{(A-9)}$$

1.3.2 Empirical Value

Experimental conical nozzle discharge coefficients obtained with air by various investigators are plotted in Figure A-3 against the indicated geometric parameter. Data sources also are listed in Figure A-3.

The values obtained by both methods are found to be in excellent agreement.

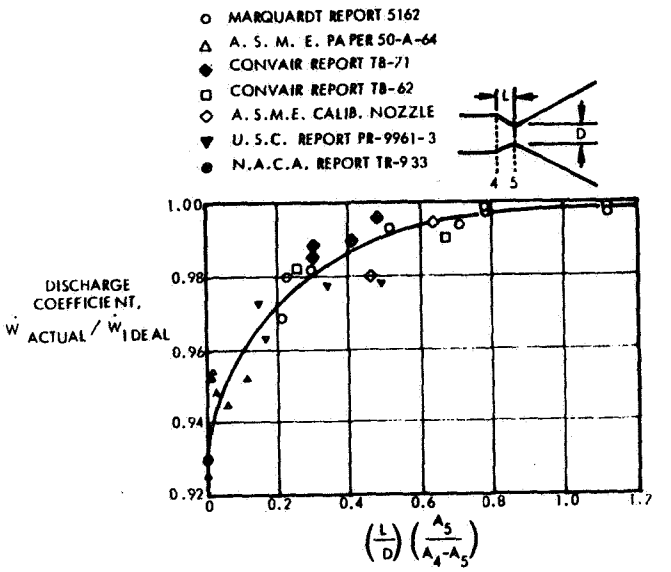

Figure A-3. Conical Nozzle Discharge Coefficient

1.4 FRICTIONAL DRAG INFLUENCE FACTOR (f_{FR})

Calculations of C* based on chamber pressure are concerned with chamber phenomena up to the nozzle throat. Drag forces to this point are small enough to be considered negligible, so that the factor f_{FR} may be taken to be unity.

1.5 ENERGY LOSS INFLUENCE FACTOR (f_{HL})

Chamber pressure and thrust are decreased by heat transfer from the combustion gases to the walls of a thrust chamber. This enthalpy loss is substantially reduced in ablative chambers and is effectively recovered in a regeneratively cooled chamber.

The effect on C* of enthalpy loss by heat transfer can be estimated from a loss of chamber enthalpy. This is determined from a two station energy balance, one at the start of nozzle convergence and the other at the throat.

$$1/2\ V_c^2 + H_c = 1/2\ V_t^2 + H_t + \dot{Q}_{conv} \qquad \text{(A-10)}$$

where:

V_c = gas velocity at chamber exit
V_t = gas velocity at nozzle throat
H_c = gas enthalpy at chamber exit
H_t = gas enthalpy at nozzle throat
$\dot{Q}_{conv}$ = heat loss in nozzle convergence

Velocity at the throat is given by:

$$V_t = [V_c^2 + 2(H_c - H_t - \dot{Q}_{conv})]^{1/2} \qquad \text{(A-11)}$$

With negligible nozzle inlet velocity

$$V_t = [2(H_c - H_t - \dot{Q}_{conv})]^{1/2} \qquad \text{(A-12)}$$

Logarithmic differentiation of Equation (A-12) gives

$$\frac{dV_t}{V_t} = 1/2\ \frac{d\ (H_c - H_t - \dot{Q}_{conv})}{(H_c - H_t - \dot{Q}_{conv})} = 1/2 \left(\frac{d\ H_c - dH_t}{H_c - H_t - \dot{Q}_{conv}} \right) \qquad \text{(A-13)}$$

Substitution of enthalpy definition into Equation (A-13) gives:

$$\frac{dV_t}{V_t} = 1/2 \left(\frac{c_{pc}\ dT_c - c_{pt}\ dT_t}{H_c - H_t - \dot{Q}_{conv}} \right) \qquad \text{(A-14)}$$

With constant $\dot{C}_p$ between the two stations,

$$\frac{dV_t}{V_t} = 1/2 \left(\frac{c_p \, dT_c}{H_c - H_t - \dot{Q}_{conv}} \right) \left(1 - \frac{dT_t}{dT_c} \right) \qquad \text{(A-15)}$$

If the specific heat ratio, γ, is assumed constant,

$$\frac{dT_t}{dT_c} = \frac{T_t}{T_c} \qquad \text{(A-16)}$$

Substituting Equation (A-16) into Equation (A-15), replacing differentials by incrementals, and noting that C* is proportional to gas velocity at the throat gives:

$$\frac{\Delta V_t}{V_t} = \frac{\Delta C^*}{C^*} = 1/2 \left(\frac{c_p \, \Delta T_c}{H_c - H_t - \dot{Q}_{conv}} \right) \left(1 - \frac{\Delta T_t}{T_c} \right) \qquad \text{(A-17)}$$

Total heat loss to the chamber walls, in Btu per pound of propellant, is obtained by summation of observed heat fluxes over the appropriate areas:

$$\text{Heat loss} = \frac{\Sigma (q/A) \, A}{\dot{w}_T} \qquad \text{(A-18)}$$

where:

q/A = experimentally observed heat flux
A = area applicable to each q/A value
$\dot{w}_T$ = total propellant flow rate

If this heat loss is equated to the change in enthalpy of the gas in the combustion chamber, $c_p \, \Delta T_c$, then substitution in Equation (A-17) gives:

$$\frac{\Delta C^*}{C^*} = 1/2 \left[\frac{\Sigma (q/A) A}{\dot{w}_T} \right] \left[\frac{1 - (T_t/T_c)}{H_c - H_t - Q_{conv}} \right] \qquad \text{(A-19)}$$

The applicable influence factor is:

$$f_{HL} = 1 + \frac{\Delta C^*}{C^*} = 1 + 1/2 \left[\frac{\Sigma (q/A) A}{\dot{w}_T} \right] \left[\frac{1 - (T_t/T_c)}{H_c - H_t - Q_{conv}} \right] \qquad \text{(A-20)}$$

An alternate expression can be obtained from the basic C* definition:

$$C^* = \frac{\sqrt{RT_c}}{\Gamma} \tag{A-21}$$

Logarithmic differentiation of this yields:

$$\frac{dc^*}{c^*} = \frac{1}{2} \frac{dT_c}{T_c} \tag{A-22}$$

Substituting incrementals from differentials in Equation (A-22) gives:

$$\frac{\Delta_c{}^*}{c^*} = \frac{1}{2} \frac{\Delta T_c}{T_c} \tag{A-23}$$

Equating ΔT_c with the heat loss from Equation (A-18) results in the following:

$$\frac{\Delta_c{}^*}{c^*} = \frac{1}{2} \left[\frac{\Sigma(q/A)A}{\dot{w}_t}\right]\left[\frac{1}{c_p T_c}\right] \tag{A-24}$$

The applicable influence factor is:

$$f_{HL} = 1 + \frac{1}{2}\left[\frac{\Sigma(q/A)A}{\dot{w}_t}\right]\left[\frac{1}{c_p T_c}\right] \tag{A-25}$$

where

c_p = specific heat at constant pressure

Although derived independently it can be shown that these two expressions, Equations (A-20) and (A-25), are nearly equivalent.

1.6 INFLUENCE FACTOR FOR CHEMICAL KINETICS (f_{KE})

The effect of finite chemical reaction rates is to produce a C* less than the corresponding theoretical equilibrium values. A TRW Systems Group developed one-dimension nonequilibrium reacting gas computer program was employed with reaction rate constants selected for the propellant system. The fluid mechanical and chemical equations were integrated from the inlet section by an implicit technique. It was determined that the effect of nonequilibrium chemistry produced a C* loss of 1.2% compared to the shifting equilibrium limits.

2. CALCULATIONS BASED ON THRUST

The alternate determination of C* efficiency is based on thrust:

$$\eta_{C^*} = \frac{F_{vac}\, g_c}{(C_F)_{vac}\, \dot{w}_T\, C^*_{theo}} \qquad \text{(A-26)}$$

where:

F_{vac} = measured thrust corrected to vacuum conditions by the equation: $F_{vac} = F + P_a A_e$

F = measured thrust, lbf

P_a = ambient pressure, psia

A_e = area of nozzle exit, in^2

g_c = conversion factor (32.174 lbm-ft/lbf-sec^2)

$(C_F)_{vac}$ = theoretical shifting thrust coefficient (vacuum)

$\dot{w}_T$ = total propellant flow rate, lbm/sec

c^*_{theo} = theoretical shifting-equilibrium characteristic velocity, ft/sec

Values of vacuum thrust are obtained by applying corrections to sea-level measurements. With these values, which include allowances for all important departures from ideality, theoretical thrust coefficients may be used for calculation of C*. C_F efficiency is taken as 100 percent if there is no combustion in the nozzle, if chemical equilibrium is maintained in the nozzle expansion process, and if energy losses from the combustion gases are accounted for.

Applicable influence factors for measured thrust are specified in the following equation:

$$\eta_{C^*} = \frac{(F + P_a A_e)\, g_c\, \phi_{FR}\, \phi_{DIV}\, \phi_{HL}\, \phi_{KE}}{(C_F)_{theo}\, (W_o + \dot{w}_f)\, (C^*)_{theo}} , \qquad \text{(A-27)}$$

where:

F = measured thrust, lb_f

P_a = ambient pressure, psia

A_e = area of nozzle exit, in^2

g_c = conversion factor (32.174 lbm-ft/lbf-sec^2)

$(C_F)_{theo}$ = theoretical shifting thrust coefficient (vacuum)

$\dot{w}_o$ = oxidizer weight flow rate, lbm/sec

$\dot{w}_f$ = fuel weight flow rate, lbm/sec

$(C^*)_{theo}$ = theoretical shifting equilibrium characteristic velocity, ft/sec

ϕ_{FR} = influence for frictional losses

ϕ_{DIV} = influence factor for nozzle divergence

ϕ_{HL} = influence factor for heat losses to chamber and nozzle walls

ϕ_{KE} = influence factor correcting C* and C_F values to account for finite chemical reaction rates

The influence factors in Equation (A-27) are applied to vacuum thrust ($F + P_a A_e$) instead of to measured site thrust (F) because, for convenience, the factors are readily calculated as changes in efficiency based on theoretical vacuum parameters. The total influence factor is then of the form $\Delta F/F_{vac}$.

Implicit in the use of theoretical C_F values are corrections to geometric throat area and to measured static chamber pressure at start of nozzle convergence. Therefore, calculation of corrected C* efficiency from thrust measurement includes all the previously described corrections plus an additional one to account for nonparallel nozzle exit flow. However, because $(C_F)_{theo}$ is essentially independent of small changes to chamber pressure and contraction ratio which are involved in corrections to P_c and A_t, these corrections are of no practical significance in calculation of C* from thrust measurements.

2.1 INFLUENCE FACTOR FOR FRICTIONAL DRAG (ϕ_{FR})

This factor corrects for energy losses caused by viscous drag forces on the thrust chamber walls. Its magnitude is estimated by a boundary layer analysis utilizing the integral momentum equation for turbulent flow, which accounts for boundary layer effects from the injector to the nozzle exit by suitable description of the boundary layer profile and local skin friction coefficient. A computer program is used to carry out a numerical

integration of the equation, including effects of pressure gradient, heat transfer, and surface roughness. The program requires a potential nozzle flow solution obtained from variable-property, axisymmetric method of characteristics calculation of the flow field outside the boundary layer; corresponding properties for the subsonic combustion chamber flow field are also calculated.

2.2 INFLUENCE FACTOR FOR NOZZLE DIVERGENCE (ϕ_{DIV})

The one-dimensional theoretical performance calculations assume that flow at the nozzle exit is uniform and parallel to the nozzle axis. The influence factor, ϕ_{DIV}, allows for nozzle divergence (i.e., for nonaxial flow) and for nonuniformity across the nozzle exit plane. It is calculated by a computer program which utilizes the axisymmetric method of characteristics for a variable-property gas. Computation begins with a transonic input near Mach 1, providing a characteristic line for use in the analysis of the supersonic portion of the nozzle. The resulting pressures are integrated over the given geometry to give the geometric efficiency.

2.3 INFLUENCE FACTOR FOR HEAT LOSS (ϕ_{HL})

To obtain the heat loss influence factor from measured thrust the approach is identical to that taken previously from the pressure measurement, except that the nozzle losses must also be included. With constant specific heat and gamma from start of nozzle convergence to exit, Equation (A-20) becomes

$$\phi_{HL} = 1 + \frac{1}{2}\left[\frac{\Sigma\left(\frac{q}{A}\right) A}{\dot{w}_T}\right]\left[\frac{1 - T_e/T_c}{H_c - H_e - \dot{Q}_{nozzle}}\right] \qquad \text{(A-28)}$$

when "e" corresponds to the exit condition, and the summation occurs over the entire combustion.

An alternate can also be derived as in Equation (A-25). This equation becomes

$$\phi_{HL} = 1 + \frac{1}{2}\left[\frac{(q/A)A}{\dot{w}_T}\right]\left[\frac{1}{c_p T_e}\right] \qquad \text{(A-29)}$$

2.4 INFLUENCE FACTOR FOR CHEMICAL KINETICS (ϕ_{KE})

The effect of finite chemical reaction rates is to produce a C* and C_F less than the corresponding theoretical equilibrium values. A TRW Systems Group developed one-dimensional nonequilibrium reacting gas computer program was employed with reaction rate constants selected for the hydrogen-oxygen propellant system. The fluid mechanical and chemical equations were integrated from the inlet section by an implicit technique.

APPENDIX B

COMPUTER PROGRAMS

The following computer programs were used to facilitate performance and heat transfer analysis during various phases of this program.

1.0 ROCKET CHEMISTRY PROGRAM

The generalized equilibrium chemistry program solves a wide range of thermodynamic problems requiring only the composition and two of the following system properties to be specified: pressure, volume, temperature, enthalpy, entropy or internal energy. The program calculates composition, either from a pair of compounds with a specified weight mixture ratio, or from a series of compounds and their respective weight percents. In addition to the usual pure condensed phases, it is possible to submit a series of ideal chemical solutions composed of selected combinations of the condensed phases; the program will determine whether or not these solutions are formed by the reaction. The possible reaction products are obtained by searching a prepared master inventory tape containing entropy and enthalpy curve fit coefficients for all elements and compounds of interest. Nongaseous phases and ionized species are treated as distinct and separate compounds. The program initially assumes an ideal all-gas system. The equilibrium gas pressures of all possible gaseous species are calculated. Using these partial pressures as initial estimates, nongaseous phases and solutions are then considered. Upon convergence of the calculations, the program eliminates all but the actual gases, condensed phases, and ideal solutions present at equilibrium. Rocket performance is computed for isentropic sonic flow through a throat by specifying exit pressures, temperatures, or area ratios. Chemical reactions only, or chemical reactions and phase changes, may be stopped at any point in the expansion. Equilibrium or frozen composition, thermodynamic parameters, and the usual rocket parameters are given in the program output.

2.0 ONE-DIMENSIONAL, ONE-PHASE EXACT KINETIC COMPUTER PROGRAM

TRW Systems had developed under contract to the National Aeronautics and Space Administration Manned Spacecraft Center (Contract NAS 9-4358), a One-Dimensional, One-Phase (1D, 1P) Reacting Gas Nonequilibrium Performance Program. The computer program calculates the inviscid one-dimensional equilibrium, frozen and nonequilibrium nozzle expansion of propellant exhaust mixtures containing the six elements: carbon, hydrogen, oxygen, nitrogen, fluorine and chlorine.

The computer program considers all significant gaseous species (19) present in the exhaust mixtures of propellants containing these elements and all gas phase chemical reactions (48) which can occur between the exhaust products. In order to reduce the computation times per case to a minimum, the program utilizes a second-order implicit integration method. This integration method has reduced the computation time, per case, several orders of magnitude compared to the computation time required when utilizing standard explicit integration methods such as fourth order Runge-Kutta or Adams-Moulton methods.

The throat size is determined for each combination of propellant system and mixture ratio through use of the given chamber pressure, thrust level, and the value of the one-dimensional thrust coefficient, C_F, computed by the Rocket Chemistry Program. The reverse reaction rate constant, $k_r = AT^{-n}e^{-B/T}$, is employed in the Kinetics Program and forms a portion of the input data to the computer program. It is usually input in chemist's units; i.e., cm^3, gm, °K, sec., and is converted internally into units consisting of ft^3, lb, °R, sec.

3.0 ONE-DIMENSIONAL, TWO-PHASE EXACT KINETIC COMPUTER PROGRAM

TRW Systems has also developed, under contract to the National Aeronautics and Space Administration Manned Spacecraft Center (Contract NAS 9-4358), a One-Dimensional, Two-Phase (1D, 2P) Reacting Gas Nonequilibrium Performance Program. This program calculates the inviscid one-dimensional equilibrium, frozen and nonequilibrium nozzle expansion of propellant exhaust mixtures containing the six elements: carbon, hydrogen, oxygen, nitrogen, fluorine and chlorine; and one metal element, either aluminum, beryllium,

boron or lithium. Energy and momentum transfer is considered between the two phases but interphase mass transfer is not considered.

In all 79 species related by 763 reactions are handled with a maximum of 46 species and 380 reactions for the boron metal element. In addition, provision is made for eight condensed species with a maximum of four condensed species at any time. Furthermore, the condensed phase can be allocated to one (or more) size group.

All the species and reactions of importance to the proposed program can be accommodated by the TRW Systems developed One-Phase and/or Two-Phase Kinetics Programs.

4.0 VISCOUS EFFECTS COMPUTER PROGRAM.

The method of Bartz for computing boundary-layer thicknesses, skin-friction, and heat flux in axisymmetric nozzles has been revised and programmed for digital computer solution. The method solves, simultaneously, the integral momentum and energy equations for thin axisymmetric boundary layers. Boundary-layer shape parameters are approximated from one-seventh power profiles of velocity and stagnation temperature; and skin-friction coefficient and Stanton number are evaluated as functions of boundary-layer thickness from the best available semiempirical relations.

This program either employs a given wall Mach number distribution as generated by, for example, the Two-Dimensional Kinetics Computer Program, or can generate internally a one-dimensional Mach number distribution as a function of local area ratio and (constant) γ, the ratio of specific heats. In addition, the program requires a wall temperature, Tw, distribution. This distribution can be produced, by an iterative procedure, from a thermal analysis of the nozzle. A constant wall temperature may be assumed in lieu of such data.

The program computes the local parameters: convective heat transfer coefficient (h_g), heat flux ($\dot{q}/A$), where A is the nozzle surface area, skin-friction coefficient (C_f), boundary-layer thickness (δ), displacement thickness (δ^*) and momentum thickness (θ). The total heat rejection load, $\dot{q}$, is found from numerical intergration of $\dot{q}/A$ versus A.

5.0 BASIC ONE-DIMENSIONAL HEAT TRANSFER PROGRAM

This program, designated 84040 on TRW's IBM 7070, computes the change in temperature of each of a number of points (called nodes) in a slab of material, at specified intervals of time, during which the slab is to be heated and/or cooled. The heating and cooling is accomplished by convection and radiation, at the slab boundaries. The program is general enough so that it can handle heat transfer through both flat plate and cylindrical sections, regardless of size, thickness, and material layer composition. Most commonly, the program is used to simulate rocket engine firing duty cycles.

Preparation of the input for this program requires the following:

1) Convective heat transfer coefficients on the inside and outside surfaces
2) Inside and outside adiabatic wall temperatures
3) Initial temperatures of the node points
4) Thermal conductivities and diffusivities of the materials in the slab
5) Thicknesses of the material layers

The output consists of temperature profiles in the slab at specified time intervals.

6.0 THREE-DIMENSIONAL PROGRAM

This is a high-speed digital program for transient problems involving all nodes or combinations of nodes of heat transfer (i.e., convection, conduction, and radiation). This program can be used for any thermal problem whose finite difference equation is analogous to the differential equation for a lumped RC electrical network and can, therefore, be visualized as an electrical circuit.

The number of connecting flux paths to any node is arbitrary. This program can handle as many as 250 node point and capacitances with approximately 800 resistances.

Four valuable features are incorporated into this program:

1) Variable thermal properties are simulated when a table showing values of each property versus temperature is entered in the input.
2) This program can hold any node at a constant temperature for a period of time and thus simulate phase transition.
3) Erosion rate schedule is entered in the input in the form of a table.
4) A cathode follower is used for the purpose of transferring a temperature from one node in the network to another with zero transfer of energy.

7.0 GAS PROPERTIES COMPUTER PROGRAM

This program is used to rapidly determine the following:

1) Nozzle thrust coefficient as a function of pressure ratio
2) Nozzle area ratio as a function of pressure ratio
3) Nozzle area ratio as a function of Mach number
4) Ratio of local to critical temperature as a function of Mach number
5) Ratio of isentropic temperature drop to inlet temperature as a function of pressure ratio

The range of values covered for each of the basic parameters is:

Mach number:	1 - 10
Pressure ratio:	3.5 - 10^4
Ratio of specific heats:	1.1 - 1.67

The effect of the ratio of specific heats is included in all the plots.

APPENDIX C

DISTRIBUTION LIST

REPORT COPIES R	D	RECIPIENT	DESIGNEE
		National Aeronautics & Space Administration Lewis Research Center 21000 Brookpark Road Cleveland, Ohio 44135	
1		Attn: Contracting Officer, MS 500-313	
5		E. A. Bourke, MS 500-203	
1		Technical Report Control Office, MS 5-5	
1		Technology Utilization Office, MS 3-16	
2		AFSC Liaison Office, 501-3	
2		Library	
1		Office of Reliability & Quality Assurance, MS 500-111	
1		J. W. Gregory	Chief, MS 500-203
3		P. N. Herr	Project Manager, MS 500-209

Director, Shuttle Technology Office, RS
Office of Aeronautics & Space Technology
NASA Headquarters
Washington, D. C. 20546

REPORT COPIES REQ'D	RECIPIENT	DESIGNEE
2	Director Space Prop. and Power, RP Office of Aeronautics & Space Technology NASA Headquarters Washington, D.C. 20546	
1	Director, Launch Vehicles & Propulsion, SV Office of Space Science NASA Headquarters Washington, D.C. 20546	
1	Director, Materials & Structures Div, RW Office of Aeronautics & Space Technology NASA Headquarters Washington, D. C. 20546	
1	Director, Advanced Manned Missions, MT Office of Manned Space Flight NASA Headquarters Washington, D.C. 20546	
37	National Technical Information Service Springfield, Virginia 22151	
1	National Aeronautics & Space Administration Ames Research Center Moffett Field, California 94035 Attn.: Library	Hans M. Mark Mission Analysis Division
1	National Aeronautics & Space Administration Flight Research Center P.O. Box 273 Edwards, California 93523 Attn: Library	
1	Director, Technology Utilization Division Office of Technology Utilization NASA Headquarters Washington, D. C. 20546	
1	Office of the Director of Defense Research & Engineering Washington, D. C. 20301 Attn: Office of Asst. Dir. (Chem Technology)	

REPORT COPIES R	D	RECIPIENT	DESIGNEE
2		NASA Scientific and Technical Information Facility P. O. Box 33 College Park, Maryland 20740 Attn: NASA Representative	
1		Nation Aeronautics & Space Administration Goddard Space Flight Center Greenbelt, Maryland 20771 Attn: Library	Merland L. Mosesor, Code 620
1		National Aeronautics & Space Administration John F. Kennedy Space Center Cocoa Beach, Florida 32931 Attn: Library	Dr. Kurt H. Debus
1		National Aeronautics & Space Administration Langley Research Center Langley Station Hampton, Virginia 23365 Attn: Library	E. Cortwright Director
1	1	National Aeronautics & Space Administration Manned Spacecraft Center Houston, Texas 77001	J. G. Thibodaux, Jr. Chief, Propulsion & Power Division
	1	Attn: Library	C. A. Vaughan
1	1	National Aeronautics & Space Administration George C. Marshall Space Flight Center Huntsville, Alabama 35912 Attn: Library	Hans G. Paul
	1		Keith Coates
1		Jet Propulsion Laboratory 4800 Oak Grove Drive Pasadena, California 91103 Attn: Library	Henry Burlage, Jr. Duane Dipprey
1		Defense Documentation Center Cameron Station Building 5 5010 Duke Street Alexandria, Virginia 22314 Attn: TISIA	

REPORT COPIES R	D	RECIPIENT	DESIGNEE
1		Arnold Engineering Development Center Air Force Systems Command Tullahoma, Tennessee 37389 Attn: Library	Dr. H. K. Doetsch
1		Aeronautical Systems Division Air Force Systems Command Wright-Patterson Air Force Base, Dayton, Ohio Attn: Library	D. L. Schmidt Code ARSCNC-2
1		Air Force Missile Test Center Patrick Air Force Base, Florida Attn: Library	L. J. Jillian
1		Air Force Systems Command Andrews Air Force Base Washington, D.C. 20332 Attn: Library	Capt. S. W. Bowen SCLT
1	1	Air Force Rocket Propulsion Laboratory (LKDS) Edwards, California 93523 Attn: Library	R. L. Wiswell W. Lawrence
1		Air Force Rocket Propulsion Laboratory(RPM) Edwards, California 93523 Attn: Library	
1		Air Force FTC (FTAT-2) Edwards Air Force Base, California 93523 Attn: Library	Donald Ross
1		Air Force Office of Scientific Research Washington, D.C. 20333 Attn: Library	SREP, Dr. J. F. Masi

REPORT COPIES R	D	RECIPIENT	DESIGNEE
1		Space & Missile Systems Organization Air Force Unit Post Office Los Angeles, California 90045 Attn: Technical Data Center	
1		Office of Research Analyses (OAR) Holloman Air Force Base, New Mexico 88330 Attn: Library RRRD	
1		U. S. Air Force Washington, D.C. Attn: Library	Col. C. K. Stambaugh, Code AFRST
1		Commanding Officer U. S. Army Research Office (Durham) Box CM, Duke Station Durham, North Carolina 27706 Attn: Library	
1		U. S. Army Missile Command Redstone Scientific Information Center Redstone Arsenal, Alabama 35808 Attn: Document Section	Dr. W. Wharton
1		Bureau of Naval Weapons Department of the Navy Washington, D.C. Attn: Library	J. Kay, Code RTMS-41
1		Commander U. S. Naval Missile Center Point Mugu, California 93041 Attn: Technical Library	
1		Commander U. S. Naval Weapons Center China Lake, California 93557 Attn: Library	
1		Commanding Officer Naval Research Branch Office 1030 E. Green Street Pasadena, California 91101 Attn: Library	

REPORT COPIES R	D	RECIPIENT	DESIGNEE
1		Director (Code 6180) U. S. Naval Research Laboratory Washington, D.C. 20390 Attn: Library	H. W. Carhart J. M. Krafft
1		Picatinny Arsenal Dover, New Jersey 07801 Attn: Library	I. Forsten
1		Air Force Aero Propulsion Laboratory Research & Technology Division Air Force Systems Command United States Air Force Wright-Patterson AFB, Ohio 45433 Attn: APRP (Library)	R. Quigley C. M. Donaldson
1		Space Division Aerojet-General Corporation 9200 East Flair Drive El Monte, California 91734 Attn: Library	S. Machlawski
1		Aerojet Liquid Rocket Company P. O. Box 15847 Sacramento, California 95813 Attn: Technical Library 2484-2015A	R. Stiff R. LaBotz
1		Aeronutronic Division of Philco Ford Corp. Ford Road Newport Beach, California 92663 Attn: Technical Information Department	Dr. L. H. Linder

REPORT COPIES R	D	RECIPIENT	DESIGNEE
1		Aerospace Corporation 2400 E. El Segundo Blvd. Los Angeles, California 90045 Attn: Library-Documents	J. G. Wilder
1		Astropower Laboratory McDonnell-Douglas Aircraft Company 2121 Paularino Newport Beach, California 92163 Attn: Library	
1		ARO, Incorporated Arnold Engineering Development Center Arnold AF Station, Tennessee 37389 Attn: Library	
1		Susquehanna Corporation Atlantic Research Division Shirley Highway & Edsall Road Alexandria, Virginia 22314 Attn: Library	
1		Beech Aircraft Corporation Boulder Facility Box 631 Boulder, Colorado Attn: Library	Douglas Pope
1		Bell Aerosystems, Inc. Box 1 Buffalo, New York 14240 Attn: Library	T. Reinhardt W. M. Smith J. Flanagan
	1		

REPORT COPIES R & D	RECIPIENT	DESIGNEE
1	Instruments & Life Support Division Bendix Corporation P.O. Box 4508 Davenport, Iowa 52808 Attention: Library	W. M. Carlson
1	Boeing Company Space Division P.O. Box 868 Seattle, Washington 98124 Attn: Library	J. D. Alexander C. F. Tiffany
1	Boeing Company P.O. Box 1680 Huntsville, Alabama 35801	Ted Snow
1	Chemical Propulsion Information Agency Applied Physics Laboratory 8621 Georgia Avenue Silver Spring, Maryland 20910	Tom Reedy
1	Chrysler Corporation Missile Division P.O. Box 2628 Detroit, Michigan Attn: Library	John Gates
1	Chrysler Corporation Space Division P.O. Box 29200 New Orleans, Louisiana 70129 Attn: Library	

REPORT COPIES R	D	RECIPIENT	DESIGNEE
1		Curtiss-Wright Corporation Wright Aeronautical Division Woodridge, New Jersey Attn: Library	G. Kelley
1		Fairchild Stratos Corporation Aircraft Missiles Division Hagerstown, Maryland Attention: Library	
1		Research Center Fairchild Hiller Corporation Germantown, Maryland Attn: Library	Ralph Hall
1		Republic Aviation Fairchild Hiller Corporation Farmington, Long Island New York	
1		General Dynamics/Convair P. O. Box 1128 San Diego, California 92112 Attn: Library	Frank Dore
1		Missiles and Space Systems Center General Electric Company Valley Forge Space Technology Center P. O. Box 8555 Philadelphia, Pa. 19101 Attn: Library	A. Cohen G. E. DeSalle
1		General Electric Company Flight Propulsion Lab. Department Cincinnati, Ohio Attn: Library	D. Suichu Leroy Smith

REPORT COPIES R	D	RECIPIENT	DESIGNEE
1		Grumman Aircraft Engineering Corporation Bethpage, Long Island, New York Attn: Library	Joseph Gavin
1		Honeywell Inc. Aerospace Division 2600 Ridgeway Road Minneapolis, Minnesota Attn: Library	
1		IIT Research Institute Technology Center Chicago, Illinois 60616 Attn: Library	C. K. Hersh
1		Kidde Aer-Space Division Walter Kidde & Company, Inc. 567 Main Street	R. J. Hanville
1		Ling-Temco-Vought Corporation P. O. Box 5907 Dallas, Texas 75222 Attn: Library	
1		Lockheed Missiles and Space Company P. O. Box 504 Sunnyvale, California 94087 Attn: Library	
1		Lockheed Propulsion Company P. O. Box 111 Redlands, California 92374 Attn: Library, Thackwell	H. L. Thackwell
1		Marquardt Corporation 16555 Saticoy Street Box 2013 - South Annex Van Nuys, California 91409	Tom Hudson

REPORT COPIES R	D	RECIPIENT	DESIGNEE
1		Martin-Marietta Corporation (Baltimore Division) Baltimore, Maryland 21203 Attn: Library	
1		Denver Division Martin-Marietta Corporation P. O. Box 179 Denver, Colorado 80201 Attn: Library	Dr. Morganthaler F. R. Schwartzberg
1		Western Division McDonnell Douglas Astronautics 5301 Bolsa Ave Huntington Beach, California 92647 Attention: Library	R. W. Hallet G. W. Burge P. Klevatt
1	1	McDonnell Douglas Aircraft Corporation P. O. Box 516 Lambert Field, Missouri 63166 Attn: Library	R. A. Herzmark L. Kohrs
1	1	Rocketdyne Division North American Rockwell Inc. 6633 Canoga Avenue Canoga Park, California 91304 Attn: Library, Department 596-306	Dr. R. J. Thompson S. F. Iacobellis R. E. Field
1		Space & Information Systems Division North American Rockwell 12214 Lakewood Blvd. Downey, California Attn: Library	
1		Northrop Space Laboratories 3401 West Broadway Hawthorne, California Attn: Library	Dr. William Howard

REPORT COPIES R	D	RECIPIENT	DESIGNEE
1		Radio Corporation of America Astro-Electronics Products Princeton, New Jersey Attn: Library	
1		Rocket Research Corporation Willow Road at 116th Street Redmond, Washington 98052 Attn: Library	F. McCullough, Jr.
1		Thiokol Chemical Corporation Redstone Division Huntsville, Alabama Attn: Library	John Goodloe
1	1	TRW Systems Inc. 1 Space Park Redondo Beach, California 90278 Attn: Tech. Lib. Doc. Acquisitions	D. H. Lee H. Burge
1		United Aircraft Corporation Corporation Library 400 Main Street East Hartford, Connecticut 06108 Attn: Library	Dr. David Rix
1		United Aircraft Corporation Pratt & Whitney Division Florida Research & Development Center P. O. Box 2691 West Palm Beach, Florida 33402 Attn: Library	R. J. Coar Dr. Schmitke

REPORT COPIES R	D	RECIPIENT	DESIGNEE
1		B. F. Goodrich Company Aerospace & Defense Products 500 South Main Street Akron, Ohio 44311	
1		Goodyear Aerospace Corporation 1210 Massillon Road Akron, Ohio 44306	D. Romick
1		Vought Astronautics Box 5907 Dallas, Texas Attn: Library	